Global effects of plant virus infection, viral noncoding RNAs, and unfolded protein response on plant gene expression

by

Pulkit Kanodia

A dissertation submitted to the graduate faculty

in partial fulfillment of the requirements for the degree of

DOCTOR OF PHILOSOPHY

Major: Genetics and Genomics

Program of Study Committee:
W. Allen Miller, Major Professor
Stephen H. Howell
Steven A. Whitham
Dior Kelley
Peng Liu

The student author, whose presentation of the scholarship herein was approved by the program of study committee, is solely responsible for the content of this dissertation. The Graduate College will ensure this dissertation is globally accessible and will not permit alterations after a degree is conferred.

Iowa State University

Ames, Iowa

2021

DEDICATION

"Science appears calm and triumphant when it is completed; but science in the process of being done is only contradiction and torment, hope and disappointment." ― Pierre Paul Émile Roux, French bacteriologist.

I dedicate my dissertation to my mom, dad, and my brother, Dhoundhu, who always supported and encouraged me to pursue my dreams. My family blessed me with some privileges: the most important one was to give me the freedom to choose my career. They provided me with the resources and the capabilities without which I would never have been able to pursue Ph. D. They gave me the strength and moral support, during all the set-backs, which motivated me to carry-on and succeed.

I also dedicate this dissertation to my friend, Mahima, who kept me sane during my Ph.D. Being able to share my personal and professional ups and down with her during the last seven years was one of the main reasons why I did not quit Ph.D. during difficult times, but instead, was able to stay motivated and on-track to achieve my goals.

I would also like to dedicate my research to the people around the world who have suffered through hunger, famine and diseases because of viruses. I sincerely hope that my work will serve as, at the very least, a tiny pebble of knowledge in the vast ocean of unknowns that, along with the work of others, can help make the world satiated, healthy, and a better place.

TABLE OF CONTENTS

Page

LIST OF FIGURES

Page

LIST OF TABLES

Page

NOMENCLATURE

3’ CITE	3’ Cap-independent translation element
3’ TE-DR1	3’ Translation element of *Dianthovirus* RNA1
BNYVV	Beet necrotic yellow vein virus
BP	Blocking primer
BTE	BYDV-like translation element
BYDV	Barley yellow dwarf virus
CDS	Coding DNA sequence
CP	Coat protein
DEG	Differentially expressed genes
DeSCo-PCR	Detection of smaller coterminal RNA by PCR
dpi	Days post inoculation
dsRNA	Double-stranded RNA
DTG	Differentially translated genes
eIF	Eukaryotic translation initiation factor
ER	Endoplasmic reticulum
FP	Forward primer
gRNA	Genomic RNA
IRES	Internal ribosome entry site
IVT	*In vitro* transcribed/transcription
LDFE	Long-distance frameshift element
lncRNA	Long noncoding RNA
LRR	Leucine rich receptor

miRNA	Micro RNA
MP	Movement protein
mRNA	Messenger RNA
NB-LRR	Nucleotide-binding leucine rich receptor
NBH	Northern blot hybridization
ncRNA	Noncoding RNA
ncsgRNA	Noncoding subgenomic RNA
NGS	Next generation sequencing
nt	Nucleotide
ORF	Open reading frame
PCR	Polymerase chain reaction
PEB	Polysome extraction buffer
PERK	PKR-like ER kinase
PKR	Protein kinase R
PR	Pathogenesis-related
PRF	Programmed ribosomal frameshifting
qPCR	Quantitative PCR
RCNMV	Red clover necrotic mosaic virus
RdRp	RNA-dependent RNA polymerase
Ribo-seq	Ribosome profiling
RLK	Receptor-like kinase
RLP	Receptor-like protein
RNA-seq	RNA sequencing

RNAi	RNA interference
RP	Reverse primer
RPF	Ribosome-protected fragments/footprints
rRNA	Ribosomal RNA
RT-PCR	Reverse transcription PCR
SG	Stress granules
sgRNA	Subgenomic RNA
siRNA	Short interfering RNA
ssRNA	Single-stranded RNA
SUnSET	Surface sensing of translation
TA	Trans-activator sequence in RCNMV RNA2
TA-BS	TA-binding site in RCNMV RNA1
TE	Translation efficiency
uORF	Upstream open reading frame
UPR	Unfolded protein response
UTR	Untranslated region
VRC	Virus replication complex
Wt/wt	Wild type
XRN	Exoribonuclease
xeRNA	Exoribonuclease-evading RNA
xrRNA	Exoribonuclease-resistant RNA
ZIKV	Zika virus

ACKNOWLEDGMENTS

First and foremost, I would like to thank my advisor and academic father, Dr. W. Allen Miller, who truly nurtured me into an independent researcher that I can confidently claim to be now. Allen gave me the freedom to think independently, patiently listened to my ideas and hypothesis, and provided me with the resources to test those ideas. He trained me to be a good scientific writer, taught me the scientific method, and most importantly, he taught me how to think about science. For the reasons I have mentioned, and numerous others like his contagious enthusiasm for virology, I would like to sincerely thank him again.

I would also like to thank my committee members: (i) Dr. Peng Liu and Dr. Stephen H. Howell for giving me the opportunity to collaborate with them and learn from them, (ii) Dr. Steve Whitham for guiding me throughout my research journey and always being willing to answer the countless questions that I bombarded him with, and (iii) Dr. Dior Kelley for guiding me and helping me keep my research on track.

I would like to thank my friends Akshay, Ashley, Bhakti, Gaurav, Juliette, Sambit, Talon, and Viraj, along with Surya and Saranya (plus their kids Sanav and Sanvi) for being my family in Ames. They made my life in Ames worth living and helped me become a better scientist and a better person. Additionally, I thank my friends and colleagues Keisuke, Liz, Manju, Megan, Renu, Ryan, Weihui, and Zach for the skills they helped me learn, for the help they provided me, and for making the time spent in the lab more fun and an enjoyable experience.

In addition, I would also like to thank the department staff, especially Dai, Linda, and Carla, for making my life easier and my time at Iowa State University a wonderful experience. Finally, I would like to thank all the researchers who collaborated with me on my projects, without whom this thesis would not have been possible.

ABSTRACT

Plants are subject to a variety of abiotic and biotic stresses, including virus infection. This leads to enormous losses in crop yield and quality worldwide. Understanding how plants respond to these stresses can enable researchers to develop more healthy and robust plant varieties. The main objective of my research is to explore (i) the transcriptional and translational control of cellular gene expression in response to virus infection and (ii) the role(s) of viral noncoding subgenomic (ncsg)RNAs during infection. For this, I used red clover necrotic mosaic virus (RCNMV) as a model for economically important *Tombusvirids*. RCNMV generates a 3' coterminal viral ncsgRNA, called SR1f, that belongs to the class of viral subgenomic (sg)RNAs that are functional in human flavivirus pathogenesis but which are still understudied in plant virus infection. Additionally, I also explored how translation is regulated in plants during unfolded protein response (UPR), which is elicited by many viruses and abiotic stresses.

A prerequisite for investigating viral sgRNAs is an RNA detection method that can distinguish between the coterminal genomic and sgRNAs. Using RCNMV SR1f and the analogous ncsgRNA from Zika virus (sfRNA), I developed a novel RT-PCR-based method, called DeSCo-PCR (Detection of smaller coterminal RNAs by PCR), for simple, quick, quantitative, and specific detection of viral sgRNAs. I demonstrate its advantages over the traditionally-used northern blot hybridization for detecting viral sgRNAs. This is the first RT-PCR method that distinguishes genomic from sgRNAs in most positive-sense RNA viruses.

Next, I wanted to assess the role(s) of RCNMV SR1f during infection. RCNMV SR1f belongs to the class of exoribonuclease-resistant (xr)RNA-derived viral ncsgRNAs. In plants, viral ncsgRNAs play a role in determining the severity of symptoms and the success of infection. Therefore, to explore the functions and effects of SR1f, I (i) used RNA sequencing (RNA-seq) to

compare how infection with RCNMV constructs, which can or cannot produce SR1f, affect the transcriptomes of *Nicotiana benthamiana* and RCNMV, (ii) assessed the role of SR1f in counteracting the antiviral RNA silencing response in *Arabidopsis thaliana*, and (iii) determined the requirement of XRN4 for generating RCNMV SR1f in *A. thaliana*.

Next, I used ribosome profiling (Ribo-seq) to assess how host and viral genes are translationally regulated in RCNMV-infected plants. Most genome-wide host-virus interaction studies have used RNA-seq, which does not provide any information on translational control. Translational control is a tightly-regulated process that provides a more rapid change in gene expression than a transcriptional response. Furthermore, viruses rely completely on cellular translation machinery for viral protein synthesis. However, translational control during plant virus-host interaction has rarely been studied at the genome-wide level. Therefore, I used Ribo-seq to (i) assess the effects of RCNMV infection on the transcriptome and the translatome of *A. thaliana* at early and late stages of infection, (ii) identify cellular genes that are transcriptionally and translationally-regulated in response to virus infection, and (iii) assess the translational landscape of RCNMV mRNAs in infected cells.

Finally, I also used Ribo-seq to assess the translational control in roots of *Zea mays* seedlings during UPR. The PKR-like ER kinase (PERK)-mediated UPR pathway, which results in phosphorylation of eIF2α and subsequent inhibition of global translation in mammalian cells, is absent in the plant system. Therefore, I wanted to determine if translational control is as important in plants as it is in mammalian cells during UPR. I used Ribo-seq and other molecular assays to (i) determine if there is global inhibition of translation in plants during UPR, (ii) calculate the translational efficiencies of several UPR-responsive mRNAs, and (iii) determine the fate of the UPR-responsive mRNAs that were transcriptionally upregulated during UPR.

CHAPTER 1. GENERAL INTRODUCTION

"We think of something that has four legs and wags its tail as being alive. We look at a rock and say it's not living. Yet when we get down to the no man's land of virus particles and replicating molecules, we are hard put to define what is living and what is non-living." (Cyril Ponnamperuma, 'The Seeds of Life', The Omni Interviews, 1984).

Since the emergence of severe acute respiratory syndrome coronavirus 2 (SARS-CoV-2) in 2019, the usage of the term "viruses" has gone viral among the general population worldwide. Globally, SARS-CoV-2 has resulted in over 245 million cases (reported) of the coronavirus disease 2019 (COVID-19) and over 4.9 million deaths (reported) by October 2021 (World Health Organization). In addition to the deaths and hospitalizations, the toll on human mental health (1–3), physical health (4, 5), and world economy (6, 7) has significantly exacerbated during this pandemic.

In spite of the increased awareness of the importance of studying viruses, the attention is mostly given to human viruses by the funding agencies and the general population alike. Relatively little importance is given to plant viruses. It is surprising because plant viral diseases have a direct implication to human health and the world economy (8). A rapidly growing human population demands a rapid increase in agricultural productivity. However, plant pathogens and pests, in addition to the weather extremes caused by climate change, pose a serious threat to global food security. Almost 40% yield of crops like maize, soybean, rice, wheat, and potato is lost worldwide due to plant pathogen and pests, among which viruses are the most consequential as they account for ~50% of the plant pathogens (9, 10). Furthermore, the economic impact of plant viral diseases is estimated to be greater than $30 billion annually (11–13). With the

increasing plant viral diseases, crop quality, yield, and nutrition value is suffering. The resulting global shortage of food supply and the increased malnutrition rate further worsen human health and makes us more susceptible to diseases. Unfortunately, the epidemic of plant diseases disproportionally affects developing countries. For example, maize lethal necrosis disease (MLND) in east Africa, where maize is the major crop for subsistence, has devasted yields and sometimes resulted in complete loss of the crop (14). MLND is caused by synergistic infection of two RNA viruses: maize chlorotic mottle virus (MCMV) and a virus from the *Potyviridae* family, such as sugarcane mosaic virus (SCMV). In another example, mungbean yellow mosaic disease (MYMD) caused by mungbean yellow mosaic virus (MYMV), from the *Geminiviridae* family, has had a significant impact on the production of several legumes in India, Pakistan, Sri Lanka, Bangladesh, Indonesia, Thailand, and Philippines (15). It has been a serious concern mainly in India as pulses are the major source of protein, especially for the large vegetarian population. Therefore, the development of crops that are resistant to viruses and other pathogens is of utmost importance.

In order to develop virus-resistant plants, basic research to understand how viral infections perturb and exploit host gene expression is crucial. It is also important to understand the intricate mechanisms by which a virus regulates its own gene expression during infection. Because human and plant viruses share a plethora of similarities, the knowledge gained by studying plant viruses also sheds light on the infection mechanisms used by human viruses. My doctoral research *(Fig. 1.1)* mainly focuses on a plant virus, called red clover necrotic mosaic virus (RCNMV), and the noncoding subgenomic (ncsg)RNA of RCNMV, called SR1f. I have developed a novel method to quantitatively detect viral coterminal subgenomic RNAs, including SR1f and a ncsgRNA of Zika virus *(Chapter 2 published in ref. 16)*. Subsequently, I assessed

how RCNMV SR1f affects the host and viral gene expression at the level of RNA abundance in RCNMV-infected *Nicotiana benthamiana (Chapter 3)*. Furthermore, I investigated how RCNMV infection affects host as well as viral gene expression patterns, both at the level of RNA abundance and their translatability to proteins in RCNMV-infected *Arabidopsis thaliana (Chapter 4)*.

In addition to my work on plant viruses, I also explored how protein synthesis is regulated in the roots of *Zea mays* seedlings during the unfolded protein response *(Chapter 5 published in ref. 17)*. Because my research involves a few distinct-but-related concepts *(Fig. 1.1)*, I would like to introduce them one by one in the following section and discuss them in detail in the respective chapters.

Red clover necrotic mosaic virus (RCNMV)

RCNMV (genus *Dianthovirus*, family *Tombusviridae*) is a bipartite plant virus with the virion size of ~36 nm *(Fig. 1.2-A)* (18, 19). Its genome is segmented into two positive-sense single-stranded genomic (g)RNAs, RNA1 and RNA2 *(Fig. 1.2-B)* (20–22). The genome organization of RCNMV is depicted *(Fig. 1.2-C)* along with a northern blot that shows the mobilities of subgenomic (sg)RNAs produced during the infection in Arabidopsis plants (*Fig. 1.2-D)*.

RNA1 (~3.89 kb) has three open reading frames (ORFs) *(Fig. 1.2-C)*, two of which are translated from RNA1 to make p27 (27-kDa) and p88 (88-kDa) proteins (23). p27 is an essential replication protein (22) and p88, which is a C-terminal extension of p27, is an RNA-dependent RNA polymerase (RdRp) (24). The p88 protein is translated by a -1 programmed ribosomal frameshift (-1 PRF) event immediately upstream of the p27 stop codon (25, 26). The p27-p27 and p27-p88 interactions are required for the formation of a 480-kDa replicase complex that

interacts with RCNMV RNAs and host factors to tightly associate with the endoplasmic reticulum (ER) (27–30). This results in the formation of virus replication complexes (VRCs) at the ER, the site of RCNMV replication (27, 28). It has also been shown that the formation of the 480-kDa replicase complex and the subsequent replication of RNA1 or RNA2 can suppress the antiviral RNA silencing response in *N. benthamiana* (31, 32). The 3'-proximal ORF on RNA1 *(Fig. 1.2-C)* is translated from a coat protein (CP)sgRNA to make the 37-kDa CP (33, 34). CP is not required for replication or cell-to-cell movement but is required for long-distance movement for systemic infection of a plant (35). RNA2 (~1.45 kb) has a single ORF *(Fig. 1.2-C)* encoding a 35-kDa movement protein (MP) that is required for cell-to-cell movement in plants (35, 36). Additionally, MP also functions as a viral suppressor of RNA silencing (37).

Similar to other tombusvirids, RCNMV RNAs lack a 5' methyl guanosine cap and a 3' poly(A) tail that are normally required for efficient translation (23, 36, 38, 39). Instead, RNA1 possesses a cap-independent translation element (CITE) in the 3' untranslated region (UTR) (39) that recruits the host translation machinery in order to synthesize the p27 and p88 proteins. The 3' CITEs function by binding translation initiation factors for ribosomal recruitment and translation initiation (40, 41). The 3' CITE of RCNMV is called 3' TE-DR1 *(Fig. 1.2-C)* and belongs to the barley yellow dwarf virus (BYDV)-like translation element (BTE) class of 3' CITEs (39). BTEs associate with the translation initiation factor eIF4F via binding to the eIF4G subunit for recruitment of translation machinery (42–45). As RNA1 and CPsgRNA have the same 3' UTR, CP translation from CPsgRNA is considered to occur via 3'TE-DR1-dependent mechanism (39). In contrast, RNA2 lacks any known 3' CITEs that can replace the function of the cap and therefore, RNA2 sequence by itself, in the presence of translation machinery, is insufficient for translation in the absence of a 5' cap (46). Despite this, translation of RNA2

occurs in the presence of p27 and p88, which are required for RNA2 replication, possibly from the newly replicated RNA2 molecules by coupling translation to its replication (46). In addition to the viral proteins and the coding CPsgRNA, RCNMV also makes a noncoding sgRNA, called SR1f, which is discussed in the later section.

Viral subgenomic RNAs

Subgenomic (sg)RNAs refer to truncated functional RNA species that are generated from the viral genomic (g)RNAs in infected cells. The gRNAs and sgRNAs usually have the same 3' ends *(Fig. 1.2-C)* (47, 48). Viral sgRNAs can be coding (i.e., contain an ORF for translation of a viral protein) or noncoding. Examples of sgRNA-producing medically important human viruses and economically important plant viruses include dengue virus (DENV) (49), Zika virus (ZIKV) (50), chikungunya virus (51), SARS-CoV (52), SARS-CoV-2 (53), barley yellow dwarf virus (54), and maize chlorotic mottle virus (55).

Coding sgRNAs are made for the translation of 5'-distal ORFs in polycistronic genomic RNAs, i.e., RNA with multiple ORFs. This is because during eukaryotic mRNA translation, only the 5'-proximal ORF is translated by the 80S ribosomes which dissociate into 40S and 60S ribosomal sub-units upon encountering the stop codon (56, 57). Therefore, ORFs encoding viral proteins required early during infection, such as replicase proteins, are located 5'-proximal and can be directly translated from the gRNA. Other ORFs encoding viral proteins that are required at an intermediate or late stage of infection, such as coat protein, are usually located 5'-distal and are translated from sgRNAs, thereby regulating the expression of viral proteins, both quantitatively and temporally, during an infection. Almost all the mechanisms of sgRNA production are viral RNA replication-dependent and have been reviewed earlier (47, 48).

The mechanism by which RCNMV CPsgRNA is synthesized is via transcription from a prematurely-terminated RNA1 negative-strand *(Fig. 1.3-A)* (34, 58). RCNMV RNA2 MP coding region has a 34 bp stem-loop element, called trans-activator (TA) *(Fig. 1.3-A)*. The 8 bp in the loop of TA are complementary to an 8 bp sequence in RNA1, called TA-binding site (TA-BS). The intermolecular interaction between RNA2 TA and RNA1 TA-BS blocks the viral polymerase, upstream of the CPsgRNA promoter, during the synthesis of RNA1 negative-strand. This results in a truncated RNA1 negative-strand that is transcribed to make the CPsgRNA positive-strand from which CP is translated *(Fig. 1.3-A)*. Coding sgRNA production is one of the many different strategies evolved by viruses for the translation of 5'-distal ORFs (48, 59–62). A few other strategies for translation of 5'-distal ORFs include translation initiation from internal ribosome entry sites (IRESs) (63) and translation reinitiation (64, 65).

Noncoding (nc)sgRNAs refer to the truncated but functional RNAs, without an ORF, derived from the UTRs of viral gRNAs. RCNMV generates an ncsgRNA, called SR1f *(Fig. 1.2-C, D)* (66). SR1f is generated by a host-dependent mechanism that is different from CPsgRNA production. In the last decade, this new strategy for the production of sgRNAs was discovered that is independent of virus replication but instead depends on the host 5'$\rightarrow$ 3' exoribonuclease (XRN) (66–74). Considering RCNMV as an example *(Fig. 1.3-B)*, the host cell initiates the degradation of the uncapped RCNMV RNA1 and CPsgRNA via the plant XRN, progressing from 5' to 3' end of the RNA. However, a stable exoribonuclease-resistant (xr)RNA structure at the 5'end of the 3' UTR *(Fig. 1.2-C, 1.3-B)* blocks the progression of XRN resulting in the accumulation of a truncated left-over degradation product, SR1f *(Fig. 1.3-B)*.

Most xrRNA elements that have been identified in viruses are located in the 3' UTR and, therefore, results in the formation of xrRNA-derived ncsgRNAs (66, 67, 69, 71, 75, 76).

However, a few xrRNA elements located in intergenic regions have also been identified that may result in coding xrRNA-derived sgRNAs (72, 74, 77). xrRNA-derived ncsgRNAs (simply referred to as ncsgRNAs hereafter) have been shown to have important functions during infection. The extensively studied ncsgRNAs of flaviviruses, called sfRNAs, have multiple functions, some of which include inhibition of translation of interferon-stimulated genes in mammalian cells, suppression of siRNA- and miRNA-induced RNAi pathways in insect and mammalian cells, and regulation of the stability of host mRNAs (75, 78–85). The ncsgRNA of beet necrotic yellow vein virus (BNYVV), called ncRNA3, has been shown to boost the viral RNA silencing suppression activity of BNYVV and enables long-distance virus movement in plants (69, 86). As more xrRNA elements, that are structurally-diverse but functionally-conserved, are being discovered *in silico* and experimentally in diverse virus families, it suggests that the xrRNAs provide an evolutionary advantage to viruses (72, 77).

As discussed above, sgRNAs (coding or noncoding) play important roles in virus life cycle. For studying these 3' coterminal sgRNAs, an obvious requirement is a method to detect them. Because sgRNAs are, simply, nucleic acids, reverse transcription (RT)-PCR would seem to be the first choice. However, conventional RT-PCR cannot distinguish sgRNA from the gRNA. This is because any primer pair designed to hybridize to sgRNA will also hybridize to the gRNA and result in amplification, irrespective of the presence of sgRNA. Because of this fundamental limitation of RT-PCR, northern blot hybridization (NBH) (87, 88) is widely used for the detection of sgRNAs. Northern blots have advantages over RT-PCR: (i) Northern blots can detect all coterminal sgRNAs simultaneously and (ii) there is no requirement for sequence information of the 5' ends of sgRNAs. However, northern blots suffer from several disadvantages: (i) A large amount of input RNA is needed for northern blots, (ii) It is time-,

labor-, and cost-intensive, (iii) It is a complex method with several steps and therefore, training is required, (iv) It involves hazardous chemicals like formaldehyde and usually radioactive isotopes. Non-radioactive northern blot methods exist but are more expensive, time-consuming, and less sensitive. To overcome these disadvantages of northern blots, I developed a novel RT-PCR-based approach for quantitative and specific detection of sgRNAs, which I call DeSCo-PCR (Detection of Smaller Coterminal RNAs by PCR). This is described in detail in *Chapter 2*. To demonstrate the utility of this method, my collaborators and I used a plant virus (RCNMV) and a human virus (ZIKV) to detect their 3'coterminal ncsgRNAs. Compared to northern blots, DeSCo-PCR is simpler, quicker, cost-, and labor-effective (16).

Next, I wanted to assess the effect(s) of plant viral ncsgRNAs in infected plants using SR1f of RCNMV as a model *(Chapter 3)*. To do that, I used wt RCNMV, which generates SR1f in infected cells, and mutant RCNMVΔSR1f, which does not generate SR1f. I showed that SR1f is not required for RCNMV replication or systemic movement in *N. benthamiana*, which is consistent with the previous report (66), but the absence of SR1f results in reduced viral RNA accumulation and symptom severity. In wt Arabidopsis plants, only wt RCNMV replication was detected even though it did not produce any symptoms. In transgenic Arabidopsis plants, which were knocked-out in antiviral RNA silencing machinery, only wt RCNMV replication was detected with severely symptomatic plants, consistently and reproducibly. Because knocking-out the antiviral silencing machinery did not rescue the replication of RCNMVΔSR1f, I concluded that the primary function of SR1f is something other than the suppression of RNA silencing. I also show that Arabidopsis 5'→ 3' exoribonuclease, XRN4, which is widely assumed to be responsible for generating plant viral ncsgRNAs, is not required for the generation of SR1f. Additionally, I conducted a comparative transcriptomic analysis of wt RCNMV- and

RCNMVΔSR1f- infected *N. benthamiana* to assess the effects of virus infection with or without SR1f. More details about the experiments, results, possible functions of SR1f, and the limitations of our study are discussed in *Chapter 3*.

Furthermore, I was also interested in understanding how plant virus infection affects the host and viral gene expression in RCNMV-infected Arabidopsis, both by transcriptional and translational regulation, on a genome-wide scale. The importance of studying translational control of gene expression and the technique used, called ribosome profiling, are discussed below.

Translational regulation of gene expression

Translation refers to the process of protein synthesis programmed by the sequence information encoded in the mRNA. The process of translation can be broadly divided into four stages (89–91): (i) Translation initiation includes recruitment of the 40S ribosomal subunit and the initiator methionyl transfer RNA (Met-tRNA$_i^{Met}$) to the 5' end of a capped mRNA with the help of several eukaryotic translation initiation factors (eIFs), scanning of the 5' leader sequence of an mRNA by the 40S ribosomal subunit in association with eIFs until it encounters the start codon of an ORF, and the subsequent association of 60S ribosomal subunit to the 40S subunit, with the release of eIFs, for the formation of 80S ribosomes with Met-tRNA$_i^{Met}$ in the ribosomal P-site, (ii) translation elongation includes the synthesis of polypeptide chain by ribosomal translocation from one codon (3 nt) to the next, with aminoacylated tRNAs bringing the amino acids to the ribosomes where peptidyl transferase activity of ribosomes synthesize the polypeptide chains with the help of eukaryotic elongation factors (eEFs), (iii) translation termination that occurs when ribosomes encounter the stop codon of an ORF where eukaryotic release factors (eRFs) enable the release of the polypeptide chain and dissociation of 80S

ribosomes into subunits, (iv) ribosome recycling includes the use of these ribosomal subunits for subsequent rounds of translation.

The process of translation is faster than the total time taken by transcription, mRNA processing, nuclear export, and translation for synthesis of a protein. Therefore, a translational response is much quicker than the transcriptional control (which includes translation), and in response to any internal or external stimuli, regulating the translation of the required proteins can yield a much faster and finely-tuned response (92). Additionally, translation is a highly energy-intensive process and therefore, needs to be tightly regulated to minimize wasteful expenditure of cellular energy (93–95). Translational control of gene expression has been shown to be important in a variety of cellular, developmental, and neurological processes (96–100). Dysregulated translation has been implicated in a gamut of human diseases (101) including cancer (102, 103) and several neurological disorders (99, 104, 105).

Translational control is important during virus infection as well. Viruses are obligate intracellular parasites that rely completely on the cellular translation machinery for the synthesis of viral proteins. Therefore, host cells can regulate cellular translation to inhibit viral protein synthesis that limits the viral infection and spread (106–108). For example, in vertebrates, the cellular protein kinase R (PKR) gets activated when it senses dsRNA that is produced as replication-intermediates during ssRNA virus replication (109). Subsequently, activated PKR phosphorylates the alpha subunit of the translation initiation factor 2 (eIF2α) resulting in global inhibition of translation initiation, including the translation of viral proteins (110). However, certain cellular antiviral mRNAs and those required for homeostasis can still be translated (111, 112). Even though host cells can regulate translation to limit virus infection, viruses have also evolved counter-strategies to selectively limit the translation of cellular antiviral mRNAs and

preferentially translate viral mRNAs and proviral cellular mRNAs (62, 113–117). For example, (i) Rift Valley fever virus can induce the degradation of PKR, thereby preventing eIF2α phosphorylation and global translation inhibition (118), (ii) polio virus-protease cleaves cellular eIF4Gs, which are essential for cap-dependent translation. This inhibits the translation of the capped cellular mRNAs whereas the uncapped polio virus mRNA is preferentially translated by cap-independent mechanisms via an IRES (119).

In plants, translational regulation has been shown to be important under stressed conditions, including virus infection where translational control can be used either by plants to inhibit virus infection or by viruses to inhibit the translation of cellular antiviral mRNA and preferentially translate viral and proviral cellular mRNAs (17, 120–128). For example, (i) overexpression of sucrose nonfermenting (SNF)-related kinase 1 (SnRK1) in plants has been shown to limit geminivirus infection (129), possibly because of the global translation inhibition via SnRK1-mediated phosphorylation of eIF4E and eIFiso4E (127, 130), (ii) Interaction between a nucleotide-binding-leucine rich receptor (NB-LRR) protein in *N. benthamiana* and a virus elicitor confers virus resistance by Argonaute 4 (AGO4)-dependent selective inhibition of viral mRNA translation (131), (iii) Cauliflower mosaic virus (CaMV)-encoded transactivator protein (TAV) not only promotes reinitiation of downstream ORFs in the polycistronic mRNAs but it also binds to cellular eIF3 and ribosomal protein L24 to promote viral mRNA translation (132). Even though translation is a highly conserved process among eukaryotes (133), there are certain unique aspects of translational control in plants that have been extensively reviewed before (134, 135). A couple of examples include (i) the existence of multiple isoforms of eIF4E/eIFiso4E and eIF4G/eIFiso4Gs only in plants that have redundant as well as specialized functions (89, 135, 136), (ii) phosphorylation of eIF2α by the only known plant eIF2α kinase, GCN2, does not

necessarily lead to global inhibition of translation (137, 138), unlike mammalian and yeast systems, where eIF2α phosphorylation results in global translation inhibition (139). However, whether eIF2α phosphorylation always results in global inhibition of translation, even in other non-plant eukaryotes, is still debated (140).

Several molecular techniques exist for the assessment of global and specific changes in translation (124, 141–144). Some techniques, such as pulse labeling of translating polypeptides with radioactive amino acid or the non-radioactive puromycin-based SUnSET (surface sensing of translation) assay (145, 146), can directly measure the total amount of newly synthesized proteins per unit time. However, these techniques monitor global change in translation and cannot provide specific gene- or protein-level information. Other proteomics-based methods such as p-SILAC (pulsed- stable isotope labeling of amino acids in culture) (147, 148) and BONCAT (bio-orthogonal non-canonical amino acid tagging) (149) can be also be used for proteome-wide direct quantification of nascent proteins. The proteomic approach assesses the composition of the protein but, owing to the highly variable half-lives of proteins, it cannot be ascertained that the high content of any protein is due to the high stability of the protein or due to increased gene expression (150). Furthermore, if the increased protein content is due to increased gene expression, it cannot be inferred whether the change is due to global change in mRNA abundance or global change in the efficiency of translation of mRNAs, i.e., these techniques do not decipher the translational control. To overcome this, researchers have used various methods to isolate polysomal mRNAs (151) either via polysome profiling (152, 153) or TRAP (translating ribosome affinity purification) followed by RNA quantification methods such as RNA sequencing, microarrays, or qRT-PCR of selected genes (154–157) to assess the extent of ribosome occupancy on the mRNAs as a proxy for translation status. This can be coupled

with RNA sequencing from total RNA to ascertain the changes due to translational control. Simple polysome profiles without any subsequent RNA measurements can also be used to monitor global changes in translation. However, these methods provide low-resolution genome-wide information on translationally regulated genes and cannot distinguish between translating or stalled ribosomes on the mRNA. For example, ribosomes translating the upstream (u)ORFs on an mRNA have been shown to repress the translation of the main ORF (158). Therefore, polysomal mRNAs will include those mRNAs in which ribosomes are present only on the uORFs with no translation occurring from the main ORF but such mRNAs will be incorrectly identified as being translated. A technique that bypasses these limitations to provide high-throughput genome-wide information on translationally-regulated genes with single-codon resolution is ribosome profiling (159).

Ribosome profiling

Since the advent of next generation sequencing (NGS) technology, researchers have been able to investigate an organism's transcriptome and its regulation on a genome-wide scale in a high-throughput manner (160). The majority of the NGS-related studies use RNA-sequencing (RNA-seq) that measures the steady-state RNA abundance for differential gene expression analysis (161). Even though steady-state RNA abundance takes both transcription and RNA decay into account, it is generally assumed that changes in RNA abundance are caused by transcriptional regulation, which is not always true (162, 163). Furthermore, RNA abundance or transcription is used as a proxy for protein abundance but this proxy may be inaccurate because protein abundance can also be regulated post-transcriptionally at the level of translation. In fact, previous reports have shown that compared to RNA abundance, the translation rate is a better predictor of protein abundance (148, 164–172).

The translation rate is determined by the translation initiation step, which regulates how many ribosomes are translating (ribosome occupancy) any given mRNA. Although translation rate can be regulated at any stage of the translation process, translation initiation is considered to be the main step that regulates translation rate as it is the slowest step compared to translation elongation, termination, and ribosome recycling (124, 173). Therefore, ribosome occupancy (other related terms include ribosome density or translation efficiency) can be used to assess the translation rate of any mRNA. A simplistic illustration of how the interplay between RNA abundance and ribosome occupancy determines the overall control of gene expression (protein synthesis) is described as follows *(Fig. 1.4)*: (i) Change in mRNA levels with the same number of ribosomes per mRNA would yield only transcription control, (ii) change in the number of ribosomes per mRNA without any change in mRNA levels yield translational control, and (iii) changes in both the mRNA levels and the number of ribosomes per mRNA yield transcriptional and translational control of gene expression.

To assess the genome-wide translational control with a single-nucleotide resolution, an NGS-based technique, called ribosome profiling, emerged in 2009 (166). Ribosome profiling (Ribo-seq) is a modified RNA-seq-based technique for genome-wide measurement of translation. Instead of estimating the number of fragments of total RNA via RNA-seq, Ribo-seq estimates only the number of fragments/mRNA regions that were occupied by the translating ribosomes. The basis for this technique originated over 50 years ago in which a report showed that eukaryotic ribosomes protect a discrete length of mRNA region from ribonuclease digestion and this can be used to precisely map the positions of the ribosomes on an mRNA (174, 175). In 2009, Nicholas Ingolia and colleagues in Jonathan Weissman's lab developed Ribo-seq by deep sequencing these ribosome-protected fragments (166).

Ribo-seq can provide a panorama of the whole translation process (150, 159, 176–182). Depending on the research objectives, translation initiation inhibitors, such as harringtonine (183) or lactimidomycin (184), and translation elongation inhibitors, such as cycloheximide (166) or emetine (183), can be used individually or in combination to arrest translating ribosomes on mRNAs. Some of the aspects of translation that can be characterized using Ribo-seq include, but are not limited to, identification of novel AUG-initiated ORFs, overlapping ORFs, uORFs, small (s)ORFs, ORFs with a non-AUG start codon (166, 185–191) and unexpected translation from RNAs that were previously annotated as noncoding RNAs (192–196). It can also be used to (i) identify ribosomal pause sites that can regulate protein synthesis, co-translational protein folding, and protein localization (197–200), (ii) identify translation recoding events such as programmed ribosomal frameshifting and stop-codon readthrough (201–205), (iii) identify mRNA features that regulate the translation of selective mRNAs in response to a certain stimulus (206–211), and (iv) assess translation elongation kinetics and mechanics (112, 183, 212–215).

Similar to RNA-seq, which can describe the entire transcriptome, Ribo-seq can be used for the characterization of the entire translatome of a tissue or an organism (188, 216–221). Ribo-seq has also been used to explore the canonical and non-canonical mechanisms of viral mRNA translation, explore and study the breadth of virus-encoded peptides or proteins that remained unidentified by other methods (186, 222–228). Conducting Ribo-seq and RNA-seq from the same sample with cycloheximide can be used for genome-wide differential gene expression analysis, both at the level of RNA abundance (transcriptional regulation) and translation efficiency (translational regulation) (17, 121, 234, 235, 166, 208, 225, 229–233).

The general methodology of Ribo-seq for the assessment of differentially translated genes is described as follows *(Fig. 1.5)*. Cells or tissues are lysed in a buffer that can maintain the integrity of polysomes. Most importantly, the buffer contains a translation elongation inhibitor, usually cycloheximide, that freezes the eukaryotic translating ribosomes on the mRNA by halting ribosome translocation. The lysis buffer may also contain chloramphenicol for arresting mitochondrial, chloroplastic, or prokaryotic translation. Following cell lysis, the crude cell lysate is clarified by centrifugation and treated with a sequence-nonspecific endoribonuclease (RNase) (236). The RNase digests the mRNAs except the regions that are protected by the translating 80S ribosomes, yielding monosomes, i.e., mRNA fragments with single ribosome on them. These protected fragments are called ribosome protected fragments (RPFs). The monosomes are pelleted by ultracentrifugation through a sucrose cushion followed by RNA purification. The RPFs of the size 28-34 nt are excised from a denaturing gel following electrophoresis. Subsequently, a DNA library is prepared from the size-selected RPFs via a small RNA library preparation protocol and deep sequenced using an Illumina NGS instrument. For RNA-seq *(Fig. 1.5)*, total RNA is extracted from an aliquot of the same clarified lysate that was used for Ribo-seq, followed by alkaline hydrolysis that results in random fragmentation of the total RNA. The RNA fragments of the size 25-40 nt are excised from a denaturing gel following electrophoresis. Subsequently, a DNA library is prepared from the size-selected RNA via a small RNA library preparation protocol and deep sequenced using an Illumina NGS instrument.

The bioinformatic analysis of Ribo-seq and RNA-seq data starts by assessing the quality of raw data by tools such as FastQC (237), followed by processing via quality- and adapter-trimming by tools such as Cutadapt (238). Subsequently, the processed reads are aligned to the

organism's reference sequences for the ribosomal (r)RNAs, transfer (t)RNAs, and small nucleolar (sno)RNAs by alignment tools such as Bowtie (239, 240). The reads that do not align to the previously-mentioned sequences are subsequently aligned to the reference transcriptome using tools such as Bowtie (239, 240) or to reference genome using splice-aware tools such as STAR (241). These mapped reads can be used for further downstream analysis depending on the research objective. Some of the downstream analyses include P-site identification, determining the hallmark quality characteristics of Ribo-seq data, *de novo* identification of ORFs, and identifying genes that are differentially expressed, both at the level of transcription and translation efficiency. A variety of bioinformatics tools have been developed for analyzing Ribo-seq data (179, 242, 243).

There are specific hallmarks of Ribo-seq data that are absent in RNA-seq data. Because RNA fragments similar to RPF-length can arise from secondary RNA structures and non-polysomal ribonucleoprotein complexes, it is essential to determine if the majority of RPFs are indeed true RPFs and not artifacts. The following hallmarks of true RPFs can be used to assess the quality of Ribo-seq data.

(i) Narrow length distribution: Because ribosomes protect a specific number of nucleotides from RNAse digestion, depending on the organism and RNase digestion conditions, the length distribution of high-quality Ribo-seq data is enriched at a single or only a few RPF length(s) *(Fig. 1.6-A)*. In contrast, RNA-seq data gives a broad read-length distribution *(Fig. 1.6-B)*. It has been shown that a narrow length-distribution of RPFs with the specific RPF length usually yields good triplet periodicity (explained below). For example, Hsu et al. (2016) showed that their narrow length distribution of RPFs in Arabidopsis, with a peak at 28-nt, gave a good triplet periodicity from 28-nt RPFs (188). On the other hand, the RPF length distribution in

Arabidopsis from Liu et al. (2013) (244) and Merchante et al. (2015) (206) was much broader and did not have a peak at 28-nt RPFs but still, the best triplet periodicity was displayed by 28-nt RPFs (188). The following are some of the studies with the RPF length that yields good triplet periodicity: 28/29-nt RPFs in Arabidopsis (188, 209) *(our data in Chapter 4, Fig. 4.3-A),* tomato (218), rice (219, 245), yeast (166) and 29-31 nt RPFs in maize (17, 220).

(ii) CDS enrichment: Because Ribo-seq captures RPFs only from the 80S translating ribosomes, it is expected that when these RPFs are mapped to the reference transcriptome, the majority of the reads will map back to the coding DNA sequence (CDS) and very few reads will map to the untranslated regions (UTRs) of an mRNA *(Fig. 1.6-C).* In contrast, RNA-seq data is obtained from random fragmentation of total RNA and therefore, would include a substantial proportion of reads that map to the UTRs as well *(Fig. 1.6-D).*

(iii) Triplet periodicity: If any specific nucleotide (let's say the first nucleotide) of an RPF is mapped to the reference transcriptome, it would correspond to a certain reading frame, which is described here as frame 0, 1, or 2, according to the nucleotide position relative to the start codon *(Fig. 1.6-E).* During translation elongation, because ribosomes pause at each codon (3 nt) after translocation, we would get more reads at every third nucleotide, i.e., at a specific reading frame *(Fig. 1.6-E).* This 3-nt phasing of Ribo-seq data is called triplet periodicity. In contrast, because RNA-seq data is obtained from random fragmentation of total RNA, we do not expect to see any triplet periodicity *(Fig. 1.6-F).* In addition, CDS enrichment in Ribo-seq data and lack thereof in RNA-seq data can be observed in the same triplet periodicity plot, also called metagene analysis *(Fig. 1.6-E, F).* Another way to assess Ribo-seq data quality is to determine triplet periodicity over CDS and UTRs separately *(Fig. 1.6-G, H).* Only the Ribo-seq reads mapping only to the CDS (true RPFs) would show triplet periodicity *(Fig. 1.6-G).* In contrast,

Ribo-seq reads mapping to UTRs and RNA-seq reads mapping either to CDS or UTRs would not show triplet periodicity *(Fig. 1.6-G, H)*.

The rationale behind Ribo-seq is based on the fact that an mRNA that is translated efficiently will have more ribosomes initiating translation, which will yield more RPFs, than an inefficiently translated mRNA. RPFs represent the translated mRNA and its abundance is proportional to mRNA abundance and the rate of translation initiation on that mRNA. To uncouple both of these effects, translation efficiency (TE) is estimated to assess the translational control of gene expression. TE is calculated as the ratio of RPF abundance to RNA abundance and represents how well an mRNA is being translated. RNA abundance from RNA-seq can be used to measure how transcription is regulated, and translation efficiency can be used to study translational control.

In this dissertation, I used Ribo-seq to study the extent of translational regulation of gene expression in Arabidopsis in response to RCNMV infection and explore the translational landscape of RCNMV RNAs during infection *(Chapter 4)*. I collected systemic non-inoculated leaves of RCNMV-infected *dcl2-1/dcl4-2t* Arabidopsis plants at early and late infection stages. I identified the genes that were transcriptionally- and/or translationally-regulated. I found that the early translational response was specific to the plant's defense response against pathogen infection whereas the late translational response included many pathways that were dysregulated as a result of RCNMV infection. I showed that the unfolded protein response was elicited by RCNMV during the late infection stages. My collaborators and I also analyzed the Ribo-seq and RNA-seq reads that mapped to RCNMV. Ribo-seq data clearly demonstrated the translation of RCNMV p88 protein by -1 PRF. We also identified a putative ribosomal pause site in the MP ORF of RCNMV RNA2.

I also used Ribo-seq to study the translational control of gene expression in the roots of maize seedlings during unfolded protein response *(Chapter 5)*.

Unfolded protein response

The correct three-dimensional conformation of proteins is responsible and required for their proper localization and function. After the mRNA recruits the translation machinery and initiates translation, an endoplasmic reticulum (ER)-targeting signal peptide at the N-terminal of the protein is translated first that emerges out of the ribosomes and targets the protein, co- or post-translationally, into the ER lumen (246–248). In the ER lumen, several molecular chaperones and co-chaperones associate with the nascent protein and initiate co-translational protein folding in a step-wise manner via several steps such as cleaving off the signaling peptide, sequential addition and trimming of N-linked glycans, and formation of disulfide bonds (249–258). Once the correct conformation is achieved, the protein is exported out of the ER to the Golgi for further modifications and protein sorting (259–261).

Protein folding is an error-prone process that is easily disturbed by a variety of different biotic and abiotic stressors. Improperly folded proteins are detected via the ER-quality control (ERQC) system and degraded by the ER-associated degradation (ERAD) system (262–265). However, aggregation of misfolded proteins faster than their refolding or degradation results in an increased accumulation of misfolded proteins in the ER triggering ER-stress (266–268). ER-stress can potentially be toxic to the cell and therefore, in response, the cell elicits an adaptive response, called unfolded protein response (UPR) that aims to increase the folding capacity of the ER (266, 269–273). In humans, the accumulation of misfolded proteins and dysregulated UPR have been shown to be responsible for many diseases (274–277), including neurodegenerative diseases such as Alzheimer's and Parkinson's disease (278–280). In plants,

biotic stress such as pathogen infection, pest infestations, and abiotic stress such as high temperature, drought, and salinity can trigger ER-stress (264). An important point to note is that several stressors that do not disrupt protein folding can also elicit the UPR (281). In addition to the UPR elicited by the stressors, UPR is also involved in normal plant vegetative and reproductive development (282). Elicitation of UPR can serve to limit pathogen infection but can also be exploited by pathogens, mainly by viruses, to exploit UPR as a proviral process (282).

Even though UPR is a highly conserved process among eukaryotes, there are certain features that differ between plant and mammalian systems. There are three arms of the mammalian UPR signaling pathway, two of which are present in plants as well *(discussed further in Chapter 5)* (267, 270). The third arm of the pathway that is not present in plants involves protein kinase RNA-like ER kinase (PERK). In mammalian cells, PERK-dependent inhibition of global translation via eIF2α phosphorylation is observed during UPR (283). This serves to reduce the protein folding load on the ER. Because plants lack any known PERK homolog, it needs to be determined if there is a global inhibition of translation during UPR in plants and if there is, what is the mechanism?

For studying UPR in a plant system, we induced persistent ER-stress in maize seedling by tunicamycin (Tm) treatment (284) followed by ribosome profiling of the roots at 0, 6, and 12 hours post Tm-treatment *(Chapter 5)*. We found that Tm-treatment resulted in bzip60 splicing, a marker of UPR. However, unlike mammalian systems, we did not detect any global translation inhibition. Instead, we determined that the translation efficiencies of several mRNAs, including UPR-responsive genes, were modestly decreased. Furthermore, we found that the reduction in translation efficiency was not due to reduced ribosome loading (or reduced translation) but

instead, was due to increased transcription of UPR-responsive genes without the concomitant increase in ribosomes on those mRNAs. Most of those mRNAs became sequestered in stress granules (SGs). Therefore, the calculated translation efficiency (RPF abundance to RNA abundance ratio) decreased because of the increase in the abundance of mRNAs that were not being translated. We proposed a model in which UPR leads to the increased transcriptional upregulation of UPR genes from which only a subpopulation of mRNA molecules is translated while the rest are temporarily sequestered in SGs. As and when required, the cell can release those mRNA molecules from the SG for translation. This strategy ensures a low protein-folding load on the ER and a quick fine-tuned response according to the cellular needs while conserving energy.

Summary

My doctoral research is divided into four separate projects as follows: (i) A rapid and simple quantitative method for specific detection of smaller coterminal RNA by PCR (DeSCo-PCR): Application to the detection of viral subgenomic RNAs *(Chapter 2 published in ref. 16).* (ii) Effects of the noncoding subgenomic RNA of red clover necrotic mosaic virus in virus infection *(Chapter 3, manuscript under review).* (iii) Translational regulation of gene expression in Arabidopsis in response to virus infection *(Chapter 4, manuscript in preparation).* (iv) Control of translation during the unfolded protein response in maize seedlings: life without PERKs *(Chapter 5 published in ref. 17).*

References

1. Khan KS, Mamun MA, Griffiths MD, Ullah I. 2020. The Mental Health Impact of the COVID-19 Pandemic Across Different Cohorts. Int J Ment Health Addict 1–7.

2. Boden M, Zimmerman L, Azevedo KJ, Ruzek JI, Gala S, Abdel Magid HS, Cohen N, Walser R, Mahtani ND, Hoggatt KJ, McLean CP. 2021. Addressing the mental health impact of COVID-19 through population health. Clin Psychol Rev 85: 102006.

3. Kola L, Kohrt BA, Hanlon C, Naslund JA, Sikander S, Balaji M, Benjet C, Cheung EYL, Eaton J, Gonsalves P, Hailemariam M, Luitel NP, Machado DB, Misganaw E, Omigbodun O, Roberts T, Salisbury TT, Shidhaye R, Sunkel C, Ugo V, van Rensburg AJ, Gureje O, Pathare S, Saxena S, Thornicroft G, Patel V. 2021. COVID-19 mental health impact and responses in low-income and middle-income countries: reimagining global mental health. The Lancet Psychiatry 8: 535–550.

4. Narici M, Vito G De, Franchi M, Paoli A, Moro T, Marcolin G, Grassi B, Baldassarre G, Zuccarelli L, Biolo G, di Girolamo FG, Fiotti N, Dela F, Greenhaff P, Maganaris C. 2021. Impact of sedentarism due to the COVID-19 home confinement on neuromuscular, cardiovascular and metabolic health: Physiological and pathophysiological implications and recommendations for physical and nutritional countermeasures. Eur J Sport Sci 21: 614–635.

5. Griffiths D, Sheehan L, van Vreden C, Petrie D, Grant G, Whiteford P, Sim MR, Collie A. 2021. The Impact of Work Loss on Mental and Physical Health During the COVID-19 Pandemic: Baseline Findings from a Prospective Cohort Study. J Occup Rehabil 31: 455–462.

6. Chowdhury EK, Khan II, Dhar BK. 2021. Catastrophic impact of Covid-19 on the global stock markets and economic activities. Bus Soc Rev basr.12219.

7. Jena PR, Majhi R, Kalli R, Managi S, Majhi B. 2021. Impact of COVID-19 on GDP of major economies: Application of the artificial neural network forecaster. Econ Anal Policy 69: 324–339.

8. He S, Creasey Krainer KM. 2020. Pandemics of People and Plants: Which Is the Greater Threat to Food Security? Mol Plant 13: 933–934.

9. Savary S, Willocquet L, Pethybridge SJ, Esker P, McRoberts N, Nelson A. 2019. The global burden of pathogens and pests on major food crops. Nat Ecol Evol 3: 430–439.

10. Jones RAC. 2021. Global Plant Virus Disease Pandemics and Epidemics. Plants (Basel) 10: 233.

11. Sastry KS, Zitter TA. 2014. Management of Virus and Viroid Diseases of Crops in the Tropics, p. 149–480. In Sastry, KS, Zitter, TA (eds.), Plant Virus and Viroid Diseases in the Tropics Vol. 2, Epidemiology and Management. Springer Netherlands, Dordrecht.

12. Nicaise V. 2014. Crop immunity against viruses: outcomes and future challenges. Front Plant Sci 5: 660.

13. Patil BL. 2021. Plant Viral Diseases: Economic Implications, p. 81–97. In Bamford, DH, Zuckerman, M (eds.), Encyclopedia of Virology 4th edition. Academic Press UK, Oxford.

14. Deressa T, Demissie G. 2017. Maize Lethal Necrosis Disease (MLND)-A Review. Journal of Natural Sciences Research 7: 38-42.

15. Rishi N. 2009. Significant plant virus diseases in India and a glimpse of modern disease management technology. J Gen Plant Pathol 75: 1–18.

16. Kanodia P, Prasanth KR, Roa-Linares VC, Bradrick SS, Garcia-Blanco MA, Miller WA. 2020. A rapid and simple quantitative method for specific detection of smaller coterminal RNA by PCR (DeSCo-PCR): application to the detection of viral subgenomic RNAs. RNA 26: 888–901.

17. Kanodia P, Vijayapalani P, Srivastava R, Bi R, Liu P, Miller WA, Howell SH. 2020. Control of translation during the unfolded protein response in maize seedlings: Life without PERKs. Plant Direct 4: e00241.

18. Sherman MB, Guenther RH, Tama F, Sit TL, Brooks CL, Mikhailov AM, Orlova EV, Baker TS, Lommel SA. 2006. Removal of Divalent Cations Induces Structural Transitions in Red Clover Necrotic Mosaic Virus, Revealing a Potential Mechanism for RNA Release. J Virol 80: 10395–10406.

19. Martin SL, Guenther RH, Sit TL, Swartz PD, Meilleur F, Lommel SA, Rose RB. 2010. Crystallization and preliminary X-ray diffraction analysis of red clover necrotic mosaic virus. Acta Crystallogr Sect F Struct Biol Cryst Commun 66: 1458–1462.

20. Gould AR, Francki RIB, Hatta T, Hollings M. 1981. The bipartite genome of red clover necrotic mosaic virus. Virology 108: 499–506.

21. Hiruki C. 1987. The Dianthoviruses: A Distinct Group of Isometric Plant Viruses with Bipartite Genome. Adv Virus Res 33: 257-300.

22. Okuno T, Hiruki C. 2013. Molecular Biology and Epidemiology of Dianthoviruses. Adv Virus Res 87: 37-74.

23. Xiong Z, Lommel SA. 1989. The complete nucleotide sequence and genome organization of red clover necrotic mosaic virus RNA-1. Virology 171: 543–554.

24. Koonin EV. 1991. The phylogeny of RNA-dependent RNA polymerases of positive-strand RNA viruses. J Gen Virol 72: 2197–2206.

25. Kim KH, Lommel SA. 1994. Identification and Analysis of the Site of -1 Ribosomal Frameshifting in Red Clover Necrotic Mosaic Virus. Virology 200: 574–582.

26. Kim KH, Lommel SA. 1998. Sequence Element Required for Efficient −1 Ribosomal Frameshifting in Red Clover Necrotic Mosaic Dianthovirus. Virology 250: 50–59.

27. Turner KA, Sit TL, Callaway AS, Allen NS, Lommel SA. 2004. Red clover necrotic mosaic virus replication proteins accumulate at the endoplasmic reticulum. Virology 320: 276–290.

28. Mine A, Takeda A, Taniguchi T, Taniguchi H, Kaido M, Mise K, Okuno T. 2010. Identification and Characterization of the 480-Kilodalton Template-Specific RNA-Dependent RNA Polymerase Complex of Red Clover Necrotic Mosaic Virus. J Virol 84: 6070–6081.

29. Kusumanegara K, Mine A, Hyodo K, Kaido M, Mise K, Okuno T. 2012. Identification of domains in p27 auxiliary replicase protein essential for its association with the endoplasmic reticulum membranes in Red clover necrotic mosaic virus. Virology 433: 131–141.

30. Mine A, Hyodo K, Tajima Y, Kusumanegara K, Taniguchi T, Kaido M, Mise K, Taniguchi H, Okuno T. 2012. Differential Roles of Hsp70 and Hsp90 in the Assembly of the Replicase Complex of a Positive-Strand RNA Plant Virus. J Virol 86: 12091–12104.

31. Takeda A, Tsukuda M, Mizumoto H, Okamoto K, Kaido M, Mise K, Okuno T. 2005. A plant RNA virus suppresses RNA silencing through viral RNA replication. EMBO J 24: 3147–3157.

32. Mine A, Hyodo K, Takeda A, Kaido M, Mise K, Okuno T. 2010. Interactions between p27 and p88 replicase proteins of Red clover necrotic mosaic virus play an essential role in viral RNA replication and suppression of RNA silencing via the 480-kDa viral replicase complex assembly. Virology 407: 213–224.

33. Zavriev SK, Hickey CM, Lommel SA. 1996. Mapping of the Red Clover Necrotic Mosaic Virus Subgenomic RNA. Virology 216: 407–410.

34. Sit TL, Vaewhongs AA, Lommel SA. 1998. RNA-mediated trans-activation of transcription from a viral RNA. Science 281: 829–32.

35. Xiong Z, Kim KH, Giesman-Cookmeyer D, Lommel SA. 1993. The Roles of the Red Clover Necrotic Mosaic Virus Capsid and Cell-to-Cell Movement Proteins in Systemic Infection. Virology 192: 27–32.

36. Lommel SA, Weston-Fina M, Xiong Z, Lomonossoff GP. 1988. The nucleotide sequence and gene organization of red clover necrotic mosaic virus RNA-2. Nucleic Acids Res 16: 8587–8602.

37. Powers JG, Sit TL, Heinsohn C, George CG, Kim KH, Lommel SA. 2008. The Red clover necrotic mosaic virus RNA-2 encoded movement protein is a second suppressor of RNA silencing. Virology 381: 277–286.

38. Xiong Z, Lommel SA. 1991. Red clover necrotic mosaic virus infectious transcripts synthesized *in vitro*. Virology 182: 388–392.

39. Mizumoto H, Tatsuta M, Kaido M, Mise K, Okuno T. 2003. Cap-Independent Translational Enhancement by the 3′ Untranslated Region of Red Clover Necrotic Mosaic Virus RNA1. J Virol 77: 12113–12121.

40. Simon AE, Miller WA. 2013. 3′ Cap-Independent Translation Enhancers of Plant Viruses. Annu Rev Microbiol 67: 21–42.

41. Truniger V, Miras M, Aranda MA. 2017. Structural and Functional Diversity of Plant Virus 3′-Cap-Independent Translation Enhancers (3′-CITEs). Front Plant Sci 8: 2047.

42. Treder K, Pettit Kneller EL, Allen EM, Wang Z, Browning KS, Miller WA. 2007. The 3' cap-independent translation element of Barley yellow dwarf virus binds eIF4F via the eIF4G subunit to initiate translation. RNA 14: 134–147.

43. Kraft JJ, Treder K, Peterson MS, Miller WA. 2013. Cation-dependent folding of 3′ cap-independent translation elements facilitates interaction of a 17-nucleotide conserved sequence with eIF4G. Nucleic Acids Res 41: 3398–3413.

44. Sharma S Das, Kraft JJ, Miller WA, Goss DJ. 2015. Recruitment of the 40S Ribosome Subunit to the 3′-Untranslated Region (UTR) of a Viral mRNA, via the eIF4 Complex, Facilitates Cap-independent Translation. J Biol Chem 290: 11268–11281.

45. Zhao P, Liu Q, Miller WA, Goss DJ. 2017. Eukaryotic translation initiation factor 4G (eIF4G) coordinates interactions with eIF4A, eIF4B, and eIF4E in binding and translation of the barley yellow dwarf virus 3′ cap-independent translation element (BTE). J Biol Chem 292: 5921–5931.

46. Mizumoto H, Iwakawa H, Kaido M, Mise K, Okuno T. 2006. Cap-Independent Translation Mechanism of Red Clover Necrotic Mosaic Virus RNA2 Differs from That of RNA1 and Is Linked to RNA Replication. J Virol 80: 3781–3791.

47. Miller WA, Koev G. 2000. Synthesis of Subgenomic RNAs by Positive-Strand RNA Viruses. Virology 273: 1–8.

48. Sztuba-Solińska J, Stollar V, Bujarski JJ. 2011. Subgenomic messenger RNAs: Mastering regulation of (+)-strand RNA virus life cycle. Virology 412: 245–255.

49. Chapman EG, Moon SL, Wilusz J, Kieft JS. 2014. RNA structures that resist degradation by Xrn1 produce a pathogenic Dengue virus RNA. Elife 3: e01892.

50. Akiyama BM, Laurence HM, Massey AR, Costantino DA, Xie X, Yang Y, Shi PY, Nix JC, Beckham JD, Kieft JS. 2016. Zika virus produces noncoding RNAs using a multi-pseudoknot structure that confounds a cellular exonuclease. Science 354: 1148–1152.

51. Strauss JH, Strauss EG. 1994. The alphaviruses: gene expression, replication, and evolution. Microbiol Rev 58: 491–562.

52. Hussain S, Pan J, Chen Y, Yang Y, Xu J, Peng Y, Wu Y, Li Z, Zhu Y, Tien P, Guo D. 2005. Identification of Novel Subgenomic RNAs and Noncanonical Transcription Initiation Signals of Severe Acute Respiratory Syndrome Coronavirus. J Virol 79: 5288–5295.

53. Wang D, Jiang A, Feng J, Li G, Guo D, Sajid M, Wu K, Zhang Q, Ponty Y, Will S, Liu F, Yu X, Li S, Liu Q, Yang XL, Guo M, Li X, Chen M, Shi ZL, Lan K, Chen Y, Zhou Y. 2021. The SARS-CoV-2 subgenome landscape and its novel regulatory features. Mol Cell 81: 2135-2147.e5.

54. Koev G, Miller WA. 2000. A Positive-Strand RNA Virus with Three Very Different Subgenomic RNA Promoters. J Virol 74: 5988–5996.

55. Lommel SA, Kendall TL, Xiong Z, Nutter RC. 1991. Identification of the Maize chlorotic mottle virus capsid protein cistron and characterization of its subgenomic messenger RNA. Virology 181: 382–385.

56. Dever TE, Green R. 2012. The Elongation, Termination, and Recycling Phases of Translation in Eukaryotes. Cold Spring Harb Perspect Biol 4: a013706.

57. Nürenberg E, Tampé R. 2013. Tying up loose ends: ribosome recycling in eukaryotes and archaea. Trends Biochem Sci 38: 64–74.

58. Guenther RH, Sit TL, Gracz HS, Dolan MA, Townsend HL, Liu G, Newman WH, Agris PF, Lommel SA. 2004. Structural characterization of an intermolecular RNA-RNA interaction involved in the transcription regulation element of a bipartite plant virus. Nucleic Acids Res 32: 2819–2828.

59. Firth AE, Brierley I. 2012. Non-canonical translation in RNA viruses. J Gen Virol 93: 1385–1409.

60. Miras M, Miller WA, Truniger V, Aranda MA. 2017. Non-canonical Translation in Plant RNA Viruses. Front Plant Sci 8.

61. Pooggin MM, Ryabova LA. 2018. Ribosome Shunting, Polycistronic Translation, and Evasion of Antiviral Defenses in Plant Pararetroviruses and Beyond. Front Microbiol 9: 644.

62. Jaafar ZA, Kieft JS. 2019. Viral RNA structure-based strategies to manipulate translation. Nat Rev Microbiol 17: 110–123.

63. Martinez-Salas E, Francisco-Velilla R, Fernandez-Chamorro J, Embarek AM. 2018. Insights into Structural and Mechanistic Features of Viral IRES Elements. Front Microbiol 8: 2629.

64. Ryabova L, Park HS, Hohn T. 2004. Control of translation reinitiation on the cauliflower mosaic virus (CaMV) polycistronic RNA. Biochem Soc Trans 32: 592–596.

65. Powell ML, Brown TDK, Brierley I. 2008. Translational termination–re-initiation in viral systems. Biochem Soc Trans 36: 717–722.

66. Iwakawa H, Mizumoto H, Nagano H, Imoto Y, Takigawa K, Sarawaneeyaruk S, Kaido M, Mise K, Okuno T. 2008. A Viral Noncoding RNA Generated by cis -Element-Mediated Protection against 5′→3′ RNA Decay Represses both Cap-Independent and Cap-Dependent Translation. J Virol 82: 10162–10174.

67. Pijlman GP, Funk A, Kondratieva N, Leung J, Torres S, van der Aa L, Liu WJ, Palmenberg AC, Shi PY, Hall RA, Khromykh AA. 2008. A Highly Structured, Nuclease-Resistant, Noncoding RNA Produced by Flaviviruses Is Required for Pathogenicity. Cell Host Microbe 4: 579–591.

68. Silva PAGC, Pereira CF, Dalebout TJ, Spaan WJM, Bredenbeek PJ. 2010. An RNA Pseudoknot Is Required for Production of Yellow Fever Virus Subgenomic RNA by the Host Nuclease XRN1. J Virol 84: 11395–11406.

69. Peltier C, Klein E, Hleibieh K, D'Alonzo M, Hammann P, Bouzoubaa S, Ratti C, Gilmer D. 2012. Beet necrotic yellow vein virus subgenomic RNA3 is a cleavage product leading to stable non-coding RNA required for long-distance movement. J Gen Virol 93: 1093–1102.

70. Flobinus A, Chevigny N, Charley PA, Seissler T, Klein E, Bleykasten-Grosshans C, Ratti C, Bouzoubaa S, Wilusz J, Gilmer D. 2018. Beet necrotic yellow vein virus noncoding rna production depends on a 5 ′ →3 ′ xrn exoribonuclease activity. Viruses 10: 137.

71. Steckelberg AL, Akiyama BM, Costantino DA, Sit TL, Nix JC, Kieft JS. 2018. A folded viral noncoding RNA blocks host cell exoribonucleases through a conformationally dynamic RNA structure. Proc Natl Acad Sci 115: 6404–6409.

72. Steckelberg AL, Vicens Q, Kieft JS. 2018. Exoribonuclease-Resistant RNAs Exist within both Coding and Noncoding Subgenomic RNAs. MBio 9: e02461-18.

73. Gunawardene CD, Newburn LR, White KA. 2019. A 212-nt long RNA structure in the Tobacco necrosis virus-D RNA genome is resistant to Xrn degradation. Nucleic Acids Res 47: 9329–9342.

74. Ilyas M, Du Z, Simon AE. 2021. Opium Poppy Mosaic Virus Has an Xrn-Resistant, Translated Subgenomic RNA and a BTE 3′ CITE. J Virol 95: e02109-20.

75. Slonchak A, Khromykh AA. 2018. Subgenomic flaviviral RNAs: What do we know after the first decade of research. Antiviral Res 159: 13–25.

76. Szucs MJ, Nichols PJ, Jones RA, Vicens Q, Kieft JS. 2020. A New Subclass of Exoribonuclease-Resistant RNA Found in Multiple Genera of *Flaviviridae*. MBio 11: 1–15.

77. Steckelberg AL, Vicens Q, Costantino DA, Nix JC, Kieft JS. 2020. The crystal structure of a Polerovirus exoribonuclease-resistant RNA shows how diverse sequences are integrated into a conserved fold. RNA 26: 1767–1776.

78. Moon SL, Anderson JR, Kumagai Y, Wilusz CJ, Akira S, Khromykh AA, Wilusz J. 2012. A noncoding RNA produced by arthropod-borne flaviviruses inhibits the cellular exoribonuclease XRN1 and alters host mRNA stability. RNA 18: 2029–2040.

79. Schnettler E, Sterken MG, Leung JY, Metz SW, Geertsema C, Goldbach RW, Vlak JM, Kohl A, Khromykh AA, Pijlman GP. 2012. Noncoding Flavivirus RNA Displays RNA Interference Suppressor Activity in Insect and Mammalian Cells. J Virol 86: 13486–13500.

80. Bidet K, Garcia-Blanco MA. 2014. Flaviviral RNAs: weapons and targets in the war between virus and host. Biochem J 462: 215–230.

81. Roby JA, Pijlman GP, Wilusz J, Khromykh AA. 2014. Noncoding subgenomic flavivirus RNA: multiple functions in West Nile virus pathogenesis and modulation of host responses. Viruses 6: 404–27.

82. Bidet K, Dadlani D, Garcia-Blanco MA. 2014. G3BP1, G3BP2 and CAPRIN1 Are Required for Translation of Interferon Stimulated mRNAs and Are Targeted by a Dengue Virus Non-coding RNA. PLoS Pathog 10: e1004242.

83. Moon SL, Dodd BJT, Brackney DE, Wilusz CJ, Ebel GD, Wilusz J. 2015. Flavivirus sfRNA suppresses antiviral RNA interference in cultured cells and mosquitoes and directly interacts with the RNAi machinery. Virology 485: 322–329.

84. Donald CL, Brennan B, Cumberworth SL, Rezelj V V., Clark JJ, Cordeiro MT, Freitas de Oliveira França R, Pena LJ, Wilkie GS, Da Silva Filipe A, Davis C, Hughes J, Varjak M, Selinger M, Zuvanov L, Owsianka AM, Patel AH, McLauchlan J, Lindenbach BD, Fall G, Sall AA, Biek R, Rehwinkel J, Schnettler E, Kohl A. 2016. Full Genome Sequence and sfRNA Interferon Antagonist Activity of Zika Virus from Recife, Brazil. PLoS Negl Trop Dis 10: e0005048.

85. Michalski D, Ontiveros JG, Russo J, Charley PA, Anderson JR, Heck AM, Geiss BJ, Wilusz J. 2019. Zika virus noncoding sfRNAs sequester multiple host-derived RNA-binding proteins and modulate mRNA decay and splicing during infection. J Biol Chem 294: 16282–16296.

86. Flobinus A, Hleibieh K, Klein E, Ratti C, Bouzoubaa S, Gilmer D. 2016. A Viral Noncoding RNA Complements a Weakened Viral RNA Silencing Suppressor and Promotes Efficient Systemic Host Infection. Viruses 8: 272.

87. Kessler C, Holtke HJ, Seibl R, Burg J, Muhlegger K. 1990. Non-radioactive Labeling and Detection of Nucleic Acids. I. A Novel DNA Labeling and Detection System Based on Digoxigenin: Anti-Digoxigenin ELISA Principle (Digoxigenin System). Biol Chem Hoppe Seyler 371: 917–927.

88. Amiss T, Presnell SC. 2006. Nucleic Acid Blotting Techniques, p. 31–46. In Coleman, WB, Tsongalis, GJ (eds.), Molecular Diagnostics. Humana Press, Totowa, NJ.

89. Browning KS, Bailey-Serres J. 2015. Mechanism of Cytoplasmic mRNA Translation. Arabidopsis Book 13: e0176.

90. Schuller AP, Green R. 2018. Roadblocks and resolutions in eukaryotic translation. Nat Rev Mol Cell Biol 19: 526–541.

91. Merrick WC, Pavitt GD. 2018. Protein Synthesis Initiation in Eukaryotic Cells. Cold Spring Harb Perspect Biol 10: a033092.

92. Sonenberg N, Hinnebusch AG. 2009. Regulation of Translation Initiation in Eukaryotes: Mechanisms and Biological Targets. Cell 136: 731–745.

93. Buttgereit F, Brand MD. 1995. A hierarchy of ATP-consuming processes in mammalian cells. Biochem J 312: 163–167.

94. Hershey JWB, Sonenberg N, Mathews MB. 2019. Principles of Translational Control. Cold Spring Harb Perspect Biol 11: a032607.

95. Gabut M, Bourdelais F, Durand S. 2020. Ribosome and Translational Control in Stem Cells. Cells 9: 497.

96. Sonenberg N, Hinnebusch AG. 2007. New Modes of Translational Control in Development, Behavior, and Disease. Mol Cell 28: 721–729.

97. Kong J, Lasko P. 2012. Translational control in cellular and developmental processes. Nat Rev Genet 13: 383–394.

98. Teixeira FK, Lehmann R. 2019. Translational Control during Developmental Transitions. Cold Spring Harb Perspect Biol 11: a032987.

99. Sossin WS, Costa-Mattioli M. 2019. Translational Control in the Brain in Health and Disease. Cold Spring Harb Perspect Biol 11: a032912.

100. Park Y, Page N, Salamon I, Li D, Rasin MR. 2021. Making sense of mRNA landscapes: Translation control in neurodevelopment. WIREs RNA e1674.

101. Tahmasebi S, Khoutorsky A, Mathews MB, Sonenberg N. 2018. Translation deregulation in human disease. Nat Rev Mol Cell Biol 19: 791–807.

102. Truitt ML, Ruggero D. 2016. New frontiers in translational control of the cancer genome. Nat Rev Cancer 16: 288–304.

103. Robichaud N, Sonenberg N, Ruggero D, Schneider RJ. 2019. Translational Control in Cancer. Cold Spring Harb Perspect Biol 11: a032896.

104. Smith M. 2020. MRNA Transcription, Translation, and Defects in Developmental Cognitive and Behavioral Disorders. Front Mol Biosci 7: 240.

105. Lin JQ, van Tartwijk FW, Holt CE. 2021. Axonal mRNA translation in neurological disorders. RNA Biol 18: 936–961.

106. Hoang HD, Graber TE, Alain T. 2018. Battling for Ribosomes: Translational Control at the Forefront of the Antiviral Response. J Mol Biol 430: 1965–1992.

107. Hoang HD, Neault S, Pelin A, Alain T. 2021. Emerging translation strategies during virus–host interaction. WIREs RNA 12: e1619.

108. Liu Y, Wang M, Cheng A, Yang Q, Wu Y, Jia R, Liu M, Zhu D, Chen S, Zhang S, Zhao XX, Huang J, Mao S, Ou X, Gao Q, Wang Y, Xu Z, Chen Z, Zhu L, Luo Q, Liu Y, Yu Y, Zhang L, Tian B, Pan L, Rehman MU, Chen X. 2020. The role of host eIF2α in viral infection. Virol J 17: 112.

109. Lemaire PA, Anderson E, Lary J, Cole JL. 2008. Mechanism of PKR Activation by dsRNA. J Mol Biol 381: 351–360.

110. García MA, Meurs EF, Esteban M. 2007. The dsRNA protein kinase PKR: Virus and cell control. Biochimie 89: 799–811.

111. Lee YY, Cevallos RC, Jan E. 2009. An Upstream Open Reading Frame Regulates Translation of GADD34 during Cellular Stresses That Induce eIF2α Phosphorylation. J Biol Chem 284: 6661–6673.

112. Andreev DE, O'Connor PBF, Fahey C, Kenny EM, Terenin IM, Dmitriev SE, Cormican P, Morris DW, Shatsky IN, Baranov P V. 2015. Translation of 5' leaders is pervasive in genes resistant to eIF2 repression. Elife 4: e03971.

113. Walsh D, Mathews MB, Mohr I. 2013. Tinkering with Translation: Protein Synthesis in Virus-Infected Cells. Cold Spring Harb Perspect Biol 5: a012351–a012351.

114. Jan E, Mohr I, Walsh D. 2016. A Cap-to-Tail Guide to mRNA Translation Strategies in Virus-Infected Cells. Annu Rev Virol 3: 283–307.

115. Cao S, Dhungel P, Yang Z. 2017. Going against the Tide: Selective Cellular Protein Synthesis during Virally Induced Host Shutoff. J Virol 91: e00071-17.

116. Dai A, Cao S, Dhungel P, Luan Y, Liu Y, Xie Z, Yang Z. 2017. Ribosome Profiling Reveals Translational Upregulation of Cellular Oxidative Phosphorylation mRNAs during Vaccinia Virus-Induced Host Shutoff. J Virol 91: e01858-16.

117. Stern-Ginossar N, Thompson SR, Mathews MB, Mohr I. 2019. Translational Control in Virus-Infected Cells. Cold Spring Harb Perspect Biol 11: a033001.

118. Mudhasani R, Tran JP, Retterer C, Kota KP, Whitehouse CA, Bavari S. 2016. Protein Kinase R Degradation Is Essential for Rift Valley Fever Virus Infection and Is Regulated by SKP1-CUL1-F-box (SCF)FBXW11-NSs E3 Ligase. PLoS Pathog 12: e1005437.

119. Kempf BJ, Barton DJ. 2008. Poliovirus 2A Pro Increases Viral mRNA and Polysome Stability Coordinately in Time with Cleavage of eIF4G. J Virol 82: 5847–5859.

120. Muñoz A, Castellano MM. 2012. Regulation of Translation Initiation under Abiotic Stress Conditions in Plants: Is It a Conserved or Not so Conserved Process among Eukaryotes? Comp Funct Genomics 2012: 406357.

121. Juntawong P, Girke T, Bazin J, Bailey-Serres J. 2014. Translational dynamics revealed by genome-wide profiling of ribosome footprints in Arabidopsis. Proc Natl Acad Sci 111: E203–E212.

122. Lei L, Shi J, Chen J, Zhang M, Sun S, Xie S, Li X, Zeng B, Peng L, Hauck A, Zhao H, Song W, Fan Z, Lai J. 2015. Ribosome profiling reveals dynamic translational landscape in maize seedlings under drought stress. Plant J 84: 1206–1218.

123. Machado JPB, Calil IP, Santos AA, Fontes EPB. 2017. Translational control in plant antiviral immunity. Genet Mol Biol 40: 292-304.

124. Merchante C, Stepanova AN, Alonso JM. 2017. Translation regulation in plants: an interesting past, an exciting present and a promising future. Plant J 90: 628–653.

125. Sesma A, Castresana C, Castellano MM. 2017. Regulation of Translation by TOR, eIF4E and eIF2α in Plants: Current Knowledge, Challenges and Future Perspectives. Front Plant Sci 8: 644.

126. Xu T, Lei L, Shi J, Wang X, Chen J, Xue M, Sun S, Zhan B, Xia Z, Jiang N, Zhou T, Lai J, Fan Z. 2019. Characterization of maize translational responses to sugarcane mosaic virus infection. Virus Res 259: 97–107.

127. Miller WA, Dinesh-Kumar SP. 2019. A new mechanism for translational control in plants. FEBS J 286: 3775–3777.

128. Wu X, Valli A, García J, Zhou X, Cheng X. 2019. The Tug-of-War between Plants and Viruses: Great Progress and Many Remaining Questions. Viruses 11: 203.

129. Hao L, Wang H, Sunter G, Bisaro DM. 2003. Geminivirus AL2 and L2 Proteins Interact with and Inactivate SNF1 Kinase. Plant Cell 15: 1034–1048.

130. Bruns AN, Li S, Mohannath G, Bisaro DM. 2019. Phosphorylation of Arabidopsis eIF 4E and eIF iso4E by Sn RK 1 inhibits translation. FEBS J 286: 3778–3796.

131. Bhattacharjee S, Zamora A, Azhar MT, Sacco MA, Lambert LH, Moffett P. 2009. Virus resistance induced by NB-LRR proteins involves Argonaute4-dependent translational control. Plant J 58: 940–951.

132. Park HS, Himmelbach A, Browning KS, Hohn T, Ryabova LA. 2001. A Plant Viral "Reinitiation" Factor Interacts with the Host Translational Machinery. Cell 106: 723–733.

133. Jackson RJ, Hellen CUT, Pestova TV. 2010. The mechanism of eukaryotic translation initiation and principles of its regulation. Nat Rev Mol Cell Biol 11: 113–127.

134. Urquidi Camacho RA, Lokdarshi A, Arnim AG. 2020. Translational gene regulation in plants: A green new deal. WIREs RNA 11: e1597.

135. Castellano MM, Merchante C. 2021. Peculiarities of the regulation of translation initiation in plants. Curr Opin Plant Biol 63: 102073.

136. Lellis AD, Allen ML, Aertker AW, Tran JK, Hillis DM, Harbin CR, Caldwell C, Gallie DR, Browning KS. 2010. Deletion of the eIFiso4G subunit of the Arabidopsis eIFiso4F translation initiation complex impairs health and viability. Plant Mol Biol 74: 249–263.

137. Izquierdo Y, Kulasekaran S, Benito P, López B, Marcos R, Cascón T, Hamberg M, Castresana C. 2018. Arabidopsis nonresponding to oxylipins locus NOXY7 encodes a yeast GCN1 homolog that mediates noncanonical translation regulation and stress adaptation. Plant Cell Environ 41: 1438–1452.

138. Zhigailov AV, Alexandrova AM, Nizkorodova AS, Stanbekova GE, Kryldakov RV, Karpova OV, Polimbetova NS, Halford NG, Iskakov BK. 2020. Evidence That Phosphorylation of the α-Subunit of eIF2 Does Not Essentially Inhibit mRNA Translation in Wheat Germ Cell-Free System. Front Plant Sci 11: 936.

139. Wek RC. 2018. Role of eIF2α Kinases in Translational Control and Adaptation to Cellular Stress. Cold Spring Harb Perspect Biol 10: a032870.

140. Boye E, Grallert B. 2020. eIF2α phosphorylation and the regulation of translation. Curr Genet 66: 293–297.

141. King HA, Gerber AP. 2014. Translatome profiling: methods for genome-scale analysis of mRNA translation. Brief Funct Genomics 15: 22–31.

142. Iwasaki S, Ingolia NT. 2017. The Growing Toolbox for Protein Synthesis Studies. Trends Biochem Sci 42: 612–624.

143. Dermit M, Dodel M, Mardakheh FK. 2017. Methods for monitoring and measurement of protein translation in time and space. Mol Biosyst 13: 2477–2488.

144. Mazzoni-Putman SM, Stepanova AN. 2018. A Plant Biologist's Toolbox to Study Translation. Front Plant Sci 9: 873.

145. Schmidt EK, Clavarino G, Ceppi M, Pierre P. 2009. SUnSET, a nonradioactive method to monitor protein synthesis. Nat Methods 6: 275–277.

146. Van Hoewyk D. 2016. Use of the non-radioactive SUnSET method to detect decreased protein synthesis in proteasome inhibited Arabidopsis roots. Plant Methods 12: 20.

147. Ong SE, Blagoev B, Kratchmarova I, Kristensen DB, Steen H, Pandey A, Mann M. 2002. Stable Isotope Labeling by Amino Acids in Cell Culture, SILAC, as a Simple and Accurate Approach to Expression Proteomics. Mol Cell Proteomics 1: 376–386.

148. Selbach M, Schwanhäusser B, Thierfelder N, Fang Z, Khanin R, Rajewsky N. 2008. Widespread changes in protein synthesis induced by microRNAs. Nature 455: 58–63.

149. Dieterich DC, Link AJ, Graumann J, Tirrell DA, Schuman EM. 2006. Selective identification of newly synthesized proteins in mammalian cells using bioorthogonal noncanonical amino acid tagging (BONCAT). Proc Natl Acad Sci 103: 9482–9487.

150. Michel AM, Baranov P V. 2013. Ribosome profiling: a Hi-Def monitor for protein synthesis at the genome-wide scale. WIREs RNA 4: 473–490.

151. Mustroph A, Juntawong P, Bailey-Serres J. 2009. Isolation of Plant Polysomal mRNA by Differential Centrifugation and Ribosome Immunopurification Methods. Methods Mol Biol 553: 109-26.

152. Arava Y, Wang Y, Storey JD, Liu CL, Brown PO, Herschlag D. 2003. Genome-wide analysis of mRNA translation profiles in Saccharomyces cerevisiae. Proc Natl Acad Sci 100: 3889–3894.

153. Mašek T, Valášek L, Pospíšek M. 2011. Polysome Analysis and RNA Purification from Sucrose Gradients. Methods Mol Biol 703: 292-309.

154. Zanetti ME, Chang IF, Gong F, Galbraith DW, Bailey-Serres J. 2005. Immunopurification of Polyribosomal Complexes of Arabidopsis for Global Analysis of Gene Expression. Plant Physiol 138: 624–635.

155. Heiman M, Schaefer A, Gong S, Peterson JD, Day M, Ramsey KE, Suárez-Fariñas M, Schwarz C, Stephan DA, Surmeier DJ, Greengard P, Heintz N. 2008. A Translational Profiling Approach for the Molecular Characterization of CNS Cell Types. Cell 135: 738–748.

156. Sanz E, Yang L, Su T, Morris DR, McKnight GS, Amieux PS. 2009. Cell-type-specific isolation of ribosome-associated mRNA from complex tissues. Proc Natl Acad Sci 106: 13939–13944.

157. Mustroph A, Zanetti ME, Jang CJH, Holtan HE, Repetti PP, Galbraith DW, Girke T, Bailey-Serres J. 2009. Profiling translatomes of discrete cell populations resolves altered cellular priorities during hypoxia in Arabidopsis. Proc Natl Acad Sci 106: 18843–18848.

158. Morris DR, Geballe AP. 2000. Upstream Open Reading Frames as Regulators of mRNA Translation. Mol Cell Biol 20: 8635–8642.

159. Brar GA, Weissman JS. 2015. Ribosome profiling reveals the what, when, where and how of protein synthesis. Nat Rev Mol Cell Biol 16: 651–664.

160. Wang Z, Gerstein M, Snyder M. 2009. RNA-Seq: a revolutionary tool for transcriptomics. Nat Rev Genet 10: 57–63.

161. Stark R, Grzelak M, Hadfield J. 2019. RNA sequencing: the teenage years. Nat Rev Genet 20: 631–656.

162. Hayles B, Yellaboina S, Wang D. 2010. Comparing Transcription Rate and mRNA Abundance as Parameters for Biochemical Pathway and Network Analysis. PLoS One 5: e9908.

163. Furlan M, de Pretis S, Pelizzola M. 2021. Dynamics of transcriptional and post-transcriptional regulation. Brief Bioinform 22: 1–13.

164. Lu P, Vogel C, Wang R, Yao X, Marcotte EM. 2007. Absolute protein expression profiling estimates the relative contributions of transcriptional and translational regulation. Nat Biotechnol 25: 117–124.

165. Baek D, Villén J, Shin C, Camargo FD, Gygi SP, Bartel DP. 2008. The impact of microRNAs on protein output. Nature 455: 64–71.

166. Ingolia NT, Ghaemmaghami S, Newman JRS, Weissman JS. 2009. Genome-wide analysis *in vivo* of translation with nucleotide resolution using ribosome profiling. Science 324: 218–23.

167. Maier T, Güell M, Serrano L. 2009. Correlation of mRNA and protein in complex biological samples. FEBS Lett 583: 3966–3973.

168. de Sousa Abreu R, Penalva LO, Marcotte EM, Vogel C. 2009. Global signatures of protein and mRNA expression levels. Mol Biosyst 5: 1512–1526.

169. Vogel C, de Sousa Abreu R, Ko D, Le S, Shapiro BA, Burns SC, Sandhu D, Boutz DR, Marcotte EM, Penalva LO. 2010. Sequence signatures and mRNA concentration can explain two-thirds of protein abundance variation in a human cell line. Mol Syst Biol 6: 400.

170. Plotkin JB. 2010. Transcriptional regulation is only half the story. Mol Syst Biol 6: 406.

171. Schwanhäusser B, Busse D, Li N, Dittmar G, Schuchhardt J, Wolf J, Chen W, Selbach M. 2011. Global quantification of mammalian gene expression control. Nature 473: 337–342.

172. Vogel C. 2011. Translation's coming of age. Mol Syst Biol 7: 498.

173. Fujita T, Kurihara Y, Iwasaki S. 2019. The Plant Translatome Surveyed by Ribosome Profiling. Plant Cell Physiol 60: 1917–1926.

174. Steitz JA. 1969. Polypeptide Chain Initiation: Nucleotide Sequences of the Three Ribosomal Binding Sites in Bacteriophage R17 RNA. Nature 224: 957–964.

175. Wolin SL, Walter P. 1988. Ribosome pausing and stacking during translation of a eukaryotic mRNA. EMBO J 7: 3559–69.

176. Weiss RB, Atkins JF. 2011. Translation Goes Global. Science 334: 1509–1510.

177. Ingolia NT. 2014. Ribosome profiling: new views of translation, from single codons to genome scale. Nat Rev Genet 15: 205–13.

178. Ingolia NT. 2016. Ribosome Footprint Profiling of Translation throughout the Genome. Cell 165: 22–33.

179. Calviello L, Ohler U. 2017. Beyond Read-Counts: Ribo-seq Data Analysis to Understand the Functions of the Transcriptome. Trends Genet 33: 728–744.

180. Ingolia NT, Hussmann JA, Weissman JS. 2019. Ribosome Profiling: Global Views of Translation. Cold Spring Harb Perspect Biol 11: a032698.

181. Wang Y, Zhang H, Lu J. 2020. Recent advances in ribosome profiling for deciphering translational regulation. Methods 176: 46–54.

182. Kage U, Powell JJ, Gardiner DM, Kazan K. 2020. Ribosome profiling in plants: what is not lost in translation? J Exp Bot 71: 5323–5332.

183. Ingolia NT, Lareau LF, Weissman JS. 2011. Ribosome Profiling of Mouse Embryonic Stem Cells Reveals the Complexity and Dynamics of Mammalian Proteomes. Cell 147: 789–802.

184. Lee S, Liu B, Lee S, Huang SX, Shen B, Qian SB. 2012. Global mapping of translation initiation sites in mammalian cells at single-nucleotide resolution. Proc Natl Acad Sci 109: E2424–E2432.

185. Brar GA, Yassour M, Friedman N, Regev A, Ingolia NT, Weissman JS. 2012. High-Resolution View of the Yeast Meiotic Program Revealed by Ribosome Profiling. Science 335: 552–557.

186. Stern-Ginossar N, Weisburd B, Michalski A, Le VTK, Hein MY, Huang SX, Ma M, Shen B, Qian SB, Hengel H, Mann M, Ingolia NT, Weissman JS. 2012. Decoding Human Cytomegalovirus. Science 338: 1088–1093.

187. Mouilleron H, Delcourt V, Roucou X. 2016. Death of a dogma: Eukaryotic mRNAs can code for more than one protein. Nucleic Acids Res 44: 14–23.

188. Hsu PY, Calviello L, Wu HYL, Li FW, Rothfels CJ, Ohler U, Benfey PN. 2016. Super-resolution ribosome profiling reveals unannotated translation events in Arabidopsis. Proc Natl Acad Sci 113: E7126–E7135.

189. Cao X, Slavoff SA. 2020. Non-AUG start codons: Expanding and regulating the small and alternative ORFeome. Exp Cell Res 391: 111973.

190. Li YR, Liu MJ. 2020. Prevalence of alternative AUG and non-AUG translation initiators and their regulatory effects across plants. Genome Res 30: 1418–1433.

191. Eisenberg AR, Higdon AL, Hollerer I, Fields AP, Jungreis I, Diamond PD, Kellis M, Jovanovic M, Brar GA. 2020. Translation Initiation Site Profiling Reveals Widespread Synthesis of Non-AUG-Initiated Protein Isoforms in Yeast. Cell Syst 11: 145-160.e5.

192. Chew GL, Pauli A, Rinn JL, Regev A, Schier AF, Valen E. 2013. Ribosome profiling reveals resemblance between long non-coding RNAs and 5’ leaders of coding RNAs. Development 140: 2828–2834.

193. Guttman M, Russell P, Ingolia NT, Weissman JS, Lander ES. 2013. Ribosome Profiling Provides Evidence that Large Noncoding RNAs Do Not Encode Proteins. Cell 154: 240–251.

194. Ingolia NT, Brar GA, Stern-Ginossar N, Harris MS, Talhouarne GJS, Jackson SE, Wills MR, Weissman JS. 2014. Ribosome profiling reveals pervasive translation outside of annotated protein-coding genes. Cell Rep 8: 1365–79.

195. Ji Z, Song R, Regev A, Struhl K. 2015. Many lncRNAs, 5'UTRs, and pseudogenes are translated and some are likely to express functional proteins. Elife 4: e08890.

196. Chekulaeva M, Rajewsky N. 2019. Roles of Long Noncoding RNAs and Circular RNAs in Translation. Cold Spring Harb Perspect Biol 11: a032680.

197. Gawroński P, Jensen PE, Karpiński S, Leister D, Scharff LB. 2018. Pausing of Chloroplast Ribosomes Is Induced by Multiple Features and Is Linked to the Assembly of Photosynthetic Complexes. Plant Physiol 176: 2557–2569.

198. Gelsinger DR, Dallon E, Reddy R, Mohammad F, Buskirk AR, DiRuggiero J. 2020. Ribosome profiling in archaea reveals leaderless translation, novel translational initiation sites, and ribosome pausing at single codon resolution. Nucleic Acids Res 48: 5201–5216.

199. Collart MA, Weiss B. 2020. Ribosome pausing, a dangerous necessity for co-translational events. Nucleic Acids Res 48: 1043–1055.

200. Chyżyńska K, Labun K, Jones C, Grellscheid SN, Valen E. 2021. Deep conservation of ribosome stall sites across RNA processing genes. NAR Genom Bioinform 3: Iqab038.

201. Napthine S, Ling R, Finch LK, Jones JD, Bell S, Brierley I, Firth AE. 2017. Protein-directed ribosomal frameshifting temporally regulates gene expression. Nat Commun 8: 15582.

202. Cook GM, Shang P, Li Y, Brown KA, Dinan A, Fang Y, Firth A, Brierley I. 2019. Ribosome profiling of porcine reproductive and respiratory syndrome virus. Access Microbiol 1: 313.

203. Rodnina MV, Korniy N, Klimova M, Karki P, Peng BZ, Senyushkina T, Belardinelli R, Maracci C, Wohlgemuth I, Samatova E, Peske F. 2020. Translational recoding: canonical translation mechanisms reinterpreted. Nucleic Acids Res 48: 1056–1067.

204. De Lise F, Strazzulli A, Iacono R, Curci N, Di Fenza M, Maurelli L, Moracci M, Cobucci-Ponzano B. 2021. Programmed Deviations of Ribosomes From Standard Decoding in Archaea. Front Microbiol 12: 1352.

205. Bhatt PR, Scaiola A, Loughran G, Leibundgut M, Kratzel A, Meurs R, Dreos R, O'Connor KM, McMillan A, Bode JW, Thiel V, Gatfield D, Atkins JF, Ban N. 2021. Structural basis of ribosomal frameshifting during translation of the SARS-CoV-2 RNA genome. Science 372: 1306–1313.

206. Merchante C, Brumos J, Yun J, Hu Q, Spencer KR, Enríquez P, Binder BM, Heber S, Stepanova AN, Alonso JM. 2015. Gene-Specific Translation Regulation Mediated by the Hormone-Signaling Molecule EIN2. Cell 163: 684–697.

207. Gandin V, Masvidal L, Hulea L, Gravel SP, Cargnello M, McLaughlan S, Cai Y, Balanathan P, Morita M, Rajakumar A, Furic L, Pollak M, Porco JA, St-Pierre J, Pelletier J, Larsson O, Topisirovic I. 2016. nanoCAGE reveals 5′ UTR features that define specific modes of translation of functionally related MTOR-sensitive mRNAs. Genome Res 26: 636–648.

208. Xu G, Greene GH, Yoo H, Liu L, Marqués J, Motley J, Dong X. 2017. Global translational reprogramming is a fundamental layer of immune regulation in plants. Nature 545: 487–490.

209. Chung BYW, Balcerowicz M, Di Antonio M, Jaeger KE, Geng F, Franaszek K, Marriott P, Brierley I, Firth AE, Wigge PA. 2020. An RNA thermoswitch regulates daytime growth in Arabidopsis. Nat Plants 6: 522–532.

210. Rao S, Hoskins I, Tonn T, Garcia PD, Ozadam H, Sarinay Cenik E, Cenik C. 2021. Genes with 5′ terminal oligopyrimidine tracts preferentially escape global suppression of translation by the SARS-CoV-2 Nsp1 protein. RNA 27: 1025–1045.

211. Couto Bordignon P, Pechmann S. 2021. Inferring translational heterogeneity from Saccharomyces cerevisiae ribosome profiling. FEBS J 288: 4541–4559.

212. Lareau LF, Hite DH, Hogan GJ, Brown PO. 2014. Distinct stages of the translation elongation cycle revealed by sequencing ribosome-protected mRNA fragments. Elife 2014: 1–16.

213. Andreev DE, O'Connor PBF, Loughran G, Dmitriev SE, Baranov PV, Shatsky IN. 2017. Insights into the mechanisms of eukaryotic translation gained with ribosome profiling. Nucleic Acids Res 45: 513–526.

214. Bazin J, Baerenfaller K, Gosai SJ, Gregory BD, Crespi M, Bailey-Serres J. 2017. Global analysis of ribosome-associated noncoding RNAs unveils new modes of translational regulation. Proc Natl Acad Sci 114: E10018–E10027.

215. Riba A, Di Nanni N, Mittal N, Arhné E, Schmidt A, Zavolan M. 2019. Protein synthesis rates and ribosome occupancies reveal determinants of translation elongation rates. Proc Natl Acad Sci 116: 15023–15032.

216. de Klerk E, Fokkema IFAC, Thiadens KAMH, Goeman JJ, Palmblad M, den Dunnen JT, von Lindern M, 't Hoen PAC. 2015. Assessing the translational landscape of myogenic differentiation by ribosome profiling. Nucleic Acids Res 43: 4408–4428.

217. Trösch R, Barahimipour R, Gao Y, Badillo-Corona JA, Gotsmann VL, Zimmer D, Mühlhaus T, Zoschke R, Willmund F. 2018. Commonalities and differences of chloroplast translation in a green alga and land plants. Nat Plants 4: 564–575.

218. Wu HYL, Song G, Walley JW, Hsu PY. 2019. The Tomato Translational Landscape Revealed by Transcriptome Assembly and Ribosome Profiling. Plant Physiol 181: 367–380.

219. Yang X, Song B, Cui J, Wang L, Wang S, Luo L, Gao L, Mo B, Yu Y, Liu L. 2021. Comparative ribosome profiling reveals distinct translational landscapes of salt-sensitive and -tolerant rice. BMC Genomics 22: 612.

220. Chotewutmontri P, Barkan A. 2021. Ribosome profiling elucidates differential gene expression in bundle sheath and mesophyll cells in maize. Plant Physiol 187: 59–72.

221. Wang N, Wang D. 2021. Genome-wide transcriptome and translatome analyses reveal the role of protein extension and domestication in liver cancer oncogenesis. Mol Genet Genomics 296: 561–569.

222. Arias C, Weisburd B, Stern-Ginossar N, Mercier A, Madrid AS, Bellare P, Holdorf M, Weissman JS, Ganem D. 2014. KSHV 2.0: A Comprehensive Annotation of the Kaposi's Sarcoma-Associated Herpesvirus Genome Using Next-Generation Sequencing Reveals Novel Genomic and Functional Features. PLoS Pathog 10: e1003847.

223. Stern-Ginossar N, Ingolia NT. 2015. Ribosome Profiling as a Tool to Decipher Viral Complexity. Annu Rev Virol 2: 335-349.

224. Yang Z, Cao S, Martens CA, Porcella SF, Xie Z, Ma M, Shen B, Moss B. 2015. Deciphering Poxvirus Gene Expression by RNA Sequencing and Ribosome Profiling. J Virol 89: 6874–6886.

225. Irigoyen N, Firth AE, Jones JD, Chung BYW, Siddell SG, Brierley I. 2016. High-Resolution Analysis of Coronavirus Gene Expression by RNA Sequencing and Ribosome Profiling. PLoS Pathog 12: e1005473.

226. Irigoyen N, Dinan AM, Brierley I, Firth AE. 2018. Ribosome profiling of the retrovirus murine leukemia virus. Retrovirology 15: 10.

227. Stewart H, Brown K, Dinan AM, Irigoyen N, Snijder EJ, Firth AE. 2018. Transcriptional and Translational Landscape of Equine Torovirus. J Virol 92: e00589-18.

228. Finkel Y, Mizrahi O, Nachshon A, Weingarten-Gabbay S, Morgenstern D, Yahalom-Ronen Y, Tamir H, Achdout H, Stein D, Israeli O, Beth-Din A, Melamed S, Weiss S, Israely T, Paran N, Schwartz M, Stern-Ginossar N. 2021. The coding capacity of SARS-CoV-2. Nature 589: 125–130.

229. Smircich P, Eastman G, Bispo S, Duhagon MA, Guerra-Slompo EP, Garat B, Goldenberg S, Munroe DJ, Dallagiovanna B, Holetz F, Sotelo-Silveira JR. 2015. Ribosome profiling reveals translation control as a key mechanism generating differential gene expression in Trypanosoma cruzi. BMC Genomics 16: 443.

230. Jiang Z, Yang J, Dai A, Wang Y, Li W, Xie Z. 2017. Ribosome profiling reveals translational regulation of mammalian cells in response to hypoxic stress. BMC Genomics 18: 638.

231. Shamimuzzaman M, Vodkin L. 2018. Ribosome profiling reveals changes in translational status of soybean transcripts during immature cotyledon development. PLoS One 13: e0194596.

232. Reid DW, Campos RK, Child JR, Zheng T, Chan KWK, Bradrick SS, Vasudevan SG, Garcia-Blanco MA, Nicchitta CV. 2018. Dengue Virus Selectively Annexes Endoplasmic Reticulum-Associated Translation Machinery as a Strategy for Co-opting Host Cell Protein Synthesis. J Virol 92: e01766-17.

233. Hu Z, Xia B, Postnikoff SDL, Shen ZJ, Tomoiaga AS, Harkness TA, Seol JH, Li W, Chen K, Tyler JK. 2018. Ssd1 and Gcn2 suppress global translation efficiency in replicatively aged yeast while their activation extends lifespan. Elife 7: e35551.

234. Poidevin L, Forment J, Unal D, Ferrando A. 2021. Transcriptome and translatome changes in germinated pollen under heat stress uncover roles of transporter genes involved in pollen tube growth. Plant Cell Environ 44: 2167–2184.

235. Finkel Y, Gluck A, Nachshon A, Winkler R, Fisher T, Rozman B, Mizrahi O, Lubelsky Y, Zuckerman B, Slobodin B, Yahalom-Ronen Y, Tamir H, Ulitsky I, Israely T, Paran N, Schwartz M, Stern-Ginossar N. 2021. SARS-CoV-2 uses a multipronged strategy to impede host protein synthesis. Nature 594: 240–245.

236. Gerashchenko MV, Gladyshev VN. 2017. Ribonuclease selection for ribosome profiling. Nucleic Acids Res 45: e6.

237. Andrews S. 2010. FastQC: A Quality Control Tool for High Throughput Sequence Data [Online]. Available online at: http://www.bioinformatics.babraham.ac.uk/projects/fastqc.

238. Martin M. 2011. Cutadapt removes adapter sequences from high-throughput sequencing reads. EMBnet.journal 17: 10–12.

239. Langmead B, Trapnell C, Pop M, Salzberg SL. 2009. Ultrafast and memory-efficient alignment of short DNA sequences to the human genome. Genome Biol 10: 1-10.

240. Langmead B, Salzberg SL. 2012. Fast gapped-read alignment with Bowtie 2. Nat Methods 9: 357–359.

241. Dobin A, Davis CA, Schlesinger F, Drenkow J, Zaleski C, Jha S, Batut P, Chaisson M, Gingeras TR. 2013. STAR: ultrafast universal RNA-seq aligner. Bioinformatics 29: 15–21.

242. Wang H, Wang Y, Xie Z. 2019. Computational resources for ribosome profiling: from database to Web server and software. Brief Bioinform 20: 144–155.

243. Kiniry SJ, Michel AM, Baranov PV. 2020. Computational methods for ribosome profiling data analysis. WIREs RNA 11: e1577.

244. Liu MJ, Wu SH, Wu JF, Lin WD, Wu YC, Tsai TY, Tsai HL, Wu SH. 2013. Translational Landscape of Photomorphogenic Arabidopsis. Plant Cell 25: 3699–3710.

245. Yang X, Cui J, Song B, Yu Y, Mo B, Liu L. 2020. Construction of High-Quality Rice Ribosome Footprint Library. Front Plant Sci 11: 1381.

246. Zimmermann R, Eyrisch S, Ahmad M, Helms V. 2011. Protein translocation across the ER membrane. Biochim Biophys Acta 1808: 912–924.

247. Saraogi I, Shan S. 2011. Molecular Mechanism of Co-translational Protein Targeting by the Signal Recognition Particle. Traffic 12: 535–542.

248. Paul P, Simm S, Blaumeiser A, Scharf KD, Fragkostefanakis S, Mirus O, Schleiff E. 2013. The protein translocation systems in plants – composition and variability on the example of Solanum lycopersicum. BMC Genomics 14: 189.

249. Helenius A. 1994. How N-linked oligosaccharides affect glycoprotein folding in the endoplasmic reticulum. Mol Biol Cell 5: 253–265.

250. Vitale A, Denecke J. 1999. The Endoplasmic Reticulum—Gateway of the Secretory Pathway. Plant Cell 11: 615–628.

251. Helenius A, Aebi M. 2004. Roles of N-Linked Glycans in the Endoplasmic Reticulum. Annu Rev Biochem 73: 1019–1049.

252. Young JC, Agashe VR, Siegers K, Hartl FU. 2004. Pathways of chaperone-mediated protein folding in the cytosol. Nat Rev Mol Cell Biol 5: 781–791.

253. Bukau B, Weissman J, Horwich A. 2006. Molecular Chaperones and Protein Quality Control. Cell 125: 443–451.

254. Braakman I, Hebert DN. 2013. Protein Folding in the Endoplasmic Reticulum. Cold Spring Harb Perspect Biol 5: a013201.

255. Oka OBV, Bulleid NJ. 2013. Forming disulfides in the endoplasmic reticulum. Biochim Biophys Acta 1833: 2425–2429.

256. Melnyk A, Rieger H, Zimmermann R. 2015. Co-chaperones of the Mammalian Endoplasmic Reticulum. Subcell Biochem 78: 179-200.

257. Nagashima Y, von Schaewen A, Koiwa H. 2018. Function of N-glycosylation in plants. Plant Sci 274: 70–79.

258. Urade R. 2019. Oxidative protein folding in the plant endoplasmic reticulum. Biosci Biotechnol Biochem 83: 781–793.

259. Watson P, Stephens DJ. 2005. ER-to-Golgi transport: Form and formation of vesicular and tubular carriers. Biochim Biophys Acta 1744: 304–315.

260. Gomez-Navarro N, Miller E. 2016. Protein sorting at the ER–Golgi interface. J Cell Biol 215: 769–778.

261. Brandizzi F. 2018. Transport from the endoplasmic reticulum to the Golgi in plants: Where are we now? Semin Cell Dev Biol 80: 94–105.

262. Araki K, Nagata K. 2011. Protein Folding and Quality Control in the ER. Cold Spring Harb Perspect Biol 3: a007526.

263. Strasser R. 2018. Protein Quality Control in the Endoplasmic Reticulum of Plants. Annu Rev Plant Biol 69: 147–172.

264. Liu JX, Howell SH. 2010. Endoplasmic Reticulum Protein Quality Control and Its Relationship to Environmental Stress Responses in Plants. Plant Cell 22: 2930–2942.

265. Sun JL, Li JY, Wang MJ, Song ZT, Liu JX. 2021. Protein Quality Control in Plant Organelles: Current Progress and Future Perspectives. Mol Plant 14: 95–114.

266. Hetz C. 2012. The unfolded protein response: controlling cell fate decisions under ER stress and beyond. Nat Rev Mol Cell Biol 13: 89–102.

267. Howell SH. 2013. Endoplasmic Reticulum Stress Responses in Plants. Annu Rev Plant Biol 64: 477–499.

268. Liu JX, Howell SH. 2016. Managing the protein folding demands in the endoplasmic reticulum of plants. New Phytol 211: 418–428.

269. Walter P, Ron D. 2011. The Unfolded Protein Response: From Stress Pathway to Homeostatic Regulation. Science 334: 1081–1086.

270. Deng Y, Srivastava R, Howell S. 2013. Endoplasmic Reticulum (ER) Stress Response and Its Physiological Roles in Plants. Int J Mol Sci 14: 8188–8212.

271. Angelos E, Ruberti C, Kim SJ, Brandizzi F. 2017. Maintaining the factory: the roles of the unfolded protein response in cellular homeostasis in plants. Plant J 90: 671–682.

272. Nawkar GM, Lee ES, Shelake RM, Park JH, Ryu SW, Kang CH, Lee SY. 2018. Activation of the Transducers of Unfolded Protein Response in Plants. Front Plant Sci 9: 214.

273. Hetz C, Zhang K, Kaufman RJ. 2020. Mechanisms, regulation and functions of the unfolded protein response. Nat Rev Mol Cell Biol 21: 421–438.

274. Marciniak SJ, Ron D. 2006. Endoplasmic Reticulum Stress Signaling in Disease. Physiol Rev 86: 1133–1149.

275. Luheshi LM, Crowther DC, Dobson CM. 2008. Protein misfolding and disease: from the test tube to the organism. Curr Opin Chem Biol 12: 25–31.

276. Doultsinos D, Avril T, Lhomond S, Dejeans N, Guédat P, Chevet E. 2017. Control of the Unfolded Protein Response in Health and Disease. SLAS Discov 22: 787–800.

277. Hetz C, Papa FR. 2018. The Unfolded Protein Response and Cell Fate Control. Mol Cell 69: 169–181.

278. Hetz C, Saxena S. 2017. ER stress and the unfolded protein response in neurodegeneration. Nat Rev Neurol 13: 477–491.

279. García-González P, Cabral-Miranda F, Hetz C, Osorio F. 2018. Interplay Between the Unfolded Protein Response and Immune Function in the Development of Neurodegenerative Diseases. Front Immunol 9: 2541.

280. Uddin MS, Yu WS, Lim LW. 2021. Exploring ER stress response in cellular aging and neuroinflammation in Alzheimer's disease. Ageing Res Rev 70: 101417.

281. Howell SH. 2017. When is the unfolded protein response not the unfolded protein response? Plant Sci 260: 139–143.

282. Bao Y, Howell SH. 2017. The Unfolded Protein Response Supports Plant Development and Defense as well as Responses to Abiotic Stress. Front Plant Sci 8: 344.

283. Harding HP, Zhang Y, Ron D. 1999. Protein translation and folding are coupled by an endoplasmic-reticulum-resident kinase. Nature 397: 271–274.

284. Srivastava R, Li Z, Russo G, Tang J, Bi R, Muppirala U, Chudalayandi S, Severin A, He M, Vaitkevicius SI, Lawrence-Dill CJ, Liu P, Stapleton AE, Bassham DC, Brandizzi F, Howell SH. 2018. Response to Persistent ER Stress in Plants: A Multiphasic Process That Transitions Cells from Prosurvival Activities to Cell Death. Plant Cell 30: 1220–1242.

Figures

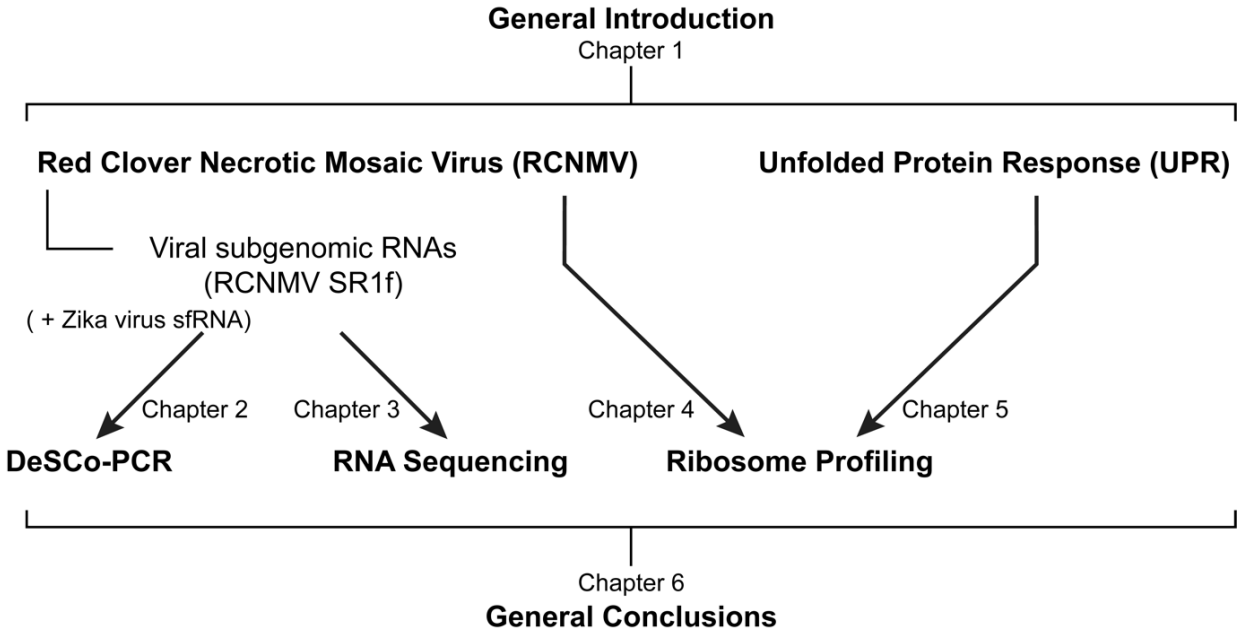

Figure 1.1. Dissertation outline.

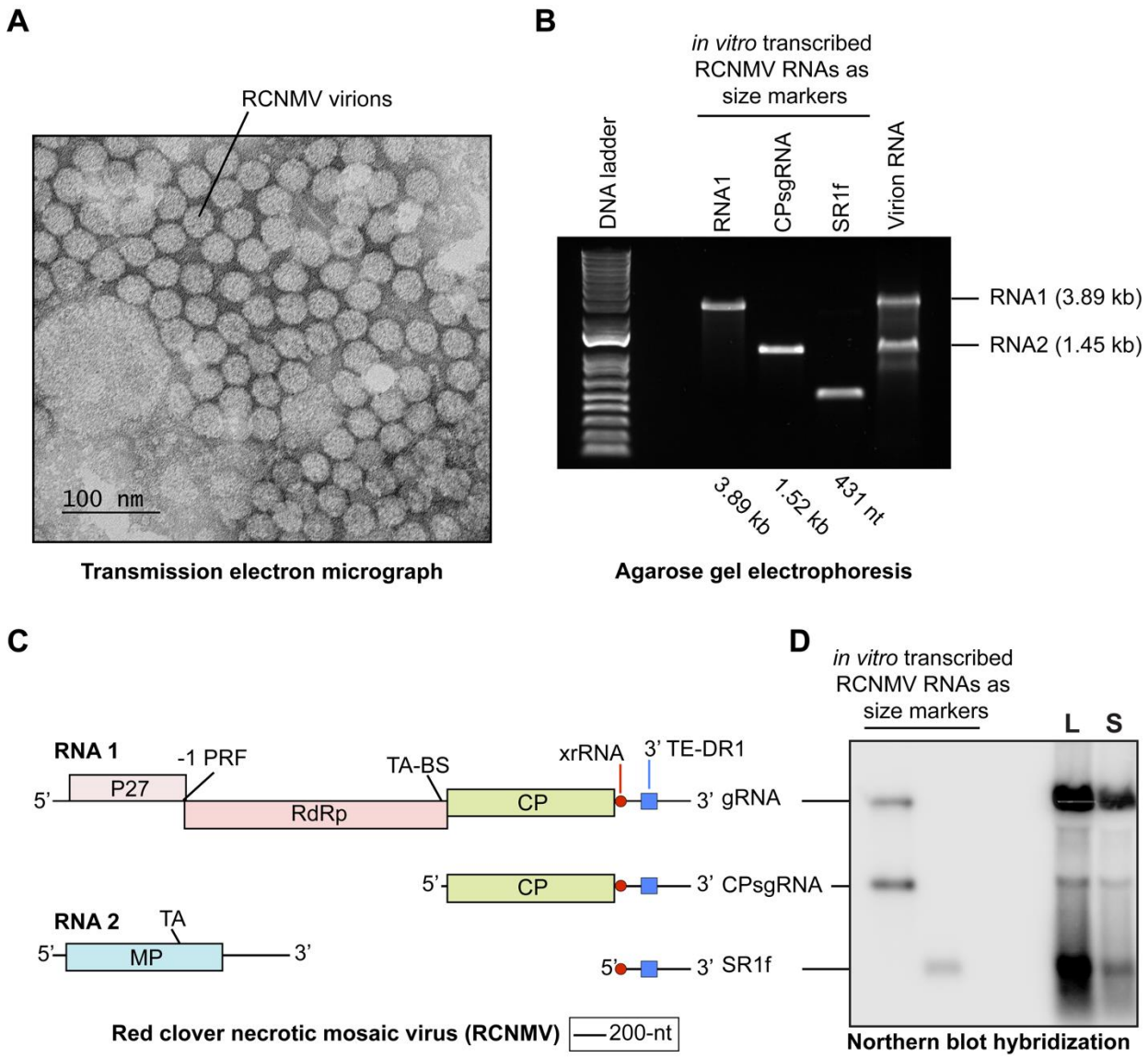

Figure 1.2. Red clover necrotic mosaic virus (RCNMV). **(A)** Transmission electron micrograph (TEM) of purified RCNMV particles from infected *N. benthamiana* plants. Virus purification was conducted according to ref. 19. TEM was conducted by Tracey P. Stewart from the microscopy facility at the Iowa State University. **(B)** Agarose gel electrophoreses showing the genomic RNAs extracted from the purified RCNMV virions. **(C)** Genome organization of RCNMV (drawn to scale) depicting RCNMV genomic and subgenomic RNAs and the translated ORFs. **(D)** Northern blot hybridization from RCNMV-infected transgenic Arabidopsis plants (*dcl2-1/dcl4-2t* double knock-out, see *Chapter 3*) with a probe complementary to the 3' UTR of RNA1. The probe detects the accumulation of RCNMV RNA1, CPsgRNA, and SR1f in the local (L) inoculated as well as systemic (S) non-inoculated leaves. (TA) trans-activator, (TA-BS) trans-activator binding site, (xrRNA) exoribonuclease-resistant RNA, (3' TE-DR1) 3' translation element of *dianthovirus* RNA1.

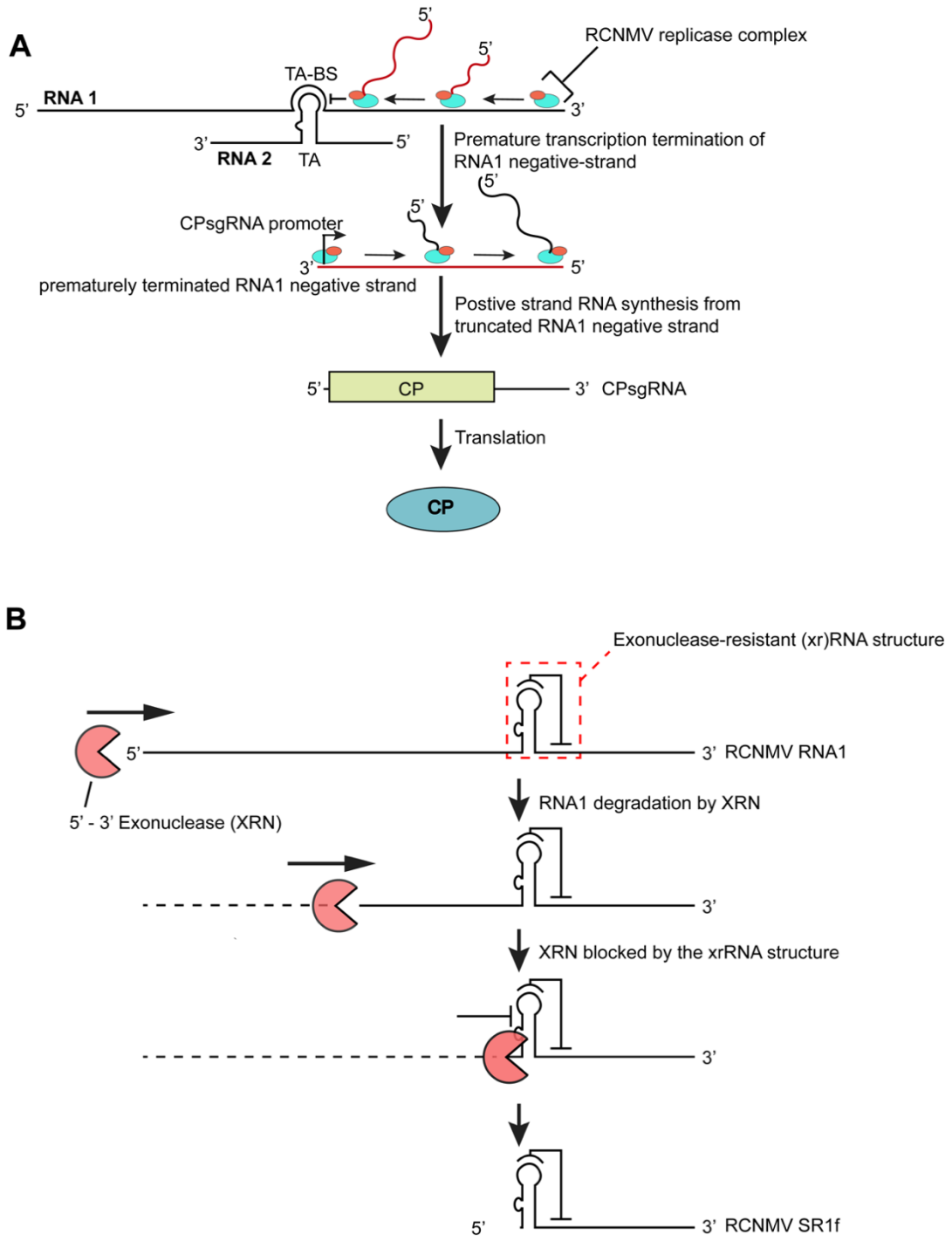

Figure 1.3. Schematics of the mechanisms for the generation of RCNMV CPsgRNA and SR1f. **(A)** Transcription of CPsgRNA from the 3'end of a truncated RNA1 negative-strand that was produced by premature transcription termination as a result of RNA1-RNA2 interaction. Black and red lines represent positive- and negative-sense strands, respectively. **(B)** Generation of SR1f via the host exoribonuclease (XRN)-dependent mechanism. Host 5'→ 3' exoribonuclease, while degrading viral RNAs, gets blocked by an XRN-resistant (xr)RNA structure in the 3'UTR of RNA1/CPsgRNA resulting in the left-over stable degradation product (SR1f). xrRNA shown is only an illustration and does not reflect the true xrRNA structure of SR1f.

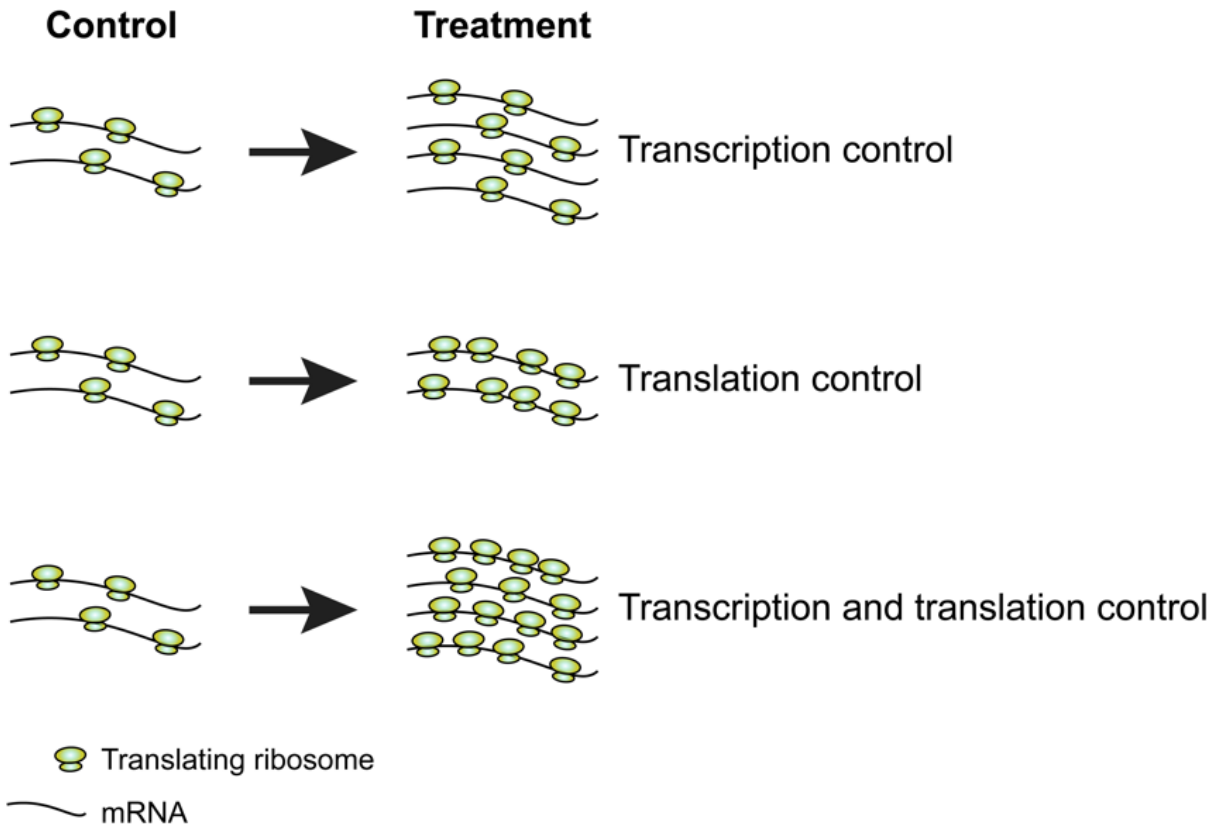

Figure 1.4. Interplay between transcriptional and translational control of gene expression to regulate the final protein abundance.

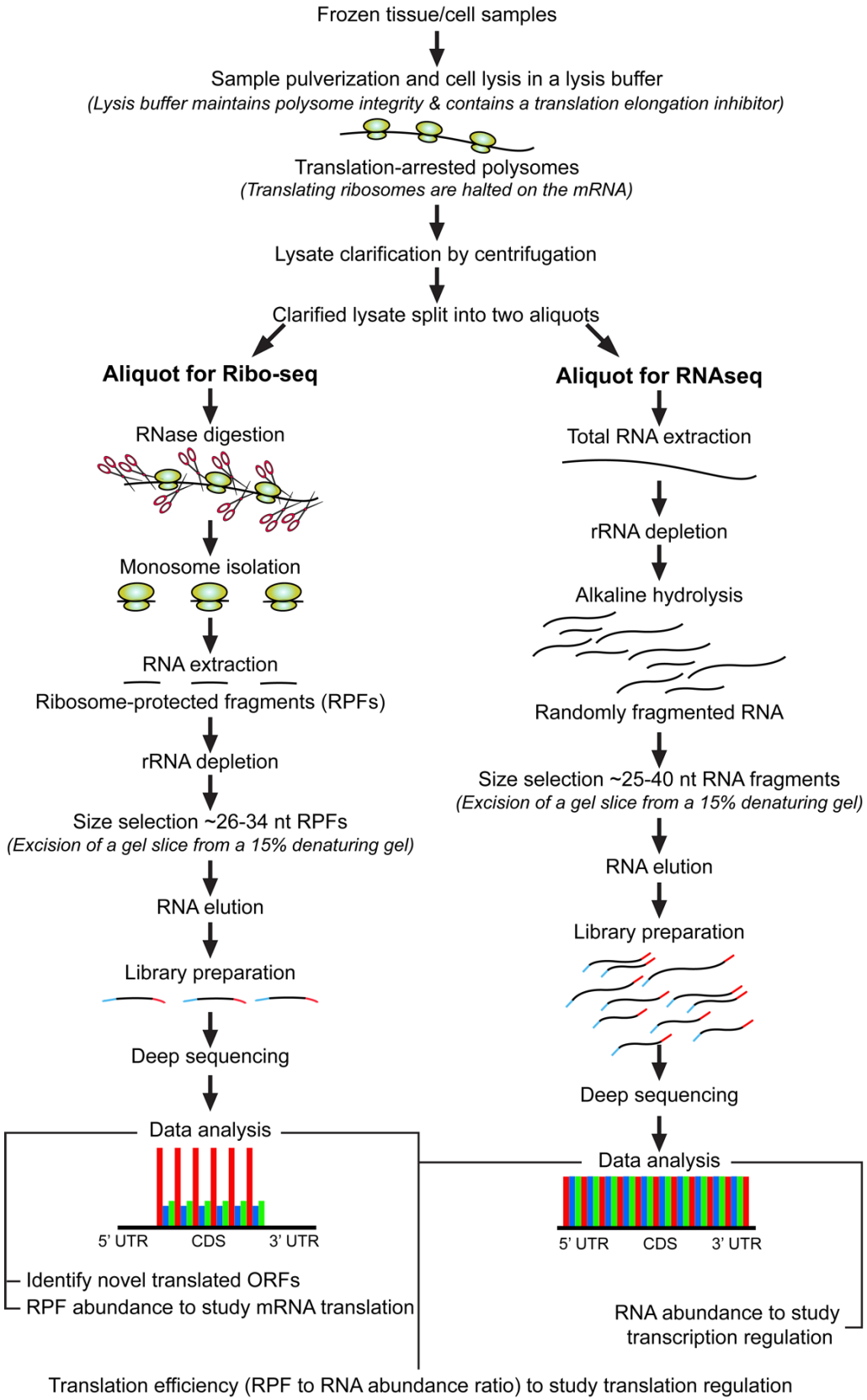

Figure 1.5. Outline of ribosome profiling and RNA sequencing methodology.

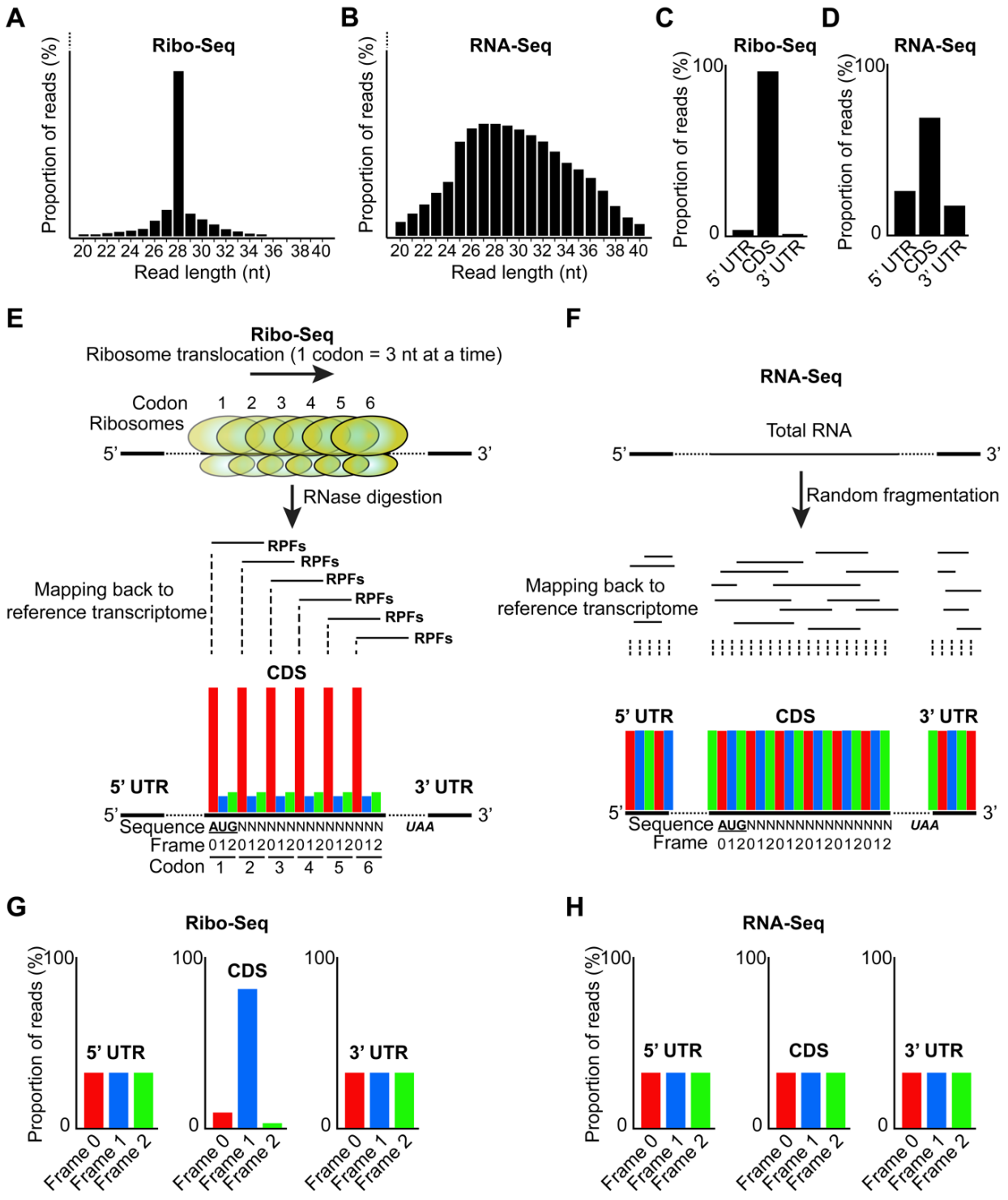

Figure 1.6. Illustration of specific hallmarks of Ribo-seq data. **(A)** Read-length distribution of Ribo-seq data shows a unimodal distribution. **(B)** Read-length distribution of RNA-seq data shows a relatively uniform and broad distribution. **(C)** Ribo-seq data maps predominantly to the CDS of all the mRNAs whereas only a few reads map to the UTRs. **(D)** Substantial number of reads from RNA-seq data map to the UTRs as well as the CDS. **(E)** Metagene analysis representing the triplet periodicity of Ribo-seq data. Because ribosomes move 3 nt at time during translation elongation, the RPFs would map to every third nt

in the reference transcriptome. **(F)** Metagene analysis representing the lack of triplet periodicity of RNA-seq data because it is obtained from random fragmentation of ribosome-free total RNAs. **(G)** Triplet periodicity of Ribo-seq data is only observed for the reads that map to the CDS (true RPFs) and not for those that map to the UTRs. **(H)** No triplet periodicity is observed in RNA-seq data for reads that map either to the CDS or to the UTRs. The figure only includes illustrations of a high-quality Ribo-seq data and does not represent real experimental data. (nt) nucleotide, (RPFs) ribosome-protected fragments, (CDS) coding DNA sequence, (UTRs) untranslated regions.

CHAPTER 2. A RAPID AND SIMPLE QUANTITATIVE METHOD FOR SPECIFIC DETECTION OF SMALLER COTERMINAL RNA BY PCR (DESCO-PCR): APPLICATION TO THE DETECTION OF VIRAL SUBGENOMIC RNAS

Pulkit Kanodia[1,2], K. Reddisiva Prasanth[3], Vicky C. Roa-Linares[3,4], Shelton S. Bradrick[3,7], Mariano A. Garcia-Blanco[3,5,6], W. Allen Miller[1,2]*

[1] Interdepartmental Genetics and Genomics Program, Iowa State University, Ames, Iowa, USA

[2] Plant Pathology and Microbiology Department, Iowa State University, Ames, Iowa, USA

[3] Department of Biochemistry and Molecular Biology, University of Texas Medical Branch, Galveston, Texas, USA

[4] Molecular and Translational Medicine Group, Institute of Medical Research, Faculty of Medicine University of Antioquia, Medellin, Colombia

[5] Programme of Emerging Infectious Diseases, Duke-NUS Medical School, Singapore

[6] Institute of Human Infections and Immunity, University of Texas Medical Branch, Galveston, Texas, USA

[7] Present address: MRIGlobal, Kansas City, MO 64110, USA

* Corresponding author: wamiller@iastate.edu

Modified from a manuscript published in *RNA*

Author Contributions: PK conceptualized the method and conducted all experiments excluding ZIKV template construction, ZIKV infections, and ZIKV northern blot hybridization. KRP conducted ZIKV infections and northern blot hybridization. VCRL constructed ZIKV templates for *in vitro* transcription. PK and WAM designed the experiments and wrote the draft manuscript. All authors edited the manuscript. WAM supervised PK, and SSB and MAGB supervised VCRL and KRP.

Abstract

RNAs that are 5′-truncated versions of a longer RNA but share the same 3′ terminus can be generated by alternative promoters in transcription of cellular mRNAs or by replicating RNA viruses. These truncated RNAs cannot be distinguished from the longer RNA by a simple two-primer RT-PCR because primers that anneal to the cDNA from the smaller RNA also anneal to—and amplify—the longer RNA-derived cDNA. Thus, laborious methods, such as northern blot hybridization, are used to distinguish shorter from longer RNAs. For rapid, low-cost, and specific detection of these truncated RNAs, we report detection of smaller coterminal RNA by PCR (DeSCo-PCR). DeSCo-PCR uses a nonextendable blocking primer (BP), which outcompetes a forward primer (FP) for annealing to longer RNA-derived cDNA, while FP outcompetes BP for annealing to shorter RNA-derived cDNA. In the presence of BP, FP, and the reverse primer, only cDNA from the shorter RNA is amplified in a single-tube reaction containing both RNAs. Many positive strand RNA viruses generate 5′-truncated forms of the genomic RNA (gRNA) called subgenomic RNAs (sgRNA), which play key roles in viral gene expression and pathogenicity. We demonstrate that DeSCo-PCR is easily optimized to selectively detect relative quantities of sgRNAs of red clover necrotic mosaic virus from plants and Zika virus from human cells, each infected with viral strains that generate different amounts of sgRNA. This technique should be readily adaptable to other sgRNA-producing viruses, and for quantitative detection of any truncated or alternatively spliced RNA.

Introduction

Many positive sense RNA viruses generate 3′ coterminal subgenomic RNAs (sgRNAs) in infected cells. These include many pathogens such as human norovirus, chikungunya, Zika, and dengue viruses, and important plant pathogens such as barley yellow dwarf (BYDV) and maize

chlorotic mottle viruses. Most viral sgRNAs, including those of the above viruses, are simply 5′-truncated versions of the viral genome, usually being less than half the length of the full-length genomic RNA (Miller and Koev 2000; Sztuba-Solińska et al. 2011). sgRNAs can serve as mRNAs for translation of open reading frames (ORFs) located downstream from the 5′-proximal ORF(s) that are translated from genomic RNA (Sztuba-Solińska et al. 2011). More recently, sgRNAs have been found that are derived from the 3′ untranslated region (UTR) of the viral genome, and thus function as noncoding sgRNAs (ncsgRNAs) (Iwakawa et al. 2008; Pijlman et al. 2008; Peltier et al. 2012).

For plant viruses in the *Tombusviridae*, *Luteoviridae*, *Solemoviridae*, *Bromoviridae*, *Virgaviridae*, *Benyviridae* families, and the order Tymovirales, and animal viruses in the *Togaviridae* (e.g., chikungunya virus), *Caliciviridae* (e.g., human norovirus), *Astroviridae* (human astrovirus) families, ORFs encoding the RNA-dependent RNA polymerase and associated replicase proteins, located in the 5′ half of the genome, are translated from the viral genomic RNA (gRNA). However, for translation of 5′ distal ORFs that encode proteins required at middle or late stages of infection, such as structural proteins, one or more sgRNAs are generated (Monroe et al. 1993; Koev and Miller 2000; Miller and Koev 2000; Sztuba-Solińska et al. 2011; Royall and Locker 2016; Contigiani and Diaz 2017). For example, the nonstructural polyprotein ORF (including the replicase) of members of *Togaviridae* is translated from gRNA, while the polyprotein ORF encoding structural proteins is translated from a sgRNA that is 3′ coterminal with the gRNA (Strauss and Strauss 1994).

Certain viruses in the *Luteoviridae* (Shen and Miller 2004; Shen et al. 2006; Miller et al. 2015), *Tombusviridae* (Scheets 2000; Iwakawa et al. 2008) and *Benyviridae* (Peltier et al. 2012; Flobinus et al. 2016, 2018) families, and all viruses in the *Flavivirus* genus (Pijlman et al. 2008;

Roby et al. 2014) generate ncsgRNAs from the 3′ UTR that play an important role in regulating virus gene expression, virus movement and transmission, with major effects on pathogenicity and symptom development. However, their mechanisms of action are only just beginning to be understood. For example, (i) BYDV sgRNA2 regulates translation of gRNA and sgRNA1 (Shen et al. 2006; Miller et al. 2015), (ii) beet necrotic yellow vein virus sgRNA3 is required for long-distance movement in plants (Peltier et al. 2012), and (iii) subgenomic flavivirus RNAs (sfRNA) interfere with the innate immune systems of mammalian and insect hosts (Schnettler et al. 2012; Bidet and Garcia-Blanco 2014; Bidet et al. 2014; Roby et al. 2014; Manokaran et al. 2015; Donald et al. 2016; Miller et al. 2016; Finol and Ooi 2019).

In this study, we detected sgRNAs of red clover necrotic mosaic virus (RCNMV) and Zika virus (ZIKV). RCNMV (Family: *Tombusviridae*, Genus: *Dianthovirus*, *Fig. 2.1-A*) is a bipartite plant virus with positive-sense single-stranded gRNA1 and gRNA2 (Gould et al. 1981; Hiruki 1987). During infection, a coding sgRNA generated from the 3′ end of gRNA1 serves as the mRNA for viral coat protein translation (Sit et al. 1998). RCNMV also generates a ncsgRNA, SR1f, as a stable degradation product formed by incomplete degradation of gRNA and coat protein sgRNA by a plant 5′ to 3′ exonuclease (Iwakawa et al. 2008; Steckelberg et al. 2018). SR1f is not required for infection of the highly susceptible host plant, *Nicotiana benthamiana*, as an RCNMV mutant that is unable to generate SR1f accumulates substantial levels of the viral genomic RNAs and the coat protein sgRNA (Iwakawa et al. 2008). However, this mutant is unable to accumulate substantially in *Arabidopsis thaliana*.

ZIKV (Family: *Flaviviridae*; Genus: *Flavivirus*; *Fig. 2.1-B*) usually causes an acute, mild febrile illness, but in the 2015 South and Central American epidemic was found to cause neurological disorders such as microcephaly in infants born to infected mothers and Guillain-

Barre syndrome in adults (Beckham et al. 2016; Ferraris et al. 2019). One of the molecular determinants of pathogenicity of ZIKV and other flaviviruses is the sfRNA, which, like SR1f, is an incomplete degradation product of gRNA by a host 5′ to 3′ exonuclease (Pijlman et al. 2008; Silva et al. 2010). RCNMV SR1f and the sfRNAs of ZIKV and other flaviviruses are not required for viral replication but increase virus titer and disease severity (Iwakawa et al. 2008; Pijlman et al. 2008; Moon et al. 2012, 2015; Schnettler et al. 2012; Schuessler et al. 2012; Bidet et al. 2014; Roby et al. 2014; Akiyama et al. 2016; Göertz et al. 2016; Lee et al. 2019). For example, dengue virus disease severity appears to correlate positively with sfRNA level in infected cells. Screening viral mutants that vary in level of sgRNA accumulation is crucial to the understanding of the role of these sgRNAs in viral infection.

In order to (i) decipher the role of ncsgRNA, (ii) identify cis- or trans-acting RNA elements in a sgRNA, (iii) understand the function of proteins encoded by sgRNAs, (iv) identify promoters required for sgRNA synthesis, (v) undertake field surveys for viral strains with particularly severe symptoms controlled by sgRNA levels, etc., rapid detection of sgRNA and measurement of expression is important. While gRNA can be measured by a simple two-primer based RT-PCR with PCR primers that can hybridize to any region across the gRNA, detection of sgRNAs as distinct from gRNA currently requires more cost- and time-intensive methods, usually northern blot hybridization (Kessler et al. 1990; Amiss and Presnell 2005). In addition, northern blot hybridization is less sensitive compared to RT-PCR and requires several micrograms of total RNA as input. Indirect ways of estimating sgRNA levels include quantitative RT-PCR (qRT-PCR) in which abundance of gRNA, as calculated by gRNA-specific qRT-PCR, is subtracted from total abundance of gRNA and sgRNA, as calculated by qRT-PCR using primers that anneal to their coterminal region (Bidet et al. 2014), or deep sequencing (e.g.,

Illumina) of total RNA in an infected cell and simply comparing the number of reads that map to the sgRNA region vs the upstream gRNA. However, this too is expensive, time-consuming and requires much bioinformatics analysis post-sequencing. Also, Illumina read counts can vary significantly across a viral genome in the absence of sgRNA (Xu et al. 2019).

To overcome the difficulties and costs associated with the above methods, an RT-PCR approach would be preferable. However, as mentioned above, a simple two-primer based RT-PCR cannot distinguish sgRNA-derived cDNA (sgRNA cDNA) from gRNA-derived cDNA (gRNA cDNA). For an RT-PCR reaction with coterminal RNAs, any primer-pair designed to amplify the sgRNA cDNA will also anneal to the gRNA cDNA, owing to their coterminal ends, resulting in amplification from both, making RT-PCR futile for specific detection of sgRNA. To prevent amplification from gRNA cDNA and enable selective amplification from sgRNA cDNA, we have developed a three-primer based RT-PCR approach, which we name DeSCo-PCR (detection of smaller coterminal RNA by PCR). This method is easy to optimize, relatively simple, quick and inexpensive for specific detection of sgRNAs.

Results

Overview of the DeSCo-PCR method

DeSCo-PCR utilizes a nonextendable blocking primer (BP) with two amplification primers to prevent amplification of gRNA under conditions that permit amplification of the sgRNA *(Fig. 2.2)*. Firstly, cDNA to be used as template for DeSCo-PCR is prepared from total RNA, using a virus sequence-specific reverse primer *(Fig. 2.2-A)*. DeSCo-PCR uses three primers *(Fig. 2.2-B)*: (i) a reverse primer (RP) that anneals to gRNA cDNA and sgRNA cDNA at their coterminal 5′ end (complementary to the 3′-coterminal ends of the viral RNAs), (ii) a forward primer (FP), containing the sequence of the 5′ end of the sgRNA, that can anneal to both

gRNA cDNA and sgRNA cDNA, and (iii) a long (~50-nt) forward nonextendable BP containing a contiguous gRNA sequence upstream and downstream from the sgRNA 5′ end followed by a tract of nonviral bases at its 3′ end, which makes it nonextendable by the polymerase (explained in detail below). Under PCR conditions, BP out-competes FP for annealing to gRNA cDNA because it has more bases that can anneal to gRNA cDNA. However, BP is nonextendable and hence, amplification cannot occur from gRNA cDNA. For annealing to sgRNA cDNA, FP outcompetes BP because FP has more bases that can anneal to sgRNA cDNA, resulting in amplification of sgRNA cDNA. Thus, in the presence of all three primers, only sgRNA cDNA is amplified but not the gRNA cDNA *(Fig. 2.2-C).*

Blocking primer design for DeSCo-PCR

Blocking primer (BP) is a DeSCo-PCR specific primer that is 50–60-nt long and has three regions *(Fig. 2.2-B; dashed box)*: (i) competitive region (CR), the first ~40-nt of the primer that can anneal only to gRNA sequence (just upstream of the 5′ end of sgRNA sequence) but not to sgRNA sequence; (ii) blocking region (BR), the ~10-nt middle region of the primer that can anneal to both gRNA and sgRNA sequences at the 5′ end of the sgRNA (entire sequence of BR is present in the FP); (iii) nonextendable region (NER), the 3′-terminal ~6-nt of the primer with any nontemplate bases that ensure that the 3′ end of the primer cannot anneal to either the gRNA or sgRNA sequence. Because the 3′ end of the primer cannot anneal, the polymerase cannot extend and hence, amplify from the template. FP and CR-BR sequences of BP can anneal to gRNA sequence. The melting temperature (Tm) of CR-BR should be significantly higher than FP so that BP will out-compete FP for annealing to gRNA sequence during PCR. FP and BR can anneal to sgRNA sequence. Tm of FP should be higher than that of BR so that FP will out-

compete BP for annealing to sgRNA sequence. The NER should not be included for any Tm calculations. It is preferable to calculate Tm according to buffer conditions of the PCR reaction. For example, if Promega GoTaq master mix is used, Tm should be calculated using the "Tm for Oligos" tool on its website (https://www.promega.com/resources/tools/biomath/) with the appropriate master mix specified.

General guidelines for optimizing DeSCo-PCR

For optimizing DeSCo-PCR conditions, either *in vitro* transcribed gRNA and sgRNA can be reverse transcribed and the resulting first-strand cDNA product can be used as template for PCR, or one can use DNA templates with (i) sequence of sgRNA and (ii) at least partial gRNA sequence that includes sgRNA sequence and ~100 nt upstream of sgRNA. All DeSCo-PCR reactions should be conducted with low ramp-rate for the annealing step of PCR.

The main determinant of PCR parameters is the template concentration. Therefore, *in vitro* transcribed (IVT) viral RNA concentration or the dilution of cDNA that gives similar band intensity by RT-PCR to that from infected tissues should be determined to serve as a positive control. Next, a gradient PCR with ~25 cycles should be performed with FP plus RP to determine the maximum annealing temperature (Tm) that results in amplification from gRNA cDNA (or sgRNA cDNA). At this Tm, DeSCo-PCR should be carried out with an increasing molar ratio of BP to FP to determine the ratio at which there is amplification predominantly from sgRNA cDNA but not (or only faintly) from gRNA cDNA. A positive control with FP plus RP, and a negative control with BP plus RP should be used with both gRNA cDNA and sgRNA cDNA templates to ensure that any lack of amplification is not because of a failed PCR reaction and any successful amplification is not from BP, respectively. Next, Tm can be finely tuned if required, with the selected BP:FP ratio at which sgRNA cDNA is amplified but amplification

from gRNA cDNA is completely blocked. Finally, DeSCo-PCR should be conducted with twofold dilution of sgRNA to determine the lower level of detection of sgRNA and the Tm can be further fine-tuned accordingly.

To use DeSCo-PCR as a quantitative assay for measuring the relative expression of sgRNA, twofold serial dilutions of sgRNA cDNA can be used as templates for simple- and DeSCo-PCR with varying number of PCR cycles to determine the optimal number of cycles at which DeSCo-PCR reflects the expected sgRNA cDNA dilution.

Proof-of-concept using *in vitro* transcribed (IVT) gRNA and sgRNA

To test the concept of DeSCo-PCR, 0.5 pmol each of *in vitro* transcribed (IVT) RCNMV RNA1, RCNMV SR1f, ZIKV gRNA-mimic1 and ZIKV sfRNA1 were reverse transcribed using either RCNMV reverse primer (RRP) for the RCNMV RNAs or ZIKV reverse primer (ZRP) for the ZIKV RNAs. ZIKV gRNA-mimic1 *(Fig. 2.1-B)* is a 5′-truncated version of the genomic RNA consisting of the 3′-terminal 1009 nt, to serve as a convenient stand-in for full-length ZIKV RNA for initial RT-PCR experiments. cDNA reaction products were diluted fivefold and 2 µL of these diluted cDNA reaction products were used as template for PCR.

Simple PCR with RRP plus RCNMV forward primer (RFP) as a positive control amplified both the cDNA from RNA1 (RNA1 cDNA) and cDNA from SR1f (SR1f cDNA), demonstrating successful amplification under PCR conditions *(Fig. 2.3-A, lanes 1,4)*. PCR with RRP plus RCNMV blocking primer (RBP) did not amplify from either RNA1 cDNA or SR1f cDNA, demonstrating that that RBP is nonextendable under these PCR conditions *(Fig. 2.3-A, lanes 2,5)*. DeSCo-PCR with RRP plus RFP plus RBP resulted in amplification only from SR1f cDNA *(Fig. 2.3-A, lane 6)* but not from RNA1 cDNA *(Fig. 2.3-A, lane 3)*. Similar results were obtained using the ZIKV primers for DeSCo-PCR on the ZIKV RNA templates *(Fig. 2.3-B)*.

It is noteworthy that an unexpected, very low molecular weight band appeared in the PCR reactions containing BP *(Fig. 2.4)*. To determine whether it is BP-derived primer-dimer, or if it is a nonspecific amplification product, we conducted PCR with BP plus RP, and FP plus BP plus RP, using sfRNA1 cDNA or water as template. The low molecular weight product appeared, even in the absence of a template, indicating that it is a BP-derived "primer-dimer" *(Fig. 2.5, lanes 2,3,5,6)*. In spite of the presence of primer-dimer, detection of sgRNA and measurement of its relative abundance (below) was not affected.

Additionally, there is a small but reproducible increase in mobility of the DeSCo-PCR product compared to the FP-RP PCR product even though both products result from amplification by the FP-RP primer pair *(Fig. 2.3)*. We found that this difference was due to the presence of the abundant primer-dimer formed only in DeSCo-PCR. We showed this by conducting PCR using ZIKV sfRNA1 cDNA as template with FP plus RP that yields only the band of interest and PCR with BP plus RP that yields only the primer-dimer, mixed these PCR products, and then loaded this mixture in a single well for agarose gel electrophoresis. Mobility of the band of interest from the FP-RP PCR, in the presence of the BP + RP primer-dimer, was identical to that from DeSCo-PCR *(Fig. 2.5, lanes 1–4)*. The reason for the slight mobility change due to the primer-dimer is unclear, but it does not affect the utility of DeSCo-PCR.

Quantitative analysis for measuring relative amounts of sgRNA by DeSCo-PCR

To test if DeSCo-PCR can be used as a quantitative assay for measuring relative amounts of sgRNA, we first tested whether PCR of sgRNA-derived cDNA (in the absence of full-length viral cDNA) was quantitative in the presence of the three primers. *In vitro* transcribed RCNMV SR1f and ZIKV sfRNA1 were reverse transcribed using RRP and ZRP, respectively, and twofold serial dilutions of the resulting cDNA were used as template for PCR. Relative amounts of

sgRNA-derived cDNA in each sample was estimated by measuring the relative intensity of each band with respect to that of undiluted sample. DeSCo-PCR with RRP plus RFP plus RBP showed reduction in band intensity with SR1f cDNA dilution *(Fig. 2.6-A)*. Furthermore, relative band intensity, as measured by DeSCo-PCR, precisely reflected the expected SR1f cDNA dilution *(Fig. 2.6-B)*.

We next tested whether DeSCo-PCR can be used as a quantitative assay in the presence of plant total RNA and RCNMV RNA1. Twofold dilutions of IVT SR1f were mixed with a constant amount of *N. benthamiana* total RNA and IVT RCNMV RNA 1 (hence, gRNA and sgRNA are in different ratios). Five hundred nanograms of *N. benthamiana* total RNA was mixed with 0.1 pmol IVT RNA1 and twofold serial dilutions of IVT SR1f starting with an undiluted amount of 0.1 pmol *(Fig. 2.6-C)*. Subsequently, the RNA mixes were reverse transcribed with RRP followed by PCR. RNA1-specific PCR with RNA1-specific forward primer (RCNMV_909_FP) plus RNA1-specific reverse primer (RCNMV_1262_RP) (both far upstream of the sgRNA region of the genome) showed that the band intensity across all samples was uniform, as expected *(Fig. 2.6-D, Gel 1)*. DeSCo-PCR with RRP plus RFP plus RBP that amplifies only SR1f showed reduction in band intensity with SR1f dilution *(Fig. 2.6-D, Gel 2)*. Relative band intensities were used as proxy for measuring the relative amounts of RNA1 or SR1f. The relative amount of RNA1 was mostly uniform across all samples as measured by RNA1-specific PCR, as expected *(Fig. 2.6-E)*. Relative amounts of SR1f (blank subtracted) from DeSCo-PCR reflected the expected SR1f dilutions *(Fig. 2.6-E)*. Relative band intensity calculation by blank-subtracted values shows that there is either a very small amount of amplification that occurs from RNA1 or it is just the background fluorescence. If relative

intensities were calculated using no-SR1f sample subtracted values, the estimation of relative amounts of SR1f became even more accurate *(Fig. 2.6-E)*.

We also tested whether the detection of ZIKV sfRNA1 by DeSCo-PCR was quantitative. As for RCNMV, DeSCo-PCR of dilutions of ZIKV sfRNA1-derived cDNA with ZRP plus ZFP plus ZBP showed a reduction in band intensity proportional to the cDNA dilution *(Fig. 2.7-A, B)*. These results show that DeSCo-PCR can precisely measure relative amounts of sgRNA cDNA.

To test if DeSCo-PCR can be used as a quantitative assay in the presence of ZIKV gRNA, twofold dilutions of IVT sfRNA1, starting at 0.1 pmol, were mixed with constant levels (0.1 pmol) of IVT gRNA-mimic1 *(Fig. 2.7-C)*. This RNA mix was reverse transcribed with ZRP followed by PCR. gRNA-mimic1-specific PCR with ZIKV gRNA-specific forward primer (ZIKV_ 9827_FP) plus ZIKV gRNA-specific reverse primer (ZIKV_10115_RP) showed that the band intensity across all samples was uniform, as we observed with RCNMV *(Fig. 2.7-D, Gel 1)*. DeSCo-PCR with ZRP plus ZFP plus ZBP that amplifies only sfRNA1 showed reduction in band intensity with sfRNA1 dilution *(Fig. 2.7-D, Gel 2)*. The relative amount of gRNA-mimic1 was uniform across all samples as measured by gRNA-mimic1-specific PCR, as expected *(Fig. 2.7-E)*. The relative amount of sfRNA1 (blank subtracted) from DeSCo-PCR reflected the expected sfRNA1 dilutions *(Fig. 2.7-E)*. If relative intensities were calculated using no-sfRNA1 sample subtracted values, the estimation of relative amounts of sfRNA1 became even more accurate. Collectively, these experiments show that DeSCo-PCR can quantitatively detect sgRNAs, even in the presence of gRNA, and allow calculation of relative differences in sgRNA/gRNA ratio.

Specific detection of sgRNA in virus-infected tissues

We next tested whether DeSCo-PCR could distinguish viral genomic from subgenomic RNA in infected tissues. We first tested RCNMV (R) in the plant host *N. benthamiana*, taking advantage of a viral mutant (RΔSR1f) we constructed, which contains a six-base substitution in its xrRNA structure at the 5′ end of the SR1f sequence, preventing it from generating the noncoding subgenomic SR1f RNA (Iwakawa et al. 2008). Northern blot hybridizations with a probe complementary to the 3′ end of RCNMV RNA1 revealed ample amounts of SR1f from *N. benthamiana* plants infected with wild-type RCNMV, and no (or vanishingly small amounts of) SR1f in plants infected with RCNMVΔSR1f, while both sets of plants accumulated substantial amounts of RCNMV genomic RNA1 and CPsgRNA *(Fig. 2.8-A)*. cDNA was prepared from 1 µg of total RNA from RCNMV-infected and RCNMVΔSR1f-infected *N. benthamiana* leaves using RRP followed by PCR. Because RCNMVΔSR1f has a six-base substitution at the 5′ end of the SR1f sequence, forward and BPs incorporating this substitution, RFP-m1 and RBP-m1, respectively, were used for PCR with cDNA from RCNMVΔSR1f-infected samples. PCR with RRP plus RFP, and RRP plus RFP-m1 resulted in amplification from both RCNMV-infected and RCNMVΔSR1f-infected cDNA samples, respectively, confirming successful virus infection *(Fig. 2.8-B, L1 and L2)*. PCR with RRP plus RBP, and RRP plus RBP-m1 primers did not result in amplification showing that the RBP and RBP-m1 are nonextendable under PCR conditions *(Fig. 2.8-B, L3 and L4)*. DeSCo-PCR with RRP plus RFP plus RBP amplified only from RCNMV-infected cDNA samples *(Fig. 2.8-B, L5)* while DeSCo-PCR with RRP plus RFP-m1 plus RBP-m1 resulted in no amplification from RCNMVΔSR1f-infected cDNA samples *(Fig. 2.8-B, L6)* demonstrating that SR1f is detected only in wild-type RCNMV-infected plants and not in RCNMVΔSR1f-infected plants.

We next tested ZIKV RNA accumulation in HeLa cells, taking advantage of a mutant, 10ΔZIKV (deletion of nts 10,650 to 10,659 in the 3′UTR) that produces a lower ratio of sfRNA1/gRNA than wild-type ZIKV (Shan et al. 2017b). Northern blot hybridization with a 3′ probe complementary to ZIKV RNA revealed much greater levels of sfRNA1 in cells infected with wild-type virus than with the mutant. In this case, the genomic RNA levels were also reduced in 10ΔZIKV infection, but the sfRNA1 was virtually undetectable by northern blot hybridization in 10ΔZIKV-infected cells *(Fig. 2.8-C)*. cDNA was prepared from 1 µg total RNA from mock-infected, wild-type ZIKV-infected and 10ΔZIKV-infected HeLa cells using ZRP. PCR of the resulting cDNA template with ZRP plus ZFP primers amplified both ZIKV-infected and 10ΔZIKV-infected cDNA samples, but not from mock-infected cDNA samples, as expected *(Fig. 2.8-D, lanes 1–3)*. There was no amplification using ZRP plus ZBP primer pairs, confirming that the ZBP is nonextendable under the PCR conditions *(Fig. 2.8-D, lanes 4,5)*. DeSCo-PCR with ZRP plus ZFP plus ZBP primers yielded a product from cDNA from cells infected with wild-type ZIKV *(Fig. 2.8-D, lane 6)*, but only a very faint band from 10ΔZIKV-infected cells *(Fig. 2.8-D, lane 7)*, reflecting the ratios of sfRNA1/gRNA observed by northern blot hybridization and published previously (Shan et al. 2017b). Collectively, these experiments demonstrate that DeSCo-PCR can be used for specific, quantitative detection of sgRNAs from hosts in different kingdoms infected by unrelated viruses.

Discussion

DeSCo-PCR is a simple, quick, inexpensive and sensitive assay that can selectively amplify a viral sgRNA from a pool of RNA containing host total RNA, viral gRNA and other sgRNAs. Even though northern blot hybridization has certain advantages (e.g., the entire sequence of sgRNA need not be known and it can detect gRNA and multiple sgRNAs

simultaneously), DeSCo-PCR can easily detect sgRNAs in a variety of experimental settings to rapidly screen for sgRNA production. Similar to northern blot hybridization, DeSCo-PCR can be used for measuring relative abundance of sgRNAs in different experimental conditions such as those from mutant viral genomes or in transgenic hosts. While it does not measure absolute amounts of RNA, DeSCo-PCR quantitatively measures relative amounts of sgRNA and can detect differences in ratios of sgRNA:gRNA between different virus isolates. The advantages of DeSCo-PCR are particularly beneficial for experiments where several viral mutants or isolates need to be screened rapidly to identify the relative amount of a particular sgRNA each viral isolate produces. For examples, 10ΔZIKV produces sfRNA1 at a very low sfRNA1/genomic RNA ratio and has reduced accumulation and attenuated pathogenicity compared to wild-type ZIKV. This makes 10ΔZIKV a vaccine candidate against ZIKV infection (Shan et al. 2017a, b).

In addition, DeSCo-PCR can be used by clinics or laboratories that do not have access to radioisotopes, expensive nonradioactive chemiluminescent northern blot reagents or an imager required for detection of fluorescent probes used in northern blots. For viruses that require replication to generate sgRNAs, DeSCo-PCR could be used as a quick or confirmatory assay to determine whether a virus is replicating, without need for measuring increases in total RNA or infectious units over time.

DeSCo-PCR is not limited to virology. It can be used for detecting smaller coterminal RNAs of any origin. Coterminal RNAs are present in eukaryotes as truncated RNA isoforms transcribed by alternative transcription start sites (TSS) or may be produced as alternatively spliced RNA isoforms. These truncated mRNA isoforms may differ in their 5′ UTR, affecting their stability and translation efficiency or differ in their encoded protein domains, affecting their localization, function and protein stability (Rojas-Duran and Gilbert 2012; Wang et al. 2016;

Galipon et al. 2017). For example, in humans, adenosine deaminases acting on RNA (ADARs) are involved in RNA editing, and the ADAR1 gene produces two coterminal mRNA isoforms, ADAR1-p150 and ADAR1-p110 from an interferon-inducible promoter and a constitutive promoter, respectively (Galipon et al. 2017). Additionally, next-generation sequencing and computational analysis are often used to identify, predict functions and determine differential expression of these transcript isoforms with a certain degree of confidence (Kandoi and Dickerson 2017, 2019; Qin et al. 2018). However, these analyses are often followed by molecular assays for validation and DeSCo-PCR provides a simple alternative to northern blot hybridization for confirming the production of a truncated RNA isoform with coterminal ends and measuring their relative abundance.

Because DeSCo-PCR involves competition between blocking and forward primers for selective annealing to gRNA or sgRNA cDNA, it may be possible to design primers that tolerate a few mismatched bases at the 5′ end of sgRNA in cases where the exact 5′ end nucleotide of the sgRNA has not been determined precisely. Also, it may be possible to use a BP terminating in a dideoxynucleotide (Sanger et al. 1977) to make it universally nonextendable, instead of the mismatched 3′ terminal sequence on our BPs. This may eliminate the production of BP-derived primer-dimer and therefore, make DeSCo-PCR adaptable to qRT-PCR. In addition, a BP with a few locked nucleic acid (LNA) (Koshkin et al. 1998; Ballantyne et al. 2008; Veedu et al. 2008) nucleotides in the BP-CR region would increase its binding affinity to gRNA cDNA, helping BP to out-compete FP for annealing to gRNA cDNA at lower annealing temperatures, which would be more optimal for amplification. However, use of dideoxynucleotides or LNAs would increase primer costs many-fold. Although presently DeSCo-PCR cannot be used for absolute quantification of the number of copies of a sgRNA by qRT-PCR because of amplification of

primer-dimer *(Fig. 2.4)*, it can reliably be used to quantitatively compare the relative abundance of sgRNAs of different virus strains or mutants in a highly sensitive manner. Similar to northern blot hybridization, DeSCo-PCR requires some optimization with every virus, but this can be done in a short time (2 or 3 d) *(Table 2.1)*. In summary, DeSCo-PCR provides a simple, readily optimized, cost-effective method for rapid, sensitive quantification of viral subgenomic RNAs in only a limited amount of total RNA and without the use of expensive and hazardous chemicals.

Materials and Methods

Oligonucleotide synthesis

All primers were synthesized by Integrated DNA Technologies and purified by standard desalting. Sequences and genomic positions of primers that were used for construction of pRC169c, pRSR1f, pR1m1, ZIKV gRNA-mimic1 PCR product, and ZIKV sfRNA1 PCR product are listed in *Table 2.2*. Sequences and genomic positions of primers that were used for all RT-PCR experiments, including DeSCo-PCR, are listed in *Table 2.3*.

Plasmid construction

Full-length infectious cDNA clones of RCNMV Australian strain RNA1 (pRC169) and RNA2 (pRC2|G) (Xiong and Lommel 1991; Sit et al. 1998) were kindly provided by Dr. Tim L. Sit and Dr. S.A. Lommel. pRC169 and pRC2|G are cDNA clones with a T7-promoter for *in vitro* transcription of infectious RNA1 and RNA2, respectively. pRC169 was sequenced by Sanger sequencing and was found to contain several base changes compared to the sequence from NCBI (GenBank: J04357). Two of the base changes, at positions 3462 and 3494, were present near the 5′ end of SR1f and therefore, were changed from C to T and G to A, respectively, using Q5 Site-Directed Mutagenesis kit (NEB #E0554) according to manufacturer's

protocol with primers 3UTR_R1_corrected_for and 3UTR_R1_corrected_rev. The corrected plasmid, pRC169c, was used as template for construction of pRSR1f and pR1m1, and as template for *in vitro* transcription of infectious RCNMV RNA1.

pRSR1f. pRSR1f is a cDNA clone with T7-promoter followed by SR1f sequence for *in vitro* transcription of SR1f. A Q5 Site-Directed Mutagenesis kit (NEB #E0554) was used according to manufacturer's protocol. A DNA fragment with the T7 promoter sequence, vector sequence and SR1f sequence was amplified from pRC169c with the following PCR reaction composition and conditions: Q5-hot start high fidelity 2× master mix (1×), T7-rev primer (0.5 µM), SR1f_for primer (0.5 µM), pRC169c as template (10 ng); initial denaturation at 98°C for 30 sec; 25 cycles of denaturation at 98°C for 10 sec, annealing at 60°C for 30 sec, extension at 72°C for 2.5 min; final extension at 72°C for 2 min. This was followed by ligation, according to manufacturer's protocol, to circularize the PCR product. Subsequently, the plasmid was transformed in *E. coli* sigma 10 cells and colonies were screened in LB-agar plates with ampicillin. Plasmids were extracted from selected colonies and the sequence was verified by Sanger sequencing.

pR1m1. pR1m1 is an infectious cDNA clone of RCNMV RNA1 (RNA1-m1) that does not generate SR1f during infection. pR1m1 has a six-base substitution ("TGTAGC" to "ACGTTG") in pRC169c (nts 3462 to 3467) that disrupts the xrRNA structure required for SR1f production (Iwakawa et al. 2008). A Q5 Site-Directed Mutagenesis kit (NEB #E0554) was used according to manufacturer's protocol. The DNA fragment was amplified by PCR with the following reaction composition and conditions: Q5-hot start high fidelity 2× master mix (1×), SR1f.m1_for primer (0.5 µM), SR1f.m1_rev primer (0.5 µM), pRC169c as template (10 ng); initial denaturation at 98°C for 30 sec; 25 cycles of denaturation at 98°C for 10 sec, annealing at

59°C for 30 sec, extension at 72°C for 4 min; final extension at 72°C for 2 min. This was followed by ligation, according to manufacturer's protocol, to circularize the PCR product. Subsequently, the plasmid was transformed in *E. coli* sigma 10 cells and colonies were screened in LB-agar plates with ampicillin. Plasmids were extracted from selected colonies and the sequence was verified by Sanger sequencing.

All RCNMV cDNA clones were linearized at a unique SmaI restriction site at the precise 3′ end of the RCNMV 3′ UTR prior to *in vitro* transcription.

ZIKV gRNA-mimic1 PCR product. ZIKV gRNA-mimic1 PCR product is a DNA fragment with a T7 promoter followed by a partial sequence of ZIKV gRNA (nts 9799 to 10807). It was amplified from pFLZIKV (Shan et al. 2016) using the primers NS5 (+) forward primer 1 and sfRNA (−) reverse primer. ZIKV gRNA-mimic1 PCR product was used for *in vitro* transcription to make noninfectious ZIKV gRNA-mimic1 that was used for DeSCo-PCR experiments.

ZIKV sfRNA1 PCR product. ZIKV sfRNA1 PCR product is a DNA fragment with a T7-promoter followed by the sequence of ZIKV sfRNA1 (nts 10392 to 10807). It was amplified from pFLZIKV (Shan et al. 2016) using the primers sfRNA (+) forward primer and sfRNA (−) reverse primer. ZIKV sfRNA1 PCR product was used for *in vitro* transcription to make ZIKV sfRNA1 that was used for DeSCo-PCR experiments.

In vitro transcription

One µg linearized plasmid for all RCNMV constructs, 200 ng ZIKV sfRNA1 PCR product, and 500 ng ZIKV gRNA mimic1 PCR product were used as templates for *in vitro* transcription using MEGAscript T7 Transcription kit (Invitrogen #AM1334) followed by DNase treatment according to manufacturer's protocol. The transcription reaction was carried out at

37°C for 4 h and DNase treatment at 37°C for 30 min. Subsequently, RNA was purified using Zymo RNA Clean & Concentrator -5 kit (Zymo Research #R1015) and eluted in nuclease-free water.

Virus inoculation and RNA extraction

RCNMV. *Nicotiana benthamiana* plants at the four-leaf stage were used for inoculations. Two leaves per plant were inoculated. Per leaf, 1 µg *in vitro*-transcribed (IVT) RCNMV RNA1 plus 1 µg IVT RCNMV RNA2 were mixed in 10 mM sodium phosphate buffer (pH 6.8) and rubbed on the leaves. These are referred to as RCNMV-infected plants that make SR1f. Similarly, 1 µg IVT RCNMV RNA1-m1 plus 1 µg IVT RCNMV RNA2 were mixed in 10 mM sodium phosphate buffer (pH 6.8) and rubbed on the leaves. These are referred to as RCNMVΔSR1f-infected plants that do not make SR1f. For *Fig. 2.8*, leaves from RCNMV- and RCNMVΔSR1f-infected *N. benthamiana* were collected at 5 d post inoculation (dpi) for PCR and at 14 dpi for northern blot hybridization, pulverized and total RNA was extracted using Zymo Direct-zol RNA Miniprep (Zymo Research #R2051).

ZIKV. Hela cells were seeded at a density of 3 × 105 cells per well in a six-well plate. One day later, cells were infected with the wild-type (ZIKV-Cambodia) or mutant (10ΔZIKV) virus at an MOI of 3. After 48 h post-infection, cells were washed with PBS and total RNA was extracted from cells using the Direct-zol RNA MiniPrep kit (Zymo Research).

cDNA synthesis

Amount of *in vitro* transcribed RNA or plant/cell total RNA that were reverse transcribed is indicated in the results section. RNA (IVT or total RNA) and virus-specific reverse primer (15 pmol; same reverse primer as used for DeSCo-PCR) were mixed in nuclease-free water to 12 µL

and incubated at 65°C for 5 min, transferred to ice followed by addition of 4 µL reaction buffer, 1 µL RiboLock, 2 µL 10 mM dNTPs and 1 µL RT enzyme from RevertAid First Strand cDNA Synthesis kit (Thermo Scientific #K1621). The reaction mix was incubated at 42°C for 60 min followed by enzyme deactivation at 70°C for 5 min. The cDNA reaction products from IVT RNAs were diluted fivefold and considered as "undiluted samples" for experiments with serially diluted templates while cDNA reaction products from total RNA from infected samples were not diluted but used as is for PCR.

PCR

GoTaq G2 green master mix (Promega #M7823) was used for all PCR reactions. Simple PCR with RP plus FP as positive control, RP plus BP as negative control, DeSCo-PCR with RP plus FP plus BP, and gRNA-specific PCR were carried out in a thermocycler with the capability of controlling the ramp rate. Ramp rate of 0.5°C per second was used for the PCR reactions specified below. A 20 µL PCR reaction mix was prepared with 2-µL template and final concentration of each of the primers, if used, were as follows: 0.2 µM RP, 0.2 µM FP, 4 µM BP. BP: FP = 20: 1 was determined, empirically, as optimum for RCNMV and ZIKV, for successful DeSCo-PCR to selectively amplify sgRNA cDNA and completely block amplification from gRNA cDNA (data not shown). The primers used are mentioned below and the primer sequences can be found in *Table 2.3*. PCR conditions were as follows:

RCNMV. 98°C (2 min); 18 cycles of 98°C (30 sec), 65°C (20 sec, ramp rate = 0.5°C/sec), 72°C (30 sec); 72°C (2 min); 4°C hold. Primers used were RFP, RRP, RBP, RFP-m1, and RBP-m1.

RCNMV (RNA1-specific PCR). 98°C (2 min); 18 cycles of 98°C (30 sec), 60°C (20 sec), 72°C (30 sec); 72°C (2 min); 4°C hold. Primers used were RCNMV_909_FP and RCNMV_1262_RP.

ZIKV (with IVT templates). 98°C (2 min); 22 cycles of 98°C (30 sec), 66.5°C (20 sec, ramp rate = 0.5°C/sec), 72°C (40 sec); 72°C (2 min); 4°C hold. Primers used were ZFP, ZRP, and ZBP. ZIKV gRNA-specific PCR was carried out in the same conditions as above with primers ZKV_9827_FP and ZKV_10115_RP.

ZIKV (with infected samples as templates). 98°C (2 min); 30 cycles of 98°C (30 sec), 65°C (20 sec, ramp rate = 0.5°C), 72°C (40 sec); 72°C (2 min); 4°C hold. Primers used were ZFP, ZRP, and ZBP.

PCR reaction products were run on a 1% agarose gel, with SYBR Safe DNA gel stain (Invitrogen #S33102), in 1× TBE buffer and visualized on a Bio-Rad Gel doc. The gel images shown were cropped to show the band of interest. One thing to note is that all DeSCo-PCR performed with RCNMV and ZIKV resulted in amplification of BP-derived primer-dimer but it did not affect the relative band intensity measurement.

Measurement of relative expression of sgRNA

When the agarose gels were imaged for quantitative analysis, the exposure time was set for maximum duration at which no saturating intensity was observed in the amplified bands. Fiji software (ImageJ) was used to measure band intensity. Intensity of the background was measured from three separate regions of the gel where no band/DNA is expected, and the values were averaged. The averaged background intensity, referred to as “blank,” was subtracted from the intensity of each band from gRNA-specific PCR. For DeSCo-PCR, either the “blank” values or the band intensity of “No sgRNA” samples were considered as background intensity and were

subtracted from the band intensity of each sample. This was done three times for each gel and background-subtracted values from the three measurements were averaged. The final values were normalized with respect to the band intensity of undiluted cDNA. The values obtained from DeSCo-PCR are the relative band intensity representing the relative amount of sgRNA in each sample. For all results shown with the relative measurement of sgRNA, PCR was carried out three times and the values for the relative band intensities were averaged and plotted on a graph using Microsoft Excel. Error bars represent the standard deviation of the relative band intensities obtained from three PCR reactions.

Radiolabeled RNA probe preparation

A DNA template with SP6-promoter for transcribing a radiolabeled RNA probe that can hybridize to a positive sense strand of RCNMV RNA1 3′ UTR (nts 3605 to 3800) was prepared by PCR with the following composition and conditions: An amount of 50 µL reaction with GoTaq G2 green master mix (1×), R1.3UTR.for *(0.2 µM, 5′-TCGGACCCTGGGAAACAGGT-3′)*, R1.3UTR.SP6.rev *(5′-GATATTTAGGTGACACTATAGAGGTATGCGCCCTCTGAGC-3′, 0.2 µM)*, pRC169 as template (10 ng); initial denaturation at 95°C for 2 min; 25 cycles of denaturation at 95°C for 30 sec, annealing at 56°C for 30 sec, extension at 72°C for 30 sec; final extension at 72°C for 5 min. The underlined bases in the primer sequence represent SP6 promoter sequence. The amplified product was purified using QIAquick PCR Purification kit (Qiagen #28104) and used as a template for making a radiolabeled probe using MEGAscript SP6 Transcription kit (Invitrogen #AM1330) with the following reaction composition: An amount of 2 µL 10× reaction buffer, 2 µL 5mM AUG mix, 2.5 µL 0.1 mM CTP, 50 ng DNA template, 0.5 µL RNase OUT (Invitrogen #10777019), 2 µL SP6 enzyme, 2.5 µL CTP (α-32P; PerkinElmer #BLU008X250UC). The reaction was incubated at 37°C for 3 h followed by DNase treatment

with 1 µL Turbo DNase at 37°C for 15 min and a radiolabeled RNA probe was purified using Micro Bio-spin 30 columns (Bio-Rad #732-6251) and stored at −20°C.

Northern blot hybridization

RCNMV. An amount of 9.5 µg total RNA from noninoculated leaves of RCNMV- and RCNMVΔSR1f-infected *N. benthamiana* were mixed with an equal volume of 2× RNA loading dye (NEB #B0363S), denatured by incubating at 70°C for 10 min and 5 min on ice and loaded on a 1.2% agarose-formaldehyde gel (1.2% [w/v] agarose, 20 mM sodium phosphate buffer [pH 6.8], 8 mL of 37% formaldehyde per 100 mL of gel). Electrophoresis was carried out at 100 V for 2 h in running buffer (74 mL of 37% formaldehyde per 1 L of running buffer, 20 mM sodium phosphate buffer [pH 6.8]). Integrity and equal loading of RNA were verified by visualizing the gel on a Bio-Rad Gel doc. The gel was washed in sterile water for 5 min at room temperature (RT) and blotted to a nitrocellulose membrane by the capillary transfer method overnight using 10x saline-sodium citrate (SSC) buffer (Invitrogen #AM9763). Post-transfer, the membrane was washed in 5× SSC for 5 min at RT, dried on a paper towel, and UV-crosslinked in StrataGene UV Stratalinker 1800 using the "Auto Cross Link" option. The membrane was placed in a glass cylindrical bottle and incubated in 5 mL hybridization buffer (50% [v/v] formamide, 5× SSC buffer, 0.2 mg/mL polyanetholsulphonic acid, 0.1% [w/v] SDS, 20 mM sodium phosphate buffer [pH 6.8]) at 65°C for 1 h in a hybridization oven (VWR). The buffer was discarded, and fresh 5 mL hybridization buffer was added to the bottle with 5 µL radiolabeled RNA probe. Probe hybridization was carried out overnight in a hybridization oven at 65°C. Post hybridization washes were carried out in a hybridization oven as follows: two washes with 50 mL high salt concentration buffer (1× SSC, 0.1% [w/v] SDS) at RT for 20 min, two washes with 50 mL low salt concentration buffer (0.2× SSC, 0.1% [w/v] SDS) at 68°C for 20 min, and one wash with 50

mL 0.1× SSC buffer at RT for 20 min. The membrane was dried on a paper towel, covered in a saran wrap and placed inside the phosphor cassette with phosphor screen, imaged by autoradiography using Bio-Rad PharosFX Plus Molecular Imager.

ZIKV. An amount of 5 μg of total RNA from mock and ZIKV-infected cells was mixed with 2× formaldehyde loading buffer (Thermo Fisher Scientific), and denatured by incubating at 65°C for 15 min and 2 min on ice. Electrophoresis was performed in 1% denaturing agarose gel and stained with ethidium bromide. After electrophoresis, the gel was incubated in the alkaline buffer (0.01 N NaOH, 3 M NaCl) for 20 min and subsequently transferred to a Biodyne B nylon membrane (Thermo Fisher Scientific) by upward transfer. The membrane was crosslinked using a UV Stratalinker and blocked at 42°C using ULTRAhyb Oligo hybridization for 1 h while rotating. Blots were probed overnight rotating at 42°C with a Biotin-labeled DNA probe prepared as described in Soto-Acosta et al. (2018). After hybridization, the membrane was washed in wash buffer for 15 min at 42°C four times. The blot was incubated for 1 h at room temperature with IRDYE 800CW streptavidin (LI-COR Biosciences) in Odyssey Blocking Buffer (LI-COR Biosciences) with 1% of SDS. Later the membrane was washed three times with TBS buffer containing 0.1% tween, and the membrane was scanned using an LI-COR Odyssey.

Acknowledgments

We thank Dr. Tim L. Sit and Dr. S.A. Lommel for providing us with RCNMV clones, Dr. Surapathrudu Kanakala for his support, critique, and advice on developing the method, and Dr. Steve Whitham for advising on the manuscript. This work was supported by Iowa State University Plant Sciences Institute Faculty Scholar award (WAM); National Institute of General Medical Sciences (grant number R01 GM067104) (WAM); start-up funds from the University of

Texas Medical Branch and a University of Texas STARs Award (MAGB.); and financial support from Comité para el Desarrollo de la Investigación of University of Antioquia/Grant 2014-1041 (VCRL).

Conflict of Interest

The authors declare no conflict of interest associated with the work described in this manuscript.

References

Akiyama BM, Laurence HM, Massey AR, Costantino DA, Xie X, Yang Y, Shi PY, Nix JC, Beckham JD, Kieft JS. 2016. Zika virus produces noncoding RNAs using a multi-pseudoknot structure that confounds a cellular exonuclease. Science 354: 1148–1152. doi:10.1126/science.aah3963.

Amiss T, Presnell SC. 2006. Nucleic acid blotting techniques: theory and practice. In Molecular diagnostics: for the clinical laboratorian (ed. Coleman WB, Tsongalis GJ), pp. 31–46. Humana Press, Totowa, NJ.

Ballantyne KN, van Oorschot RAH, Mitchell RJ. 2008. Locked nucleic acids in PCR primers increase sensitivity and performance. Genomics 91: 301–305. doi:10.1016/j.ygeno.2007.10.016.

Beckham JD, Pastula DM, Massey A, Tyler KL. 2016. Zika virus as an emerging global pathogen: neurological complications of zika virus. JAMA Neurol 73: 875–879. doi:10.1001/jamaneurol.2016.0800.

Bidet K, Garcia-Blanco MA. 2014. Flaviviral RNAs: weapons and targets in the war between virus and host. Biochem J 462: 215–230. doi:10.1042/BJ20140456.

Bidet K, Dadlani D, Garcia-Blanco MA. 2014. G3BP1, G3BP2 and CAPRIN1 are required for translation of interferon stimulated mRNAs and are targeted by a dengue virus non-coding RNA. PLoS Pathog 10: e1004242. doi:10.1371/journal.ppat.1004242.

Contigiani MS, Diaz LA. 2017. *Togaviridae*. In Arthropod borne diseases (ed. Marcondes CB), pp. 115–135. Springer International Publishing, Cham.

Donald CL, Brennan B, Cumberworth SL, Rezelj VV, Clark JJ, Cordeiro MT, Freitas de Oliveira França R, Pena LJ, Wilkie GS, Da Silva Filipe A, Davis C, Hughes J, Varjak M, Selinger M, Zuvanov L, Owsianka AM, Patel AH, McLauchlan J, Lindenbach BD, Fall G, Sall AA, Biek R, Rehwinkel J, Schnettler E, Kohl A. 2016. Full genome sequence and sfRNA interferon antagonist activity of zika virus from Recife, Brazil. PLoS Negl Trop Dis 10: e0005048. doi:10.1371/journal.pntd.0005048.

Ferraris P, Yssel H, Missé D. 2019. Zika virus infection: an update. Microbes Infect 21: 353–360. doi:10.1016/j.micinf.2019.04.005.

Finol E, Ooi EE. 2019. Evolution of subgenomic RNA shapes dengue virus adaptation and epidemiological fitness. iScience 16: 94–105. doi:10.1016/j.isci.2019.05.019.

Flobinus A, Hleibieh K, Klein E, Ratti C, Bouzoubaa S, Gilmer D. 2016. A viral noncoding RNA complements a weakened viral RNA silencing suppressor and promotes efficient systemic host infection. Viruses 8: 272. doi:10.3390/v8100272.

Flobinus A, Chevigny N, Charley PA, Seissler T, Klein E, Bleykasten-Grosshans C, Ratti C, Bouzoubaa S, Wilusz J, Gilmer D. 2018. Beet necrotic yellow vein virus noncoding RNA production depends on a 5′→3′ Xrn exoribonuclease activity. Viruses 10: 137. doi:10.3390/v10030137.

Galipon J, Ishii R, Suzuki Y, Tomita M, Ui-Tei K. 2017. Differential binding of three major human ADAR isoforms to coding and long noncoding transcripts. Genes (Basel) 8: 68. doi:10.3390/genes8020068.

Göertz GP, Fros JJ, Miesen P, Vogels CBF, van der Bent ML, Geertsema C, Koenraadt CJM, van Rij RP, van Oers MM, Pijlman GP. 2016. Noncoding subgenomic flavivirus RNA is processed by the mosquito RNA interference machinery and determines West Nile virus transmission by Culex pipiens mosquitoes. J Virol 90: 10145–10159. doi:10.1128/JVI.00930-16.

Gould AR, Francki RIB, Hatta T, Hollings M. 1981. The bipartite genome of red clover necrotic mosaic virus. Virology 108: 499–506. doi:10.1016/0042-6822(81)90457-8.

Hiruki C. 1987. The dianthoviruses: a distinct group of isometric plant viruses with bipartite genome. Adv Virus Res 33: 257–300. doi:10.1016/S0065-3527(08)60320-6.

Iwakawa HO, Mizumoto H, Nagano H, Imoto Y, Takigawa K, Sarawaneeyaruk S, Kaido M, Mise K, Okuno T. 2008. A viral noncoding RNA generated by cis-element-mediated protection against 5′→3′ RNA decay represses both cap-independent and cap-dependent translation. J Virol 82: 10162–10174. doi:10.1128/JVI.01027-08.

Kandoi G, Dickerson JA. 2017. Differential alternative splicing patterns with differential expression to computationally extract plant molecular pathways. In 2017 IEEE International Conference on Bioinformatics and Biomedicine (BIBM), pp. 2163–2170, IEEE, NY.

Kandoi G, Dickerson JA. 2019. Tissue-specific mouse mRNA isoform networks. Sci Rep 9: 13949. doi:10.1038/s41598-019-50119-x.

Kessler C, Höltke HJ, Seibl R, Burg J, Mühlegger K. 1990. Non-radioactive labeling and detection of nucleic acids. I. A novel DNA labeling and detection system based on digoxigenin: antidigoxigenin ELISA principle (Digoxigenin System). Biol Chem Hoppe Seyler 371: 917–927. doi:10.1515/bchm3.1990.371.2.917.

Koev G, Miller WA. 2000. A positive-strand RNA virus with three very different subgenomic RNA promoters. J Virol 74: 5988–5996. doi:10.1128/JVI.74.13.5988-5996.2000.

Koshkin AA, Singh SK, Nielsen P, Rajwanshi VK, Kumar R, Meldgaard M, Olsen CE, Wengel J. 1998. LNA (locked nucleic acids): synthesis of the adenine, cytosine, guanine, 5-methylcytosine, thymine and uracil bicyclonucleoside monomers, oligomerisation, and unprecedented nucleic acid recognition. Tetrahedron 54: 3607–3630. doi:10.1016/S0040-4020(98) 00094-5.

Lee J, Shin O, Lee JK, Shin OS. 2019. Advances in Zika virus–host cell interaction: current knowledge and future perspectives. Int J Mol Sci 20: 1101. doi:10.3390/ijms20051101.

Manokaran G, Finol E, Wang C, Gunaratne J, Bahl J, Ong EZ, Tan HC, Sessions OM, Ward AM, Gubler DJ, Harris E, Garcia-Blanco MA, Ooi EE. 2015. Dengue subgenomic RNA binds TRIM25 to inhibit interferon expression for epidemiological fitness. Science 350: 217–221. doi:10.1126/science.aab3369.

Miller WA, Koev G. 2000. Synthesis of subgenomic RNAs by positive strand RNA viruses. Virology 273: 1–8. doi:10.1006/viro.2000.0421.

Miller WA, Jackson J, Feng Y. 2015. Cis- and trans-regulation of luteovirus gene expression by the 3′ end of the viral genome. Virus Res 206: 37–45. doi:10.1016/j.virusres.2015.03.009.

Miller WA, Shen R, Staplin W, Kanodia P. 2016. Noncoding RNAs of plant viruses and viroids: sponges of host translation and RNA interference machinery. Mol Plant-Microbe Interact 29: 156–164. doi:10.1094/MPMI-10-15-0226-FI.

Monroe SS, Jiang B, Stine SE, Koopmans M, Glass RI. 1993. Subgenomic RNA sequence of human astrovirus supports classification of *Astroviridae* as a new family of RNA viruses. J Virol 67:3611–3614. doi:10.1128/JVI.67.6.3611-3614.1993.

Moon SL, Anderson JR, Kumagai Y, Wilusz CJ, Akira S, Khromykh AA, Wilusz J. 2012. A noncoding RNA produced by arthropod-borne flaviviruses inhibits the cellular exoribonuclease XRN1 and alters host mRNA stability. RNA 18: 2029–2040. doi:10.1261/rna.034330.112.

Moon SL, Dodd BJT, Brackney DE, Wilusz CJ, Ebel GD, Wilusz J. 2015. Flavivirus sfRNA suppresses antiviral RNA interference in cultured cells and mosquitoes and directly interacts with the RNAi machinery. Virology 485: 322–329. doi:10.1016/j.virol.2015.08.009.

Peltier C, Klein E, Hleibieh K, D'Alonzo M, Hammann P, Bouzoubaa S, Ratti C, Gilmer D. 2012. Beet necrotic yellow vein virus subgenomic RNA3 is a cleavage product leading to stable non-coding RNA required for long-distance movement. J Gen Virol 93:1093–1102. doi:10.1099/vir.0.039685-0.

Pijlman GP, Funk A, Kondratieva N, Leung J, Torres S, van der Aa L, Liu WJ, Palmenberg AC, Shi PY, Hall RA, Khromykh AA. 2008. A highly structured, nuclease-resistant, noncoding RNA produced by flaviviruses is required for pathogenicity. Cell Host Microbe 4: 579–591. doi:10.1016/j.chom.2008.10.007.

Qin Z, Stoilov P, Zhang X, Xing Y. 2018. SEASTAR: systematic evaluation of alternative transcription start sites in RNA. Nucleic Acids Res 46: e45. doi:10.1093/nar/gky053.

Roby JA, Pijlman GP, Wilusz J, Khromykh AA. 2014. Noncoding subgenomic flavivirus RNA: multiple functions in West Nile virus pathogenesis and modulation of host responses. Viruses 6: 404–427. doi:10.3390/v6020404.

Rojas-Duran MF, Gilbert WV. 2012. Alternative transcription start site selection leads to large differences in translation activity in yeast. RNA 18: 2299–2305. doi:10.1261/rna.035865.112.

Royall E, Locker N. 2016. Translational control during calicivirus infection. Viruses 8: 104. doi:10.3390/v8040104.

Sanger F, Nicklen S, Coulson AR. 1977. DNA sequencing with chain-terminating inhibitors. Proc Natl Acad Sci 74: 5463–5467. doi:10.1073/pnas.74.12.5463.

Scheets K. 2000. Maize chlorotic mottle machlomovirus expresses its coat protein from a 1.47-kb subgenomic RNA and makes a 0.34-kb subgenomic RNA. Virology 267: 90–101. doi:10.1006/viro.1999.0107.

Schnettler E, Sterken MG, Leung JY, Metz SW, Geertsema C, Goldbach RW, Vlak JM, Kohl A, Khromykh AA, Pijlman GP. 2012. Noncoding flavivirus RNA displays RNA interference suppressor activity in insect and mammalian cells. J Virol 86: 13486–13500. doi:10.1128/JVI.01104-12.

Schuessler A, Funk A, Lazear HM, Cooper DA, Torres S, Daffis S, Jha BK, Kumagai Y, Takeuchi O, Hertzog P, Silverman R, Akira S, Barton DJ, Diamond MS, Khromykh AA. 2012. West Nile virus noncoding subgenomic RNA contributes to viral evasion of the type I interferon-mediated antiviral response. J Virol 86:5708–5718. doi:10.1128/JVI.00207-12.

Shan C, Xie X, Muruato AE, Rossi SL, Roundy CM, Azar SR, Yang Y, Tesh RB, Bourne N, Barrett AD, Vasilakis N, Weaver SC, Shi PY. 2016. An infectious cDNA clone of Zika virus to study viral virulence, mosquito transmission, and antiviral inhibitors. Cell Host Microbe 19: 891–900. doi:10.1016/j.chom.2016.05.004.

Shan C, Muruato AE, Jagger BW, Richner J, Nunes BTD, Medeiros DBA, Xie X, Nunes JGC, Morabito KM, Kong WP, Pierson TC, Barrett AD, Weaver SC, Rossi SL, Vasconcelos PFC, Graham BS, Diamond MS, Shi PY. 2017a. A single-dose live-attenuated vaccine prevents Zika virus pregnancy transmission and testis damage. Nat Commun 8: 676. doi:10.1038/s41467-017-00737-8.

Shan C, Muruato AE, Nunes BTD, Luo H, Xie X, Medeiros DBA, Wakamiya M, Tesh RB, Barrett AD, Wang T, Weaver SC, Vasconcelos PFC, Rossi SL, Shi PY. 2017b. A live-attenuated Zika virus vaccine candidate induces sterilizing immunity in mouse models. Nat Med 23: 763–767. doi:10.1038/nm.4322.

Shen R, Miller WA. 2004. Subgenomic RNA as a riboregulator: negative regulation of RNA replication by Barley yellow dwarf virus subgenomic RNA 2. Virology 327: 196–205. doi:10.1016/j.virol.2004.06.025.

Shen R, Rakotondrafara AM, Miller WA. 2006. Trans regulation of cap-independent translation by a viral subgenomic RNA. J Virol 80:10045–10054. doi:10.1128/JVI.00991-06.

Silva PAGC, Pereira CF, Dalebout TJ, Spaan WJM, Bredenbeek PJ. 2010. An RNA pseudoknot is required for production of yellow fever virus subgenomic RNA by the host nuclease XRN1. J Virol 84:11395–11406. doi:10.1128/JVI.01047-10.

Sit TL, Vaewhongs AA, Lommel SA. 1998. RNA-mediated trans-activation of transcription from a viral RNA. Science 281: 829–832. doi:10.1126/science.281.5378.829.

Soto-Acosta R, Xie X, Shan C, Baker CK, Shi PY, Rossi SL, Garcia-Blanco MA, Bradrick S. 2018. Fragile X mental retardation protein is a Zika virus restriction factor that is antagonized by subgenomic flaviviral RNA. Elife 7: e39023. doi:10.7554/eLife.39023.

Steckelberg AL, Akiyama BM, Costantino DA, Sit TL, Nix JC, Kieft JS. 2018. A folded viral noncoding RNA blocks host cell exoribonucleases through a conformationally dynamic RNA structure. Proc Natl Acad Sci 115: 6404–6409. doi:10.1073/pnas.1802429115.

Strauss JH, Strauss EG. 1994. The alphaviruses: gene expression, replication, and evolution. Microbiol Rev 58: 491–562. doi:10.1128/MMBR.58.3.491-562.1994.

Sztuba-Solińska J, Stollar V, Bujarski JJ. 2011. Subgenomic messenger RNAs: mastering regulation of (+)-strand RNA virus life cycle. Virology 412: 245–255. doi:10.1016/j.virol.2011.02.007.

Veedu RN, Vester B, Wengel J. 2008. Polymerase chain reaction and transcription using locked nucleic acid nucleotide triphosphates. J Am Chem Soc 130: 8124–8125. doi:10.1021/ja801389n.

Wang X, Hou J, Quedenau C, Chen W. 2016. Pervasive isoform-specific translational regulation via alternative transcription start sites in mammals. Mol Syst Biol 12: 875. doi:10.15252/msb.20166941.

Xiong Z, Lommel SA. 1991. Red clover necrotic mosaic virus infectious transcripts synthesized *in vitro*. Virology 182: 388–392. doi:10.1016/0042-6822(91)90687-7.

Xu T, Lei L, Shi J, Wang X, Chen J, Xue M, Sun S, Zhan B, Xia Z, Jiang N, Zhou T, Lai J, Fan Z. 2019. Characterization of maize translational responses to sugarcane mosaic virus infection. Virus Res 259: 97–107. doi:10.1016/j.virusres.2018.10.013.

Figures

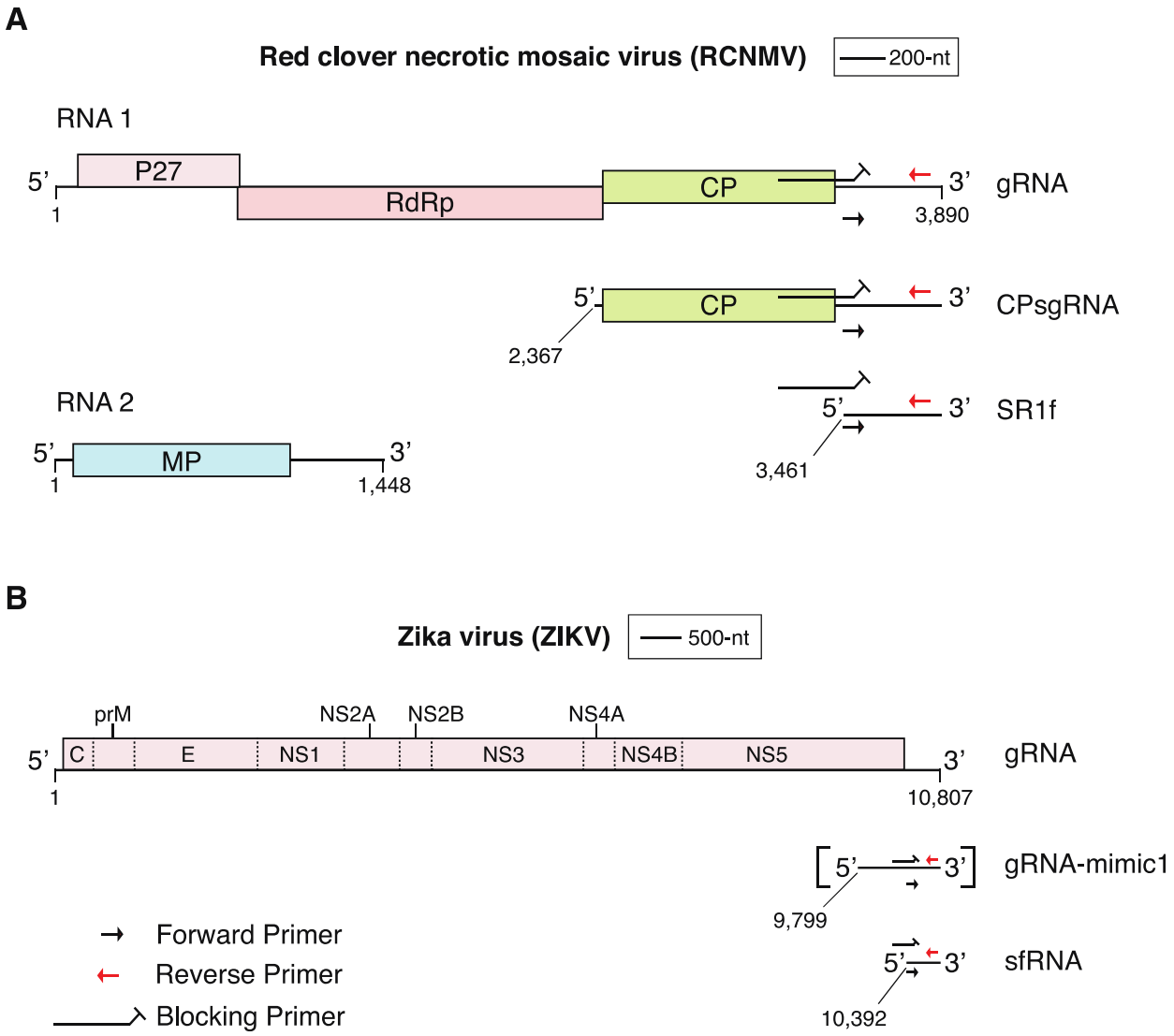

Figure 2.1. Genome organization of **(A)** Red clover necrotic mosaic virus (RCNMV) and **(B)** Zika virus (ZIKV). ZIKV gRNA-mimic1 (square brackets) was transcribed *in vitro* and is not produced during ZIKV infection. Approximate positions of DeSCo-PCR primers (not drawn to scale) are shown to depict the approximate location of the primers discussed in *Fig. 2.2*.

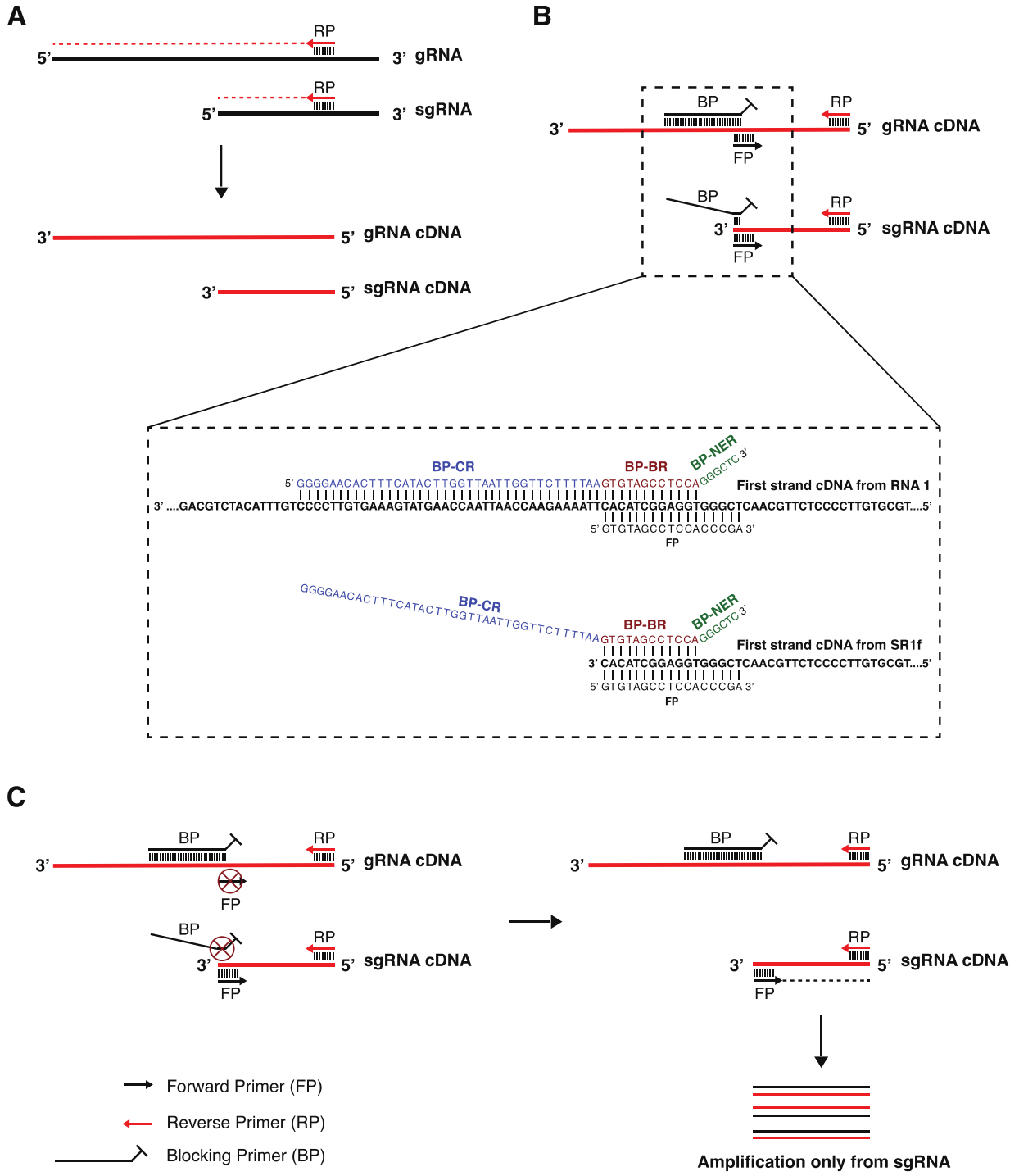

Figure 2.2. Schematic diagram of DeSCo-PCR. **(A)** First-strand cDNA synthesis (red line) using template-specific reverse primer (RP) annealed to viral positive-strand RNA (bold black line). **(B)** Primer schematics indicating annealing of BP mostly upstream but extending downstream from the 5′ end of sgRNA sequence and annealing of FP to a longer tract starting exactly at the 5′ end of sgRNA sequence. This allows BP to win the annealing competition for gRNA and FP to win the annealing competition for the 5′ end of sgRNA. The dashed box shows the sequences of BP and FP primers and the partial cDNA sequences of RCNMV RNA1 and SR1f to which the primers anneal. **(C)** Primer competition at annealing

step and subsequent extension step of DeSCo-PCR. Vertical lines represent base-pairing between the primers and the cDNA template. Circled X indicates primer that does not anneal in the presence of competing primer. (gRNA) genomic RNA, (sgRNA) subgenomic RNA, (FP) forward primer, (BP) blocking primer, (CR) competitive region (blue letters), (BR) blocking region (red letters), (NER) nonextendable region (green letters).

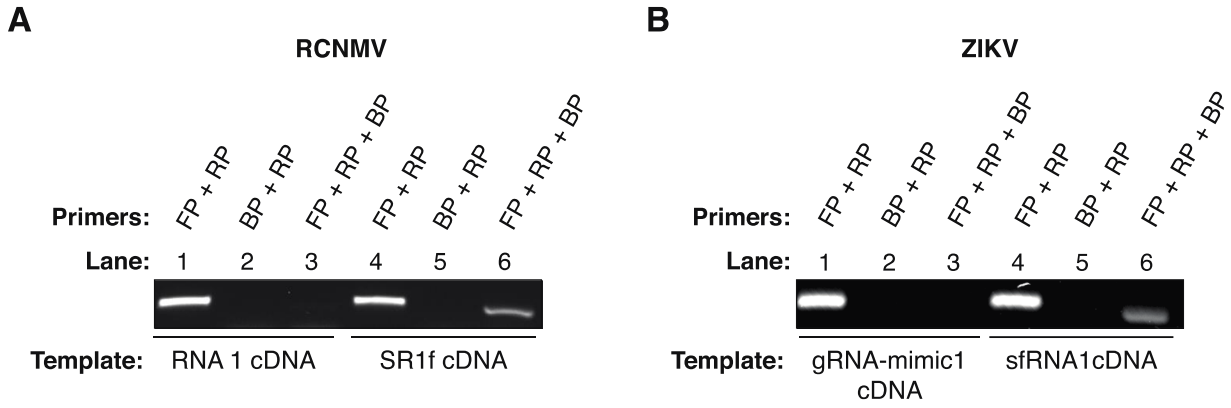

Figure 2.3. Proof of concept of DeSCo-PCR. **(A)** Selective amplification of cDNA from *in vitro* transcribed RCNMV SR1f by DeSCo-PCR. **(B)** Selective amplification of cDNA from *in vitro* transcribed ZIKV sfRNA1 by DeSCo-PCR. (FP) forward primer, (RP) reverse primer, (BP) blocking primer.

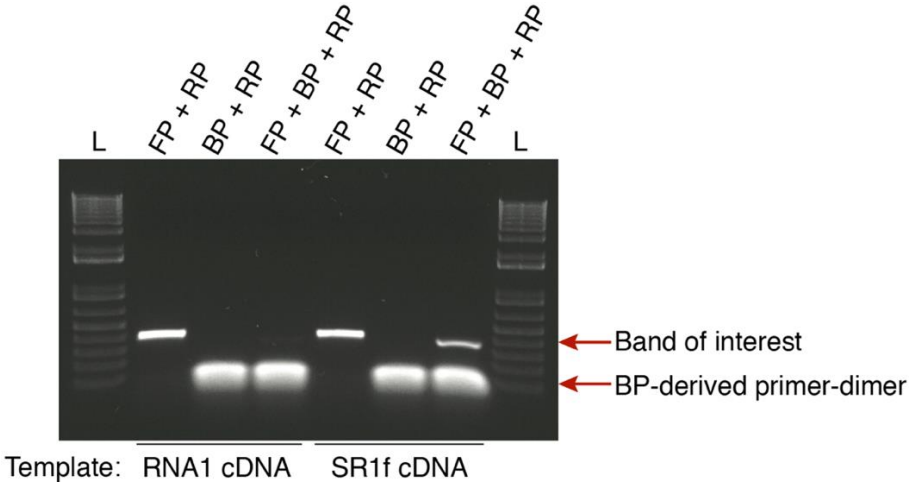

Figure 2.4. Uncropped DeSCo-PCR gel image from *Fig. 2.3-A* shows amplification of primer-dimer from PCR in samples with blocking primer. RCNMV RNA1-derived cDNA and SR1f-derived cDNA were used as templates for the PCR reaction. (FP) forward primer, (BP) blocking primer, (RP) reverse primer, (L) Invitrogen 1kb plus DNA ladder.

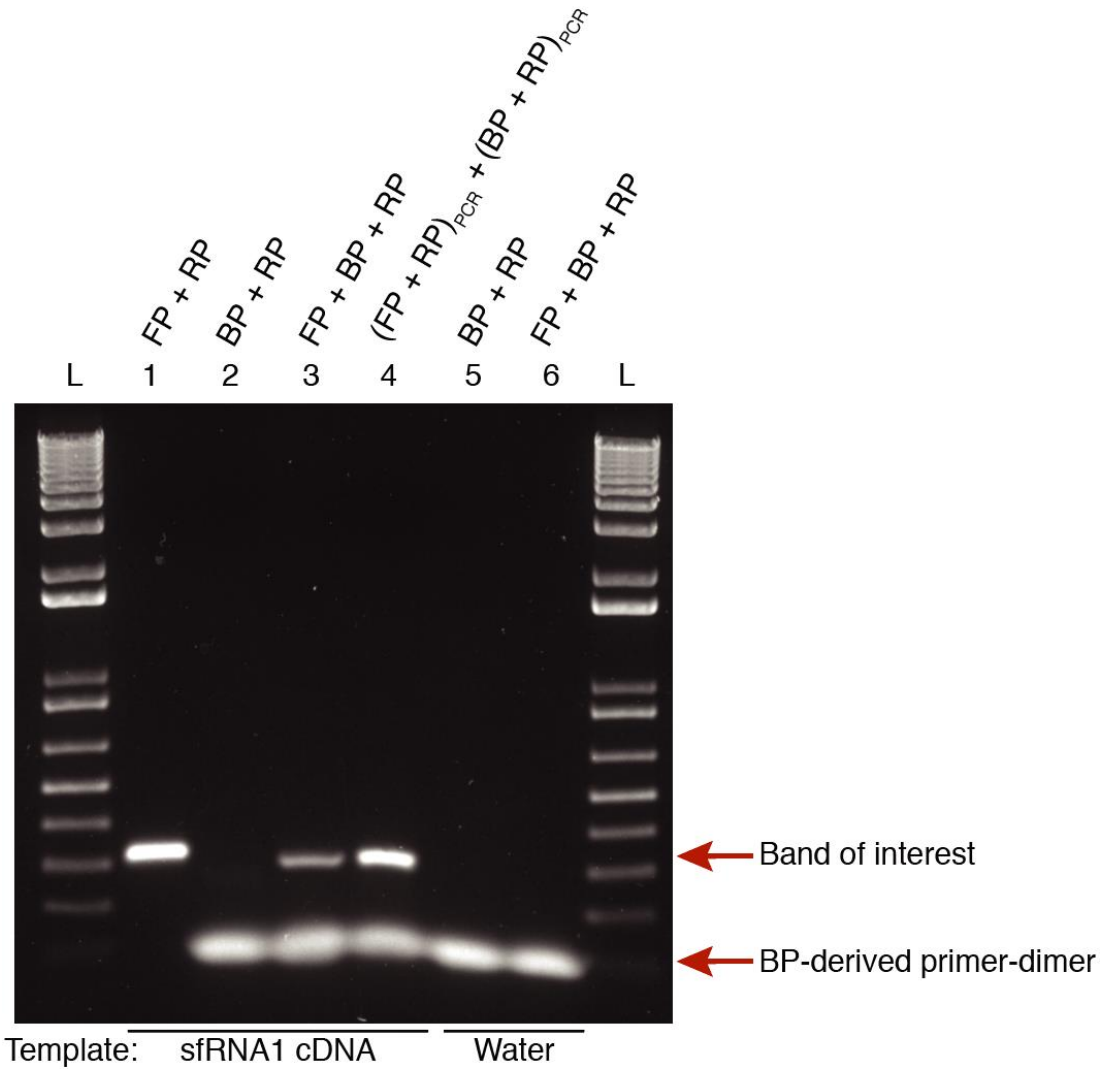

Figure 2.5. Presence of a BP-derived "primer-dimer" in sample slightly increases the mobility of the band of interest. PCR using BP plus RP yields a low molecular weight band in the presence of either ZIKV sfRNA1-derived cDNA, or no template (water) (L2-3, L5-6). In addition, the band of interest migrates slightly faster in the presence of the primer-dimer in DeSCo-PCR reactions (L3) compared to the same sized FP-RP PCR product (L1). This is shown by mixing the FP-RP PCR product that yields only the band of interest (L1) with BP-RP PCR product that yields only the primer-dimer (L2) and loading the mixture in a single well for agarose gel electrophoresis (L4). Mobility of the band of interest from the FP-RP PCR, in the presence of primer-dimer (L4), was similar to that from DeSCo-PCR (L3) and faster than that of FP-RP alone (L1). (FP) forward primer, (BP) blocking primer, (RP) reverse primer, (L) Invitrogen 1kb plus DNA ladder.

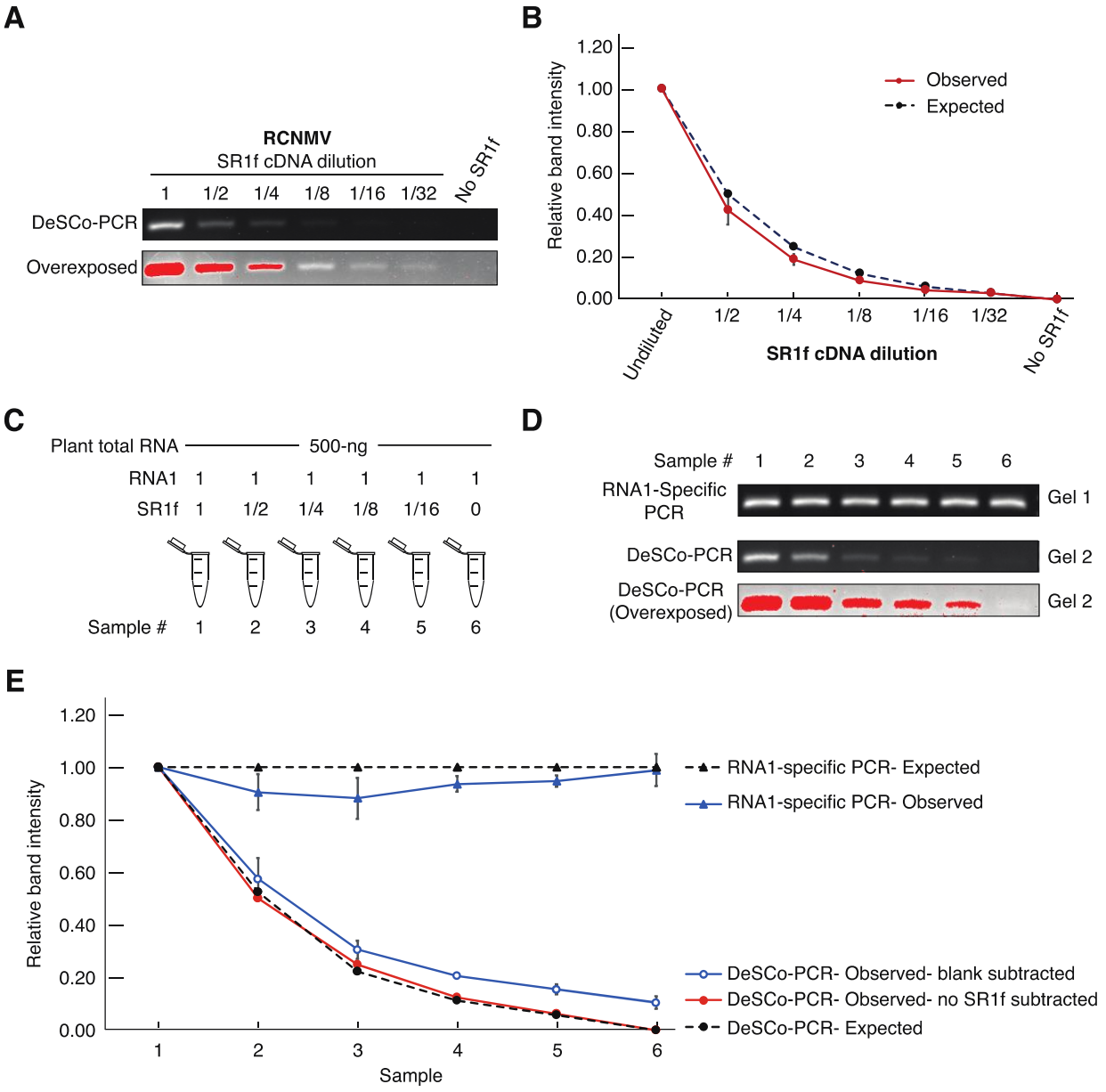

Figure 2.6. Measurement of relative amounts of *in vitro* transcribed RCNMV SR1f by DeSCo-PCR. **(A)** DeSCo-PCR gel image. **(B)** Graph of relative amounts of RCNMV SR1f as estimated by relative intensity measurements when only SR1f RNA was used for cDNA synthesis. 1, 1/2, 1/4, 1/8, 1/16, 1/32 denotes the SR1f cDNA dilution, starting with 0.1 pmol of SR1f. **(C)** Composition of RNA mix for reverse transcription containing dilutions of SR1f in the presence of fixed amounts of RCNMV RNA1 and total plant RNA. 1, 1/2, 1/4, 1/8, 1/16 denotes the SR1f dilution. **(D)** DeSCo-PCR gel image of dilutions in C. **(E)** Graph of relative RNA abundance as calculated by measuring the band intensities of the PCR products. Gel1: RNA1-specific PCR (both primers upstream of SR1f sequence), Gel2: DeSCo-PCR. Red bands in the gel images denote saturated pixels from overexposing the gel.

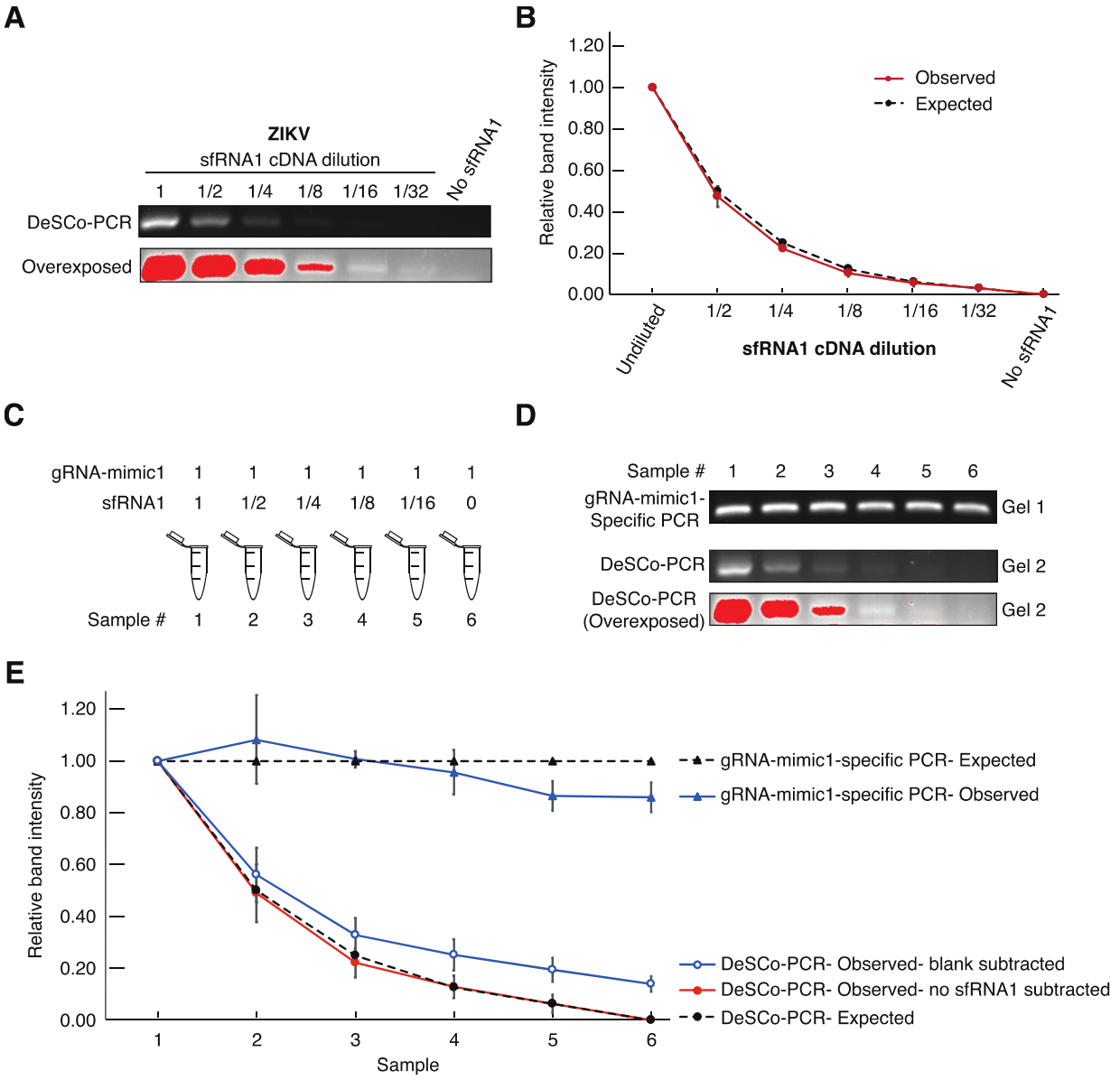

Figure 2.7. Measurement of relative amounts of *in vitro* transcribed ZIKV sfRNA1 by DeSCo-PCR. **(A)** DeSCo-PCR gel image. **(B)** Graph of relative amounts of ZIKV sfRNA1 as estimated by relative intensity measurements when only sfRNA1 was used for cDNA synthesis. 1, 1/2, 1/4, 1/8, 1/16, 1/32 denotes the sfRNA1 cDNA dilution, starting with 0.1 pmol of sfRNA. **(C)** Composition of RNA mix for reverse transcription containing dilutions of sfRNA1 in the presence of fixed amounts of gRNA-mimic1. 1, 1/2, 1/4, 1/8, 1/16 denotes the sfRNA1 dilution. **(D)** DeSCo-PCR gel image of dilutions in C. **(E)** Graph of relative RNA abundance as calculated by measuring the band intensities of PCR products. Gel1: gRNA-mimic1-specific PCR (both primers upstream of sfRNA1 sequence), Gel2: DeSCo-PCR. Red bands in the gel images denote saturated pixels from overexposing the gel.

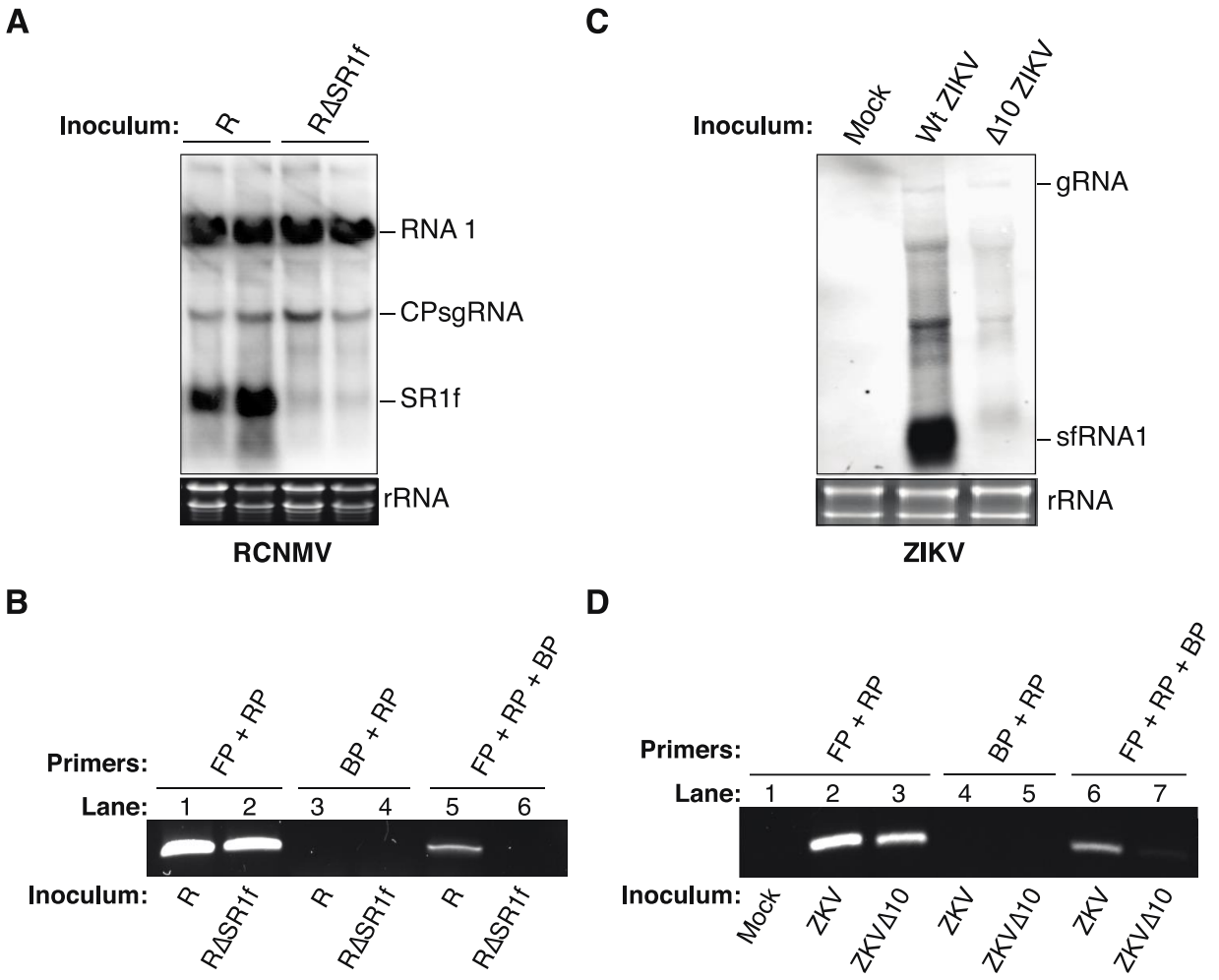

Figure 2.8. Detection of sgRNAs in virus-infected plants or HeLa cells. **(A)** Northern blot hybridization of total RNA from *N. benthamiana* leaves 14 d after inoculation with wild-type (R) or mutant (RΔSR1f) RCNMV. Stained gel shows ribosomal RNA as loading control for each lane. Duplicate samples are shown for each treatment. **(B)** Detection of SR1f in total RNA from plants infected with indicated wild-type or mutant RCNMV by DeSCo-PCR. Primer combinations used to generate the PCR products are shown above each lane of the gel. **(C)** Northern blot hybridization of total RNA from HeLa cells 48 h after inoculation with wild-type (Wt) or mutant 10ΔZIKV. Stained gel shows ribosomal RNA as loading control for each lane. **(D)** Detection of sfRNA1 in total RNA from cells infected with indicated wild-type or mutant ZIKV by DeSCo-PCR. Primer combinations used to generate the PCR products are shown above each lane of the gel. (FP) forward primer, (RP) reverse primer, (BP) blocking primer.

Tables

Table 2.1. Comparison of northern blot hybridization to DeSCo-PCR.

	Northern blot hybridization	**DeSCo-PCR**
Input amount of total RNA	5-15 µg	0.5-2 µg
Time Consumed	Electrophoresis (~2 h) Transfer to membrane (overnight) Probe preparation (~2 h) Pre-hybridization incubation (~1-2 h) Probe hybridization (overnight) Washing (~2.5 h) Autoradiography (few hours to days) Clean-up (~0.5-1 h)	cDNA synthesis (~1 h) PCR (1-2 h) Gel Imaging (~5-10 min) Clean-up (10 min)
Hazardous reagents	Formaldehyde Radioactive isotope	None
Sequence information of 5' end of sgRNA	Not required	Required. But it can tolerate a few mismatch bases
Detect multiple sgRNAs simultaneously	Yes	May be possible with some modifications

Table 2.2. Primers used for construction of DNA templates for *in vitro* transcription.

Primer	**Nucleotide position [a]**	**Sequence (5'----3') [b, c]**
3UTR_R1_corrected_for	3487- 3506	GGGGAAC**A**CGCAGTCTCGCC
3UTR_R1_corrected_rev	3448- 3486	TCTTGCAACTCGGGTGGAGGCTAC**A**CTTAAAAGA ACCAA
T7-rev	-	CTATAGTGAGTCGTATTAGGGTACCGAGC
SR1f_for	3461-3480	GTGTAGCCTCCACCCGAGTT
SR1f.m1_for	3465-3485	**TTG**CTCCACCCGAGTTGCAAG
SR1f.m1_rev	3429-3464	**CGT**CTTAAAAGAACCAATTAACCAAGTATGAAAG TG
NS5 (+) forward primer 1	9799-9819	GCTAATACGACTCACTATAGGGCTCCCACCACTTC AACAAGC
sfRNA (-) reverse primer	10787-10807	AGACCCATGGATTTCCCCACA
sfRNA (+) forward primer	10392-10416	GCTAATACGACTCACTATAGTGTTGTCAGGCCTGC TAGTCAGCC

[a] nucleotide position is with respect to the gRNA sequence of RCNMV (GenBank J04357) and ZIKV (Genbank KU955593).

[b] Sequence that was substituted in the template is in bold.

[c] T7-promoter sequence is underlined

Table 2.3. Primers used for RT-PCR and DeSCo-PCR.

Primer	**Nucleotide position [a]**	**Sequence (5'----3') [b]**
RCNMV reverse primer (RRP)	3871- 3890	GGGGTACCTAGCCGTTATAC
RCNMV forward primer (RFP)	3461- 3477	GTGTAGCCTCCACCCGA
RFP-m1	3461- 3477	GACGTTGCTCCACCCGA
RCNMV blocking primer (RBP)	3423- 3478	GGGGAACACTTTCATACTTGGTTAATTGGTT CTTTTAAGTGTAGCCTCCAgggctc
RBP-m1	3423- 3478	GGGGAACACTTTCATACTTGGTTAATTGGTT CTTTTAAGACGTTGCTCCAgggctc
RCNMV_909_FP	909- 926	AAGCGGGCCAGTAGAGTC
RCNMV_1262_RP	1244-1262	TCTCCATTGCACAGGTTTC
ZIKV reverse primer (ZRP)	10691-10711	GCGTCAATATGCTGTTTTGCG
ZIKV forward primer (ZFP)	10392-10410	GTGTTGTCAGGCCTGCTAG
ZIKV blocking primer (ZBP)	10356-10410	GGGTCCACACCTGGAGTGCTATAAGCACCA ATCTTAGTGTTGTCAGGCCacgatc
ZIKV_9827_FP	9827-9846	CAAGGACGGGAGGTCCATTG
ZIKV_10115_RP	10095-10115	GTTCCACACCACAAGCATGTC

[a] nucleotide position is with respect to the gRNA sequence of RCNMV (GenBank J04357) and ZIKV (Genbank KU955593).

[b] bases in small case letters in blocking primers do not anneal to either gRNA or sgRNA making the primer non-extendable.

CHAPTER 3. EFFECTS OF THE NONCODING SUBGENOMIC RNA OF RED CLOVER NECROTIC MOSAIC VIRUS IN VIRUS INFECTION

Pulkit Kanodia[1,2] and W. Allen Miller[1,2,3]*

[1] Plant Pathology and Microbiology Department, Iowa State University, Ames, IA, USA

[2] Interdepartmental Genetics and Genomics Major, Iowa State University, Ames, IA, USA

[3] Plant Science Institute, Iowa State University, Ames, IA, USA

* Corresponding author: wamiller@iastate.edu

Modified from a manuscript under review in *Journal of Virology*

Author Contributions: PK and WAM designed the experiments, PK conducted all the experiments. RNA-seq data was processed and analyzed by the Genome Informatics Facility at Iowa State University and PK. PK and WAM wrote the manuscript.

Abstract

In recent years, a new class of viral noncoding subgenomic (ncsg)RNA has been identified. This RNA is generated as a stable degradation product via an exoribonuclease-resistant (xr) RNA structure, which blocks the progression of 5'→ 3' exoribonuclease on viral RNAs in infected cells. Here, we assess the effects of the ncsgRNA of red clover necrotic mosaic virus (RCNMV), called SR1f, in infected plants. We demonstrate: (i) absence of SR1f reduces symptoms and decreases viral RNA accumulation in *Nicotiana benthamiana* and *Arabidopsis thaliana* plants; (ii) SR1f has an essential function other than suppression of RNA silencing; and (iii) the cytoplasmic exoribonuclease involved in mRNA turnover in plants, XRN4, is not required for SR1f production or virus infection. A comparative transcriptomic analysis in *N. benthamiana* infected with wildtype RCNMV or an SR1f-deficient mutant

RCNMV revealed that wt RCNMV infection, which produces SR1f and much higher levels of virus, has a greater and more significant impact on cellular gene expression than the SR1f-deficient mutant. Upregulated pathways include plant hormone signaling, plant-pathogen interaction, MAPK signaling, and several metabolic pathways, while photosynthesis-related genes were downregulated. We compare this to host genes known to participate in infection by other tombusvirids. Viral reads revealed a 10 to 100-fold ratio of positive to negative strand, and the abundance of reads of both strands mapping to the 3' region of RCNMV RNA1 support the premature mechanism of synthesis for the coding sgRNA. These results provide a framework for future studies of the interactions and functions of noncoding RNAs of plant viruses.

Importance

Knowledge of how RNA viruses manipulate host and viral gene expression is crucial to our understanding of infection and disease. Unlike viral protein-host interactions, little is known about the control of gene expression by viral RNA. Here we begin to address this question by investigating the noncoding subgenomic (ncsg)RNA of red clover necrotic mosaic virus (RCNMV), called SR1f. Similar exoribonuclease-resistant RNAs of flaviviruses are well-studied, but the roles of plant viral ncsgRNAs, and how they arise, are poorly understood. Surprisingly, we find the likely exoribonuclease candidate, XRN4, is not required to generate SR1f, and we assess the effects of SR1f on virus accumulation and symptom development. Finally, we compare the effects of infection by wildtype RCNMV vs an SR1f-deficient mutant on host gene expression in *Nicotiana benthamiana*, which reveals that ncsgRNAs such as SR1f are key players in virus-host interactions to facilitate productive infection.

Introduction

Long noncoding RNAs (lncRNAs) play important roles in diverse cellular processes, regulating gene expression during development, maintaining homeostasis, and responding to various abiotic and biotic stresses (Zhang and Chen 2013; Wang et al. 2017a; Nejat and Mantri 2018; Sun et al. 2018; Salviano-Silva et al. 2018; Yu et al. 2019; Tsagakis et al. 2020; Gil and Ulitsky 2020; Kumar and Chakraborty 2021). Similar to the host counterparts during infection, some viruses make lncRNAs that are instrumental in regulating virus and host gene expression to modulate virus life cycle and the host's antiviral response (Tycowski et al. 2015; Miller et al. 2016; Wang et al. 2017b). For instance, (i) polyadenylated nuclear (PAN) RNA is a long ncRNA encoded by Kaposi's sarcoma-associated herpesvirus (KSHV) that regulates viral gene expression (Rossetto et al. 2013), (ii) Citrus tristeza virus (CTV) produces LMT1, a long noncoding RNA, that counteracts plant defense responses via inhibition of the antiviral salicylic acid signaling (Kang et al. 2019).

In contrast to the lncRNAs that are made during replication by the viral polymerase, a new class of viral lncRNA was identified over a decade ago that is generated by incomplete degradation of viral RNAs by host cytoplasmic 5'→ 3' exoribonucleases (XRNs) (Pijlman et al. 2008; Iwakawa et al. 2008; Silva et al. 2010; Peltier et al. 2012; Flobinus et al. 2018). The 5'→ 3' XRNs in the nucleus and cytoplasm of eukaryotic cells are involved in RNA processing, RNA degradation, antiviral defenses, and regulation of gene expression, among other functions (Chang et al. 2011; Nagarajan et al. 2013). XRN1 is primarily present in the cytoplasm while XRN2 is primarily present in the nucleus of yeast and metazoans (Chang et al. 2011; Nagarajan et al. 2013). The three known 5'→ 3' XRNs in plants, such as Arabidopsis AtXRN2, AtXRN3, and AtXRN4, are orthologs of XRN2 with only AtXRN4 being localized to the cytoplasm

(Kastenmayer and Green 2000). Because no plant XRN with sequence homology to XRN1 has yet been identified, it is generally considered that AtXRN4 is a functional equivalent of XRN1 (Kastenmayer and Green 2000; Chang et al. 2011; Nagarajan et al. 2013). The cytoplasmic 5'→ 3' XRNs can use uncapped/de-capped viral RNA as a substrate and function as an antiviral factor by degrading the viral RNAs from the 5' end. However, all the viruses in the *Flavivirus* genus (Pijlman et al. 2008; Silva et al. 2010; Clarke et al. 2015; Slonchak and Khromykh 2018; MacFadden et al. 2018; Jones et al. 2021), several viruses in the *Luteoviridae, Tombusviridae* (Iwakawa et al. 2008; Steckelberg et al. 2018a; Gunawardene et al. 2019; Steckelberg et al. 2020; Ilyas et al. 2021), and *Benyviridae* (Peltier et al. 2012; Flobinus et al. 2018) families have evolved an XRN-resistant (xr)RNA secondary structure in their viral RNA that can block the progression of host 5'→ 3' XRN resulting in xrRNA-derived subgenomic (sg)RNAs. Putative xrRNA structures have also been identified *in vitro* in viruses belonging to the *Bunya-*, *Arena-*, *Betaflexi-*, *Virga-*, *Poty-*, and *Secoviridae* families (Charley et al. 2018; Dilweg et al. 2019). Even though some xrRNA structures in the viral RNA have been identified in the intergenic region that can yield coding sgRNAs (Steckelberg et al. 2018b, 2020; Ilyas et al. 2021), most of the xrRNAs identified have been located in the 3' UTR that yield noncoding (nc)sgRNAs (Pijlman et al. 2008; Iwakawa et al. 2008; Peltier et al. 2012; Slonchak and Khromykh 2018; Steckelberg et al. 2018a; Charley et al. 2018; Flobinus et al. 2018; Gunawardene et al. 2019; Dilweg et al. 2019; Szucs et al. 2020; Steckelberg et al. 2020). The xrRNA-derived ncsgRNAs have been shown to play roles in virus pathogenicity, symptom development, virus movement and transmission, and suppressing the host's antiviral responses (Bidet and Garcia-Blanco 2014; Roby et al. 2014). For example, sfRNA from WNV and dengue virus (DENV) suppresses siRNA- and miRNA-induced RNAi pathways in insect and mammalian cells (Schnettler et al.

2012; Moon et al. 2015), DENV and Zika virus (ZIKV) sfRNA inhibits translation of interferon-stimulated genes (Bidet et al. 2014; Manokaran et al. 2015; Donald et al. 2016), alters the stability of host mRNAs, and improves viral epidemiological fitness (Moon et al. 2012). Although flaviviral ncsgRNAs have been studied extensively, research on xrRNA-derived ncsgRNAs of plant viruses remains scarce. There is evidence that the xrRNA-derived ncsgRNA of beet necrotic yellow vein virus (BNYVV), called ncRNA3, partially complements the RNA silencing suppressor activity of BNYVV p14 protein, and also facilitates systemic movement in plants (Peltier et al. 2012; Flobinus et al. 2016, 2018).

The first xrRNA-derived ncsgRNA that was discovered in a plant virus is SR1f of red clover necrotic mosaic virus (RCNMV) (Iwakawa et al. 2008). RCNMV (genus *Dianthovirus*, family *Tombusviridae*) is a bipartite positive strand RNA virus with genomic RNAs 1 and 2 *(Fig. 3.1-A)* (Gould et al. 1981; Hiruki 1987). A subgenomic RNA (CPsgRNA1) that encodes the coat protein (CP) *(Fig. 3.1-A)* is made from RNA1 via premature transcription termination during the negative strand synthesis followed by positive strand synthesis from the prematurely terminated transcription product *(Chapter 1, Fig. 1.3-A)* (Sit et al. 1998). The xrRNA-derived ncsgRNA, SR1f *(Fig. 3.1-A)*, is generated as a stable degradation product formed by incomplete degradation of RNA1 and CPsgRNA1 by a still unidentified 5'→ 3' XRN (Iwakawa et al. 2008; Steckelberg et al. 2018a) *(Fig. 3.1-B)*. The 3' UTR from which SR1f is derived controls both cap-independent translation, via its Barley yellow dwarf virus-like translation element (BTE), called TE-DR1 in RCNMV (Mizumoto et al. 2003), and ribosomal frameshifting, via its long-distance frameshift element (LDFE) (Tajima et al. 2011) *(Fig. 3.1-B)*. SR1f has been shown to *trans* inhibit both cap-independent and cap-dependent translation in cell-free translation extracts and in BY-2 protoplasts (Iwakawa et al. 2008), possibly because the BTE (TE-DR1) binds key

translation factor, eIF4F, thus making fewer copies of eIF4F accessible to host or viral mRNAs. This mechanism may explain the observation that SR1f indirectly *trans* inhibits negative-strand synthesis of RNA1 *in vitro* by repressing the production of the replicase protein (Iwakawa et al. 2008).

Although SR1f is not absolutely required for a successful infection, cell-to-cell movement, and systemic movement of viral RNAs in *Nicotiana benthamiana*, the accumulation of RNA1 is significantly lower in plants infected with RCNMVΔSR1f mutant that is unable to generate SR1f (Iwakawa et al. 2008). Additionally, the functions of SR1f during RCNMV infection and how SR1f affects the plant on a molecular level are unknown. Understanding how SR1f affects host gene expression is important to determine its function, dissect the molecular mechanism by which it functions and discover a potentially novel strategy by which viruses can counteract plant defenses and stay a step ahead in the evolutionary arms race. In this study, we (i) assess RCNMV replication and symptom development in *N. benthamiana* and *Arabidopsis thaliana*, (ii) assess its role in counteracting the immune system, (iii) assess the role of host exoribonuclease XRN4 in generating SR1f, and (iv) perform a comparative transcriptomic analysis of *N. benthamiana* infected with wildtype RCNMV, which generates SR1f, and RCNMVΔSR1f, which does not make SR1f.

Results

Symptoms and viral RNA accumulation in *N. benthamiana*

To determine if the presence of SR1f plays a role in symptom development, we inoculated *N. benthamiana* plants with (i) RCNMV RNA1 plus RNA2 (referred to as wt RCNMV), which generates SR1f, or (ii) RCNMV RNA1-m1 *(Fig. 3.1-B)* plus RNA2 (referred to as RCNMVΔSR1f), which does not generate SR1f in local leaves *(Fig. 3.2-A)* or systemic

leaves (Iwakawa et al. 2008; Kanodia et al. 2020) as verified by northern blot hybridization. RCNMV RNA1-m1 contains a six-base substitution *(Fig. 3.1-B)* that disrupts the xrRNA structure in RNA1 at the 5' end of its 3' UTR (Iwakawa et al. 2008), and precludes SR1f production (Kanodia et al. 2020). At 11 days post inoculation (dpi), necrosis, leaf curling, and mosaic symptoms were observed in wt RCNMV-inoculated plants, while only very modest to no symptoms were observed in RCNMVΔSR1f- inoculated plants *(Fig. 3.2-B)*. Similarly, we observed severe symptoms in wt RCNMV inoculated plants but very modest to no symptoms in RCNMVΔSR1f-inoculated plants, even at later time-points *(Fig. 3.2-C)*. In multiple independent experiments, the same symptoms were observed even though both RCNMV RNA1 and RNA1-m1 accumulated in non-inoculated systemic leaves in both inoculations as verified by RT-PCR *(Fig. 3.2-D)*. Corresponding to the symptom phenotype and consistent with a previous report (Iwakawa et al. 2008), viral RNAs accumulated to much lower levels in RCNMVΔSR1f infection compared to wt RCNMV infection as verified by qRT-PCR *(Fig. 3.2-E)*. This indicates that the presence of SR1f contributes to symptom development and accumulation of viral RNAs during infection. Thus, the lack of symptoms in RCNMVΔSR1f-infected plants may be due to the reduced virus accumulation, and only a downstream, indirect effect of lack of SR1f.

Symptoms and viral RNA accumulation in *Arabidopsis thaliana*

We next tested how the presence of SR1f affects viral RNA accumulation and symptom development in wt *Arabidopsis thaliana* (Col-0), a model host plant with well-defined knockout mutations. Because the analogous flaviviral sfRNA1 in insect and mammalian cells and BNYVV ncRNA3 in plants have been shown to function as an RNA silencing suppressor (Schnettler et al. 2012; Moon et al. 2015; Flobinus et al. 2016), we hypothesized that RCNMV SR1f may also function as an RNA silencing suppressor. To test this hypothesis, we used

Arabidopsis *dcl2-1/dcl4-2t* mutant. It is a double knock-out line with T-DNA insertions in *DCL2* and *DCL4* genes (Xie et al. 2005). Among the four DCL proteins (DCL1, 2, 3, 4) in Arabidopsis, DCL2 and DCL4 generate virus-derived siRNAs required for antiviral RNA silencing (Deleris et al. 2006).

Arabidopsis leaves were mechanically inoculated with sap from Mock-, wt RCNMV-, and RCNMVΔSR1f-infected *N. benthamiana*. At 4 dpi, only wt RCNMV replication was detected in the local inoculated leaves of wt and *dcl2-1/dcl4-2t* Arabidopsis *(Fig. 3.3-A)*. By 28 dpi, no symptoms were observed in wt Arabidopsis inoculated with either wt RCNMV- or RCNMVΔSR1f *(Fig. 3.3-B)*. However, in *dcl2-1/dcl4-2t* Arabidopsis, symptoms such as chlorosis, necrosis, severely mosaic and epinastic leaves, and defective bolting were observed in wt RCNMV-inoculated plants but not in RCNMVΔSR1f-inoculated plants at 28 dpi *(Fig. 3.3-B)*. Consistent with the symptoms, only wt RCNMV replication was detected in the systemic leaves of only *dcl2-1/dcl4-2t* Arabidopsis *(Fig. 3.3-C)*. In wt Arabidopsis at 14 and 21 dpi, wt RCNMV replication was inconsistently detected and RCNMVΔSR1f replication was not detected in any plants *(Fig. 3.3-D, E)*. In *dcl2-1/dcl4-2t* Arabidopsis at 14 and 21 dpi, even though we consistently detected the replication of wt RCNMV, we did not detect RCNMVΔSR1f replication *(Fig. 3.3-D, E)*. Similarly, the symptoms always appeared only in wt RCNMV inoculated *dcl2-1/dcl4-2t* Arabidopsis at different time-points. In other independent experiments, which included only Arabidopsis *dcl2-1/dcl4-2t* plants, the symptoms and wt RNA1 accumulation were consistent even at early time-points *(Fig. 3.3-F, G)*. However, RNA1-m1 accumulation was neither consistent nor reproducible in RCNMVΔSR1f-inoculated *dcl2-1/dcl4-2t* plants, as detected by RT-PCR *(Fig. 3.3-G)*.

If SR1f were required only for silencing suppression, the *dcl2-1/dcl4-2t* knock-out should rescue the replication of RCNMVΔSR1f to wt RCNMV levels, because the virus would not need a silencing suppression function to infect these silencing-deficient plants. However, knocking-out the antiviral RNAi system in Arabidopsis *dcl2-1/dcl4-2t* plants did not rescue the replication of RCNMVΔSR1f to wt RCNMV levels. Therefore, we conclude that SR1f has an essential function for infection other than silencing suppression, although we do not rule out the possibility that SR1f may also play a role in silencing suppression.

Next, we asked whether the inability of RCNMVΔSR1f to replicate in Arabidopsis is because the 6-base substitution in RNA1-m1 may affect virus replication and/or translation *in cis.* To test this, we inoculated Arabidopsis plants in the *xrn4-5* knock-out mutant line with either wt RCNMV or RCNMVΔSR1f. Arabidopsis *xrn4-5* is a loss of function mutant with T-DNA insertion in the *XRN4* gene (Souret et al. 2004). XRN4 is the host cytoplasmic XRN that has been assumed to be responsible for generating xrRNA-derived ncsgRNAs from plant viruses (Flobinus et al. 2016, 2018; Gunawardene et al. 2019; Ilyas et al. 2021). However, the role of XRN4 in generating plant viral xrRNA-derived ncRNA has not been determined *in planta*. If SR1f is generated via exonucleolytic degradation by XRN4, we expect to see no SR1f production in wt RCNMV-inoculated *xrn4-5* plants. Furthermore, these plants have a functional antiviral RNA silencing machinery. Therefore, if RCNMVΔSR1f did not replicate in wt Arabidopsis owing to the lack of SR1f production, we would not expect wt RCNMV replication in *xrn4-5* Arabidopsis. In contrast, if SR1f is dispensable, and RCNMVΔSR1f did not replicate in wt Arabidopsis only because of a *cis*-acting effect of the 6-base substitution in RNA1-m1, we expect wt RCNMV replication to occur in *xrn4-5* Arabidopsis even without SR1f production. Similar to the observation in wt Arabidopsis, there were no discernable symptoms in either wt

RCNMV- or RCNMVΔSR1f inoculated *xrn4-5* plants *(Fig. 3.4-A)*. Surprisingly, wt RCNMV replication and SR1f accumulation was observed at 21 dpi *(Fig. 3.4-B)* indicating that XRN4 is not required for generating SR1f. This conclusion supports a report of the BNYVV ncRNA3 accumulation in *N. benthamiana* plants despite virus-induced gene silencing (VIGS) treatment that reduced *Xrn4* mRNA levels (Flobinus et al. 2018). Because SR1f was produced in wt RCNMV-infected *xrn4-5* Arabidopsis, we were unable to determine whether the lack of RCNMVΔSR1f replication in Arabidopsis is because of the absence of SR1f or because of the *cis*-acting effect of the 6-base substitution in RNA1-m1.

The 6-base substitution (nt 3461 to 3466) in the xrRNA structure lies at the 5' end of the 3' UTR of RNA1 *(Fig. 3.1-B)*, near the LDFE (nt 3562 to 3566) that is required for translation of RCNMV p88 protein by -1 programmed ribosomal frameshifting *(Fig. 3.1-B)* (Tajima et al. 2011), and the 3' TE-DR1 required for cap-independent translation *(Fig. 3.1-B)* (nt 3596 to 3732) (Mizumoto et al. 2003). Because of its proximity to these elements, it is possible that the 6-base substitution in RNA1-m1 could affect RNA folding and thus the activity of 3' TE-DR1 and/or LDFE and thereby suppress RNA1-m1 translation. To test if the 6-base substitution in RNA1-m1 affects its translation *in cis*, we conducted *in vitro* translation in wheat germ extract. RCNMV p27 and p88 proteins from RNA1-m1 accumulated to about 82-85% of the level obtained from wt RNA1 *(Fig. 3.5-A, B)*. This was a statistically significant but minor effect compared to the complete ablation of SR1f RNA and the 4-5-fold reduction in virus accumulation in *N. benthamiana*, caused by this 6-base substitution.

Effect of infection on host transcriptome

To understand the role, if any, of SR1f on host gene expression, we performed RNA sequencing (RNA-seq) on plants inoculated with wt RCNMV and RCNMVΔSR1f. Because

RCNMVΔSR1f did not replicate in wt Arabidopsis and its replication in *dcl2-1/dcl4-2t* Arabidopsis was not consistent and reproducible, we instead performed RNA-seq on RCNMV-infected *N. benthamiana*. At 15 days post inoculation (dpi), necrosis, leaf curling, and mosaic symptoms were observed in wt RCNMV-inoculated plants, while no symptoms were observed in RCNMVΔSR1f- inoculated plants *(Fig. 3.6-A)*. One non-inoculated leaf was collected from mock-, wt RCNMV- and RCNMVΔSR1f-inoculated plants at 15 dpi. Both the wt RCNMV and RCNMVΔSR1f infection were confirmed by RT-PCR *(Fig. 3.6-B)*. Additionally, we performed RT-PCR with RNA1-specific and RNA1-m1-specific primers to ensure there was no cross-contamination among the samples *(Fig. 3.7)*. RNA-seq libraries were prepared using 3, 4, and 4 biological replicates for mock-, wt RCNMV- and RCNMVΔSR1f-inoculated plants, respectively. The sequencing data were processed and aligned to (i) *N. benthamiana* 1.0.1 genome, (ii) RCNMV RNA1 or RNA1-m1, and (iii) RCNMV RNA2. From total host mRNA-mapped reads plus RCNMV-mapped reads, the proportion of reads (Mean ± SD) that mapped to RCNMV genome was ~17.4 ± 3.1 % in wt RCNMV infected plants and ~5.2 ± 2.2 % in RCNMVΔSR1f infected plants.

Next, DESeq2 (Love et al. 2014) was used to identify differentially expressed genes (DEGs) (output in *Supplemental file 3.1*). We compared the results from wt RCNMV vs. mock data to RCNMVΔSR1f vs. mock data to understand how the presence of SR1f affects the host's transcriptional response to virus infection. Principal component analysis (PCA) distinguished wt RCNMV infection data from mock-inoculation data and RCNMVΔSR1f infection data with 82% variance *(Fig. 3.8)*. In contrast, there was only 55% variance between mock-inoculation and RCNMVΔSR1f infection data with two biological replicates of RCNMVΔSR1f infected plants

very close to the mock-inoculated plants *(Fig. 3.8)*. This shows that the major variation in RNA-seq data among all the samples can be explained by different inocula.

Differentially expressed genes

We define differentially expressed genes (DEGs) as those having absolute (log_2-fold change) > 1 and adjusted p-values < 0.05. In wt RCNMV vs. mock data, we found 3659 DEGs in which 2508 genes were upregulated and 1151 genes were downregulated *(Fig. 3.9-A)*. In RCNMVΔSR1f vs. mock data, we found only 422 DEGs in which 192 genes were upregulated and 230 genes were downregulated *(Fig. 3.9-A)*. Consistent with the symptom observation, volcano plots show the greater impact of wt RCNMV infection on *N. benthamiana* gene expression with greater fold change and more significant results than the RCNMVΔSR1f infection *(Fig. 3.9-B)*. Next, we plotted the 52 upregulated and 116 downregulated DEGs shared among both datasets *(Fig. 3.9-C)*. The shared upregulated genes show a larger fold change (vs Mock) in wt RCNMV infection than in RCNMVΔSR1f infection, suggesting that these genes are upregulated in response to virus infection although their magnitude of expression can result from both RCNMV replication levels and/or the presence of SR1f *per se*. Interestingly, the shared downregulated genes show a similar fold change in both conditions suggesting that these genes are downregulated in response to RCNMV infection rather than by the presence of SR1f. We hypothesize that SR1f may sequester 5'→ 3' XRN protein(s) disrupting the cellular RNA decay machinery, thus stabilizing the cellular as well as viral RNAs. Further molecular assays need to be performed to test this hypothesis.

GO enrichment analysis

The differentially upregulated and downregulated genes were used separately in wt RCNMV vs. mock and RCNMVΔSR1f vs. mock for identifying the enriched GO terms. The upregulated genes in wt RCNMV vs. mock dataset enriched 977 GO terms. The top 15 significant terms classified mainly into the biological process category *(Table 3.1)*. The downregulated genes in wt RCNMV vs. mock dataset enriched 501 GO terms with the top 15 terms classifying into cellular components category and mainly related to the photosynthesis machinery *(Table 3.1)*. However, in RCNMVΔSR1f vs. mock dataset, the upregulated genes enriched only 37 GO terms and the downregulated genes enriched 319 GO terms, mainly biological process category for the top 15 terms *(Table 3.2)*.

The list of all the enriched GO terms, the genes involved in the GO term found in our dataset, and the p-values can be found in *Supplemental file 3.2*. Subsequently, the revigo tool was used to reduce the redundancy in the enriched GO term dataset and for visualization of the more relevant parent GO terms in "Biological process", "Cellular components" and "Molecular function". The terms that were highlighted in wt RCNMV vs. mock upregulated DEG dataset included "response to other organism", "carbohydrate metabolism", "vesicle", "cell wall", "calcium ion binding", "protein serine-threonine kinase activity" *(Fig. 3.10)* and the terms in the wt RCNMV vs. mock downregulated DEG dataset included "hormone-mediated signaling pathway", "plant-type cell wall loosening", "chloroplast thylakoid", "cell wall", "water channel activity", "kinase activity" *(Fig. 3.10)* among others. However, in the RCNMVΔSR1f vs. mock dataset, only a few terms were highlighted in upregulated DEG dataset whereas several terms were highlighted in the downregulated DEG dataset *(Fig. 3.11)*. Even though number of downregulated DEGs in both inoculations are very different, the number of highlighted terms that are affected are similar in both inoculations. In contrast, the upregulated DEGs in wt

RCNMV infection affect far greater number of molecular functions, biological processes and cellular pathways than in RCNMVΔSR1f infection. This suggests that the greater impact on host by wt RCNMV infection may be because of the upregulated DEGs, rather than the downregulated DEGs, and the greater proportion of DEGs being upregulated may be due to the presence of SR1f sequestering the XRN, as hypothesized above.

KEGG pathway enrichment analysis

The DEGs in wt RCNMV and RCNMVΔSR1f infection were used for KEGG pathway enrichment analysis. *A. thaliana*, *Solanum lycopersicum,* and *N. tabacum* annotations were used as background database for the analysis. Because more informative terms were found with Arabidopsis background, we focused only on those for further analysis. More details for the enriched pathways using the other two background databases can be found in *Supplemental file 3.3* and the DEGs involved in selected KEGG pathways can be found in *Supplemental file 3.4.* In wt RCNMV vs. mock dataset, 119 pathways were identified and 21 of those were enriched with "plant-pathogen interaction", "MAPK signaling pathway-plant" and "plant hormone signal transduction" being the most significant *(Supplemental file 3.3).*

The rich factor was calculated for each pathway. This is the ratio of number of DEGs in our dataset in the pathway to the total number of genes annotated in the pathway in the background database. Rich factor of 1 means all the genes annotated in the pathways are differentially expression in a dataset. In wt RCNMV vs. mock dataset, the rich factor of significantly enriched pathways ranged from 0.16 to 0.86 with "Stilbenoid, diarylheptanoid and gingerol biosynthesis", "Linoleic acid metabolism", "Sesquiterpenoid and triterpenoid biosynthesis", and "Flavonoid biosynthesis" pathways having a rich factor greater than 0.5 *(Fig. 3.12-A).* These pathways are frequently found to be enriched during viral infections (Huang et

al. 2017; Jiao et al. 2020). Most of the enriched pathways can be grouped under metabolic pathways and it shows the significant impact of wt RCNMV infection on the plant's metabolism. In contrast, 60 pathways were identified in RCNMVΔSR1f vs. mock dataset and only 12 of those were enriched with "photosynthesis", "RNA polymerase" and "Metabolic pathways" being the most significant *(Supplemental file 3.3)*. None of the enriched pathways have a rich factor greater than 0.5 *(Fig. 3.12-A)*.

In "plant-pathogen interaction" and "MAPK signaling" pathway (enriched only in wt RCNMV infection) most of the DEGs were upregulated *(Fig. 3.12-B)*. These DEGs were involved in both PAMP-triggered immunity and effector-triggered immunity affecting hypersensitive-response (HR) and defense-related gene induction *(Fig. 3.13)*. Transcripts for several calcium-dependent protein kinase (CDPK) genes and one Respiratory burst oxidase homolog protein A (RBOHA) gene accumulated at significantly higher levels in wt RCNMV-infected plants than mock or RCNMVΔSR1f-infected plants. This result was not unexpected as plants elicit a reactive oxygen species (ROS) burst as an antiviral defense response, yet RCNMV requires ROS production for efficient replication (Hyodo et al. 2017). It is possible that in wt RCNMV infection, viral RNA and proteins accumulate to a sufficient level to elicit a strong defense response, especially coat protein-mediated HR response (Adhab et al. 2019), and the virus hijacks one of those defense responses (ROS) to accelerate viral replication. This can be seen as high levels of RNA1 accumulation in wt RCNMV infection compared to RNA1-m1 in RCNMVΔSR1f infection in which the host does not elicit a strong defense or ROS response.

Plant-pathogen interactions are greatly impacted by phytohormone signaling (Alazem and Lin 2015; Zhao and Li 2021). The "Plant hormone signal transduction" pathway was enriched in both wt RCNMV and RCNMVΔSR1f infections. In this pathway, 80 and 9 genes

were differentially regulated during wt RCNMV and RCNMVΔSR1f infection, respectively *(Fig. 3.12-B)*. The salicylic acid pathway, which is key for systemic acquired resistance (SAR) and induction of PR-proteins, was upregulated only in wt RCNMV infection *(Fig. 3.14)*. The abscisic acid pathway was upregulated in both wt RCNMV and RCNMVΔSR1f infection *(Fig. 3.14)*. In the "photosynthesis" pathway, only one gene was upregulated and 35 were downregulated in wt RCNMV-infected plants whereas 18 genes were upregulated, and seven were downregulated in RCNMVΔSR1f infection *(Fig. 3.12-B and Supplemental file 3.4)*. Essentially, 19 components of photosystem I and II, cytochrome b6/f complex, photosynthetic electron transport, and F-type ATPase were mainly downregulated in wt RCNMV infection while in RCNMVΔSR1f infection, only 1 component of photosystem II was downregulated, and five components of photosystem I and II, and F-type ATPase were upregulated *(Fig. 3.15)*. In addition to the dysregulated metabolic pathways, a disruption in photosynthesis machinery may contribute to the symptom development in wt RCNMV infection. In the "Metabolic pathways", 247 genes were upregulated and 107 genes were downregulated in wt RCNMV infected plants while only 30 genes were upregulated and 40 genes were downregulated in RCNMVΔSR1f infected plants *(Fig. 3.12-B)*. In the "Protein processing in endoplasmic reticulum" pathway, enriched only in wt RCNMV-infection, 37 genes were upregulated while only 3 were downregulated *(Fig. 3.12-B)*. This may be a consequence of ER membrane remodeling during RCNMV replication (Turner et al. 2004; Hyodo et al. 2013). It would be interesting to test if RCNMV-infected cells undergo ER-stress and elicit unfolded protein response.

LRR-RLKs/RLPs and PR genes

Leucine rich repeat receptor-like kinases and proteins (LRR-RLKs/RLPs) play important roles in plant development, immunity and stress responses (Breiden and Simon 2016; Ye et al.

2017; He et al. 2018; Macho and Lozano-Duran 2019). These are the primary components that recognize the pathogen/damage-associated molecular patterns (P/DAMPS) and elicit pattern-triggered immunity (PTI). Out of the 317 LRR-RLKs and 86 LRR-RLPs identified in *N. benthamiana* (Wang et al. 2018), 38 LRR-RLKs and 15 LRR-RLPs were differentially regulated in wt RCNMV infection *(Table 3.3)*. However, none of the LRR-RLKs/RLPs were differentially regulated in RCNMVΔSR1f infection. Another component of the plant's innate immune response includes induction of Pathogenesis-related (PR) proteins upon pathogen attack. Out of 29 PR-genes identified in *N. benthamiana* (Li et al. 2018), 12 genes encoding PR-1, PR-2, PR-3, PR-4, PR-9, PR-11 proteins were differentially upregulated in wt RCNMV infection, whereas only 3 genes, all encoding PR-2 protein, were upregulated in RCNMVΔSR1f infection *(Table 3.4)*.

Validation of RNA-seq analysis using qRT-PCR

To validate our RNA-seq data analysis, we selected seven host DEGs that were involved in the enriched pathways and quantified their abundance using qRT-PCR. Candidate genes included PR-1, PR-2, Abscisic acid responsive element binding factor (ABF), WRKY transcription factor (WRKY), Respiratory burst oxidase homolog protein A (Rboh), Jasmonate-zim-domain protein (JAZ), and Proteinase inhibitor I-B (PI). The $\log_2$-fold change and their statistical significance values were consistent between the RNA-seq. and qRT-PCR analysis *(Fig. 3.16)*.

Read coverage on viral RNAs

RNA-seq reads were mapped to RCNMV RNA1 and RNA2 and the number of reads at every nucleotide position on the viral RNA were counted and scaled according to the DESeq2

scaling factor *(Fig. 3.17-A, B)*. Overall, more reads mapped to RNA1 in wt RCNMV-infected plants than RNA1-m1 in RCNMVΔSR1f-infected plants *(Fig. 3.17-A)*. This was verified using qRT-PCR *(Fig. 3.17-C)*. Read coverage across the negative strand of RNA1 or RNA1-m1 was more than ten-fold less than the positive strand for most of the genome, as expected *(Fig. 3.17-A)*. Reads mapping to negative strand clearly show that CPsgRNA1 negative strand was more abundant than RNA1 negative strand upstream of the region corresponding to CPsgRNA1 *(Fig. 3.17-A)*. However, we did not see a particularly high number of reads mapping to the SR1f region. The number of reads at the 5' ends of the genomic and subgenomic RNAs may be artificially reduced owing to the library preparation kit that we used, which may explain this unexpected observation. However, when the coverage over each nucleotide of RNA1/RNA1-m1 was normalized according to the total number of mapping hits to RNA1 or RNA1-m1, the accumulation of SR1f can clearly be seen only in wt RCNMV infected samples *(Fig. 3.18)*.

The read coverage profile on RNA2 positive strand was not much different in either infection *(Fig. 3.17-B)*. The number of reads mapping to RNA2 in both cases differed by only ~50% but the difference was not statistically significant *(Fig. 3.17-D)*. This did not agree with our qRT-PCR validation where the RNA2 abundance in RCNMVΔSR1f infection was ~20 % of that in wt-RCNMV infection and highly significant *(Fig. 3.17-D)*, similar to the decrease in RNA1 abundance *(Fig. 3.17-C)*. Additionally, the coverage profile on RNA2 positive strand was rather unexpected. The reads were highly represented in the 5' half of RNA2, then they decline near the middle of the RNA2 sequence, and then increase again toward the 3' end *(Fig. 3.17-B)*. It is unlikely that this is a library preparation artifact because we observed a similar pattern of RNA2 coverage in RCNMV-infected Arabidopsis in an independent RNA-seq experiment that used a different library preparation strategy, library preparation kit, and

sequencing read length *(Chapter 4).* Interestingly, this inflection point coincides with the trans-activator (TA) sequence in RNA2. Intermolecular base pairing between the TA sequence in RNA2 and the 8-nt sequence upstream of the coat protein subgenomic promoter on RNA1 is required to produce negative strand of CPsgRNA1 via premature transcription termination of negative strand synthesis to generate the template for CPsgRNA1 synthesis (Sit et al. 1998; Im et al. 2021). The coverage profile of reads on the negative strand RNA1 or RNA1-m1 showing greater number of reads in the CPsgRNA1 region further supports the premature transcription termination model *(Fig. 3.17-A).*

The proportion of individual viral RNAs relative to the total number of host mRNA reads revealed that positive and negative strand RNA1 and negative strand RNA2 are more abundant in wt RCNMV-infected plants compared to RCNMVΔSR1f-infected plants *(Fig. 3.17-E).* However, there is no significant difference in abundance of positive strand RNA2 in either infection *(Fig. 3.17-E).* Upon inspecting *Fig. 3.17-E* more closely, we observed that the proportion of reads from positive strand RNA2 is less than positive strand RNA1 in wt RCNMV-infected plants *(Fig. 3.17-E).* On the contrary, the proportion of reads from negative strand RNA1 is similar to negative strand RNA2 in wt RCNMV-infected plants and the proportion of reads from positive and negative strand RNA1 is similar to positive and negative strand RNA2, respectively, in RCNMVΔSR1f-infected plants *(Fig. 3.17-E).* This leads us to speculate that SR1f may negatively regulate the synthesis of positive strand RNA2 in late stages of infection.

Discussion

In this study, we assessed the role of the noncoding RNA of an RNA virus interacting with its host using *N. benthamiana* and Arabidopsis as hosts. We also provide a comparative

genome-wide transcriptomic analysis in *N. benthamiana* to assess how RCNMV infection and the presence of SR1f affect cellular gene expression.

Lack of SR1f reduces virus levels and symptoms

Reduced symptoms and decreased viral RNA accumulation in *N. benthamiana* and Arabidopsis plants inoculated with SR1f-deficient RCNMV mutant suggests an important role for SR1f in establishing a successful infection *(Fig. 3.2, 3.3).* Notable differences in symptoms in *N. benthamiana* infected with wt RCNMV and RCNMVΔSR1f *(Fig. 3.2-B, C)* contrasts with a previous report (Iwakawa et al. 2008), which reported (but did not show) mosaic symptoms in systemic leaves in *N. benthamiana* infected with several SR1f-deficient RCNMV RNA1 mutants, including the mutant, RNA1-m1, that we have used in our study. However, similar to our observation, it has been shown that a Tobacco necrosis virus (TNV)-D mutant, that cannot make the ncsgRNA, produced milder symptoms than the wt TNV-D infection in *N. benthamiana* (Gunawardene et al. 2019). The authors also showed that viral RNA accumulation was reduced in TNV-D mutant infection compared to the wt TNV-D infection, which is similar to the previous RCNMV report (Iwakawa et al. 2008) and our results *(Fig. 3.2-E, 3.17-C, D).* Thus, throughout this study, we cannot distinguish whether most differences in host response were due to SR1f *per se* or due to reduced virus load in general.

Defective antiviral RNA silencing pathway does not rescue RCNMVΔSR1f replication

Based on the previous reports that have demonstrated the RNA silencing suppressor activity of ncsgRNAs of WNV, DENV, Kunjin virus (KUNV), and BNYVV (Schnettler et al. 2012; Moon et al. 2015; Flobinus et al. 2016), we hypothesized that RCNMV SR1f may function as an RNA silencing suppressor. If this were the only function of SR1f, we would expect more

symptoms and viral RNA accumulation in RCNMVΔSR1f-inoculated *dcl2-1/dcl4-2t* Arabidopsis plants than in wt Arabidopsis because this mutant lacks the antiviral RNA silencing machinery. However, Arabidopsis *dcl2-1/dcl4-2t* mutant did not rescue the replication of RCNMVΔSR1f *(Fig. 3.3).* Furthermore, previous reports have shown that the formation of the 480 kDa RCNMV replication complex and the subsequent replication of RNA1 or RNA2 alone is sufficient to suppress RNA silencing in *N. benthamiana* (Takeda et al. 2005) and the movement protein encoded by RNA2 is also a suppressor of RNA silencing (Powers et al. 2008). Therefore, we concluded that SR1f performs an essential function other than RNA silencing suppression. This does not rule out the possibility that it may also play a role in RNA silencing suppression, for example similar to the BNYVV ncRNA3 that complements BNYVV p14 protein to suppress RNA silencing (Flobinus et al. 2016).

XRN4 is not required to generate SR1f

A key question in plants is which XRN is responsible for generating ncsgRNAs via blockage at the xrRNA structure? In plants, XRN4 is the only known cytoplasmic 5'→ 3' XRN, a functional equivalent of XRN1 in yeast and mammals and has been assumed to be responsible for generating xrRNA-derived ncsgRNAs (Flobinus et al. 2016, 2018; Gunawardene et al. 2019; Ilyas et al. 2021). A previous report showed that ectopic expression of plant XRN4 in *Saccharomyces cerevisiae (*Δ*xrn1 background)* could generate BNYVV ncRNA3 (Flobinus et al. 2018). The authors also demonstrated that VIGS knock-down of XRN4 affects BNYVV accumulation and inhibits its systemic spread in *N. benthamiana*, however, BNYVV ncRNA3 was still present (Flobinus et al. 2018) suggesting that XRN4 may not be necessary for ncRNA3 biogenesis, although residual XRN4 may be present in VIGS knock-down plants. In our

experiment, we detected high levels of SR1f in wt RCNMV-infected *xrn4-5* Arabidopsis plants *(Fig. 3.4),* which have a T-DNA insertion in exon 18 of the only *XRN4* gene so they do not make a functional XRN4 (Souret et al. 2004), thereby showing the lack of requirement for XRN4 to produce SR1f. Thus, if XRN4 can generate xrRNA, it is not the only exoribonuclease that does so. In fact, diverse 5'→ 3' exoribonucleases, unrelated to XRN1, such as yeast Dxo1 and bacterial RNase J1 have been shown to be capable of generating SR1f *in vitro* (Steckelberg et al. 2018a). Even flaviviral xrRNAs can block different 5'→ 3' exoribonucleases (MacFadden et al. 2018). This raises important questions: which exoribonuclease(s) are responsible for the production of xrRNA-derived ncsgRNAs *in planta* during infection? Is there a yet-unidentified cytoplasmic 5'→ 3' XRN in plants that is responsible for making viral ncsgRNAs? Can other plant XRNs functionally replace XRN4 in its absence? For characterization of xrRNA-derived ncsgRNAs of plant viruses, one could screen and identify Arabidopsis 5'→ 3' exoribonuclease loss of function mutants that cannot make viral ncsgRNAs.

Effects of wt RCNMV and RCNMVΔSR1f on the host transcriptome

To test how the cellular gene expression is affected in *N. benthamiana* infected with wt RCNMV and RCNMVΔSR1f, we conducted RNA-seq. Based on read counts, wt RCNMV accumulated five times as much as the RCNMVΔSR1f mutant, so we cannot distinguish effects of loss of SR1f *per se* from those due to less virus accumulation in general. However, in the plants infected with wt RCNMV, we can identify host genes that may be affected by presence of SR1f. According to our RNA-seq data, almost two-thirds of DEGs are upregulated (69 %) in wt RCNMV infection, whereas in RCNMVΔSR1f infection, an almost equal proportion of DEGs are upregulated (45 %) and downregulated (55 %) *(Fig. 3.9-A).* This pattern of a greater

proportion of DEGs being upregulated (i.e., show an increased level of mRNA) in a virus infection that produces an xrRNA-derived ncsgRNA has been reported previously in flavivirus-infected cells (Moon et al. 2012). In that report, the amount of XRN1 available for normal turnover of mRNAs was found to be reduced in infected cells, owing to its tight association with flaviviral sfRNA, thus sequestering it from its normal cellular activities, resulting in abnormal stabilization of cellular mRNAs. In their experiment, the wildtype KUNV and the sfRNA-mutant KUNV replicated to the same level and therefore they were able to attribute their results to the presence of the sfRNAs (Moon et al. 2012). However, in our case, wt RCNMV replicates to a higher level than RCNMVΔSR1f and therefore, the greater proportion of DEGs being upregulated may be due to increased cellular transcriptional response to virus replication, in addition to any increased mRNA stability arising from disruption of RNA decay pathway by sequestration of a 5'→ 3' XRN by SR1f. Even though it has not been shown that RCNMV SR1f can stabilize cellular RNAs *in vivo*, it can increase RCNMV RNA2 accumulation in BY-2 cell-free replication assays (Iwakawa et al. 2008). According to the GO term and KEGG pathway enrichment analysis, wt RCNMV infection disrupts more cellular pathways and to a greater extent than RCNMVΔSR1f infection *(Fig. 3.10 – 3.15)*. Which of these effects can be attributed to host response to virus infection in general, and which are specifically due to presence of SR1f remains to be determined. Either way, the large reduction in virus accumulation due to absence of SR1f demonstrates that SR1f plays an important role in the virus life cycle.

We also looked at the differential expression of a few cellular genes in our dataset that are known to be co-opted by RCNMV and other tombusvirids, such as tomato bushy stunt virus (TBSV) and carnation italian ringspot virus (CIRV). DEGs in the enriched pathways that are known to be recruited by RCNMV included Rboh and CDPKs (Hyodo et al. 2017). In addition

to these, genes encoding phospholipase D (PLD), heat shock protein 70 (HSP70), HSP90, ADP-ribosylation factor (Arf) were also upregulated only in wt RCNMV infected plants *(Fig. 3.9-B)*. PLD enzymes catalyze the production of phosphatidic acid which interacts with RCNMV replication protein p27 and promotes RCNMV replication (Hyodo et al. 2015). HSP70 and HSP90 interact with RCNMV p27 at the ER membrane and this interaction is required for the formation of a functional 480 kDa RCNMV replicase complex for successful RCNMV replication (Mine et al. 2012). RCNMV replication protein p27 also interacts with Arf1, which is a ubiquitous, highly conserved GTPase involved in the formation of COPI vesicles on Golgi membranes, and relocalizes it from Golgi apparatus to the RCNMV replication site on the ER (Hyodo et al. 2013). Selected DEGs that are recruited by other tombusvirids include oxysterol-binding protein-related protein (ORP), Vesicle-associated membrane protein-associated protein (VAP), Vacuolar protein-sorting protein bro1 (BRO1), all of which were upregulated only in wt RCNMV infected plants *(Fig. 3.9-B)*. ORP and VAP are co-opted by TBSV and CIRV for re-distribution of sterols to the virus replication sites (Barajas et al. 2014). BRO1 is required for efficient TBSV replication by recruiting ESCRT-III factors in the virus replication complexes (Kovalev et al. 2016). The list of unigene IDs of the above-mentioned genes and their differential expression can be found in *Table 3.5*. In summary, RCNMV induces expression of several proteins shown to be co-opted by TBSV or CIRV, while also inducing and using different proteins. This reveals the similarities and differences among viruses in different genera of the *Tombusviridae*.

Effect of RCNMV∆SR1f on viral RNA levels

RNA-seq reads mapped to RCNMV RNA1 and RNA2 that showed some expected features such as greater abundance of reads mapping to positive strand than the negative strand.

The greater number of reads mapping to CPsgRNA1 sequence in the negative strand *(Fig. 3.17-A, B)* compared to the rest of RNA1, rather than a uniform distribution of reads along the full-length negative strand of RNA1, supports the premature transcription termination model for the synthesis of negative strand CPsgRNA1 (Sit et al. 1998). According to this model, CPsgRNA1 positive strand is transcribed from the 3' terminus of incomplete RNA1 negative strand that arises as a result of premature transcription termination during the synthesis of negative strand RNA1 (Sit et al. 1998).

Corresponding with the accumulation of CPsgRNA1 and SR1f subgenomic RNAs we expected to see more reads in the positive strand in these regions compared to the upstream region of RNA1. However, we saw more reads only for the CPsgRNA1 region, which includes SR1f sequence, but no additional increase in reads was observed for SR1f-specific sequence *(Fig. 3.17-A)*. We think the lack of an even higher number of reads corresponding to the SR1f portion of RNA1 may be an artifact from the library preparation. The library preparation kit that we used utilizes random hexamer-mediated cDNA synthesis as its first step followed by bead clean-ups that retained reads of average ~300 nt. Thus, cDNAs from regions within 300 nt of the 3' end would be less than 300 bp and would have been removed and therefore, we would see fewer reads than expected mapping to this region *(Fig. 3.17-A)*. In contrast, the reads mapping to CPsgRNA1 would be mostly retained. However, most of the cDNAs synthesized from CPsgRNA1 would terminate at its 5' end and therefore only the 5' end of CPsgRNA1 would be over-represented in our sequencing data. Indeed, we observe this phenomenon at the 5' end of positive strand RNA1, CPsgRNA1, RNA2 and the co-terminal 5' ends of the negative strand RNA1 and CPsgRNA1 *(Fig. 3.17-A, B)*. Despite this limitation, the accumulation of SR1f can

clearly be seen only in wt RCNMV infected samples when the RNA1/RNA1-m1 coverage was normalized to the total number of mapping hits to RNA1 or RNA1-m1 *(Fig. 3.18)*.

Possible functions of SR1f

In summary, using RCNMV SR1f as a model to study xrRNA-derived ncsgRNAs of plant viruses, we show that SR1f plays a key role in virus accumulation and symptom development, possibly by regulating virus and host gene expression and counteracting plant's defense responses. We conclude that the primary function of SR1f is not an RNA silencing suppressor but may have an important role in counteracting plant defenses and/or modulating virus life cycle by a yet-unknown mechanism. Using a reporter system, it has been shown that RCNMV SR1f *trans*-inhibits both cap-independent and cap-polyA-dependent translation *in vitro* and *in vivo* in BY-2 protoplast and it suppresses cap-polyA-dependent translation more efficiently than it inhibits 3' TE-DR1-mediated (viral) cap-independent translation (Iwakawa et al. 2008). Therefore, the authors hypothesized that accumulation of SR1f may sequester translation initiation factors and/or ribosomal small sub-units and suppress translation of cellular mRNAs. However, how RCNMV-infection and SR1f accumulation in plants affects cellular mRNA translation has not been studied yet.

SR1f may also regulate translation of viral RNAs as has been shown for the sgRNA2 of BYDV, which, like SR1f, contains the BTE. Via its BTE, which binds translation factor eIF4G, sgRNA2 selectively inhibits translation of genomic RNA, relative to that of the subgenomic RNA that encodes, movement and coat proteins (Shen et al. 2006). As hypothesized previously (Iwakawa et al. 2008), SR1f may do the same, but favor translation of CPsgRNA1 and RNA2. Thus, absence of SR1f would perturb optimal regulation of translation of viral RNAs by viral RNA.

It has been shown that RCNMV SR1f and TNV-D svRNA are packaged in the virions (Iwakawa et al. 2008; Gunawardene et al. 2019), unlike WNV sfRNA (Pijlman et al. 2008). This suggests that SR1f may also have a role in the early stages of infection. Based on previous reports, results presented in this study and some of our unpublished data, we present the following hypothesis. In the early stages of infection when the specific antiviral pathways have not been triggered, a cytoplasmic 5'→ 3' XRN could degrade RCNMV genomic RNAs, which (unlike flavivirus RNAs) are uncapped. However, the co-packaged SR1f could sequester the XRN, thus minimizing degradation of viral genomic RNA, allowing it to initiate translation followed by replication. Having an uncapped genome may be the selective pressure resulting in the packaging of SR1f. TNV-D has an uncapped genome and its svRNA is also packaged (Gunawardene et al. 2019). BNYVV genomic RNAs are capped but we are unaware of any evidence indicating whether its ncRNA3 is packaged. In contrast to tombusvirids, the cap on flaviviral RNA may provide initial protection or delay in viral RNA degradation (thus explaining the absence of packaged sfRNA (Pijlman et al. 2008)), that in RCNMV and TNV-D may be provided by the SR1f and svRNA, respectively, which are present immediately upon RNA entry from the virion. This initial assistance from SR1f would minimize the degradation of viral genomic RNAs that can kick-start the production of the replicase proteins followed by viral RNA replication. Accumulation of viral RNAs and proteins will elicit antiviral defense responses, including the ROS burst, which is hijacked by RCNMV to accelerate its replication efficiency (Hyodo et al. 2017). At a later stage, SR1f accumulation may inhibit translation of viral RNAs by binding and sequestering eIF4F, as hypothesized before (Iwakawa et al. 2008), making them available for encapsidation similar to the riboregulator function of BYDV sgRNA2 (Shen and Miller 2004; Shen et al. 2006). On the other hand, RCNMVΔSR1f does not produce SR1f.

Therefore, 5'→ 3' XRN may quickly degrade viral genomic RNAs, thus reducing accumulation of viral products. Moreover, the plant defense responses will not be triggered and there will be no ROS burst that RCNMV exploits for an efficient replication.

Materials and Methods

In vitro transcription of RCNMV RNAs

RCNMV plasmid constructs used for *in vitro* transcription were described previously (Kanodia et al. 2020). pRC169c and pRC2|G are cDNA clones with T7-promoter for *in vitro* transcription of infectious RCNMV RNA1 and RNA2, respectively. **pR1m1** is a cDNA clone of RCNMV RNA1 (RNA1-m1) that does not generate SR1f in infected cells. One µg of SmaI-linearized pRC169c, pRC2|G and pR1m1 were used as template for *in vitro* transcription using MEGAscript T7 Transcription kit (Invitrogen AM1334) followed by DNase treatment according to manufacturer's protocol. The transcription reaction was carried out at 37 ˚C for 4 h and DNase treatment at 37 ˚C for 30 min. Subsequently, RNA was purified using Zymo RNA clean & concentrator -5 kit (Zymo Research R1015) and eluted in nuclease-free water.

Virus inoculation in Arabidopsis

Arabidopsis double knock-out mutant line, *dcl2-1/dcl4-2t* (Germplasm CS66078) (Xie et al. 2005), and the single knock-out mutant line, *xrn4-5* (Germplasm CS68822) (Souret et al. 2004), were obtained from the Arabidopsis Biological Resource center (abrc.osu.edu) and the T-DNA insertion was verified by genotyping *(Fig. 3.19, Table 3.7)* (O'Malley et al. 2015). Arabidopsis Col-0 wildtype and the mutant lines were grown in growth chambers with 16 h light at 24 ˚C and 8 h dark at 20 ˚C. Arabidopsis plants were mechanically inoculated with RCNMV using the sap from RCNMV-infected *N. benthamiana*. Firstly, three-week-old *N. benthamiana*

plants were mechanically-inoculated with RCNMV RNA1 plus RNA2 (wt RCNMV-inoculated) or RCNMV RNA1-m1 plus RNA2 (RCNMVΔSR1f-inoculated) in 10 mM sodium phosphate buffer (pH 6.8). At 7 dpi, infected *N. benthamiana* leaves were ground in 10 mM sodium phosphate buffer (pH 6.8) with mortar and pestle and the resulting sap was rubbed on 2-3 leaves per Arabidopsis plant using q-tips and carborundum. Subsequently, new non-inoculated Arabidopsis leaves were collected and pulverized. Total RNA was extracted using the TRIzol method (Invitrogen) and 2-5 µg total RNA was used for northern blot hybridization as previously described (Kanodia et al. 2020).

Virus inoculation in *N. benthamiana* for RNA sequencing

N. benthamiana plants were grown in a growth chamber with 16 h light at 24 ˚C and 8 h dark at 20 ˚C. At the 4-leaf stage (2 true leaves and 2 false leaves), 1st and 2nd true leaves were mechanically inoculated with (i) 10 mM sodium phosphate (pH 6.8) buffer (Mock-inoculated), (ii) 1 µg RNA1 plus 1 µg RNA2 in 10 mM sodium phosphate (pH 6.8) buffer per leaf (wt RCNMV inoculated), (iii) 1 µg RNA1-m1 plus 1 µg RNA2 in 10 mM sodium phosphate (pH 6.8) buffer per leaf (RCNMVΔSR1f inoculated). Five plants were inoculated for each condition. Growth conditions were changed to 16 h light at 20 ˚C and 8 h dark at 20 ˚C. At 15 dpi, the 7th leaf was collected from each plant and pulverized in liquid nitrogen followed by addition of 1 ml TRIzol (Invitrogen). Total RNA was extracted using Zymo Direct-zol miniprep columns (Zymo Research R2051) and quantified using Qubit RNA HS assay kit (Invitrogen Q32852). Subsequently, 5 µg total RNA was treated with 1 µl Turbo DNase (Invitrogen AM2238) in a 50-µl reaction with 1x Turbo DNase buffer at 37 °C for 30 min followed by addition of 1 µl more Turbo DNase and incubation at 37 °C for additional 30 min, purification by Zymo RNA clean &

concentrator −5 columns (Zymo Research R1016) and quantified using Qubit RNA HS assay kit (Invitrogen Q32852). Total RNA integrity was verified using 1% agarose gel electrophoresis.

cDNA synthesis and RT-PCR

RevertAid First Strand cDNA Synthesis kit (Thermo Scientific K1622) was used according to manufacturer's protocol with gene-specific primers. One µg total RNA and 15 pmoles RCNMV-specific reverse primer *(5'-GGGGTACCTAGCCGTTATAC-3')* were mixed in nuclease-free water to 12 µl and incubated at 65 ˚C for 5 min, transferred to ice followed by addition of 4 µl reaction buffer, 1 µl RiboLock, 2 µl 10mM dNTPs and 1 µl RT enzyme. The reaction mix was incubated at 42 ˚C for 60 min followed by enzyme deactivation at 70 ˚C for 5 min. A 20-µl PCR reaction mix was prepared with 10 ul GoTaq G2 green master mix (Promega M7823), 2 µl cDNA template, 200 nM each of forward *(5'-AAGCGGGCCAGTAGAGTC-3')* and reverse *(5'-CACAACATCCGCCAAAGAGG-3')* primer. The PCR conditions were as follows: 98 ˚C (2 min); 25 cycles of 98 ˚C (30 s), 65 ˚C (20 s), 72 ˚C (30 s); 72 ˚C (2 min); 4 ˚C hold.

RNA sequencing

One µg DNAse-treated total RNA from 3 biological replicates of mock-inoculated and four biological replicates each of wt RCNMV- and RCNMVΔSR1f- inoculated *N. benthamiana* were used for library preparation using Zymo-seq RiboFree total RNA library prep kit (Zymo Research R3000S). During the library preparation, the rRNA depletion was carried out for 45 min, and 10 cycles of library index PCR was performed using Zymo-Seq UDI primer set (Indexes 1-11, Zymo D3008). Final libraries were quantified using Qubit dsDNA HS assay kit (Invitrogen Q32854), and the library quality was assessed using an Agilent bioanalyzer high sensitivity DNA assay kit. Final libraries were sequenced using Zymo Research's services

(www.zymoresearch.com/) on one high-output lane of Illumina Hiseq 1500 instrument with pair-ended 100 bp read length. The eleven RNA-seq samples were trimmed for adapters and quality using Trim galore 0.4.5 (github.com/FelixKrueger/TrimGalore). The *N. benthamiana* 1.0.1 genome and annotation was obtained from the Sol Genomics Network (Fernandez-Pozo et al. 2015). Reads were mapped to the *N. benthamiana* (Bombarely et al. 2012) genome using Hisat2 2.1 (Kim et al. 2019), processed using Samtools 1.9 (Li et al. 2009), and counts were obtained using featureCounts in the Subread 1.6 (Liao et al. 2014). Differential expression was computed using DESeq2 (Love et al. 2014). List of all DEGs can be found in the *Supplemental file 3.1*. Principal component analysis was performed using the regularized log transformed data from DESeq2. For GO term enrichment analysis, the 4 DEG dataset (wt RCNMV upregulated, wt RCNMV downregulated, RCNMVΔSR1f upregulated and RCNMVΔSR1f downregulated) were used, and for KEGG pathway enrichment analysis, the 2 DEG dataset (wt RCNMV vs. mock and RCNMVΔSR1f vs. mock) were used as input in "kobas.cbi.pku.edu.cn/kobas3/genelist" with the following parameters: Type: "Fasta protein sequence", Species: "*Arabidopsis thaliana*", Pathway: "KEGG pathway" or GO: "GO", Statistical method: "hypergeometric test/Fisher's exact test" and FDR correction method: "Benjamini and Hochberg (1995). The enriched GO terms with their adjusted p-values were further used with Revigo (Supek et al. 2011) for visualization with the following parameters: Allowed similarity: "Medium", Database: "*Arabidopsis thaliana*", and semantic similarity measure: "SimRel". The pathway involvement was visualized using KEGG Mapper (Kanehisa and Sato 2020). The functional annotation of the selected genes was determined using the "Niben101_annotation.proteins.wdesc.fasta" file from the Sol Genomics Network (Fernandez-Pozo et al. 2015).

For analyzing RCNMV RNA abundance, the adapter trimmed reads were mapped to RCNMV RNA1/RNA1-m1 and RNA2 using Bowtie2 (Langmead and Salzberg 2012) with the "--sensitive-local" option. To obtain alignment information individually for positive and negative strands of RCNMV RNAs, the alignment file was split according to their flag information using Samtools. Subsequently, the Salmon tool (Patro et al. 2017) was used to quantify the number of reads mapping to positive and negative strands of the RCNMV genome. The read counts were normalized by dividing the read count to the DESeq2 scaling factors to account for the sequencing depth. The scaling factors were obtained using DESeq2 with the count table of reads mapping to the *N. benthamiana* genome and RCNMV genome as input. To obtain read coverage on the RCNMV genome, the Sam files were converted to bam file format, sorted, and indexed using Samtools. Subsequently, the bamCoverage function in deepTools 2.5.2 (Ramírez et al. 2016) was used with "--scaleFactor" option with the reciprocal of DESeq2 scaling factors for each sample. Additionally, the "--filterRNAstrand" option is set as "forward" or "reverse" to get read coverage on the positive and negative strands of RCNMV separately. Geometric mean of the scaled number of reads that mapped to each nucleotide position of RCNMV genome in the output bedgraph file was plotted in the *Fig. 3.17*.

In vitro translation

Wheat germ extract (WGE; Promega L4380) was used for *in vitro* translation. Triplicates of 389 ng each (25 nM final RNA concentration) of *in vitro* transcribed RCNMV RNA1 or RNA1-m1 in 3.75 µl water were incubated at 67 ˚C for 10 min and transferred to ice, followed by the addition of 1 µl amino acid mix (without methionine), 1 µl 1M potassium acetate, 0.5 µl EasyTag L-[35S]-Methionine (Perkin Elmer NEG709A), and 6.25 µl WGE. The reaction was incubated at 25 ˚C for 30 min, and translation was terminated by transferring the tubes to ice. To

the 12.5-µl reaction, 3.2 µl NuPAGE 4x LDS sample buffer (Invitrogen NP0007) and 1.5 µl NuPAGE 10x sample reducing (Invitrogen NP0009) agent was added, incubated at 70 ˚C for 10 min and 15 µl reaction was run in NuPAGE Novex 4-12% Bis-Tris Gel (Invitrogen NP0322BOX) with 1x NuPAGE MES SDS running buffer (Invitrogen NP002) at 200V for 40 min. The gel was washed three times with water for 5 min, once with fixing solution (50% methanol + 7% acetic acid) for 15 min, and three times with water for 5 min. All washing steps were carried out at room temperature. The dried gel was imaged by autoradiography using Bio Rad PharosFX Plus Molecular Imager.

qRT-PCR

One µg DNAse-treated total RNA (the same RNA used for RNA-seq) from 2 biological replicates of mock-inoculated and 4 biological replicates each of wt RCNMV- and RCNMVΔSR1f- inoculated *N. benthamiana* were reverse transcribed using RevertAid First strand cDNA synthesis kit (Thermo Scientific K1622) according to manufacturer's protocol with random hexamers. The resulting cDNA was diluted 10-fold and 20-fold for quantifying the abundance of transcripts from *N. benthamiana* and RCNMV, respectively. A 10-µl qPCR reaction was prepared with 1x iQ SYBR Green Supermix (Bio Rad 1708880), 300 nM each of forward and reverse primer, and 1 µl diluted cDNA template. The qPCR runs were carried out in 384-well plates with three technical replicates per sample in a Bio Rad CFX384 system with the following reaction conditions: 95 ˚C for 3 min (Polymerase activation and DNA denaturation), 40 cycles of 95 ˚C for 10 s (Denaturation), 60 ˚C for 60 s (Annealing, extension/Plate reading) followed by melt curve analysis (55-95 ˚C, 0.5 ˚C increment, 5 s). NbPP2A and NbL23 genes were used as reference genes for normalizing the abundance of *N. benthamiana* and RCNMV RNAs (Liu et al. 2012). Prior to using these as reference genes, we verified their consistent

expression between our experimental conditions. The primer efficiency calculation, ΔΔCt calculation, and statistical analysis were performed using the Bio Rad CFX manager software. The reference gene primer sequences were obtained from Liu et al. (2012), the NbPR1 primer sequences were obtained from Obrępalska-Stęplowska et al. (2018) and all the remaining primers were designed using the primer3 tool (primer3.ut.ee) (Koressaar and Remm 2007; Untergasser et al. 2012). To verify the specificity of the primers and determine the unigenes that would be amplified by the primers, we used Primer-BLAST tool (ncbi.nlm.nih.gov/tools/primer-blast) against the *N. benthamiana* 1.0.1 transcript sequences obtained from the Sol Genomics Network (Fernandez-Pozo et al. 2015) with default parameters. The Unigenes that gave the expected amplicon size, had maximum of two-base mismatch within the primers but no mismatch at the last three bases in the 3' end of the primers were considered and are included in *Fig. 3.16.* All the primers were synthesized by Integrated DNA Technologies and purified by standard desalting. qRT-PCR primer sequences are listed in *Table 3.6.*

Data availability

The raw sequencing fastq files, RCNMV genome-mapped read counts and *N. benthamiana* genome-mapped fragment counts were deposited in the NCBI Gene Expression Omnibus database under accession number GSE178909.

Supplemental Material

Supplemental File 3.1 (List of differentially expressed genes from DESeq2), xlsx file

Supplemental File 3.2 (List of enriched GO terms), xlsx file

Supplemental File 3.3 (List of enriched KEGG pathways), xlsx file

Supplemental File 3.4 (List of DEGs for the selected enriched KEGG pathways), xlsx file

Acknowledgments

The authors thank Dr. Rick Masonbrink and Dr. Andrew Severin from the Genome informatics facility for assisting with the RNA-seq data analysis, Dr. Akshay Yadav and Dr. Gaurav Kandoi for help with bioinformatics, and Dr. Viraj Muthye for assistance with plant cultivation. The authors also thank Dr. Surapathrudu Kanakala for his advice on the experiment design and data analysis. This project was funded by Iowa State University Plant Sciences Institute Faculty Scholar award to WAM. This paper of the Iowa Agriculture and Home Economics Experiment Station, Ames, IA, Project No. 3808 was supported in part by Hatch Act and State of Iowa funds. The authors also thank Zymo Research for providing the sample kit for RNA-seq library preparation and complimentary Illumina sequencing services.

Conflict of Interest

The authors declare no conflict of interest associated with the work described in this manuscript.

References

Adhab M, Angel C, Rodriguez A, Fereidouni M, Király L, Scheets K, Schoelz JE. 2019. Tracing the Lineage of Two Traits Associated with the Coat Protein of the *Tombusviridae*: Silencing Suppression and HR Elicitation in Nicotiana Species. Viruses 11: 588.

Alazem M, Lin N. 2015. Roles of plant hormones in the regulation of host–virus interactions. Mol Plant Pathol 16: 529–540.

Barajas D, Xu K, de Castro Martín IF, Sasvari Z, Brandizzi F, Risco C, Nagy PD. 2014. Co-opted Oxysterol-Binding ORP and VAP Proteins Channel Sterols to RNA Virus Replication Sites via Membrane Contact Sites. PLoS Pathog 10: e1004388.

Bidet K, Garcia-Blanco MA. 2014. Flaviviral RNAs: weapons and targets in the war between virus and host. Biochem J 462: 215–230.

Bidet K, Dadlani D, Garcia-Blanco MA. 2014. G3BP1, G3BP2 and CAPRIN1 Are Required for Translation of Interferon Stimulated mRNAs and Are Targeted by a Dengue Virus Non-coding RNA. PLoS Pathog 10: e1004242.

Bombarely A, Rosli HG, Vrebalov J, Moffett P, Mueller LA, Martin GB. 2012. A Draft Genome Sequence of *Nicotiana benthamiana* to Enhance Molecular Plant-Microbe Biology Research. Mol Plant-Microbe Interact 25: 1523–1530.

Breiden M, Simon R. 2016. Q&A: How does peptide signaling direct plant development? BMC Biol 14: 58.

Chang JH, Xiang S, Tong L. 2011. 5′-3′ Exoribonucleases. In Ribonucleases. Nucleic Acids and Molecular Biology (ed. A. Nicholson), pp. 167–192, Springer, Berlin, Heidelberg.

Charley PA, Wilusz CJ, Wilusz J. 2018. Identification of phlebovirus and arenavirus RNA sequences that stall and repress the exoribonuclease XRN1. J Biol Chem 293: 285–295.

Clarke BD, Roby JA, Slonchak A, Khromykh AA. 2015. Functional non-coding RNAs derived from the flavivirus 3′ untranslated region. Virus Res 206: 53–61.

Deleris A, Gallego-Bartolome J, Bao J, Kasschau KD, Carrington JC, Voinnet O. 2006. Hierarchical Action and Inhibition of Plant Dicer-Like Proteins in Antiviral Defense. Science 313: 68–71.

Dilweg IW, Gultyaev AP, Olsthoorn RC. 2019. Structural features of an Xrn1-resistant plant virus RNA. RNA Biol 16: 838–845.

Donald CL, Brennan B, Cumberworth SL, Rezelj VV, Clark JJ, Cordeiro MT, Freitas de Oliveira França R, Pena LJ, Wilkie GS, Da Silva Filipe A, Davis C, Hughes J, Varjak M, Selinger M, Zuvanov L, Owsianka AM, Patel AH, McLauchlan J, Lindenbach BD, Fall G, Sall AA, Biek R, Rehwinkel J, Schnettler E, Kohl A. 2016. Full Genome Sequence and sfRNA Interferon Antagonist Activity of Zika Virus from Recife, Brazil. PLoS Negl Trop Dis 10: e0005048.

Fernandez-Pozo N, Menda N, Edwards JD, Saha S, Tecle IY, Strickler SR, Bombarely A, Fisher-York T, Pujar A, Foerster H, Yan A, Mueller LA. 2015. The Sol Genomics Network (SGN)—from genotype to phenotype to breeding. Nucleic Acids Res 43: D1036–D1041.

Flobinus A, Hleibieh K, Klein E, Ratti C, Bouzoubaa S, Gilmer D. 2016. A Viral Noncoding RNA Complements a Weakened Viral RNA Silencing Suppressor and Promotes Efficient Systemic Host Infection. Viruses 8: 272.

Flobinus A, Chevigny N, Charley PA, Seissler T, Klein E, Bleykasten-Grosshans C, Ratti C, Bouzoubaa S, Wilusz J, Gilmer D. 2018. Beet necrotic yellow vein virus noncoding rna production depends on a 5 ′ →3 ′ xrn exoribonuclease activity. Viruses 10: 137.

Gil N, Ulitsky I. 2020. Regulation of gene expression by cis-acting long non-coding RNAs. Nat Rev Genet 21: 102–117.

Gould AR, Francki RIB, Hatta T, Hollings M. 1981. The bipartite genome of red clover necrotic mosaic virus. Virology 108: 499–506.

Gunawardene CD, Newburn LR, White KA. 2019. A 212-nt long RNA structure in the Tobacco necrosis virus-D RNA genome is resistant to Xrn degradation. Nucleic Acids Res 47: 9329–9342.

He Y, Zhou J, Shan L, Meng X. 2018. Plant cell surface receptor-mediated signaling – a common theme amid diversity. J Cell Sci 131.

Hiruki C. 1987. The Dianthoviruses: A Distinct Group of Isometric Plant Viruses with Bipartite Genome. Adv Virus Res 33: 257-300.

Huang C, Cun Y, Yu H, Tong Z, Xiao B, Song Z, Wang B, Li Y, Liu Y. 2017. Transcriptomic profile of tobacco in response to Tomato zonate spot orthotospovirus infection. Virol J 14: 153.

Hyodo K, Mine A, Taniguchi T, Kaido M, Mise K, Taniguchi H, Okuno T. 2013. ADP Ribosylation Factor 1 Plays an Essential Role in the Replication of a Plant RNA Virus. J Virol 87: 163–176.

Hyodo K, Taniguchi T, Manabe Y, Kaido M, Mise K, Sugawara T, Taniguchi H, Okuno T. 2015. Phosphatidic Acid Produced by Phospholipase D Promotes RNA Replication of a Plant RNA Virus. PLoS Pathog 11: e1004909.

Hyodo K, Hashimoto K, Kuchitsu K, Suzuki N, Okuno T. 2017. Harnessing host ROS-generating machinery for the robust genome replication of a plant RNA virus. Proc Natl Acad Sci 114: E1282–E1290.

Ilyas M, Du Z, Simon AE. 2021. Opium Poppy Mosaic Virus Has an Xrn-Resistant, Translated Subgenomic RNA and a BTE 3′ CITE. J Virol 95: e02109-20.

Im JSH, Newburn LR, Kent G, White KA. 2021. Trans-Activator Binding Site Context in RCNMV Modulates Subgenomic mRNA Transcription. Viruses 13: 2252.

Iwakawa H, Mizumoto H, Nagano H, Imoto Y, Takigawa K, Sarawaneeyaruk S, Kaido M, Mise K, Okuno T. 2008. A Viral Noncoding RNA Generated by cis -Element-Mediated Protection against 5′→3′ RNA Decay Represses both Cap-Independent and Cap-Dependent Translation. J Virol 82: 10162–10174.

Jiao Y, An M, Li X, Yu M, Zhao X, Xia Z, Wu Y. 2020. Transcriptomic and functional analyses reveal an antiviral role of autophagy during pepper mild mottle virus infection. BMC Plant Biol 20: 495.

Jones RA, Steckelberg AL, Vicens Q, Szucs MJ, Akiyama BM, Kieft JS. 2021. Different tertiary interactions create the same important 3D features in a distinct flavivirus xrRNA. RNA 27: 54–65.

Kanehisa M, Sato Y. 2020. KEGG Mapper for inferring cellular functions from protein sequences. Protein Sci 29: 28–35.

Kang SH, Sun YD, Atallah OO, Huguet-Tapia JC, Noble JD, Folimonova SY. 2019. A Long Non-Coding RNA of Citrus tristeza virus: Role in the Virus Interplay with the Host Immunity. Viruses 11: 436.

Kanodia P, Prasanth KR, Roa-Linares VC, Bradrick SS, Garcia-Blanco MA, Miller WA. 2020. A rapid and simple quantitative method for specific detection of smaller coterminal RNA by PCR (DeSCo-PCR): application to the detection of viral subgenomic RNAs. RNA 26: 888–901.

Kastenmayer JP, Green PJ. 2000. Novel features of the XRN-family in Arabidopsis: Evidence that AtXRN4, one of several orthologs of nuclear Xrn2p/Rat1p, functions in the cytoplasm. Proc Natl Acad Sci 97: 13985–13990.

Kim D, Paggi JM, Park C, Bennett C, Salzberg SL. 2019. Graph-based genome alignment and genotyping with HISAT2 and HISAT-genotype. Nat Biotechnol 37: 907–915.

Koressaar T, Remm M. 2007. Enhancements and modifications of primer design program Primer3. Bioinformatics 23: 1289–1291.

Kovalev N, de Castro Martín IF, Pogany J, Barajas D, Pathak K, Risco C, Nagy PD. 2016. Role of Viral RNA and Co-opted Cellular ESCRT-I and ESCRT-III Factors in Formation of Tombusvirus Spherules Harboring the Tombusvirus Replicase. J Virol 90: 3611–3626.

Kumar K, Chakraborty S. 2021. Roles of long non-coding RNAs in plant virus interactions. J Plant Biochem Biotechnol 1–14.

Langmead B, Salzberg SL. 2012. Fast gapped-read alignment with Bowtie 2. Nat Methods 9: 357–359.

Leicht BG and Cheng CL. 2009. Reverse genetics: Identification of Arabidopsis lines with T-DNA insertions in a gene of interest. In Tested Studies for Laboratory Teaching, Volume 30 (ed. Clase KL), pp. 282-290. Proceedings of the 30th Workshop/Conference of the Association for Biology Laboratory Education (ABLE), 403 pages. (studylib.net/doc/18550265/bringing-the-lab-into-your-lectures, ableweb.org/biologylabs/wp-content/uploads/volumes/vol-30/018.pdf)

Li H, Handsaker B, Wysoker A, Fennell T, Ruan J, Homer N, Marth G, Abecasis G, Durbin R. 2009. The Sequence Alignment/Map format and SAMtools. Bioinformatics 25: 2078–2079.

Li K, Wu G, Li M, Ma M, Du J, Sun M, Sun X, Qing L. 2018. Transcriptome analysis of *Nicotiana benthamiana* infected by Tobacco curly shoot virus. Virol J 15: 138.

Liao Y, Smyth GK, Shi W. 2014. featureCounts: an efficient general purpose program for assigning sequence reads to genomic features. Bioinformatics 30: 923–930.

Liu D, Shi L, Han C, Yu J, Li D, Zhang Y. 2012. Validation of Reference Genes for Gene Expression Studies in Virus-Infected *Nicotiana benthamiana* Using Quantitative Real-Time PCR. PLoS One 7: e46451.

Love MI, Huber W, Anders S. 2014. Moderated estimation of fold change and dispersion for RNA-seq data with DESeq2. Genome Biol 15: 550.

MacFadden A, O'Donoghue Z, Silva PAGC, Chapman EG, Olsthoorn RC, Sterken MG, Pijlman GP, Bredenbeek PJ, Kieft JS. 2018. Mechanism and structural diversity of exoribonuclease-resistant RNA structures in flaviviral RNAs. Nat Commun 9: 119.

Macho AP, Lozano-Duran R. 2019. Molecular dialogues between viruses and receptor-like kinases in plants. Mol Plant Pathol 20: 1191–1195.

Manokaran G, Finol E, Wang C, Gunaratne J, Bahl J, Ong EZ, Tan HC, Sessions OM, Ward AM, Gubler DJ, Harris E, Garcia-Blanco MA, Ooi EE. 2015. Dengue subgenomic RNA binds TRIM25 to inhibit interferon expression for epidemiological fitness. Science 350: 217–221.

Miller WA, Shen R, Staplin W, Kanodia P. 2016. Noncoding RNAs of Plant Viruses and Viroids: Sponges of Host Translation and RNA Interference Machinery. Mol Plant-Microbe Interact 29: 156–164.

Mine A, Hyodo K, Tajima Y, Kusumanegara K, Taniguchi T, Kaido M, Mise K, Taniguchi H, Okuno T. 2012. Differential Roles of Hsp70 and Hsp90 in the Assembly of the Replicase Complex of a Positive-Strand RNA Plant Virus. J Virol 86: 12091–12104.

Mizumoto H, Tatsuta M, Kaido M, Mise K, Okuno T. 2003. Cap-Independent Translational Enhancement by the 3′ Untranslated Region of Red Clover Necrotic Mosaic Virus RNA1. J Virol 77: 12113–12121.

Moon SL, Anderson JR, Kumagai Y, Wilusz CJ, Akira S, Khromykh AA, Wilusz J. 2012. A noncoding RNA produced by arthropod-borne flaviviruses inhibits the cellular exoribonuclease XRN1 and alters host mRNA stability. RNA 18: 2029–2040.

Moon SL, Dodd BJT, Brackney DE, Wilusz CJ, Ebel GD, Wilusz J. 2015. Flavivirus sfRNA suppresses antiviral RNA interference in cultured cells and mosquitoes and directly interacts with the RNAi machinery. Virology 485: 322–329.

Nagarajan VK, Jones CI, Newbury SF, Green PJ. 2013. XRN 5′→3′ exoribonucleases: Structure, mechanisms and functions. Biochim Biophys Acta 1829: 590–603.

Nejat N, Mantri N. 2018. Emerging roles of long non-coding RNAs in plant response to biotic and abiotic stresses. Crit Rev Biotechnol 38: 93–105.

O'Malley RC, Barragan CC, Ecker JR. 2015. A User's Guide to the Arabidopsis T-DNA Insertion Mutant Collections. Methods Mol Biol 1284: 323–342.

Obrępalska-Stęplowska A, Zmienko A, Wrzesińska B, Goralski M, Figlerowicz M, Zyprych-Walczak J, Siatkowski I, Pospieszny H. 2018. The Defense Response of *Nicotiana benthamiana* to Peanut Stunt Virus Infection in the Presence of Symptom Exacerbating Satellite RNA. Viruses 10: 449.

Patro R, Duggal G, Love MI, Irizarry RA, Kingsford C. 2017. Salmon provides fast and bias-aware quantification of transcript expression. Nat Methods 14: 417–419.

Peltier C, Klein E, Hleibieh K, D'Alonzo M, Hammann P, Bouzoubaa S, Ratti C, Gilmer D. 2012. Beet necrotic yellow vein virus subgenomic RNA3 is a cleavage product leading to stable non-coding RNA required for long-distance movement. J Gen Virol 93: 1093–1102.

Pijlman GP, Funk A, Kondratieva N, Leung J, Torres S, van der Aa L, Liu WJ, Palmenberg AC, Shi PY, Hall RA, Khromykh AA. 2008. A Highly Structured, Nuclease-Resistant, Noncoding RNA Produced by Flaviviruses Is Required for Pathogenicity. Cell Host Microbe 4: 579–591.

Powers JG, Sit TL, Heinsohn C, George CG, Kim KH, Lommel SA. 2008. The Red clover necrotic mosaic virus RNA-2 encoded movement protein is a second suppressor of RNA silencing. Virology 381: 277–286.

Ramírez F, Ryan DP, Grüning B, Bhardwaj V, Kilpert F, Richter AS, Heyne S, Dündar F, Manke T. 2016. deepTools2: a next generation web server for deep-sequencing data analysis. Nucleic Acids Res 44: W160–W165.

Roby JA, Pijlman GP, Wilusz J, Khromykh AA. 2014. Noncoding subgenomic flavivirus RNA: multiple functions in West Nile virus pathogenesis and modulation of host responses. Viruses 6: 404–27.

Rossetto CC, Tarrant-Elorza M, Verma S, Purushothaman P, Pari GS. 2013. Regulation of Viral and Cellular Gene Expression by Kaposi's Sarcoma-Associated Herpesvirus Polyadenylated Nuclear RNA. J Virol 87: 5540–5553.

Salviano-Silva A, Lobo-Alves S, Almeida R, Malheiros D, Petzl-Erler M. 2018. Besides Pathology: Long Non-Coding RNA in Cell and Tissue Homeostasis. Non-Coding RNA 4: 3.

Schnettler E, Sterken MG, Leung JY, Metz SW, Geertsema C, Goldbach RW, Vlak JM, Kohl A, Khromykh AA, Pijlman GP. 2012. Noncoding Flavivirus RNA Displays RNA Interference Suppressor Activity in Insect and Mammalian Cells. J Virol 86: 13486–13500.

Shen R, Miller WA. 2004. Subgenomic RNA as a riboregulator: negative regulation of RNA replication by Barley yellow dwarf virus subgenomic RNA 2. Virology 327: 196–205.

Shen R, Rakotondrafara AM, Miller WA. 2006. trans Regulation of Cap-Independent Translation by a Viral Subgenomic RNA. J Virol 80: 10045–10054.

Silva PAGC, Pereira CF, Dalebout TJ, Spaan WJM, Bredenbeek PJ. 2010. An RNA Pseudoknot Is Required for Production of Yellow Fever Virus Subgenomic RNA by the Host Nuclease XRN1. J Virol 84: 11395–11406.

Sit TL, Vaewhongs AA, Lommel SA. 1998. RNA-mediated trans-activation of transcription from a viral RNA. Science 281: 829–32.

Slonchak A, Khromykh AA. 2018. Subgenomic flaviviral RNAs: What do we know after the first decade of research. Antiviral Res 159: 13–25.

Souret FF, Kastenmayer JP, Green PJ. 2004. AtXRN4 Degrades mRNA in Arabidopsis and Its Substrates Include Selected miRNA Targets. Mol Cell 15: 173–183.

Steckelberg AL, Akiyama BM, Costantino DA, Sit TL, Nix JC, Kieft JS. 2018a. A folded viral noncoding RNA blocks host cell exoribonucleases through a conformationally dynamic RNA structure. Proc Natl Acad Sci 115: 6404–6409.

Steckelberg AL, Vicens Q, Kieft JS. 2018b. Exoribonuclease-Resistant RNAs Exist within both Coding and Noncoding Subgenomic RNAs. MBio 9: e02461-18.

Steckelberg AL, Vicens Q, Costantino DA, Nix JC, Kieft JS. 2020. The crystal structure of a Polerovirus exoribonuclease-resistant RNA shows how diverse sequences are integrated into a conserved fold. RNA 26: 1767–1776.

Sun X, Zheng H, Sui N. 2018. Regulation mechanism of long non-coding RNA in plant response to stress. Biochem Biophys Res Commun 503: 402–407.

Supek F, Bošnjak M, Škunca N, Šmuc T. 2011. REVIGO Summarizes and Visualizes Long Lists of Gene Ontology Terms. PLoS One 6: e21800.

Szucs MJ, Nichols PJ, Jones RA, Vicens Q, Kieft JS. 2020. A New Subclass of Exoribonuclease-Resistant RNA Found in Multiple Genera of *Flaviviridae*. MBio 11: 1–15.

Tajima Y, Iwakawa H, Kaido M, Mise K, Okuno T. 2011. A long-distance RNA–RNA interaction plays an important role in programmed − 1 ribosomal frameshifting in the translation of p88 replicase protein of Red clover necrotic mosaic virus. Virology 417: 169–178.

Takeda A, Tsukuda M, Mizumoto H, Okamoto K, Kaido M, Mise K, Okuno T. 2005. A plant RNA virus suppresses RNA silencing through viral RNA replication. EMBO J 24: 3147–3157.

Tsagakis I, Douka K, Birds I, Aspden JL. 2020. Long non-coding RNAs in development and disease: conservation to mechanisms. J Pathol 250: 480–495.

Turner KA, Sit TL, Callaway AS, Allen NS, Lommel SA. 2004. Red clover necrotic mosaic virus replication proteins accumulate at the endoplasmic reticulum. Virology 320: 276–290.

Tycowski KT, Guo YE, Lee N, Moss WN, Vallery TK, Xie M, Steitz JA. 2015. Viral noncoding RNAs: More surprises. Genes Dev 29: 567–584.

Untergasser A, Cutcutache I, Koressaar T, Ye J, Faircloth BC, Remm M, Rozen SG. 2012. Primer3—new capabilities and interfaces. Nucleic Acids Res 40: e115–e115.

Wang J, Meng X, Dobrovolskaya OB, Orlov YL, Chen M. 2017a. Non-coding RNAs and Their Roles in Stress Response in Plants. Genomics Proteomics Bioinformatics 15: 301–312.

Wang Y, Xu Y, Sun Y, Wang H, Qi J, Wan B, Ye W, Lin Y, Shao Y, Dong S, Tyler BM, Wang Y. 2018. Leucine-rich repeat receptor-like gene screen reveals that Nicotiana RXEG1 regulates glycoside hydrolase 12 MAMP detection. Nat Commun 9: 594.

Wang Z, Zhao Y, Zhang Y. 2017b. Viral lncRNA: A regulatory molecule for controlling virus life cycle. Non-coding RNA Res 2: 38–44.

Xie Z, Allen E, Wilken A, Carrington JC. 2005. DICER-LIKE 4 functions in trans-acting small interfering RNA biogenesis and vegetative phase change in *Arabidopsis thaliana*. Proc Natl Acad Sci 102: 12984–12989.

Ye Y, Ding Y, Jiang Q, Wang F, Sun J, Zhu C. 2017. The role of receptor-like protein kinases (RLKs) in abiotic stress response in plants. Plant Cell Rep 36: 235–242.

Yu Y, Zhang Y, Chen X, Chen Y. 2019. Plant Noncoding RNAs: Hidden Players in Development and Stress Responses. Annu Rev Cell Dev Biol 35: 407–431.

Zhang YC, Chen YQ. 2013. Long noncoding RNAs: New regulators in plant development. Biochem Biophys Res Commun 436: 111–114.

Zhao S, Li Y. 2021. Current understanding of the interplays between host hormones and plant viral infections. PLoS Pathog 17: e1009242.

Figures

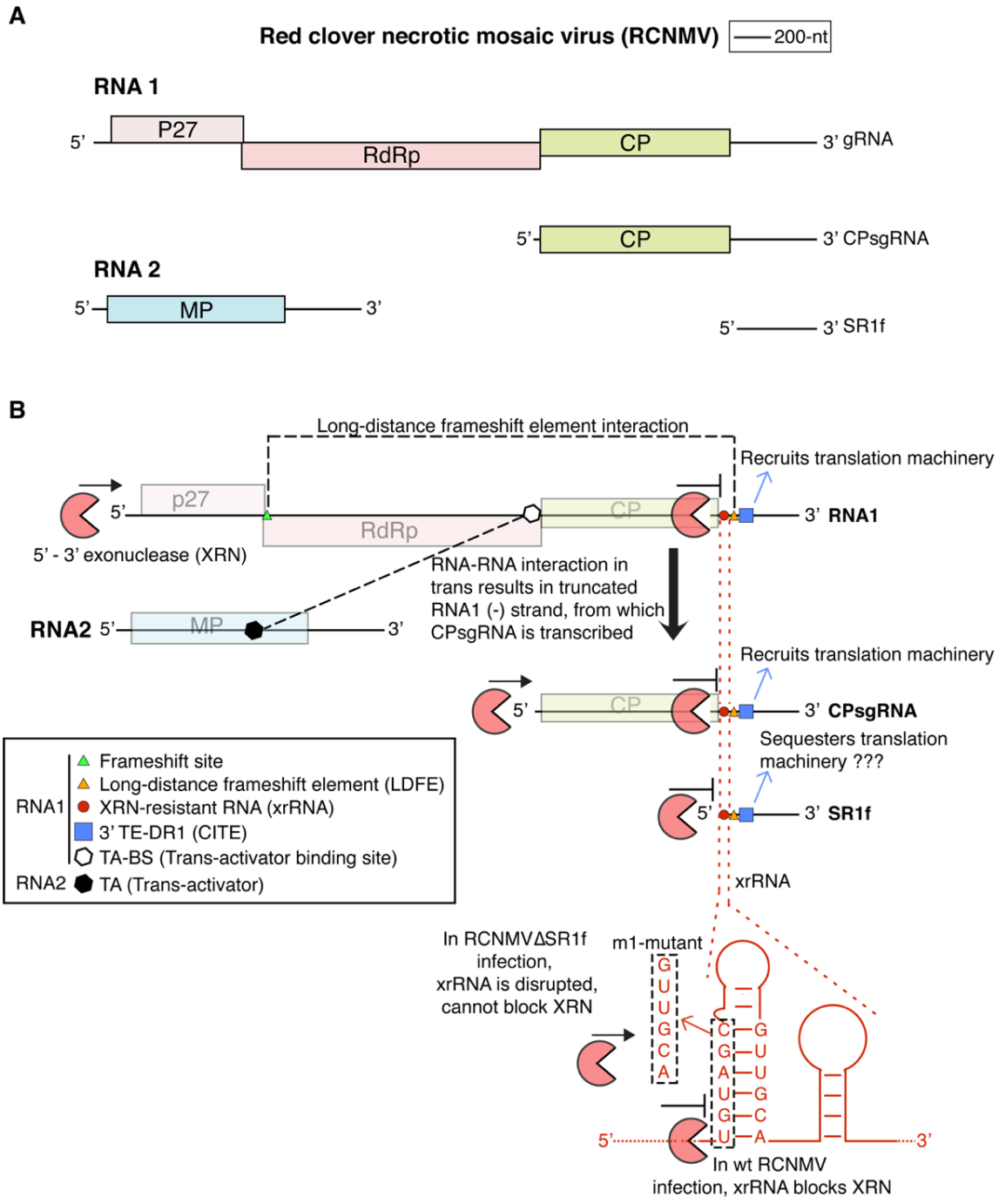

Figure 3.1. Genome organization of red clover necrotic mosaic virus (RCNMV). **(A)** RCNMV genome map (drawn to scale) depicting the genomic RNAs (RNA1 and RNA2) and subgenomic RNAs (CPsgRNA and SR1f) produced during the infection. **(B)** Schematic diagram of some important RNA elements in RCNMV RNAs that are involved in cap-independent translation of RNA1, -1 programmed ribosome frameshift for the translation of p88 protein that contains the RNA-dependent RNA polymerase (RdRp) motif, synthesis of CPsgRNA by premature transcription termination, and production of SR1f via incomplete degradation of RNA1 and CPsgRNA by the host 5'→ 3' exoribonuclease.

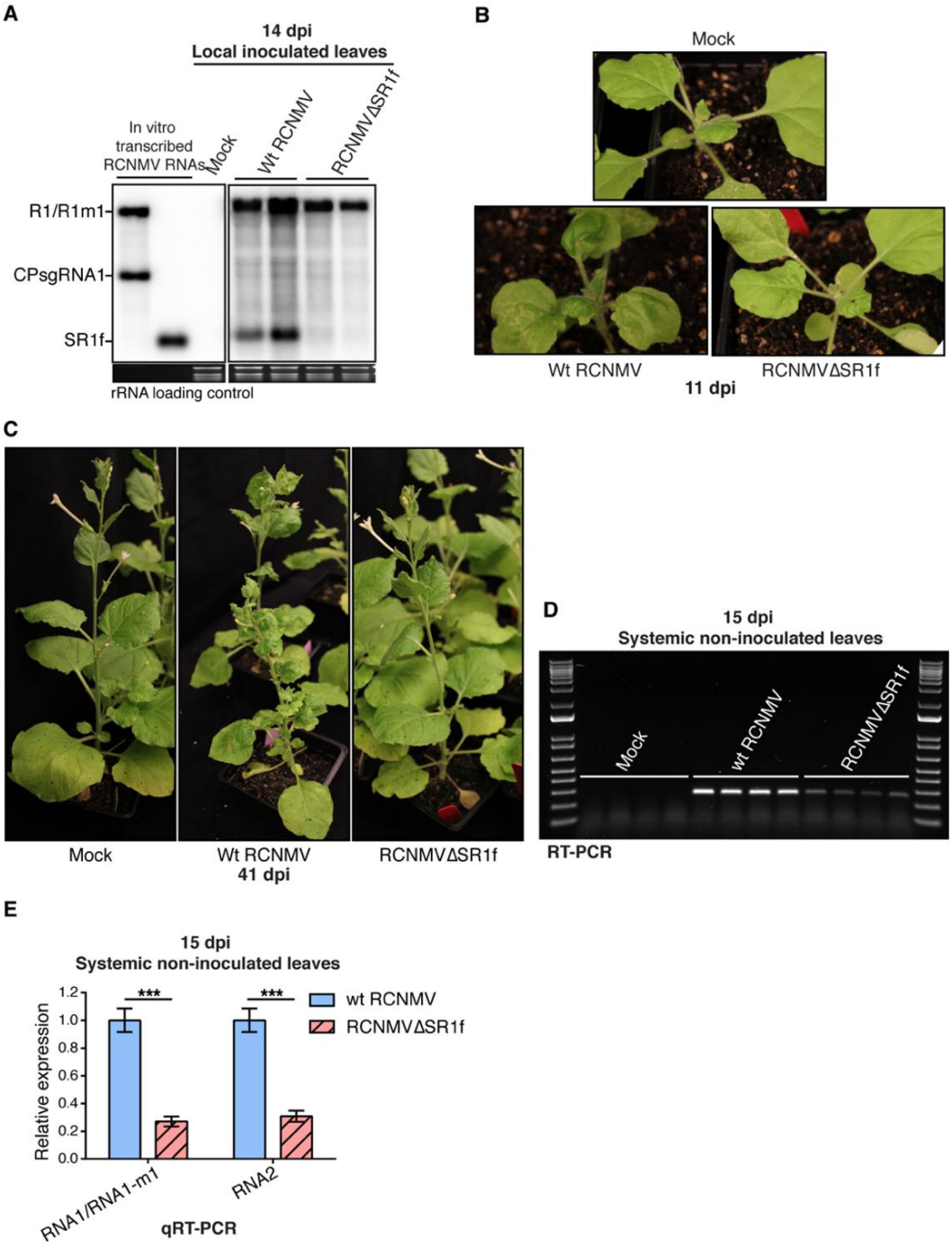

Figure 3.2. Effect of SR1f knockout on RCNMV infection in *N. benthamiana*. Wt RCNMV-infected plants were inoculated with wt RNA1 plus RNA2. RCNMVΔSR1f-infected plants were inoculated with RNA1-m1 plus RNA2. **(A)** Northern blot hybridization demonstrating that SR1f is produced only in wt RCNMV-infected plants and not in RCNMVΔSR1f-infected plants, even though viral RNA accumulation was detected in both wt RCNMV and RCNMVΔSR1f-infected plants. SYBR Safe stained rRNA was used as loading control for the northern blot. **(B)** Symptoms at 11 dpi. **(C)** Symptoms at 41 dpi. **(D)** RT-PCR to verify RNA1/RNA1-m1 accumulation. **(E)** qRT-PCR reveals relative amounts of each viral genomic RNA accumulated in wt RCNMV- and RCNMVΔSR1f-infected plants. NbPP2A and NbL23 were used as reference genes for normalization of qRT-PCR data. ***$p<0.001$. Error bars are SEMs.

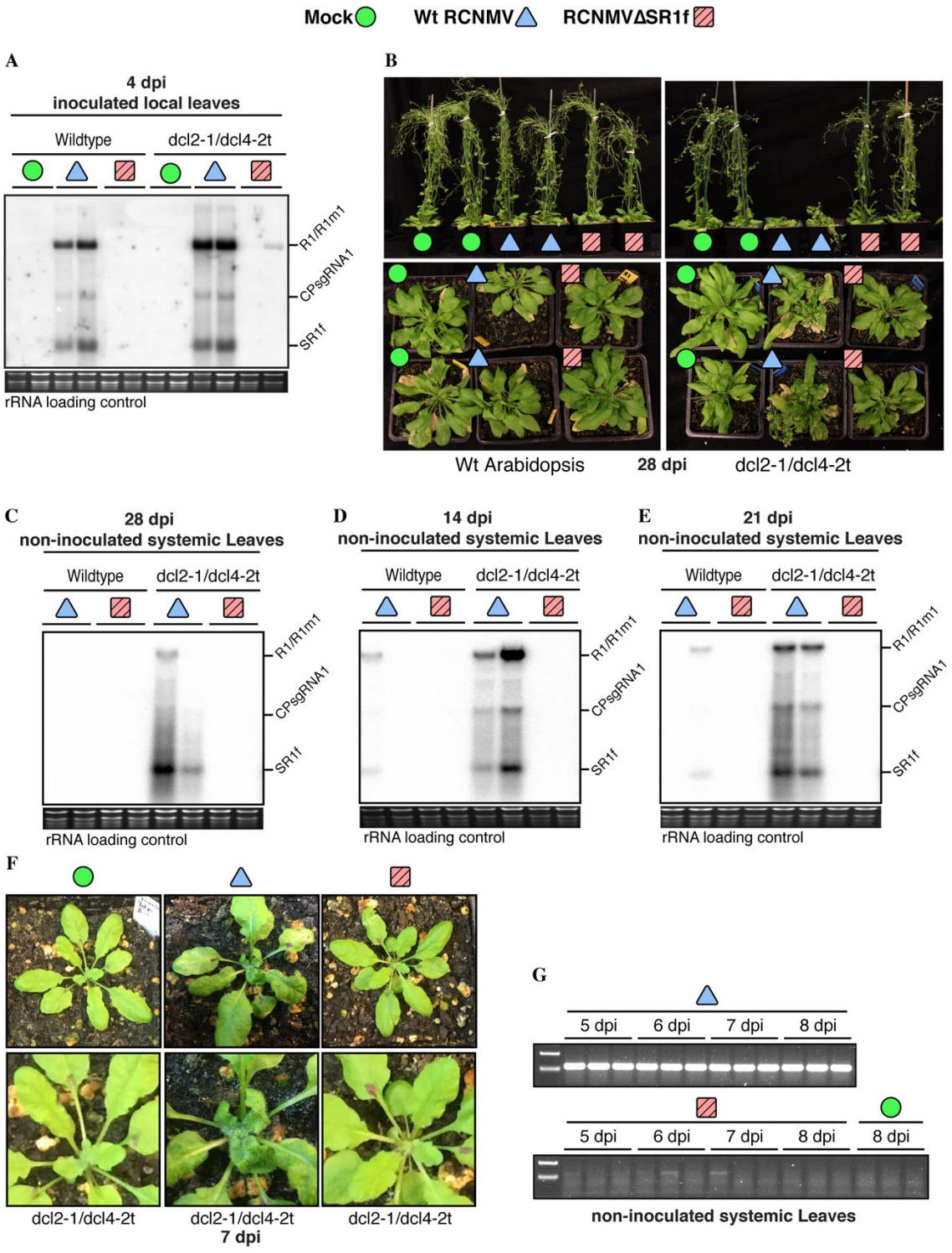

Figure 3.3. Effect of SR1f knockout on RCNMV infection in Arabidopsis. **(A)** Northern blot from RCNMV-infected wt and *dcl2-1/dcl4-2t* Arabidopsis plants at 4 dpi. **(B)** Symptoms in wildtype and *dcl2-1/dcl4-2t* Arabidopsis at 28 dpi. **(C)** Northern blot from plants shown in panel B at 28 dpi. **(D)** Northern blot from RCNMV-infected wt and *dcl2-1/dcl4-2t* Arabidopsis at 14 dpi and **(E)** 21 dpi. **(F)** Symptoms in *dcl2-1/dcl4-2t* Arabidopsis at 7 dpi. **(G)** RT-PCR to verify RNA1 or RNA1-m1 accumulation in plants from panel F. SYBR Safe stained rRNA was used as loading control for the northern blots.

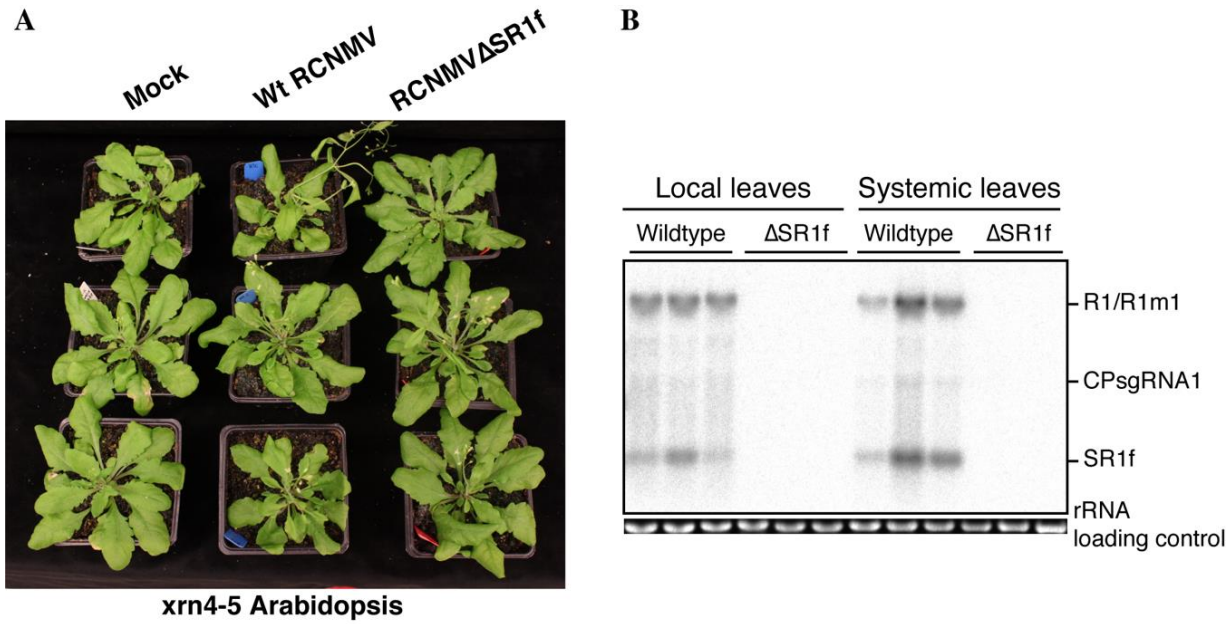

Figure 3.4. RCNMV infection in *xrn4-5* Arabidopsis. **(A)** Symptoms in *xrn4-5* Arabidopsis at 21 dpi. **(B)** Northern blot hybridization from plants shown in panel A at 21 dpi.

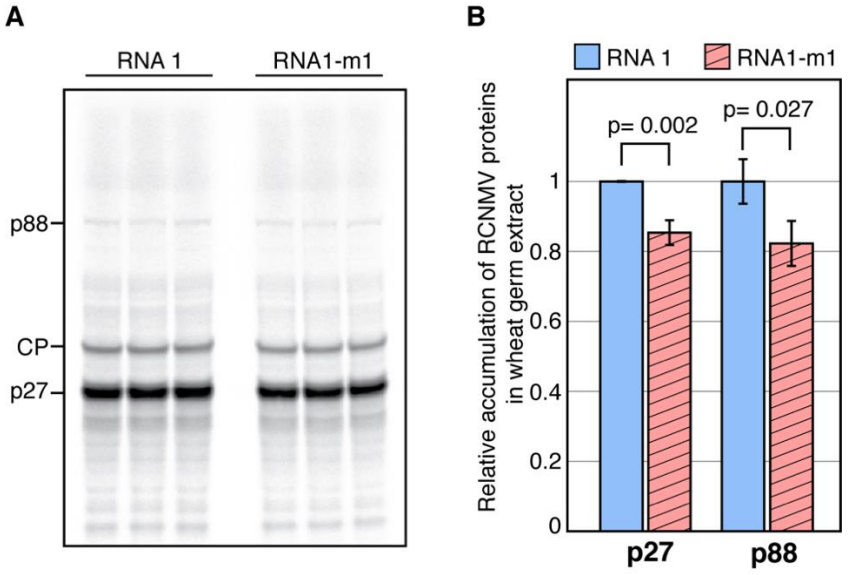

Figure 3.5. *In vitro* translation of RCNMV RNA1 and RNA1-m1 in wheat germ extract. **(A)** Polyacrylamide gel electrophoresis of ^{35}S-methionine-labeled wheat germ translation products of RCNMV RNA1 and RNA1-m1. Mobilities of viral proteins are indicated on the left. **(B)** Relative accumulation of RCNMV p27 and p88 in wheat germ extract as determined by measuring the band intensity from panel A and calculating the accumulation of viral proteins relative to those from wt RNA1. Error bars represent the S.D.

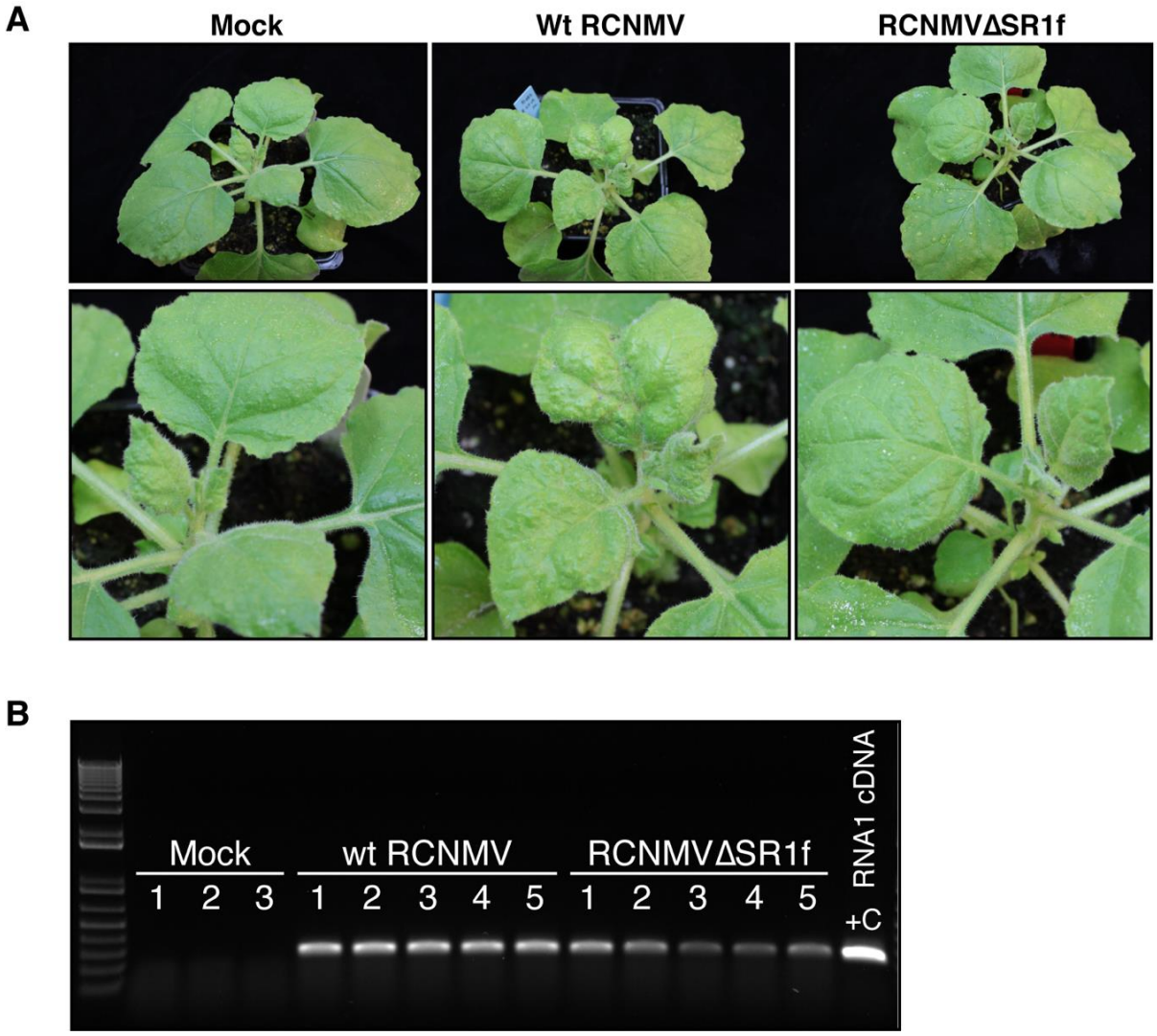

Figure 3.6. RCNMV-infected *N. benthamiana* plants used for RNA-seq analysis. **(A)** Symptoms at 15 dpi. **(B)** RT-PCR to verify the accumulation RNA1 and RNA1-m1 in wt RCNMV- and RCNMVΔSR1f-infected plants, respectively. +C refers to pR169c (RNA1 infectious clone) positive control.

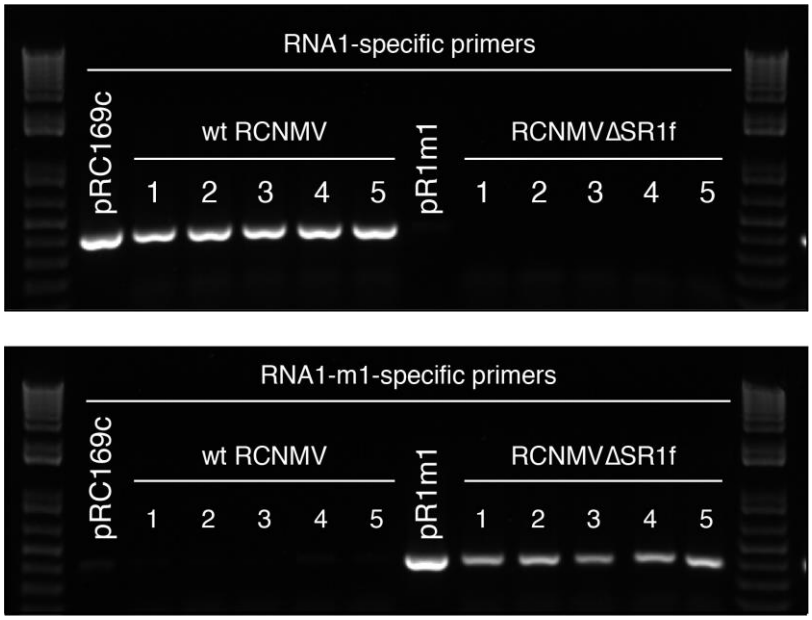

Figure 3.7. Wt RNA1 and RNA1-m1 specific RT-PCR to verify there was no cross-contamination between the samples. Total RNA was reverse transcribed as described in the Methods section. A 20 µl PCR reaction mix was prepared with 10 ul GoTaq G2 green master mix (Promega M7823), 2 µl cDNA template, 200 nM each of forward and reverse primer. PCR conditions were as follows: 98 ˚C (2 min); 25 cycles of 98 ˚C (30 s), 62 ˚C (20s), 72 ˚C (40 s); 72 ˚C (2 min); 4 ˚C hold. Primers used were *5'-GGGGTACCTAGCCGTTATAC-3'* (RCNMV-specific reverse primer) plus *5'-GTGTAGCCTCCACCCGA-3'* (wt RNA1-specific forward) or *5'-GACGTTGCTCCACCCGA-3'* (RNA1-m1- specific forward). pRC169c and pR1m1 are controls with plasmids as template for PCR.

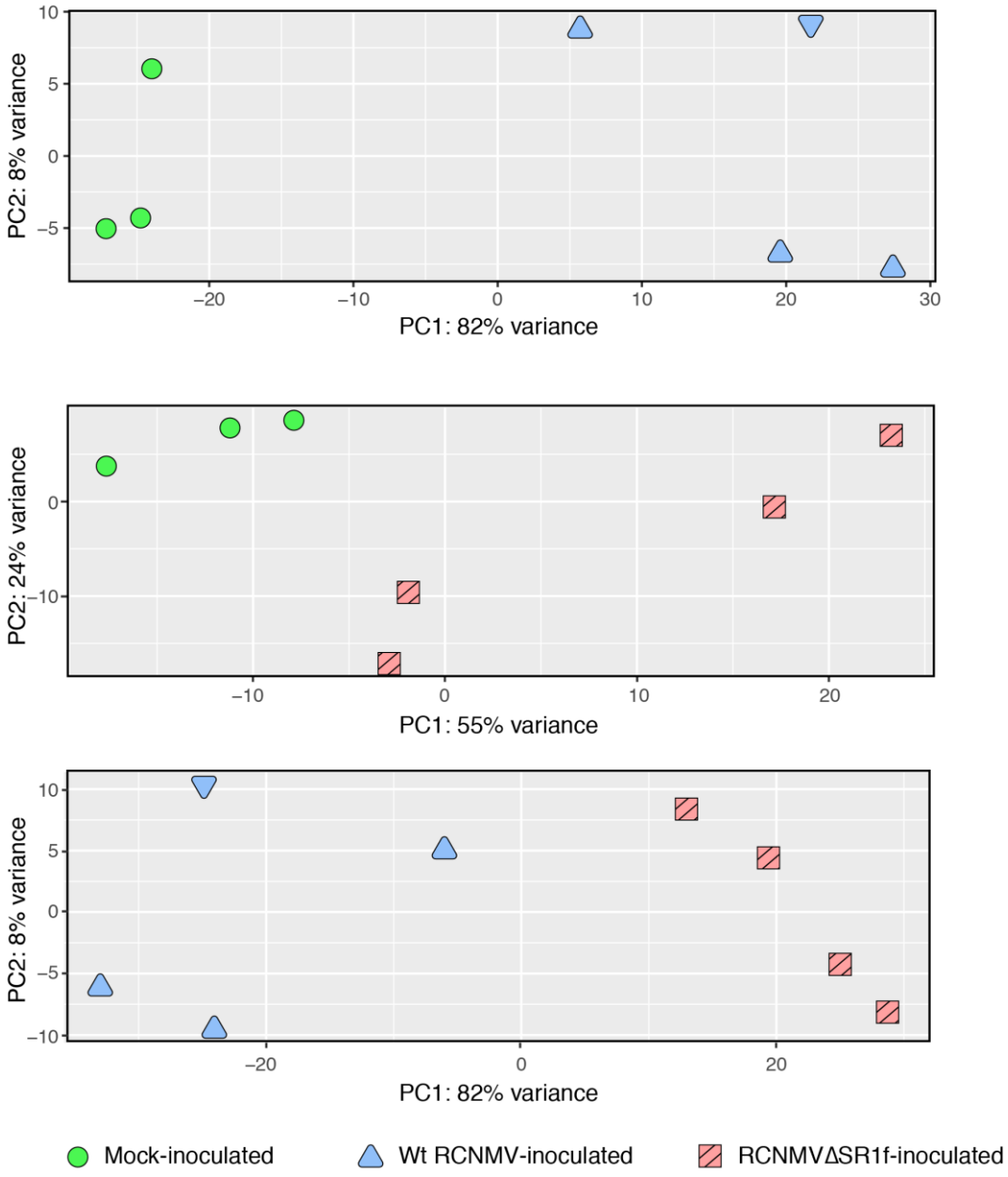

Figure 3.8. Principal component analysis (PCA) of RNA-seq data. Regularized-log transformed data from DESeq2 for each of the three comparisons was used to generate the PCA plots.

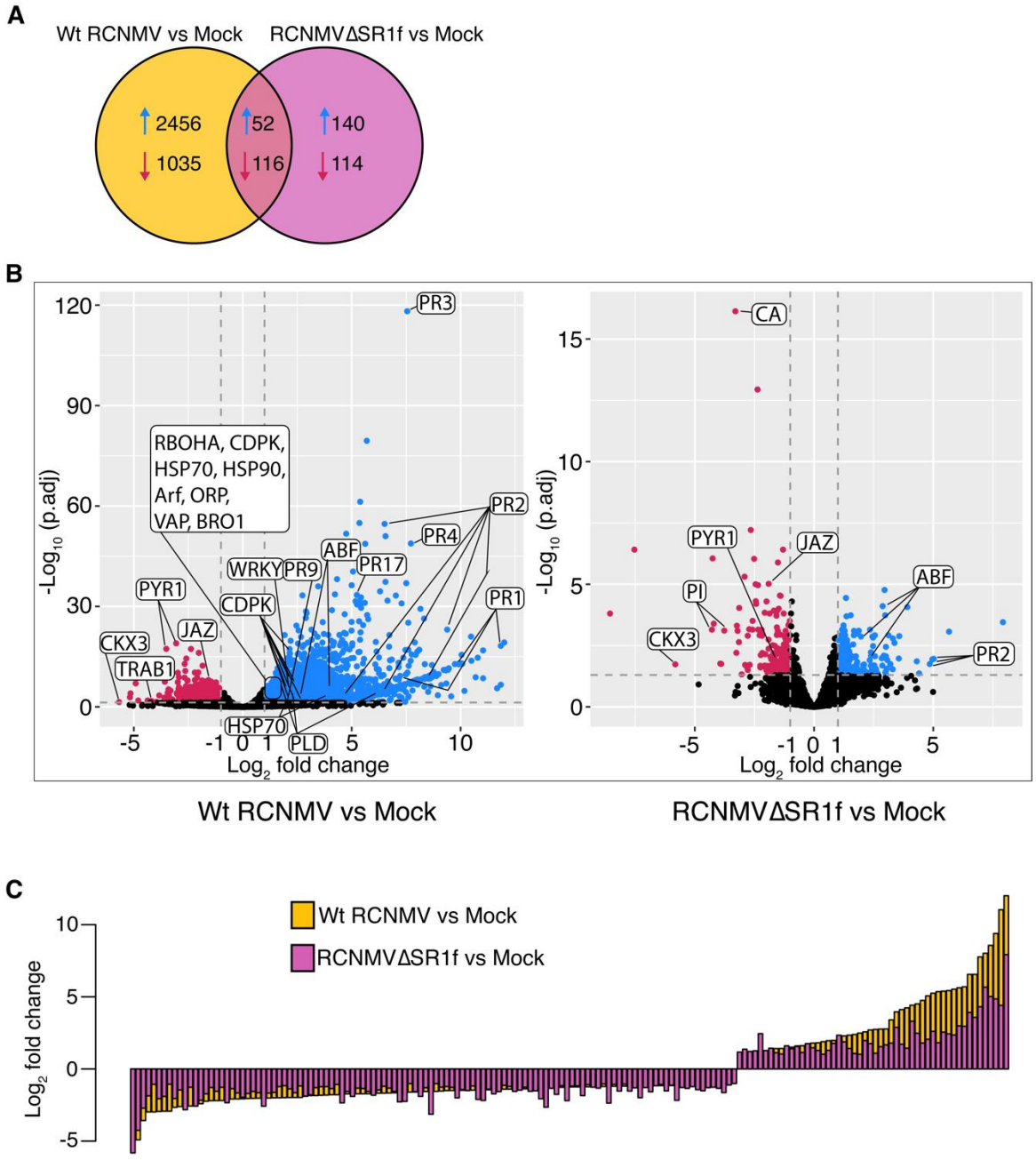

Figure 3.9. Differentially expressed genes (DEGs) in Wt RCNMV vs. Mock and RCNMVΔSR1f vs. Mock. **(A)** Venn diagram showing the number of upregulated and downregulated DEGs. **(B)** Volcano plots showing log_2-fold change and adjusted p-values for all DEGs. **(C)** Histogram comparing log_2-fold change of DEGs that are common in Wt RCNMV vs. Mock and RCNMVΔSR1f vs. Mock data. (PR) pathogenesis-related protein, (WRKY1) WRKY transcription factor, (RBOHA) respiratory burst oxidase homolog protein A, (ABF) abscisic acid responsive element-binding factor, (PYR1) abscisic acid receptor, (TRAB1) bZIP transcription factor-ABA signaling, (CKX3) cytokinin dehydrogenase, (JAZ) jasmonate-zim-domain protein 3, (CA) carbonic anhydrase, (PI) proteinase inhibitor I-B, (CDPK) calcium-dependent protein kinase, (HSP) heat shock proteins, (Arf) ADP-ribosylation factor, (ORP) oxysterol-binding protein-related protein, (VAP) Vesicle-associated membrane protein-associated protein, (BRO1) Vacuolar protein-sorting protein bro1, (PLD) phospholipase D.

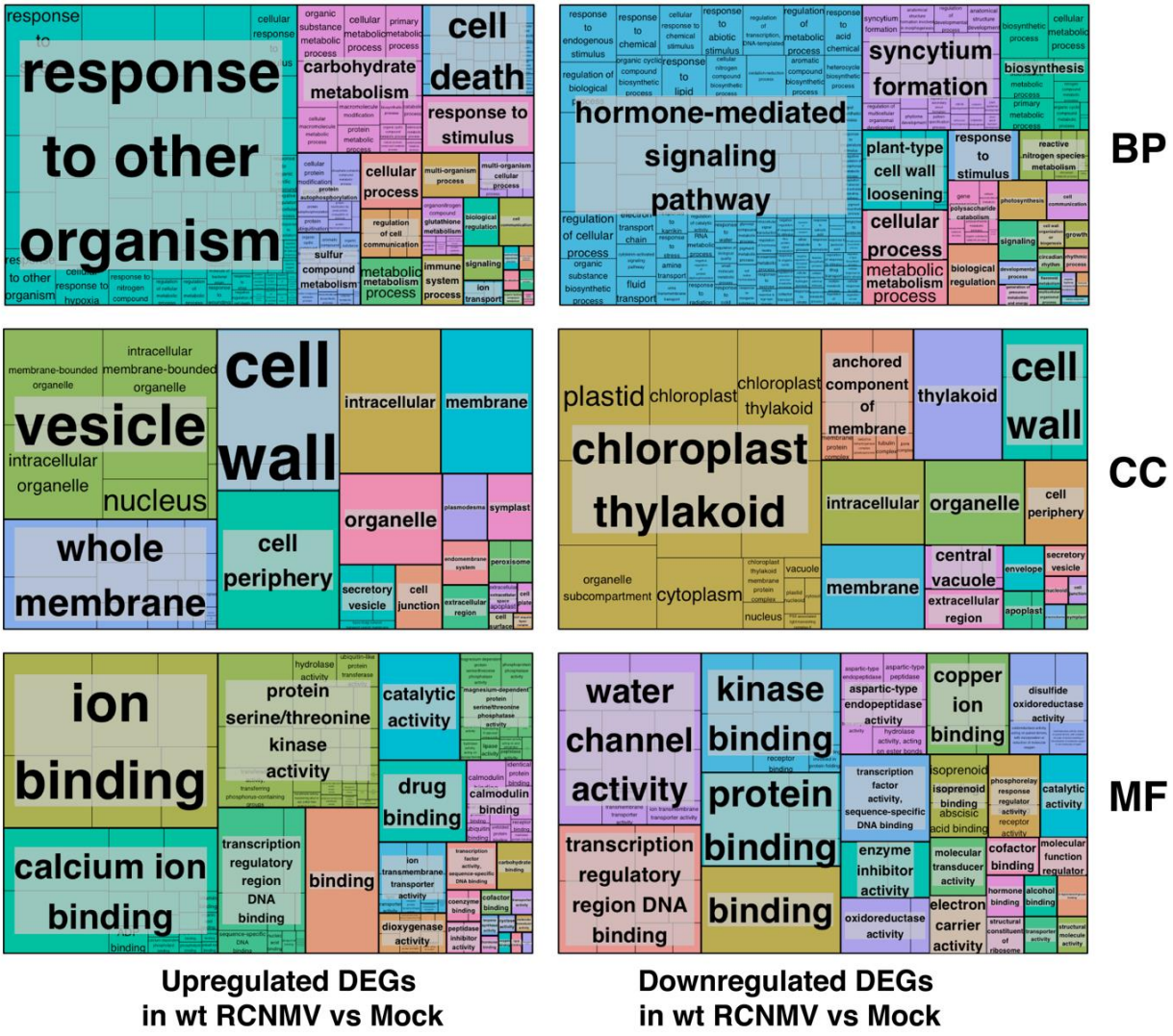

Figure 3.10. TreeMap view of enriched GO terms in wt RCNMV vs mock. The upregulated and downregulated genes were separately used to find the enriched GO terms. The absolute $\log_{10}$-p-value determines the size of the rectangles. BP: Biological process, CC: Cellular compartment, MF: Molecular function.

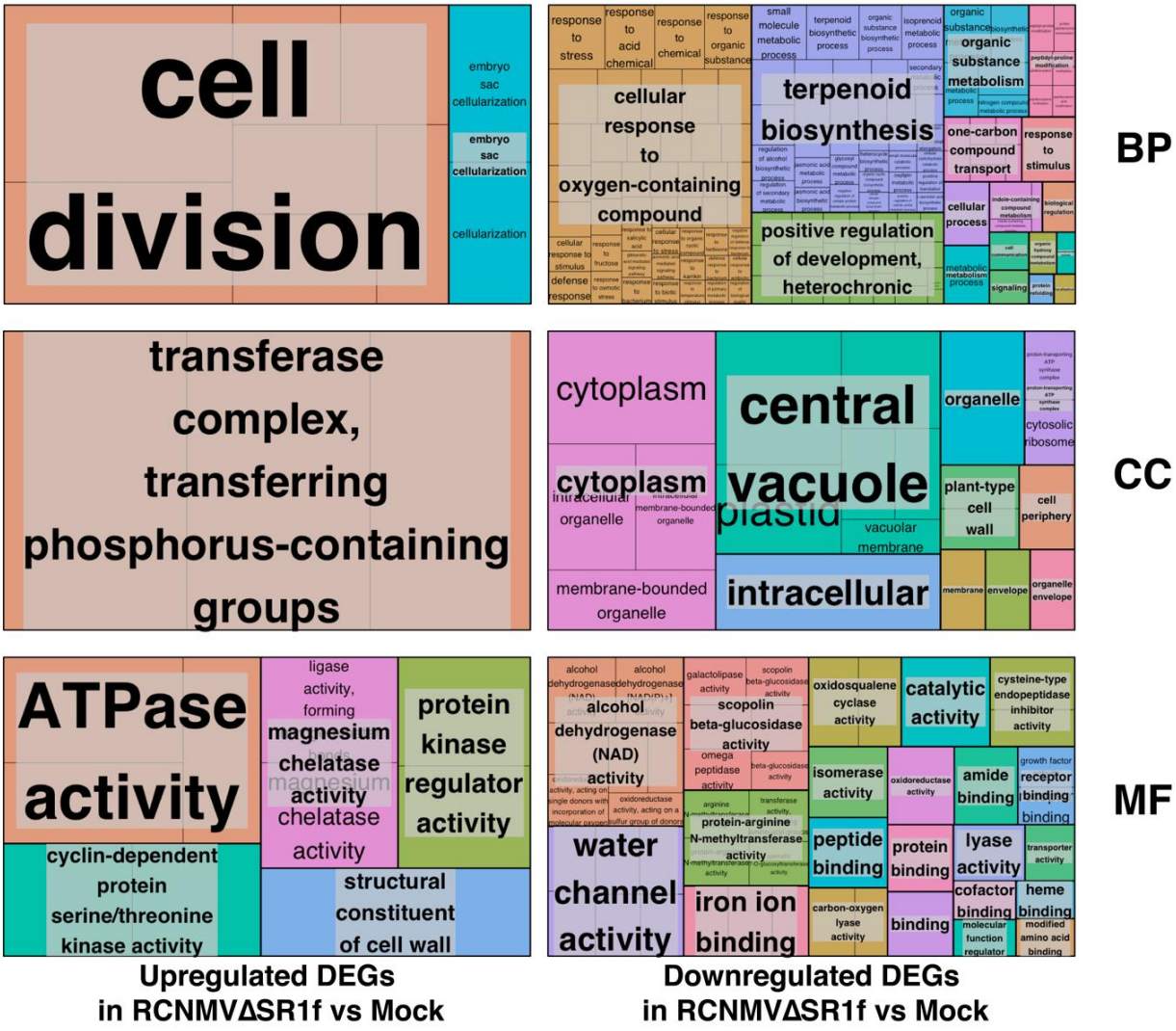

Figure 3.11. TreeMap view of enriched GO terms in RCNMVΔSR1f vs mock. The upregulated and downregulated genes were separately used to find the enriched GO terms. The absolute $\log_{10}$-p-value determines the size of the rectangles. BP: Biological process, CC: Cellular compartment, MF: Molecular function.

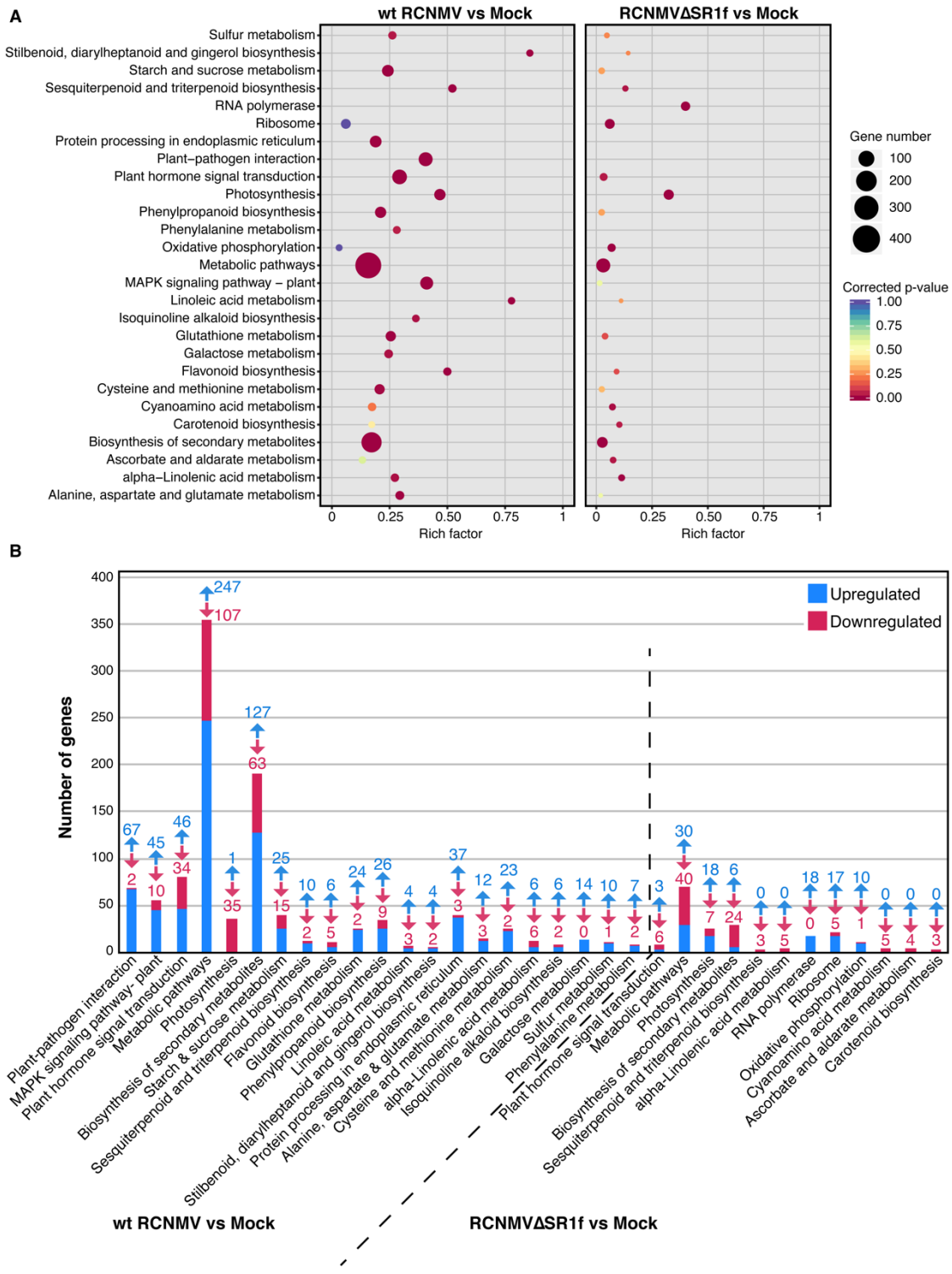

Figure 3.12. KEGG pathway enrichment analysis. **(A)** Scatterplot showing the rich factor of the KEGG pathway (x-axis), number of DEGs present in our data (size of the points), and the corrected p-values for enrichment (color). Rich factor is the ratio of number of DEGs in the pathway to the total number of genes annotated in the pathway. **(B)** Histogram showing the number of DEGs for each of the enriched KEGG pathways in wt RCNMV and RCNMVΔSR1f infection. The numbers with the arrows indicate the number of upregulated and downregulated genes in the direction of the arrow.

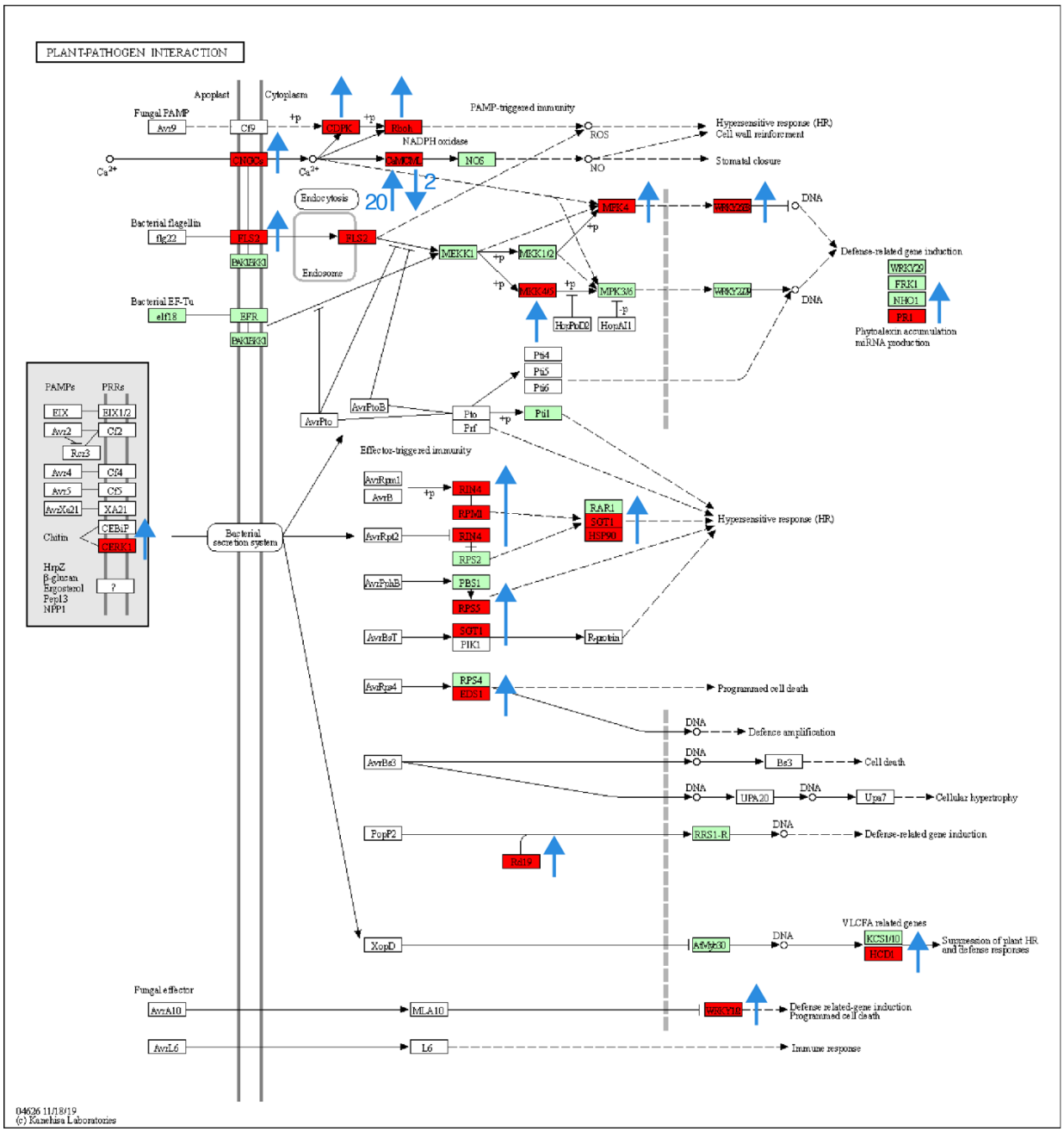

Figure 3.13. DEGs in wt RCNMV vs mock data associated with Plant-Pathogen interaction pathway. The red boxes refer to genes that were differentially expressed. The direction of blue arrows depicts if the genes were up- or down-regulated. The numbers beside the arrows refer to the number of unigenes that were regulated in the direction of the arrow. Arrows without the numbers means all the unigenes were regulated in the same direction.

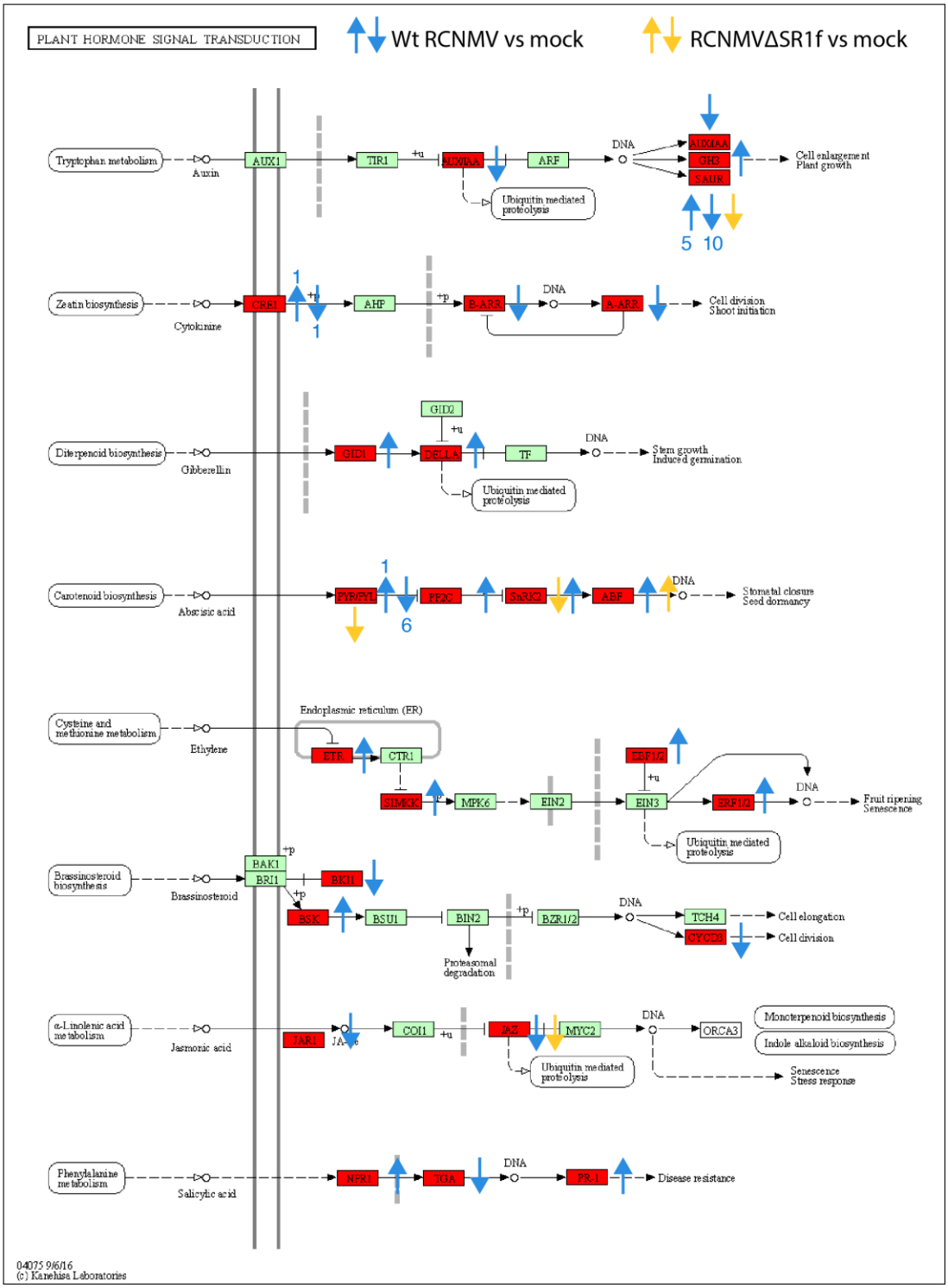

Figure 3.14. DEGs in wt RCNMV vs mock data and RCNMVSR1f vs mock data associated with Plant hormone signal transduction pathway. The red boxes refer to genes that were differentially expressed. The direction of blue and yellow arrows depicts the direction of regulation in wt RCNMV vs mock data and RCNMVΔSR1f vs mock data, respectively. The numbers beside the arrows refer to the number of unigenes that were regulated in the direction of the arrow. Arrows without the numbers means all the unigenes were regulated in the same direction.

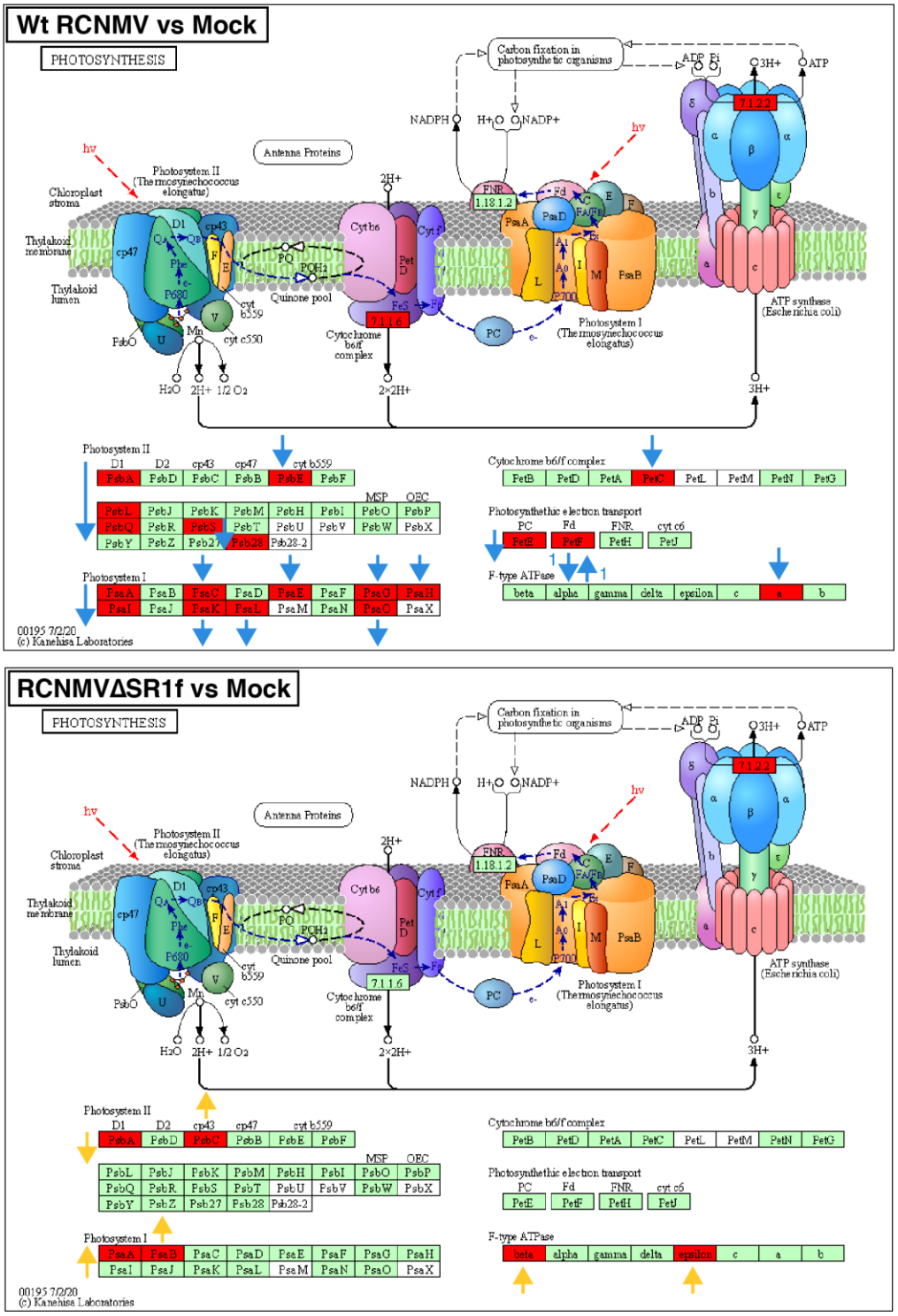

Figure 3.15. DEGs in wt RCNMV vs mock data and RCNMVSR1f vs mock data associated with Photosynthesis pathway. The red boxes refer to genes that were differentially expressed. The direction of blue and yellow arrows depicts the direction of regulation in wt RCNMV vs mock data and RCNMVΔSR1f vs mock data, respectively. The numbers beside the arrows refer to the number of unigenes that were regulated in the direction of the arrow. Arrows without the numbers means all the unigenes were regulated in the same direction.

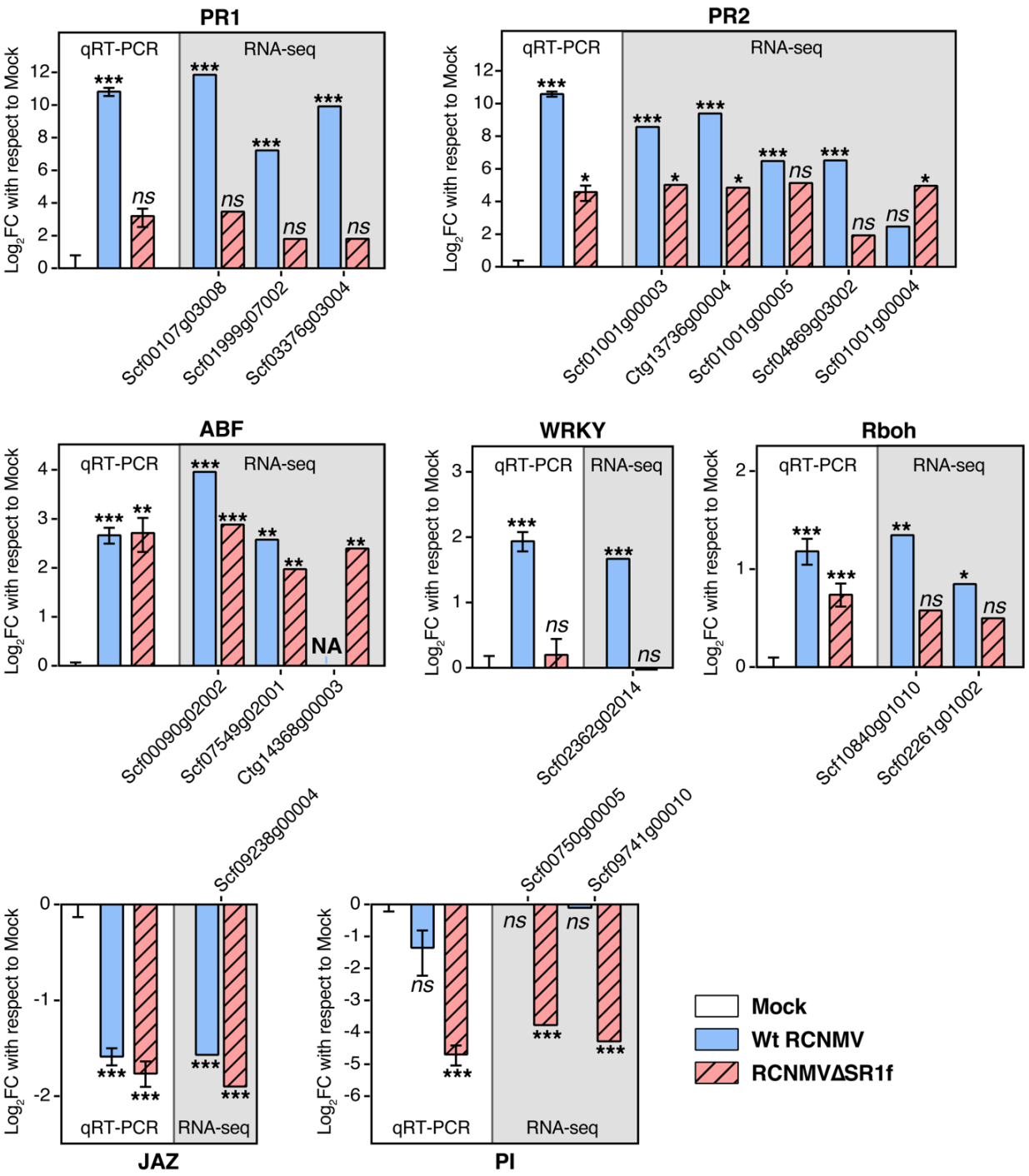

Figure 3.16. Validation of RNA-seq data by qRT-PCR of candidate genes. NbPP2A and NbL23 were used as reference genes for normalization of qRT-PCR data. Expression values are shown with respect to mock. RNA-seq data for each gene with one or more Unigene IDs are shown that could be amplified by qRT-PCR (see methods). The Unigene IDs are preceded by "Niben101". (FC) fold change, (PR) pathogenesis-related protein, (ABF) abscisic acid responsive element-binding factor, (WRKY) probable WRKY transcription factor 33, (Rboh) Respiratory burst oxidase homolog protein A, (JAZ) jasmonate-zim-domain protein 3, (PI) proteinase inhibitor I-B. *p<0.05, **p<0.01, ***p<0.001, ns: not significant. Error bars are SEMs.

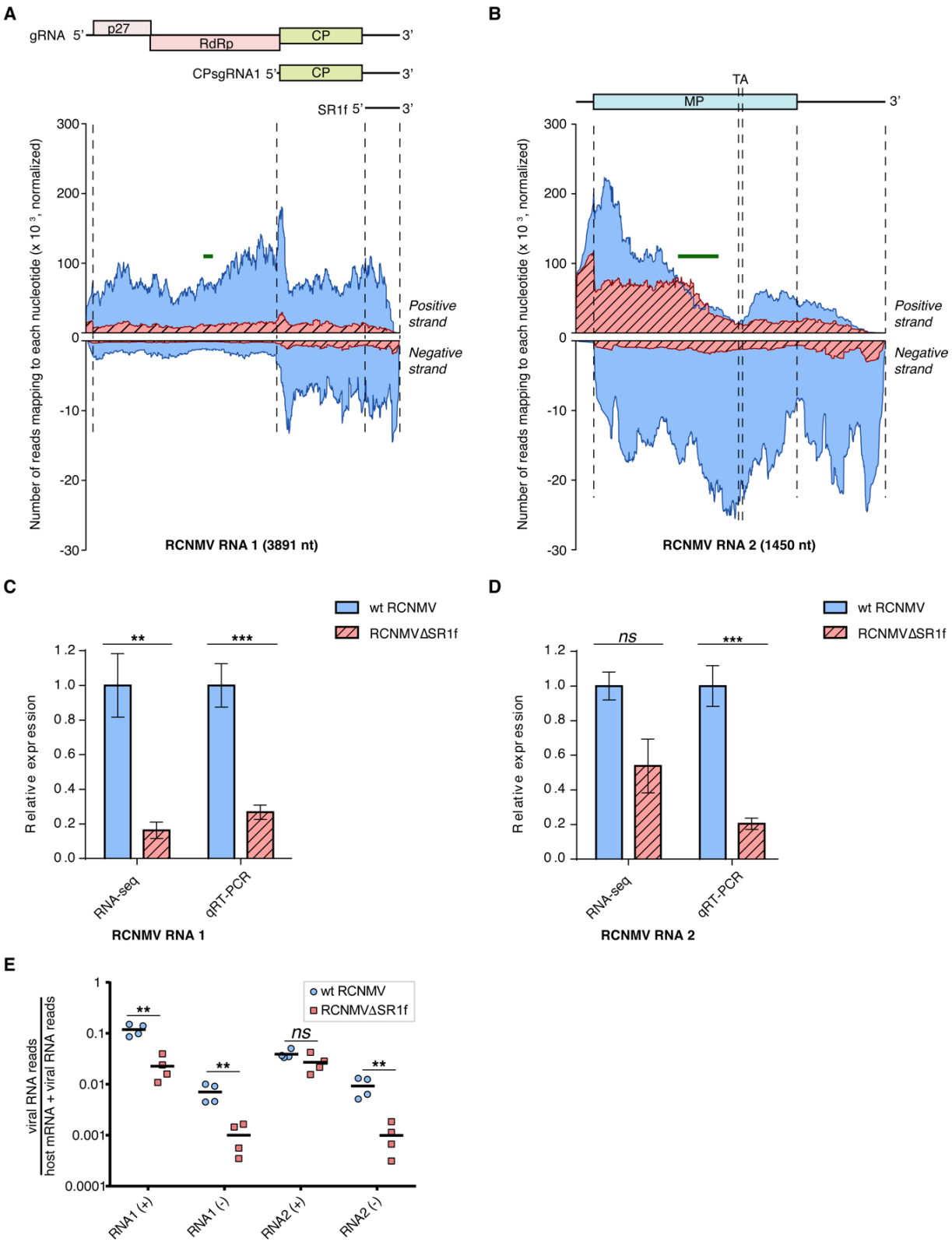

Figure 3.17. RNA-seq reads mapping to the RCNMV genome. **(A)** Coverage plots showing the reads mapping to RCNMV RNA1 positive and negative strands. **(B)** Coverage plots showing the reads

mapping to RCNMV RNA2 positive and negative strands. The RCNMV genome organization is shown above the coverage plots. The green bars denote the locations of qRT-PCR amplicon. Note that the y-axis scales used for positive and negative strand coverage differ by a factor of 10. **(C)** Relative accumulation of RNA1 (both positive and negative strand) in Wt RCNMV- and RCNMVΔSR1f-infected plants as measured by RNA-seq and qRT-PCR. **(D)** Relative accumulation of RNA2 (both positive and negative strand) in Wt RCNMV- and RCNMVΔSR1f-infected plants as measured by RNA-seq and qRT-PCR. **(E)** Proportion of viral RNA reads relative to the total number of host mRNA reads plus viral RNA reads. NbPP2A and NbL23 were used as reference genes for normalization of qRT-PCR data. DESeq2-derived scaling factors were used for normalizing RNA-seq data. Adjusted p-values *< 0.05. ** < 0.01. *** < 0.001. Error bars are SEM.

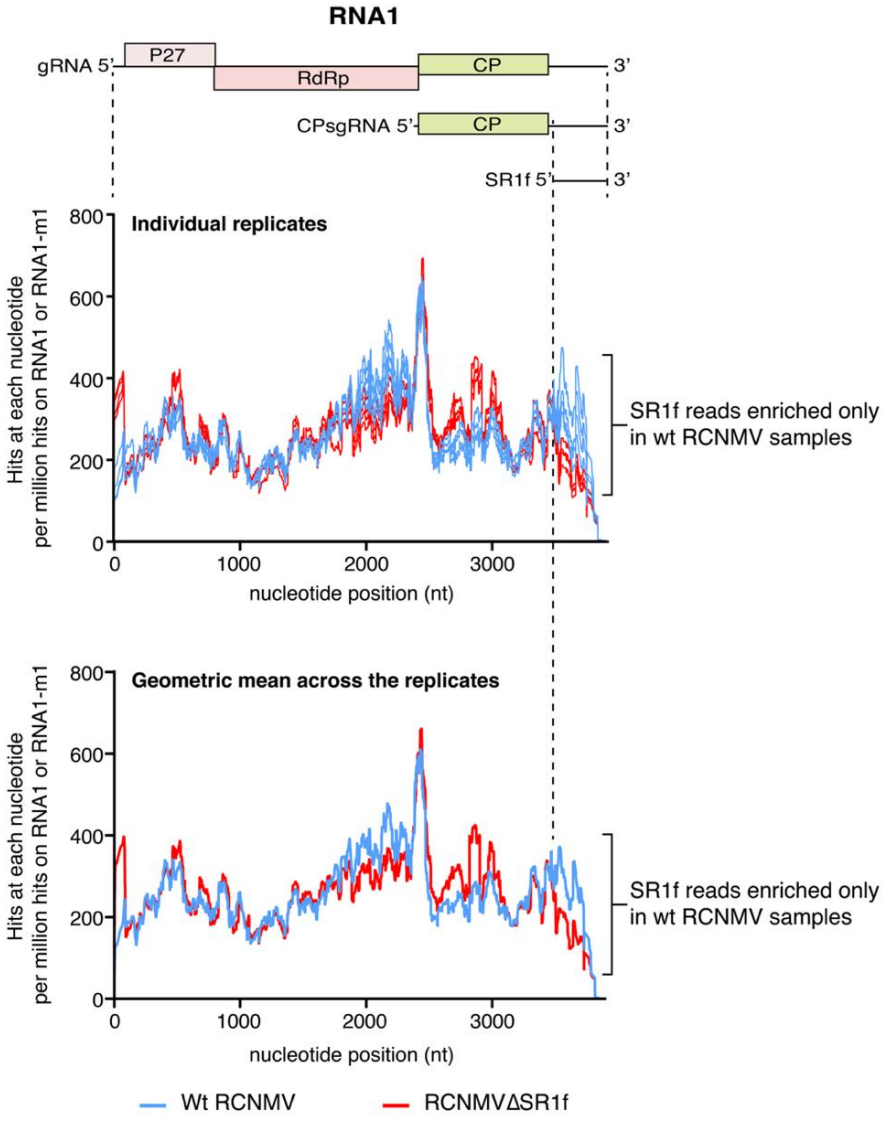

Figure 3.18. RNA-seq reads mapping to each nucleotide of RCNMV RNA1 and RNA1-m1 normalized to the total number of hits on RNA1 or RNA1-m1, respectively.

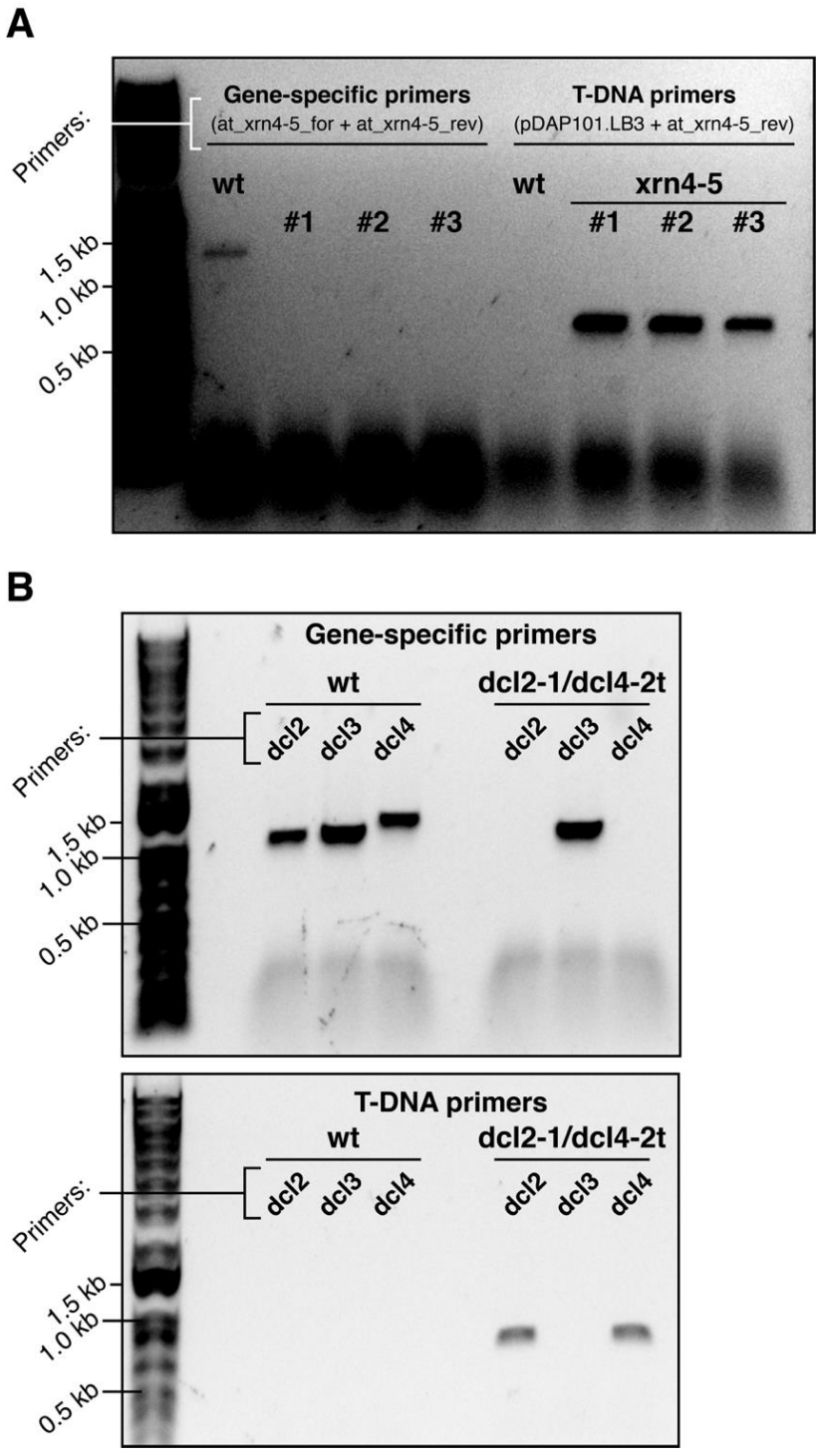

Figure 3.19. Genotyping to verify T-DNA insertions in knock-out mutants of Arabidopsis by PCR. **(A)** Genotyping *xrn4-5* mutants. Gene specific primers refer to the forward and reverse primer for *XRN4*. T-DNA primers refer to the pDAP101 vector primer with *XRN4* reverse primer. **(B)** Genotyping *dcl2-1/dcl4-2t* double knock-out mutants. Gene specific primers refer to the forward and reverse primer for the respective dcl genes. T-DNA primers refer to the *DCL2* or *DCL3* reverse primer with the pROK2 vector forward primer, and the *DCL4* reverse primer with the pAC161_8474 vector forward primer. All primer sequences are listed in *Table 3.7*.

Tables

Table 3.1. Top 15 enriched GO terms in wt RCNMV vs mock using upregulated and downregulated differentially expressed genes.

Upregulated DEG dataset

GO term	Ontology	Input number*	Background number#	Adjusted p-value
Response to stimulus	BP	971	5510	1.57E-153
Response to stress	BP	677	3196	7.96E-131
Response to chemical	BP	611	2743	1.38E-124
Cellular anatomical entity	CC	1997	20476	1.16E-115
Cell periphery	CC	643	3773	5.85E-86
Response to oxygen-containing compound	BP	376	1504	4.44E-84
Plasma membrane	CC	585	3279	1.04E-83
Cellular process	BP	1285	11150	5.01E-83
Binding	MF	1144	9385	7.44E-83
Response to organic substance	BP	402	1760	1.35E-80
Cellular response to chemical stimulus	BP	356	1412	2.64E-80
Cellular response to stimulus	BP	515	2738	2.40E-79
Intracellular	CC	1709	17437	1.48E-74
Defense response	BP	335	1361	4.98E-73
Metabolic process	BP	1173	10224	2.08E-70

Downregulated DEG dataset

GO term	Ontology	Input number*	Background number#	Adjusted p-value
Cellular anatomical entity	CC	884	20476	3.72E-43
Plastid	CC	318	4526	9.17E-37
Thylakoid	CC	93	487	1.01E-35
Chloroplast	CC	298	4164	1.42E-35
Chloroplast thylakoid	CC	84	417	7.98E-34
Plastid thylakoid	CC	84	417	7.98E-34
Chloroplast thylakoid membrane	CC	72	337	2.87E-30
Plastid thylakoid membrane	CC	72	337	2.87E-30
Photosynthetic membrane	CC	73	352	4.86E-30
Thylakoid membrane	CC	72	351	2.16E-29
Intracellular	CC	751	17437	4.94E-27
Membrane	CC	382	6756	5.75E-27
Organelle	CC	708	16128	2.38E-26
Membrane-bounded organelle	CC	700	15953	1.21E-25
Organelle subcompartment	CC	98	775	1.59E-25

BP: Biological process. CC: Cellular component. MF: Molecular function.

**Input number is the number of DEGs in our dataset annotated to the GO term.*

#*Background number is the number of genes in the background database annotated to the GO term.*

Table 3.2. Top 15 enriched GO terms in RCNMVΔSR1f vs mock using upregulated and downregulated differentially expressed genes.

Upregulated DEG dataset

GO term	Ontology	Input number*	Background number#	Adjusted p-value
Cell division	BP	14	347	8.77E-06
Cell cycle	BP	14	500	0.000335
Structural constituent of cell wall	MF	4	19	0.002280
ATPase activity	MF	11	439	0.007688
Cyclin-dependent protein kinase holoenzyme complex	CC	4	42	0.020836
Cyclin-dependent protein serine/threonine kinase regulator activity	MF	4	43	0.020836
Cell cycle process	BP	9	370	0.024266
Glucan endo-1,3-beta-D-glucosidase activity	MF	3	19	0.024266
Nucleoside-triphosphatase activity	MF	12	668	0.024266
Transferase complex, transferring phosphorus-containing groups	CC	6	161	0.024266
Regulation of cyclin-dependent protein serine/threonine kinase activity	BP	4	56	0.024266
Regulation of cyclin-dependent protein kinase activity	BP	4	56	0.024266
Serine/threonine protein kinase complex	CC	4	59	0.024266
Protein kinase complex	CC	4	60	0.024266
Mitotic cell cycle process	BP	6	172	0.024266

Downregulated DEG dataset

GO term	Ontology	Input number*	Background number#	Adjusted p-value
Cellular anatomical entity	CC	165	20476	1.17E-09
Response to stress	BP	53	3196	1.99E-09
Response to stimulus	BP	72	5510	3.79E-09
Cytoplasm	CC	116	12053	1.32E-08
Response to acid chemical	BP	29	1161	1.93E-08
Response to chemical	BP	46	2743	1.93E-08
Organic acid metabolic process	BP	27	1039	3.41E-08
Response to organic substance	BP	35	1760	5.57E-08
Small molecule metabolic process	BP	32	1496	5.57E-08
Response to oxygen-containing compound	BP	32	1504	5.70E-08
Intracellular	CC	144	17437	7.72E-08
Cellular process	BP	107	11150	9.71E-08
Cytosol	CC	45	2853	1.04E-07
Terpenoid biosynthetic process	BP	11	136	1.24E-07
Oxoacid metabolic process	BP	25	1032	2.87E-07

BP: Biological process. CC: Cellular component. MF: Molecular function.

**Input number is the number of DEGs in our dataset annotated to the GO term.*

#*Background number is the number of genes in the background database annotated to the GO term.*

Table 3.3. List of differentially expressed LRR-RLKs/RLPs genes.

	Wt RCNMV vs. mock		RCNMVΔSR1f vs. mock		
Unigene ID	**Log_2FC**	**adj. p**	**Log_2FC**	**adj. p**	**Type**
Niben101Scf03816g01001	2.72	2.09E-15	0.16	0.916	
Niben101Scf04099g05004	2.82	2.47E-12	0.11	0.955	
Niben101Scf05961g02036	1.54	2.05E-10	-0.07	0.943	
Niben101Scf06509g02006	3.94	3.12E-10	0.92	NA	
Niben101Scf05928g03007	5.45	3.10E-09	1.33	NA	
Niben101Scf20124g00014	2.33	5.33E-08	-0.06	0.970	
Niben101Scf00245g00006	7.43	3.83E-07	1.12	NA	
Niben101Scf00160g06027	5.85	3.92E-06	1.60	NA	
Niben101Scf04709g00016	1.41	5.42E-06	0.17	0.803	
Niben101Scf00541g05003	-1.65	5.62E-06	-0.71	0.231	
Niben101Scf01148g00007	1.32	1.15E-05	-0.09	0.923	
Niben101Scf04053g03008	2.04	1.51E-05	-0.39	0.789	
Niben101Scf03685g00003	1.87	1.89E-05	-0.28	0.793	
Niben101Scf03021g00010	1.38	2.55E-05	-0.04	0.971	
Niben101Scf02417g01010	2.05	6.48E-05	0.37	NA	
Niben101Scf09296g00007	-1.91	1.45E-04	-0.17	0.886	
Niben101Scf00985g06002	-1.55	1.72E-04	0.01	0.993	
Niben101Scf01237g07019	-2.06	2.62E-04	0.34	0.596	
Niben101Scf00953g00004	1.69	2.73E-04	0.51	0.692	LRR-RLK
Niben101Scf07323g01002	-1.15	3.02E-04	-0.22	0.591	
Niben101Scf03251g00016	-1.25	7.48E-04	-1.00	0.487	
Niben101Scf12414g01006	-1.28	0.001	-0.28	0.624	
Niben101Scf08564g00001	1.65	0.002	0.03	0.988	
Niben101Scf01225g04031	1.49	0.006	-0.21	0.903	
Niben101Scf05437g06022	5.02	0.007	2.95	NA	
Niben101Scf04377g07005	1.03	0.008	0.63	0.293	
Niben101Scf14708g00025	1.36	0.008	0.25	0.860	
Niben101Scf01278g09008	1.23	0.013	-0.27	0.734	
Niben101Scf09811g00006	1.18	0.014	0.06	0.967	
Niben101Scf03098g00011	-1.39	0.019	0.23	0.854	
Niben101Scf10381g03006	4.63	0.020	2.34	NA	
Niben101Scf01519g01007	1.00	0.025	-0.23	0.721	
Niben101Scf09774g00001	-1.10	0.025	-0.73	0.278	
Niben101Scf17094g01001	-1.05	0.031	0.10	0.928	
Niben101Scf04609g00013	4.09	0.033	1.17	NA	
Niben101Scf04430g01006	-1.05	0.035	-0.31	0.743	
Niben101Scf02646g03004	1.26	0.04997	0.36	0.750	
Niben101Scf00745g02015	1.70	2.07E-04	0.27	0.813	

Table 3.3 Continued

	Wt RCNMV vs. mock		RCNMVΔSR1f vs. mock		
Unigene ID	**Log_2FC**	**adj. p**	**Log_2FC**	**adj. p**	**Type**
Niben101Scf07123g01015	7.03	5.51E-34	2.42	0.140	
Niben101Scf02072g01013	3.93	3.30E-22	0.88	0.428	
Niben101Scf02252g01032	4.06	1.67E-20	0.44	0.794	
Niben101Scf03240g00007	2.33	2.05E-08	0.45	0.709	
Niben101Scf03202g08006	2.43	8.18E-08	1.01	0.780	
Niben101Scf03925g01010	3.31	1.34E-07	0.20	NA	
Niben101Scf13842g01001	2.64	5.95E-06	0.93	0.509	
Niben101Scf11676g00001	3.06	2.04E-04	-0.03	NA	LRR-RLP
Niben101Scf00714g06002	5.92	2.61E-04	NA	NA	
Niben101Scf05982g00007	2.21	0.002	-0.80	NA	
Niben101Scf03202g07009	5.31	0.003	2.30	NA	
Niben101Scf00975g01015	4.36	0.005	0.75	NA	
Niben101Scf07123g01020	1.98	0.006	1.03	NA	
Niben101Scf02646g02009	1.42	0.007	-0.11	0.946	
Niben101Scf02854g10010	1.30	0.0473	-0.85	NA	

FC: Fold change, adj. p: corrected p-values, NA: not available in DESeq2 output

Table 3.4. List of PR genes in *N. benthamiana* obtained from (Li et al. 2018) with Log_2-fold change and adjusted p-values from RNA-seq analysis using DESeq2.

			Wt RCNMV vs. mock		RCNMVΔSR1f vs. mock	
PR Family	**Protein properties**	**Unigene ID**	**Log_2FC**	**adj. p**	**Log_2FC**	**adj. p**
PR 1	Cysteine-rich secretory protein, allergen V5/Tpx-1-related	Niben101Scf13926g01014				
		Niben101Scf03376g03004	9.92	1.90E-13		
		Niben101Scf00107g03008	11.85	5.73E-19		
		Niben101Scf01999g07002	7.22	5.61E-10		
PR 2	Glucan endo-1,3-beta-glucosidase-like, Glycoside hydrolase, family 17	Niben101Scf01001g00005	6.47	4.20E-05		
		Niben101Scf01001g00004			4.96	0.0116
		Niben101Scf01001g00003	8.56	4.82E-10	5.02	0.0110
		Niben101Ctg13736g00004	9.38	8.42E-24	4.85	0.0179
		Niben101Scf04869g03002	6.51	2.19E-55		
		Niben101Scf01001g00006	4.74	0.00035		
PR 3	Chitinase 8, Glycoside hydrolase, family 19	Niben101Scf02041g00002	7.55	6.61E-119		
PR 4	Thaumatin-like protein	Niben101Scf01400g00014	7.51	1.13E-37		
		Niben101Scf03436g01016				
PR 5	Pathogenesis-related thaumatin superfamily protein	Niben101Scf00126g00008				
		Niben101Scf05554g05006				
PR 6	Cysteine-rich secretory protein, allergen V5/Tpx-1-related	Niben101Scf00953g05001				
		Niben101Scf04053g01004				
PR 9	Peroxidase 53, Haem peroxidase	Niben101Scf03460g04004	1.94	0.0046		
		Niben101Scf07182g05012				
PR 10	Major pollen allergen Bet v 1-M/N, Bet v I type allergen	Niben101Scf03526g00006				
		Niben101Scf10735g00016				
		Niben101Scf02474g01024				
		Niben101Scf01938g04007				
PR 11	Chitinase-3-like protein 2, Glycoside hydrolase superfamily	Niben101Scf06295g04023				
		Niben101Scf01789g04010				
PR 17	Plant basic secretory protein family protein, uncharacterized protein family	Niben101Scf03385g02011	5.24	3.88E-34		
		Niben101Scf03385g01006				
		Niben101Scf01341g01002				
		Niben101Ctg10643g00004				

FC: fold change, adj. p: corrected p-values

Table 3.5. Selected differentially expressed genes that are known to be co-opted by *Tombusvirids*.

			Wt RCNMV vs. mock		RCNMVΔSR1f vs. mock	
Gene	**Protein**	**Unigene ID**	**Log_2FC**	**adj. p**	**Log_2FC**	**adj. p**
Rboh	Respiratory burst oxidase homolog protein A	Niben101Scf10840g01010	1.35	1.52E-03	0.58	0.27
CDPK	Calcium-dependent protein kinase	Niben101Scf15752g00002	1.95	1.92E-06	0.63	0.37
		Niben101Scf00800g02008	2.05	6.17E-10	0.63	0.42
		Niben101Scf09296g01009	1.00	8.89E-03	0.47	0.45
		Niben101Scf09345g00003	1.43	7.89E-04	0.80	0.52
		Niben101Scf03377g04002	1.03	3.27E-04	0.38	0.59
		Niben101Scf05534g01007	2.15	5.29E-18	0.19	0.87
		Niben101Scf00539g05012	2.38	6.09E-08	0.18	0.92
		Niben101Scf01166g14001	2.41	7.41E-03	0.14	0.94
		Niben101Scf00083g00009	1.01	5.26E-04	-0.01	0.99
		Niben101Scf17776g00008	2.65	0.0213	0.03	NA
		Niben101Scf04216g07017	2.12	0.0317	0.05	NA
PLD	Phospholipase D	Niben101Scf02465g00004	1.81	2.46E-07	-0.07	0.95
		Niben101Scf00539g07022	2.24	7.01E-05	0.85	NA
		Niben101Scf03930g01018	6.05	1.20E-04	3.96	NA
HSP70	Heat shock protein 70	Niben101Scf04364g01014	1.04	1.75E-04	0.24	0.63
		Niben101Scf02771g01007	1.05	1.93E-04	0.29	0.41
		Niben101Scf07275g02012	1.36	3.18E-03	0.28	0.72
		Niben101Scf00449g06008	1.55	1.39E-04	-0.52	0.31
		Niben101Scf04490g00001	2.05	0.0473	0.41	NA
		Niben101Scf13703g01006	3.74	7.12E-04	2.48	NA
HSP90	Heat shock protein 90	Niben101Scf04331g09018	1.03	1.43E-03	0.55	0.48
		Niben101Scf01027g00003	1.38	0.0102	0.86	0.30
		Niben101Scf06890g01022	1.52	6.80E-11	0.74	0.30
		Niben101Scf27914g00006	1.60	2.92E-12	0.50	0.39
Arf	ADP-ribosylation factor	Niben101Scf01063g07014	1.24	6.30E-04	-0.19	0.89
ORP	Oxysterol-binding protein-related protein	Niben101Scf00126g06015	1.00	3.86E-03	0.56	0.22
		Niben101Scf02429g00001	1.03	1.95E-03	0.42	0.47
VAP	Vesicle-associated membrane protein-associated protein	Niben101Scf04122g05011	1.18	1.50E-04	-0.38	0.71
BRO1	Vacuolar protein-sorting protein bro1	Niben101Scf12308g00014	1.234	1.22E-06	0.57	0.19
		Niben101Scf04109g03009	1.326	1.22E-06	0.56	0.25
		Niben101Scf04973g02006	1.78	4.53E-05	0.46	0.44

FC: Fold change, adj. p: corrected p-values, NA: not available in DESeq2 output

Table 3.6. List of primers used for qRT-PCR.

Primer Name	Sequence (5'-3') *	Amplicon Size (bp)	Efficiency[#]	Miscellaneous
RCNMV_1457_FP	CAACAGGGCTCAAGGGAGAG	118	104.14 %	Amplifies RCNMV RNA 1
RCNMV_1574_RP	GAATTTGAGGGCATCGACGC			
RC_R2_479_FP	AGGGTGCGAATCACGAATAC	190	100.21 %	Amplifies RCNMV RNA 2
RC_R2_668_RP	ACTGCACGTAGGCTTCCACT			
Nbenth_PP2A_FP	GACCCTGATGTTGATGTTCGCT	123	92.76-106.91 %	Protein phosphatase 2A; TC21939 (At1g13320) [R]
Nbenth_PP2A_RP	GAGGGATTTGAAGAGAGATTTC			
Nbenth_L23_FP	AAGGATGCCGTGAAGAAGATGT	110	83.09 - 109.12 %	60S ribosomal protein; TC19271 (At2g39460) [R]
Nbenth_L23_RP	GCATCGTAGTCAGGAGTCAACC			
NbPR1_FP	GGATGCCCATAACACAGCTC	150	93.52 %	Amplifies PR1 genes
NbPR1_RP	GCTAGGTTTTCGCCGTATTG			
NbPR2_FP	GATGCCCTTTTGGATTCTATG	109	86.91 %	Amplifies PR2 genes
NbPR2_RP	TTGCTGCAGAGTTTCCTTCA			
NbABF_FP	TTGGGAAGTCCTGGAATGAG	130	102.86 %	Amplifies ABF genes
NbABF_RP	TAACAGCTCCGGCTCCTAAA			
NbWrky_FP	TCTTTAGCCGTCCAGCCTTA	169	93.86 %	Amplifies NbWRKY25/33 genes
NbWrky_RP	CGTCGTCGAAATCATCTCCT			
NbRboh_FP	TCAAGAACTCAAGCGGGTCT	176	107.75 %	Amplifies NbRboh genes
NbRboh_RP	GACCAACAAGCAGCAAGACA			
NbJAZ_FP	ACATGAGCAATCCCTCCAAC	218	104.06 %	Amplifies NbJAZ genes
NbJAZ_RP	GACCGTCCCACCATAGAAGA			
NbPro-inh_FP	GCTTTCTTGCTCCTTGCATC	175	108.66 %	Amplifies NbPI genes
NbPro-inh_RP	GTTCAGGCCATGATTGCTTT			

[#]Primer efficiency was calculated using standard curve with 5 points of dilution with each run.

[R]Used as reference genes.

*The primer sequence for NbPP2A, and NbL23 was by obtained from (Liu et al. 2012). The primer sequence for NbPR1 gene was obtained from (Obrępalska-Stęplowska et al. 2018). All the remaining primers were designed using the primer3 tool (https://primer3.ut.ee/).

Table 3.7. List of primers used for genotyping Arabidopsis mutants.

Primer Name	Sequence (5'-3') *	Amplicon Size (bp)	
at_xrn4-5_for	GTTTCTTGGTTGTTGCAGCTC	1164	
at_xrn4-5_rev	TCATGACGAATTCCTTTGAGG		593-893
pDAP101.LB3#	TAGCATCTGAATTTCATAACCAATCTCGATACAC		
at_dcl2-1_for	TGAATCATCTGGAAGAGGTGG	1060	
at_dcl2-1_rev	CTTCACAGGAGTTTTTGGCTG		459-759
pROK2_LBb1.3#	ATTTTGCCGATTTCGGAAC	546-846	
at_dcl3-1_rev	TGGAAAAGTTTGCTACAACGG		1085
at_dcl3-1_for	ACAGGTAACCTTGCCATGTTG		
at_dcl4-2t_for	AAGAGAACTTTTGCCGAAAGC	1222	
at_dcl4-2t_rev	TTTGCCAGTCTTACAAGTGGG		572-872
pAC161_8474#	ATAATAACGCTGCGGACATCTACATTTT		

#Primers for T-DNA vector sequences

*Primers were designed using T-DNA express (http://signal.salk.edu/tabout.html) according to (Leicht and Cheng 2009; O'Malley et al. 2015).

CHAPTER 4. TRANSLATIONAL CONTROL OF GENE EXPRESSION DURING RED CLOVER NECROTIC MOSAIC VIRUS INFECTION IN *ARABIDOPSIS THALIANA*

Pulkit Kanodia[1,2], Zachary Lozier[2,3], Filip Lastovka[4], Betty Chung[4], W. Allen Miller[1,2,3,5]*

[1] Interdepartmental Genetics & Genomics Program, Iowa State University, Ames, Iowa, USA

[2] Plant Pathology and Microbiology Department, Iowa State University, Ames, Iowa, USA

[3] Bioinformatics & Computational Biology Program, Iowa State University, Ames, Iowa, USA

[4] Department of Pathology, University of Cambridge, Cambridge, UK

[5] Plant Science Institute, Iowa State University, Ames, Iowa, USA

* Corresponding author: wamiller@iastate.edu

Modified from a manuscript to be submitted to *Journal of Virology*

Author Contributions: PK and WAM designed the experiments. PK conducted all the experiments. PK conducted bioinformatics and statistical analysis of host RNAs. FL, ZL, and PK conducted bioinformatics and statistical analysis of RCNMV RNAs. PK and WAM wrote the draft manuscript. WAM supervised PK and ZL, and BC supervised FL.

Abstract

During infection, viruses regulate host gene expression to create a proviral environment while the host simultaneously regulates its own and viral gene expression to restrict virus spread. The reprogramming of cellular gene expression occurs at transcriptional, post-transcriptional, translational, and post-translational levels but almost all the genome-wide studies in plant-virus interaction have focused only on transcriptional regulation. However, owing to the energy-intensive nature of translation and virus's complete reliance on the host translational machinery, it is important to assess the translational control during virus infection. Therefore, in this study,

we assessed how plant virus infection reprograms the cellular gene expression at the level of mRNA abundance and translational control using ribosome profiling. We inoculated *Arabidopsis thaliana* plants with red clover necrotic mosaic virus (RCNMV) and assessed host and viral gene expression at 5- and 8-days post inoculation. We identified the genes that are transcriptionally and/or translationally regulated during virus infection and determined that the early translational response to RCNMV infection is specific to plant immune responses unlike the translational response at a later stage when many other pathways are regulated/dysregulated by virus infection. At the later infection stage, unfolded protein response (UPR) was also elicited as demonstrated by transcriptional upregulation of canonical UPR genes. On the other hand, ribosome profiling of RCNMV RNAs (i) revealed the efficiency of the -1 programmed ribosomal frameshifting for the translation of RCNMV p88 protein with RdRp domain, (ii) determined that among viral proteins, coat protein is translated most efficiently while p88 is translated least efficiently, and (iii) identified a putative ribosomal pause site in the movement protein ORF of RCNMV RNA2. To our knowledge, this is the first genome-wide study that assesses the translational control of gene expression in plants infected with a virus from the *Tombusviridae* family.

Introduction

Plant viruses are obligate intracellular parasites with a limited coding capacity and therefore, rely heavily on cellular factors and machinery to complete their infection cycle. This includes virion disassembly, viral mRNA translation, cellular membrane remodeling to form viral replication sites, viral genome replication, virus movement, and virion assembly (Nagy and Pogany 2012; Hyodo and Okuno 2014; Wang 2015; Hyodo and Okuno 2016; Garcia-Ruiz 2018; Pitzalis and Heinlein 2018; Zhang et al. 2019; Tang et al. 2020; Hyodo and Okuno 2020; Hyodo

2021). As soon as the virus enters the cell, a molecular battle ensues between the virus and the host cell that determines the success of infection (Alexander and Cilia 2016; Harwig et al. 2017; Musidlak et al. 2017; Cheng and Wang 2017; Garcia-Moreno et al. 2018; Wu et al. 2019b; Souza and Carvalho 2019; Kushwaha et al. 2019; Wang et al. 2019; Garcia-Ruiz 2019; Li and Wang 2019; Girardi et al. 2021). This includes the reprogramming of host gene expression by the virus to create a proviral cellular environment while the host regulates the cellular and viral gene expression to restrict the infection (Lindbo et al. 2001; Hanley-Bowdoin et al. 2013; Collum et al. 2016; Nicaise and Candresse 2017; Wang et al. 2019; Kapos et al. 2019; Mauck et al. 2019; Vinutha et al. 2020; Hyodo and Okuno 2020; Ramesh et al. 2021; Wang et al. 2021). Understanding host-virus interactions on a genome-wide scale is valuable for high-throughput identification of pro- and antiviral pathways that can be exploited and targeted to develop virus-resistant plants (Rodriguez-Hernandez et al. 2012; Hashimoto et al. 2016; Gal-On et al. 2017; Zaidi et al. 2018; Gaffar and Koch 2019; Schmitt-Keichinger 2019; Esse et al. 2020; Zhao et al. 2020; Lv et al. 2020; Yoon et al. 2020; Taliansky et al. 2021; Wang et al. 2021; Garcia-Ruiz et al. 2021).

While numerous studies exist that elucidate the transcriptional and post-transcriptional regulation of cellular and viral gene expression (Dardick 2007; Havelda et al. 2008; Catoni et al. 2009; Allie and Rey 2013; Yang et al. 2014; Kaur et al. 2015; Choi et al. 2015; Fan et al. 2015; Gómez-Aix et al. 2016; Sun et al. 2016; Huang et al. 2017; Ahmed et al. 2017; Seo et al. 2018; Wu et al. 2019a; Zanardo et al. 2019; Pesti et al. 2019; Medzihradszky et al. 2019; Sun et al. 2021), there are only a few studies that assess the role of translational regulation in plant viral infection (Bhattacharjee et al. 2009; Eskelin et al. 2011; Ghoshal and Sanfaçon 2014; Karran and Sanfaçon 2014; Machado et al. 2015; Zorzatto et al. 2015; Ma et al. 2015; Meteignier et al. 2016;

Miller et al. 2016; Machado et al. 2017; Wu et al. 2020). Previously, microarrays and high-throughput sequencing of polysome associated mRNAs have been used to study translational control of plant mRNAs during pathogen infection (Moeller et al. 2012; Meteignier et al. 2017; Eskelin et al. 2019; Collum et al. 2020) but this technique suffers from poor resolution and accuracy (Ingolia et al. 2009). The advent of ribosome profiling has enabled researchers to study translational control of gene expression in a high-throughput manner at a genome-wide scale with single-nucleotide resolution (Ingolia et al. 2009). Ribosome profiling has explored the translation landscape of the cellular and viral mRNAs during infection in animal systems (Stern-Ginossar 2015; Stern-Ginossar and Ingolia 2015; Yang et al. 2015; Irigoyen et al. 2016; Khong et al. 2016; Dai et al. 2017; Irigoyen et al. 2018; Bencun et al. 2018; Gerresheim et al. 2019; Cook et al. 2019; Dinan et al. 2019; Machkovech et al. 2019; Tran et al. 2020; Echavarría-Consuegra et al. 2021; Yuan et al. 2021; Alexander et al. 2021) but there is only one published study (with the sequencing data not publicly available), to our knowledge, that uses a plant virus-host system to assess the genome-wide translational control in sugarcane mosaic virus (SCMV, *Potyvirus*, *Potyviridae*)-infected maize plants (Xu et al. 2019). Therefore, there is a need for more research into plant virus-host interaction at the translation level. Here, we used *Arabidopsis thaliana* and red clover necrotic mosaic virus (RCNMV) as a model system to study host-virus interactions.

RCNMV (*Dianthovirus*, *Tombusviridae*) is a bipartite RNA virus with uncapped and non-polyadenylated positive-sense single-stranded genomic RNAs 1 and 2 *(Chapter 1, Fig. 1.2-C)* (Gould et al. 1981; Hiruki 1987; Okuno and Hiruki 2013). Essential replicase protein (p27) and a -1 programmed ribosomal frameshift (-1 PRF) product (p88), which contains the RNA-dependent RNA-polymerase (RdRp) domain, are translated directly from RNA1 *(Chapter 1, Fig.*

1.2-C) (Xiong and Lommel 1989; Koonin 1991; Kim and Lommel 1994, 1998; Okuno and Hiruki 2013). Coat protein (CP) is translated from subgenomic RNA (CPsgRNA1) *(Chapter 1, Fig. 1.2-C, 1.3-A)* and is required for long-distance movement in the plant (Xiong et al. 1993; Zavriev et al. 1996; Sit et al. 1998). Movement protein (MP) is translated from RNA2 *(Chapter 1, Fig. 1.2-C)* and is required for cell-to-cell movement (Lommel et al. 1988; Xiong et al. 1993). Additionally, an xrRNA-derived noncoding subgenomic (ncsg)RNA, called SR1f, is generated as a stable degradation product formed by incomplete degradation of RNA1 and CPsgRNA1 by the host 5'→ 3' exoribonuclease *(Chapter 1, Fig. 1.2-C, 1.3-B)* (Iwakawa et al. 2008; Steckelberg et al. 2018). Translation of viral proteins from RNA1 and CPsgRNA1 occurs via a 3' cap-independent translation element (CITE) in the 3' UTR, called TE-DR1 *(Chapter 1, Fig. 1.2-C)* (Mizumoto et al. 2003). TE-DR1 belongs to the barley yellow dwarf virus-like translation element (BTE) class of CITEs that recruit the translation machinery via binding to eIF4G (Treder et al. 2007; Mizumoto et al. 2003; Kraft et al. 2013; Sharma et al. 2015; Zhao et al. 2017). Because TE-DR1 is also present in the 3' co-terminal SR1f *(Chapter 1, Fig. 1.2-C)*, it is hypothesized that SR1f may sequester the host translation machinery and spatio-temporally regulate viral as well as cellular translation (Iwakawa et al. 2008; Miller et al. 2016).

In this study, we utilize ribosome profiling to study how RCNMV infection in Arabidopsis affects the cellular gene expression, both at the level of transcription and translation, during an early pre-symptomatic and a late symptomatic phase. We identified genes that are differentially regulated owing to the change in their (i) mRNA abundance without any change in the proportion of ribosomes translating those mRNAs, (ii) translation efficiency, i.e., the number of translating ribosomes without any change in the mRNA abundance, and (iii) mRNA abundance as well as translation efficiency. We found out the translationally-regulated genes,

only in the early phase, are enriched in protein domains that are involved in plant defense responses. In addition to host gene expression, we also assess the ribosome profiles on viral RNAs which displayed the translation of the four known ORFs in the RCNMV genome. One appealing aspect of Ribo-seq on viral RNAs was the visualization and quantification of -1 programmed ribosomal frameshifting in translation of p88 ORF. Our data showed that the frameshift efficiency increased from 5 to 8 dpi. We also determined that, among the four ORFs, p88 ORF is translated least efficiently, as expected, and the CP ORF is translated most efficiently.

Results and Discussion

RCNMV accumulation increases steeply at 6/7 dpi in *dcl2-1/dcl4-2t* Arabidopsis

In *Chapter 3*, we determined that RCNMV infection in wildtype Arabidopsis was asymptomatic and mostly inconsistent. However, for our experiment, we require mutant Arabidopsis plants with reduced antiviral activity in which RCNMV can replicate efficiently and produce symptomatic infection. Among the four DCL proteins (DCL1, 2, 3, 4) in Arabidopsis, DCL2 and DCL4 generate virus-derived siRNAs required for antiviral RNA silencing (Deleris et al. 2006). Therefore, we tested *dcl2-1/dcl4-2t* Arabidopsis, which is a loss-of-function double knock-out line (with T-DNA insertion in *DCL2* and *DCL4* genes) with non-functional antiviral RNA silencing machinery (Xie et al. 2005), and determined that wt RCNMV produces symptomatic infection reproducibly in *dcl2-1/dcl4-2t* Arabidopsis plants *(Chapter 3)*. Thus, for our Ribo-seq experiment, we used *dcl2-1/dcl4-2t* Arabidopsis as a host for RCNMV infection.

Our first objective was to determine early and late time-points at which the infected leaves would be harvested for Ribo-seq. Compared to transcriptional regulation, translational control can yield a much quicker and finely-tuned response to any stimuli. Therefore, we expect

most gene expression changes to be translationally regulated in RCNMV-infected plants at an early time-point. We decided to choose an early time-point when we can reproducibly detect viral RNAs in the systemic leaves just before the appearance of symptoms. The late time-point refers to the time-point after the appearance of symptoms with a high viral RNA accumulation but before significant cell death. A time-course assay from 4 to 10 days post inoculation (dpi) demonstrated the appearance of strong symptoms at around 7 dpi *(Fig. 4.1-A)*. Symptoms included chlorosis, necrosis, severely mosaic, and epinastic leaves. Subsequently, RCNMV RNA1 accumulation was assessed using RT-PCR and qRT-PCR *(Fig. 4.1-B, C)*. Consistent with the appearance of symptoms, viral RNA accumulated dramatically at 6/7 dpi. These observations were repeatable in multiple independent time-course experiments. Therefore, for Ribo-seq, we chose 5 dpi as an early time-point when there are no symptoms but RCNMV RNA accumulated consistently in the systemic leaves and 8 dpi as a late time-point when all the infected plants were severely symptomatic and viral RNA levels were nearing their peak.

Ribo-seq and RNA-seq experiment design and data characteristics

Five biological replicates each of Mock and RCNMV-inoculated Arabidopsis *dcl2-1/4-2t* were collected at 5 and 8 dpi. Each replicate consisted of 3 – 4 non-inoculated young leaves per plant from 18 plants pooled together. Consistent with the time-course experiment, the symptoms appeared after 7 dpi *(Fig. 4.2-A)*. RCNMV infection was verified by RT-PCR *(Fig. 4.2-B)*. Subsequently, Ribo-seq and RNA-seq libraries were prepared using the five biological replicates of RCNMV-inoculated samples and four biological replicates of mock-inoculated samples and sequenced. The raw sequence data were bioinformatically processed, rRNA, tRNA, and snoRNA sequences were removed, and remaining reads were aligned to Arabidopsis TAIR 10 reference genome and the RCNMV genome. The read statistics, such as the number and

proportion of raw, processed, and aligned reads, can be found in *Supplemental file 4.1*. The quality characteristics of Ribo-seq and RNA-seq data were assessed using RiboToolkit (Liu et al. 2020), RiboTaper (Calviello et al. 2016), and custom scripts.

The read length distribution of Arabidopsis genome-mapped and RCNMV positive-strand-mapped Ribo-seq reads peaked at 28 nt, unlike RCNMV negative-strand-mapped Ribo-seq reads *(Fig. 4.3-A)*. In contrast, the RNA-seq read-lengths were much widely distributed *(Fig. 4.3-A)*. First, RiboToolkit was used to assess the triplet periodicity for reads of different lengths which showed that 28-nt Ribo-seq reads displayed the best triplet periodicity followed by 29-nt, 27-nt, and 26-nt reads *(Fig. 4.3-B)*. However, no such triplet periodicity was observed for RNA-seq data *(Fig. 4.3-B)*. The triplet periodicity for 26-29 nt Ribo-seq reads and lack thereof, for RNA-seq reads, was also verified using RiboTaper via metagene analysis *(Fig. 4.3-C)*. The metagene analysis also showed that Ribo-seq reads mapped predominantly to the CDS *(Fig. 4.3-C)*. Furthermore, according to the number of nucleotides protected by the ribosomes upstream of P-site *(Fig. 4.3-C, see peaks upstream of start and stop codons)*, we can see that the 5' end of RPFs are preferentially digested by the RNAse, as reported previously (Hsu et al. 2016). We also assessed the triplet periodicity separately on the CDS and the UTRs and verified that only the Ribo-seq reads that map only to the CDS display triplet periodicity *(Fig. 4.4-A)*. In contrast, Ribo-seq reads that map to the UTRs *(Fig. 4.4-A)* and the RNA-seq reads that map to the CDS and the UTRs *(Fig. 4.4-B)* do not show any triplet periodicity. Finally, we show that only a fraction of Ribo-seq reads map to the UTRs and the intergenic region *(Fig. 4.4-C)*, unlike RNA-seq reads *(Fig. 4.4-D)*. We do, however, have a significant proportion of Ribo-seq reads that map to the introns *(Fig. 4.4-C)*, which is quite different from what has been reported previously

(Hsu et al. 2016). All the above-mentioned data characteristics show the successful preparation of high-quality Ribo-seq data where the majority of the reads represent the true RPFs.

Next, the principal component analysis (PCA) showed that the major variation (PC1) among all of our datasets can be attributed to the type of library preparation, i.e., Ribo-seq or RNA-seq *(Fig. 4.4-E)*. The second major variation (PC2) can be attributed to the treatment, with 8 dpi RCNMV-inoculated samples forming one cluster, 5 dpi RCNMV-inoculated samples forming another cluster, and mock-inoculated samples, both 5 and 8 dpi, aggregating into a single cluster, as expected *(Fig. 4.4-E)*. Subsequently, the Pearson correlation analysis showed very high reproducibility among the biological replicates of each treatment for both Ribo-seq *(Fig. 4.4-F)* and RNA-seq dataset *(Fig. 4.4-G)*. Overall, these analyses demonstrate the high-quality NGS data characteristics.

Differentially expressed and translated genes

To identify differentially expressed genes (DEGs) and differentially translated genes (DTGs), we used DESeq2 (Love et al. 2014) for differential expression analysis. We define DEGs as those having absolute (log_2-fold change of RNA abundance) > 1 with adjusted p-values < 0.05, and DTGs as those having absolute (log_2-fold change of RPF abundance) > 1 with adjusted p-values < 0.05. For DTGs, the change in RPF abundance can arise due to the change in mRNA abundance (DEGs), translational control, or both. The list of DEGs and DTGs can be found in *Supplemental file 4.2*.

For RCNMV vs mock datasets at 5 dpi, we identified 356 DEGs and 500 DTGs whereas at 8 dpi, we identified 3441 DEGs and 3263 DTGs *(Fig. 4.5-A)*. As expected, a far greater number of genes were differentially regulated at both the RNA and RPF levels at 8 dpi when all the plants were severely symptomatic. We would also like to emphasize the fact that for the

genes that do not pass the significance threshold at RNA or RPF level, it does not mean they are unchanged at RNA or RPF levels, rather, it just means that we do not have sufficient evidence to claim they are DEGs or DTGs. Therefore, interpreting only the Venn diagram to assess the genes that are identified only as DTGs would be considered a misinterpretation. Instead, we plotted the genes with a valid log_2-fold change output from DESeq2 for both RNA-seq and Ribo-seq data *(Fig. 4.5-B)*. In the resulting scatter plot, the blue points are DTGs with non-significant change in mRNA abundance, green points are DEGs with non-significant change in RPF abundance, and red points are genes that are both DEGs and DTGs *(Fig. 4.5-B)*. More information about the genes included in the scatterplot *(Fig. 4.5-B)* can be found in *Supplemental file 4.4*. To assess if the protein products from the translationally-regulated genes have any common features, we conducted protein-domain enrichment analysis using ThaleMine (Krishnakumar et al. 2017). For stringent criteria, we focused only on the DTGs (blue) in the yellow shaded area which are most likely the translationally-regulated genes. Among the 101 translationally-upregulated genes at 5 dpi, several protein domains such as protein kinase, leucine-rich repeat (LRR), Toll/interleukin-1 receptor homology (TIR), and Gnk2-homologous domains, among others, were enriched *(Fig. 4.5-B)*. These domains are in proteins that are central to plant innate immunity (Takken et al. 2006; Tena et al. 2011; Miyakawa et al. 2014; Ve et al. 2015; Dubey and Singh 2018; Hake and Romeis 2019; Macho and Lozano-Duran 2019; Vaattovaara et al. 2019; Bayless and Nishimura 2020; Yu et al. 2021). The 6 translationally-downregulated genes were insufficient for enrichment analysis. Even though there were a far greater number of translationally-regulated genes at 8 dpi, no protein domains were enriched in the 280 translationally-upregulated and 250 translationally-downregulated genes *(Fig. 4.5-B)*. This led us to conclude that the early translationally-regulated response to virus infection is

specific and targeted towards ameliorating the virus infection. In contrast, translationally-regulated response at a later stage was not specific to plant innate immunity but may be a by-product of dysregulated pathways during the infection.

Among the translationally-regulated genes *(Fig. 4.5-B, blue points in yellow shaded area)*, only two genes were common at both the time-points, namely AT4G09770 (TRAF-like family protein), that had a high change in RPF abundance, and AT5G12940 (LRR-family protein) *(Fig. 4.5-C)*, that only had a modest change in RPF abundance. By plotting the DESeq2-normalized counts for AT4G09770 (TRAF-like family protein) across Ribo-seq and RNA-seq samples in all treatment conditions *(Fig. 4.5-D)*, we can see that this gene is actually upregulated at the level of translation. In mammals, there are 7 TRAF (Tumor necrosis factor receptor-associated factor) proteins that interact with various cell surface receptors via the TRAF-domain and play key roles in the immune response and apoptosis (Park 2018). Arabidopsis genome has more than 70 TRAF domain-containing proteins (Qi et al. 2021). AT4G09770 (TRAF-like family protein) belongs to the TRAF/MATH-only class of TRAF proteins that are shown to be involved in regulating autophagy, plant immunity, and gametophyte development (Qi et al. 2021). Two other TRAF-proteins belonging to the same class, MUSE13 and MUSE14, have been shown to form a TRAFasome that degrades NLR immune receptors, SNC1 and RPS2, via modulating ubiquitination (Huang et al. 2016). During RCNMV infection, whether AT4G09770 (TRAF-like family protein) is translationally-upregulated by the plant to prevent overaccumulation of plant NLR proteins or by the RCNMV as a counter-defense strategy still needs to be determined. We also found 4 genes, identified as both DEGs and DTGs, that were regulated in opposite directions, i.e., upregulated transcriptionally but downregulated translationally *(Fig. 4.5-B)*. These genes included

AT5G18290 (SIP-Aquaporin-like superfamily protein), AT4G32295 (KIX9-histone acetyltransferase), AT1G10610 (bHLH DNA-binding superfamily), and AT4G29270 (HAD superfamily). Altogether, we have identified the list of translationally regulated genes at the early and the late time-points and it would be very interesting to ascertain the mRNA features and the mechanisms that contribute to the translational regulation of the specific genes.

KEGG pathway enrichment analysis

In the RNA-seq dataset at 5 dpi, only the "plant-pathogen interaction" term was enriched, whereas in the Ribo-seq dataset, "plant-pathogen interaction" and "MAPK signaling pathway-plant" terms were enriched *(Fig. 4.6-A)*. All the DEGs and DTGs in these pathways were upregulated, signifying that the early gene expression response to virus infection was specific to the plant's defense responses. By 8 dpi, many more pathways were enriched for both RNA-seq and Ribo-seq datasets, such as "Metabolic pathways", "Plant hormone signal transduction", and "Protein processing in endoplasmic reticulum", among others. This demonstrates that by the time that plants get symptomatic, virus infection disrupts several cellular pathways. More information for the enriched pathways can be found in *Supplemental file 4.5*.

Next, we plotted the DEGs and DTGs that were present in the enriched pathways *(Fig. 4.6-B)*. At both 5 and 8 dpi, most of the genes seem to be regulated at a transcriptional level *(Fig. 4.6-B, points near the x = y dotted line)*. A few other genes (denoted as blue triangles) were identified as DTGs but did not have any DESeq2 output from the RNA-seq data, mostly because of the low read counts. Because the RNA abundance did not increase to a detectable level in the RCNMV infected plants, but the RPF levels did increase, it is likely that these genes are regulated at the translational level. Examples include defense-related genes such as ERF1 (Ethylene response factor, AT3G23240), RPS2 (Resistant to *Pseudomonas syringae* 2,

AT4G26090), PDF1.2 (Plant defensin 1.2, AT5G44420), and CML43 (Calmodulin-like 43, AT5G44460), which were identified only as DTGs at both the time-points. More information about the genes included in the scatterplot *(Fig. 4.6-B)* can be found in *Supplemental file 4.6*.

Interestingly, the genes in the pathway "Protein processing in endoplasmic reticulum" that were identified as DEGs and DTGs at 8 dpi were regulated only at the level of transcription. These genes included BiP1, BiP2, BiP3, PDILs, CRT, CNX, HSP70, HSP90, and ERDJ3B which are known to be upregulated downstream of IRE1-mediated bZIP60 splicing in the cytoplasm that occurs during unfolded protein response (UPR) (Deng et al. 2011; Howell 2013; Srivastava et al. 2018). The function of these canonical UPR-responsive gene products is to ameliorate the ER-stress by increasing the capacity of the ER for protein folding, import, export, and quality control (Walter and Ron 2011; Hetz 2012; Deng et al. 2013; Angelos et al. 2017; Nawkar et al. 2018; Hetz et al. 2020). The elicitation of UPR pathways has been shown in a variety of plant-virus infections (Ye and Verchot 2011; Ye et al. 2011; Zhang and Wang 2016; Shen et al. 2017; Qiao et al. 2018; Li et al. 2018; Herath et al. 2020; Li et al. 2020; Verchot and Pajerowska-Mukhtar 2021). RCNMV forms virus replication complexes at the ER by restructuring the ER membrane (Turner et al. 2004; Mine et al. 2010b; Kusumanegara et al. 2012), thus, it is likely that RCNMV upregulates the UPR genes to increase the ER membrane surface area. Over-accumulation of viral proteins can also elicit UPR to alleviate ER-stress related cell death (Ye et al. 2011). Similar to our previous report on UPR in maize seedlings *(Chapter 5)*, we observed that, during RCNMV infection, the UPR genes are upregulated only transcriptionally *(Fig. 4.6-B)*. The upregulation of UPR genes supports the findings in a previous report that showed an increased amount of BiP proteins that are associated with the ER during RCNMV infection (Turner et al. 2004). Because BiP and other ER-resident genes are

upregulated at 8 dpi *(Fig. 4.6-B)*, we conclude that RCNMV infection elicits UPR in Arabidopsis. However, it still needs to be investigated whether UPR elicitation during RCNMV infection acts as a (i) proviral mechanism to increase virus replication by increased formation of virus replication complexes at the ER, (ii) proviral mechanism to increase the protein folding capacity of the ER for efficient synthesis of functional viral proteins, (iii) proviral or plant's prosurvival pathway to reduce ER stress-mediated cell death, or (iv) antiviral defense response to limit RCNMV infection.

Proportion of RCNMV-mapped RNA-seq and Ribo-seq reads

The proportion of RCNMV-mapped reads were calculated as the number of reads that uniquely mapped to RCNMV RNAs divided by the sum of the reads that uniquely mapped to RCNMV RNAs and Arabidopsis reference genome. The details can be found in *Supplemental file 4.1*. From 5 to 8 dpi, the proportion of RNA-seq reads mapping to the RCNMV RNAs increased from ~ 0.2 % to ~ 21.5 % *(Fig. 4.7-A)*. On the other hand, the proportion of 26-29 nt Ribo-seq reads mapping to the RCNMV RNAs increased from ~ 0.02 % to ~ 1.7 % *(Fig. 4.7-A)*. Such a high proportion of RCNMV RNA-seq reads with a relatively lower proportion of Ribo-seq reads was not surprising as the RNA-seq reads also include those derived from replication complexes and also packaged virus particles in which viral RNAs are not being translated. Even though at 5 dpi, only ~0.2% of the mapped reads were derived from RCNMV genome, RCNMV RNAs seemed to be quite abundant compared to the individual Arabidopsis RNAs *(Fig. 4.7-B)* but lower than many nuclear- and chloroplast-genome-encoded mRNA. With ~21.5% RNA-seq reads, RCNMV RNAs were the most abundant RNA species at 8 dpi *(Fig. 4.7-B)*. A similar pattern can be seen for the Ribo-seq reads *(Fig. 4.7-B)*. At 8 dpi, although only ~1.7% RPFs were derived from RCNMV mRNAs, at the individual mRNA level, RPFs from RCNMV

mRNAs were substantially greater than any host mRNA *(Fig. 4.7-B)*. However, the RPFs derived from chloroplast genome may be underestimated because we used only the 26-29 nt Ribo-seq reads for the analysis and the RPFs from the chloroplasts are known to be longer than the cytosolic RPFs (Chotewutmontri and Barkan 2016; Chotewutmontri et al. 2018).

Integrated RNA-seq density on RCNMV genome

The integrated density of RNA-seq reads over RCNMV genome was visualized by plotting all the nucleotides of the RNA-seq reads to the RCNMV RNA1 and RNA2 sequence from all the replicates together *(Fig. 4.8)*. Even though the RNA-seq experiment in *Chapter 3* used a different host species (*Nicotiana benthamiana*), RNA extraction protocol, library preparation strategy/kit, and sequencer, we observed similar characteristics of the RNA coverage profiles in this RNA-seq experiment *(Fig. 4.8)* to what we observed in the RNA-seq that we conducted previously *(Chapter 3, Fig. 3.17)*: (i) We did not see any marked abundance of CPsgRNA and SR1f, even though we attributed that to the library preparation artifact in *Chapter 3*, (ii) CPsgRNA negative-strand accumulated to much higher levels than the upstream portion of RNA1 negative-strand supporting the premature transcription termination mechanism for the generation of CPsgRNA (Sit et al. 1998; Guenther 2004), (iii) there are more reads towards the 5' end of RNA2 than the 3' end, with an inflection point near the trans-activator (TA) region. We speculated previously as to whether the peculiar pattern of reads across RNA2 is an artifact or actually has biological meaning. Because we observe the same pattern again in an entirely different experimental set-up, it seems less likely that this is an artifact. It would be interesting to explore this peculiar RNA coverage profile in future experiments.

Ribo-seq profiles on the RCNMV genome

The 28 nt RNA-seq and Ribo-seq reads that mapped to the RCNMV genome were visualized using the riboSeqR package (Chung et al. 2015). riboSeqR plots only the first nucleotide of the RNA-seq and Ribo-seq reads to the RNA sequence for visualization. RNA-seq reads are represented as gray bars and the Ribo-seq reads are represented as colored bars according to the reading frame the first nucleotide of the RPF maps to *(Fig. 4.9, 4.10).* The RNA-seq and Ribo-seq profiles on RCNMV genome looked reproducible across the biological replicates. Furthermore, riboSeqR correctly identified the three ORFs in RNA1 *(Fig. 4.9, red and blue horizontal bars over the profile)* and one ORF in RNA2 *(Fig. 4.10, green horizontal bars over the profile)* as being translated. Except for the increase in the number of reads, we did not see any other change in coverage pattern from 5 dpi to 8 dpi in these profiles.

In RNA1, we can observe the -1 PRF, as the translating frame changes at the frameshift site, denoted by the red frame at p27 ORF and blue frame in RdRp ORF *(Fig. 4.9, see the zoomed image).* Next, we quantified the frameshift efficiency, which was ~8% at 5 dpi, and increased to ~16% by 8 dpi *(Fig. 4.11).* Previous studies have reported the frameshift efficiency in RCNMV to be ~ 7.5% in the *in vitro* and protoplast-reporter assays (Kim and Lommel 1998). It has been hypothesized previously that -1 PRF product from RCNMV can act as a switch from translation to replication of viral RNAs (Okamoto et al. 2008; Tajima et al. 2011), similar to the model proposed for BYDV (Barry and Miller 2002). This hypothesis is based on the fact that p88 can act only in *cis* for the replication of RCNMV RNA1 (Okamoto et al. 2008; Iwakawa et al. 2011). This means that only the RNA1 molecule that undergoes -1 PRF to synthesize p88 protein is used as a template for negative-strand RNA1 synthesis. Therefore, upon -1 PRF, the translated p88 protein can bind to the 3' UTR of RNA1, assemble the 480-kDa virus replication complex with p27 at the ER, and initiate negative-strand RNA synthesis while inhibiting 3'TE-

DR1-mediated translation of RNA1 (Mine et al. 2010a, 2010b; Iwakawa et al. 2011). Therefore, the dependence of RNA1 replication on the -1 PRF product (p88) synthesized in *cis*, suggests that increased frameshift efficiency would increase RCNMV replication by producing more RdRps. Here, the observed increase in frameshift efficiency with the steep increase in RCNMV RNA1 accumulation supports the proposed model *(Fig. 4.11)*.

Even though -1 PRF is detected by Ribo-seq, we did not detect any ribosomal pausing, as indicated by the lack of an increase in the number of RPFs, at the frameshift site *(Fig. 4.9)*. Previously, it was considered that ribosomal pausing occurs at the frameshift site and the pause is required, although insufficient, for PRF (Tu et al. 1992; Somogyi et al. 1993; Lopinski et al. 2000; Brierley et al. 2010; Dinman 2012). Kontos et al. (2001) has argued against correlating ribosomal pausing and frameshifting, rather, speculated that pausing could occur as a result of the interaction between the ribosome and the stem-loop/pseudoknot and may not have any effect on frameshifting. Ribosome profiling has also failed to detect ribosomal pausing at frameshift sites in other viruses (Irigoyen et al. 2016; Napthine et al. 2017, 2019; Finkel et al. 2021). For example, (i) -1 PRF efficiency during the late stages of encephalomyocarditis virus (EMCV) is shown to be very high (~70%) (Napthine et al. 2017). However, ribosome pausing was not markedly detectable at the frameshift site of wildtype EMCV (Napthine et al. 2017). (ii) Ribo-seq in murine coronavirus-infected cells showed that no ribosomal pausing occurs at the frameshift site (Irigoyen et al. 2016). The authors speculated that RPFs at the pause site could be longer and were excluded from the experiment because of the narrow size range of RPFs that were selected after RNase digestion. However, upon conducting Ribo-seq even with longer RPFs, no ribosomal pausing was detected (Irigoyen et al. 2016). (iii) Ribosomal pausing was not detected at the PRF site in SARS-CoV-2 RNA (Finkel et al. 2021). In contrast, modified

nuclease digestion (disome footprint profiling) with SARS-CoV-2-infected cells did show ribosome pausing at the frameshift site and this observation was verified using cryo-EM (Bhatt et al. 2021). Therefore, whether Ribo-seq is suitable for assessing ribosomal pausing during frameshifting is still debatable. In case of RCNMV, using the conventional Ribo-seq method with only the 26-29 nt RPFs, we did not detect any ribosomal pausing at or near the frameshift site *(Fig. 4.9)*.

According to the RNA-seq data, abundance of reads across RNA1 seems to be uniform suggesting very low or no accumulation of CPsgRNA *(Fig. 4.9)*. However, the number of Ribo-seq reads mapping to CP ORF is substantially higher than those mapping to the p27 and RdRp ORFs, indicating the CP is translated with a very high efficiency *(Fig. 4.9)*. This suggests that either CPsgRNA has a much higher translation efficiency than RNA1 and/or there is an internal ribosome entry site (IRES) in RNA1 just upstream of the CP ORF. Another result that supports the latter hypothesis is the accumulation of CP from the *in vitro* translation of RNA1 in wheat germ extract *(Chapter 3, Fig. 3.5-A)*. Previously, we speculated that CP translation might have occurred from partially degraded RNA1 but the ribosome profiling results show the need to investigate the possibility of an IRES, upstream of CP ORF, as has been reported for other Tombusvirids (Koh et al. 2003; Fernández-Miragall and Hernández 2011; May et al. 2017).

In RNA2, RPF read density was very low, showing that RNA2 is not translated very efficiently *(Fig. 4.10)*. Interestingly, we observe an RPF peak *(Fig. 4.10, red arrow)* in the MP ORF that was present in all the samples at both time-points. That could be an artifact or an authentic ribosomal pause site. It would be interesting to assess the RNA structure and codon composition near the putative pause site. Ribosomal pausing may occur to aid co-translational folding of MP. However, because the inflection point at the TA region in our RNA coverage

profile *(Fig. 4.8, 4.10)* is near the potential ribosomal pause site, we speculate if ribosomal pausing leads to stacking of stalled ribosomes that may elicit No-Go decay pathway, resulting in an endonucleolytic cleavage upstream of the pause site (Simms et al. 2017; Navickas et al. 2020). If this hypothesis were true, it would explain the big green peak in the Ribo-seq profile, unusual RNA2 coverage pattern, and low translation of RNA2 as evidenced by sparsely distributed RPFs over RNA2 *(Fig. 4.10)*.

Conclusion

In this study, we determined that the early translational response to RCNMV infection is specific to the plant defense responses. We identified the genes that are differentially expressed and differentially translated in RCNMV-infected plants. Future work would include the identification of the sequence and structural features of the UTRs of translationally-regulated mRNAs to explore the mechanisms by which specific mRNAs are translationally controlled during RCNMV infection. We also investigated the RNA-seq and Ribo-seq read profiles across RCNMV RNA1 and RNA2 sequences. We found that the frameshift efficiency of RNA1 increased during the late phase of infection, which correlates with the increased accumulation of RCNMV RNA1. We also identified a putative ribosomal pause site in the MP ORF of RNA2. The authenticity of the ribosomal pause site and its biological significance needs to be tested. Furthermore, my hypothesis that ribosomal pausing leads to No-Go decay of RNA2 also needs to be investigated as this could explain the unusual RNA-seq read coverage across RNA2 sequence. Lastly, the high-quality Ribo-seq and RNA-seq data obtained in this study, with several biological replicates showing excellent reproducibility, provide a valuable source of transcriptomic and translatomic data that could further be explored to dissect plant virus-host interactions.

Materials and Methods

In vitro transcription of RCNMV RNAs

RCNMV plasmid constructs used for *in vitro* transcription were described previously (Kanodia et al. 2020a). pRC169c and pRC2|G are cDNA clones with T7-promoter for *in vitro* transcription of infectious RCNMV RNA1 and RNA2, respectively. One µg of SmaI-linearized pRC169c and pRC2|G were used as templates for *in vitro* transcription using MEGAscript T7 Transcription kit (Invitrogen AM1334) followed by DNase treatment according to manufacturer's protocol. The transcription reaction was carried out at 37˚C for 4 h and DNase treatment at 37˚C for 30 min. Subsequently, RNA was purified using Zymo RNA clean & concentrator -5 kit (Zymo Res. R1015) and eluted in nuclease-free water.

RCNMV-infected sap preparation

N. benthamiana plants were grown in a growth chamber with 16 h light at 24˚C and 8 h dark at 20˚C. Four-week-old plants were mechanically inoculated with (i) 10 mM sodium phosphate (pH 6.8) buffer (Mock-inoculated), or (ii) 1 µg RNA1 plus 1 µg RNA2 in 10 mM sodium phosphate (pH 6.8) buffer per leaf (RCNMV-inoculated) and the growth conditions were changed to 12 h light at 20˚C and 12 h dark at 20˚C. After the appearance of symptoms, RT-PCR was used to verify RCNMV replication in the non-inoculated systemic leaves. Subsequently, the leaves were ground in 10 mM sodium phosphate (pH 6.8) buffer using mortar and pestle and the resulting sap was used for inoculating Arabidopsis plants.

Inoculating Arabidopsis with RCNMV

Arabidopsis double knock-out mutant line, *dcl2-1/dcl4-2t* (Germplasm CS66078) (Xie et al. 2005) was obtained from the Arabidopsis Biological Resource Center (abrc.osu.edu) and the

T-DNA insertion was verified by genotyping (O'Malley et al. 2015). The plants were grown in growth chambers with 16 h light at 24˚C and 8 h dark at 20˚C. After 3 weeks, the growth condition was changed to 12 h light at 20˚C and 12 h dark at 20˚C. The sap from mock- or RCNMV-inoculated *N. benthamiana* plants was rubbed on 2-3 leaves per Arabidopsis plant (4-week-old) using q-tips and carborundum.

RT-PCR and qRT-PCR

For the time-course experiment, 3-4 leaves per plant were pooled from 3 plants to make 1 biological replicate and 3 of these biological replicates were collected at 4, 5, 6, 7, 8, 9, and 10 dpi for RCNMV-infected plants and at 10 dpi for mock-infected plants. The leaves were pulverized in a tissue lyzer at 1500 rpm for 30 s (twice). Total RNA was extracted using Zymo Direct-zol RNA Miniprep kit (Zymo Res. R2050) according to the manufacturer's protocol followed by quantification using Qubit RNA HS assay kit (Invitrogen Q32852). Total RNA integrity was verified by agarose gel electrophoresis. RevertAid First Strand cDNA Synthesis kit (Thermo Scientific K1622) was used for DNase treatment and cDNA synthesis (with random hexamers) according to the manufacturer's protocol.

For RT-PCR, a 10 µl PCR reaction mix was prepared with 5 µl GoTaq G2 green master mix (Promega M7823), 1 µl 10-fold diluted cDNA template, 200 nM each of RCNMV_1457_FP *(5'-CAACAGGGCTCAAGGGAGAG-3')* and RCNMV_1574_RP primers *(5'-GAATTTGAGGGCATCGACGC-3')*. The PCR conditions were as follows: 98˚C (2 min); 30 cycles of 98˚C (10 s), 60˚C (15 s), 72˚C (15 s); 72˚C (2 min); 4˚C hold.

For qRT-PCR, a 10 µl qPCR reaction was prepared with 1x iQ SYBR Green Supermix (Bio Rad 1708880), 300 nM each of forward and reverse primers, and 1 µl 10-fold diluted cDNA template. The qPCR runs were carried out in 384-well plates with 3 technical replicates per

sample in a Bio Rad CFX384 system with the following reaction conditions: 95˚C for 3 min (Polymerase activation and DNA denaturation), 40 cycles of 95˚C for 10 s (Denaturation), 60˚C for 60 s (Annealing, extension/Plate reading) followed by melt curve analysis (55-95˚C, 0.5˚C increment, 5 s). AtSAND and AtPDF2 genes were used as reference genes with the primer pairs Athal_PDF2_FP *(5'-TCATTCCGATAGTCGACCAAG-3')* plus Athal_PDF2_RP *(5'-TTGATTTGCGAAATACCGAAC-3')* and Athal_SAND_FP *(5'-GTTGGGTCACACCAGATTTTG-3')* plus Athal_SAND_RP *(5'-GCTCCTTGCAAGAACACTTCA-3')* (Lilly et al. 2011). Prior to using these as reference genes, we verified their consistent expression between our experimental conditions. The primer efficiency calculation, ΔΔCt calculation, and statistical analysis were performed using the Bio Rad CFX manager software.

All the primers were synthesized by Integrated DNA Technologies (IDT) and purified by standard desalting.

Ribosome profiling

Ribosome profiling protocols from (Hsu et al. 2016; Chung et al. 2020; Kanodia et al. 2020b) were used with modifications.

Lysate preparation. For ribosome profiling, 5 biological replicates were collected each for mock- and RCNMV-infected plants at 5 and 8 dpi. Each biological replicate consisted of 3-4 young leaves per plant pooled together from 18 plants. The tissues were collected in 50 ml falcon tubes and coarsely pulverized by vigorously shaking the tube with two 4.8 mm metal beads in it. An aliquot of coarsely ground tissues were finely pulverized in 1.5 ml tubes using tissue lyzer at 1500 rpm for 30 s (twice) followed by the addition of 800 µl of polysome extraction buffer (PEB; 20 mM Tris-HCl pH 7.5, 140 mM KCl, 5 mM MgCl2, 1% (v/v) Triton

X-100, 0.5% (v/v) Igepal CA 630, 146.1 mM sucrose, 100 µg/ml cycloheximide, 100 µg/ml chloramphenicol, 0.5 mM DTT, 0.5 µl/ml Turbo DNase (Invitrogen AM2238), and EDTA-free protease inhibitor (Thermo Scientific A32965)). The crude lysate was incubated in ice for 20 min on a rocker followed by clarification using two rounds of centrifugation (21,100 x g, 15 min, 4˚C). Subsequently, the absorbance of the lysate was adjusted with PEB to A254 (Lysate - PEB) = ~A260 (Lysate - PEB) = ~6. Subsequently, 400 µl of the absorbance-adjusted lysate was used for ribosome profiling and 200 µl for RNA sequencing.

RNase1 digestion. 400 µl lysate was centrifuged (21,100 x g, 5 min, 4˚C) to remove any remaining debris. Subsequently, 2 µl (200 U) RNAse1 (Invitrogen AM2295) was added and the RNase digestion was carried out for 60 min at 28˚C in a thermomixer at 400 rpm. The tubes were immediately transferred to ice and 5 µl Superase-IN (Invitrogen AM2696) was added to terminate the RNase digestion reaction.

Pelleting the monosomes. To the RNase-treated lysate, PEB was added to make the total volume ~750 µl and was carefully layered on a precooled 350 µl sucrose cushion (35% (w/v) sucrose, 20 mM Tris-HCl pH 7.5, 140 mM KCl, 5 mM MgCl2, 100 µg/ml cycloheximide, 100 µg/ml chloramphenicol, 0.5 mM DTT, 5 µl/ml Superase-IN (Invitrogen AM2696)) in mini-ultracentrifuge tubes (Thermo Scientific 45237) followed by ultracentrifugation at 57,000 rpm (131,500 x g) for 90 min at 4˚C with slow acceleration and deceleration in a Sorvall mini ultracentrifuge (Discovery M150) with S150-AT fixed angle rotor (Thermo Scientific 45582). Subsequently, the supernatant was removed and the pellet was carefully rinsed with 500 µl nuclease-free water.

Ribo-seq RNA purification. 600 µl proteinase-K buffer (10 mM Tris-HCl pH 7.5, 1% SDS, 200 µg/ml proteinase K (Thermo Scientific EO0491)), prewarmed to 42˚C, was added to

the monosome pellet and incubated at room temperature for 5 min, the pellet was resuspended by pipetting, transferred to 1.5 ml microfuge tubes, and incubated at 42˚C for 30 min. Subsequently, the suspension was heated to 65˚C for 2 min and immediately subjected to RNA purification using the hot acid-phenol chloroform method as follows. 600 µl acid-phenol chloroform (5:1, pH 4.5, Invitrogen AM9720), prewarmed to 65˚C, was added and mixed, incubated at 65˚C for 5 min, mixed intermittently, incubated in ice for 5 min, and centrifuged (21,100 x g, 2 min). The aqueous phase was transferred to new tubes, 600 µl acid-phenol chloroform, at room temperature, was added, mixed, incubated at room temperature for 5 min, centrifuged, from which ~500 µl aqueous phase was transferred to new tubes. Subsequently, 500 µl chloroform-isoamyl alcohol (24:1, Sigma-Aldrich 25666) was added and mixed, incubated at room temperature for 1 min, centrifuged and ~400 µl aqueous phase was transferred to a 1.5-ml tube containing 2 µl Glyco Blue (Invitrogen AM9516) and 45 µl 3M sodium acetate pH 5.5 (Invitrogen AM9740). RNA was precipitated by the addition of ~450 µl ice-cold 100% isopropanol and overnight incubation at -80˚C. The RNA pellet was collected by centrifugation (21,100 x g, 45 min, 4˚C), washed twice with 1 ml ice-cold 80% ethanol, air-dried, and resuspended in nuclease-free water followed by Nanodrop quantification.

DNase treatment. A 50 µl reaction with 10 µg RNA, 1 µl Turbo DNase (Invitrogen AM2238), and 5 µl 10x Turbo DNase buffer was incubated at 37˚C for 30 min, followed by addition of 1 µl more Turbo DNase and incubation at 37˚C for another 30 min. DNase-treated RNA was purified using Zymo RNA clean & concentrator -5 kit (Zymo Res. R1015) according to the manufacturer's protocol, except with one modification (1.5 volume of ethanol was used instead of 1 volume). Clean DNase-treated RNA was eluted in nuclease-free water and quantified using Nanodrop. Quality of RPFs was assessed by electrophoresis of denatured RNA

in a 15% TBE-Urea gel (Invitrogen EC6885BOX) at 120 V for 5 min and 200 V for 75 min. The gel was stained with SYBR gold (Invitrogen S11494) and the sharpness of the RPF band between the 28 nt *(5'-AUGUACACGGAGUCGACCCGCAACGCGA-3', Sigma, HPLC purified)* and the 34 nt *(5'-AUGUACACGGAGUCGAGCUCAACCCGCAACGCGA-3', Sigma, HPLC purified)* RNA oligos was determined

rRNA-depletion. One half-reaction of Ribo-Zero for plant seed/root kit (Illumina MRZSR116) was used per ~5 µg of DNAse-treated RNA according to the manufacturer's protocol, except with one modification (the 50˚C incubation step was not performed for Ribo-seq samples). Subsequently, rRNA-depleted RNA was purified using Zymo RNA clean & concentrator -5 kit (Zymo Res. R1015) according to modified Zymo protocol described above and eluted in 11 µl nuclease-free water.

Size-selection. Denatured rRNA-depleted RNA was subjected to electrophoresis on a 15% TBE-Urea gel (Invitrogen EC6885BOX) at 120 V for 5 min and 200 V for 75 min, stained with SYBR gold (Invitrogen S11494) for 1 min, and visualized on a blue light transilluminator. A mix of 28 nt and 34 nt RNA oligos was run as size markers. The gel slice corresponding to the region between the bottom of 28 nt and bottom of 34 nt RNA size markers was excised and transferred to a 0.5 ml tube with a hole at the bottom made by an 18 G syringe needle, and the tube was placed in a 2 mL microfuge tube. The tube was then centrifuged (21,100 x g, 2 min, 4˚C) to crush the gel slice and transfer its contents to the 2 mL microfuge tube. 500 µL of RNA gel extraction buffer (0.3 M NaOAc pH5.5, 1 mM EDTA pH 8, 10 mM Tris-HCl pH 7.5, 0.25% (w/v) SDS) was added and incubated overnight at 4˚C on a shaker. Eluted RPFs were filtered through 0.22 µ SpinX cellulose acetate filter columns (Sigma-Aldrich CL8161). 2 µL Glyco Blue (Invitrogen AM9516) and an equal volume of ice-cold 100% isopropanol were added to the

supernatant and RPFs were precipitated overnight at -80˚C. The RNA pellet was collected by centrifugation (21,100 x g, 45 min, 4˚C), washed twice with 1 ml ice-cold 80% ethanol, air-dried, and resuspended in 3.25 µl nuclease-free water.

Library preparation. Prior to library preparation, RPF ends were repaired using T4PNK kit (Thermo Scientific EK0031) as follows. 3.25 µl RNA was incubated at 70˚ C for 3 min, transferred to ice, followed by the addition of 0.5 µl 10x T4 PNK buffer A (no ATP), 0.25 µl Superase-IN, 0.5 µl T4PNK enzyme. The reaction was incubated at 37˚C for 30 min, then 0.5 µl 10 mM ATP was added, and incubated at 37˚C for 1 h. The reaction was stopped by adding 5.5 µl nuclease-free water, then incubation at 75˚C for 10 min, after which it was transferred to ice.

Subsequently, cDNA libraries were prepared using NEXTflex Small RNA-Seq kit v3 (Perkin Elmer NOVA-5132-05) according to manufacturer's protocol with the following specifications: The 3' and 5' 4N adapters were diluted 1/3-fold for step A and step D, incubation in step A was carried out overnight, bead clean-up for step F was conducted according to the "No size-selection" protocol (https://perkinelmer-appliedgenomics.com/nextflex_small_rna_v3_no_size_selection_supplement-2/). 11 cycles of PCR were performed with barcoded primers and the final libraries were cleaned using the PAGE size selection and clean-up (Step H2) according to the manufacturer's protocol. The quality of the libraries was assessed using an Agilent bioanalyzer high sensitivity DNA Assay kit. Libraries were quantified using Qubit dsDNA HS Assay kit (Invitrogen Q32854), diluted, pooled together, and sequenced at the Iowa State University DNA Sequencing Facility using the Illumina NovaSeq 6000 on the two lanes of S1 flow cell to yield 100-bp single-end reads.

RNA Sequencing

200 µl lysate prepared (see lysate preparation) above was used for total RNA extraction. Most of the steps are same as that for Ribo-seq with a few modifications listed below.

Total RNA purification. Prewarmed 400 µl proteinase-K buffer was added to 200 µl lysate and incubated at 42˚C for 30 min. Subsequently, it was heated to 65˚C for 5 min and immediately subjected to RNA purification using hot acid-phenol chloroform method as described for Ribo-seq, except three rounds of extraction was done using the acid-phenol chloroform, instead of two (two rounds with 65˚C incubation and one round with room temperature incubation).

DNase treatment. This was the same as for Ribo-seq samples. DNase-treated RNA was purified using Zymo RNA clean & concentrator -5 kit (Zymo Res. R1015) according to the manufacturer's protocol without any modifications. Total RNA integrity was verified by electrophoresis of denatured RNA in a 15% TBE-Urea gel at 120 V for 5 min and 200 V for 50 min.

rRNA-depletion. One half-reaction of Ribo-Zero for plant seed/root kit (Illumina MRZSR116) was used per ~5 µg of DNAse-treated RNA according to the manufacturer's protocol without any modifications. Subsequently, rRNA-depleted RNA was purified using Zymo RNA clean & concentrator -5 kit (Zymo Res. R1015) according to manufacturer's protocol and eluted in 11 µl nuclease-free water.

Alkaline fragmentation. 10 µl 2x fragmentation buffer (2 mM EDTA pH 8, 12 mM Na2CO3, 88 mM NaHCO3) was added to 10 µl rRNA-depleted RNA and incubated at 95˚C for 20 min followed by immediate addition of 280 µl stop solution (0.3 M NaOAc pH5.5, 53.6 µg/mL Glyco Blue (Invitrogen AM9516)) and 750 µl ice-cold 100 % ethanol. After overnight precipitation at -80˚C, the pellet was collected and washed as described above.

Size-selection. Denatured rRNA-depleted RNA was subjected to electrophoresis on a 15% TBE-Urea gel at 120 V for 5 min and 200 V for 50 min, stained with SYBR gold for 1 min, and visualized on a blue light transilluminator. 50 ng of single-stranded DNA ladder (IDT 51-05-15-01) was run as size markers. The gel slice corresponding to the region between the top of the 30 nt band and top of the 40 nt band of the IDT ladder was excised and transferred to a 0.5 ml tube with a hole at the bottom made by an 18 G syringe needle, and the tube was placed in a 2 ml microfuge tube. RNA was eluted from the gel slice using the same protocol as described for Ribo-seq samples.

Library preparation. This was the same as for Ribo-seq samples. RNA-seq libraries were pooled and sequenced using the Illumina NovaSeq 6000 on the two lanes of SP flow cell to yield 100 bp single-end reads.

Ribo-seq and RNA-seq data analysis

Data preprocessing. The sequencing data from both lanes were concatenated for each sample. The quality of raw sequencing reads was assessed using FastQC v.0.11.7 (Andrews 2010). The adapters were removed from raw sequencing reads (parameters: "-a TGGAATTCTCGGGTGCCAAGG --discard-untrimmed --minimum-length 23"), further processed to trim the four random bases (parameters: "-u 4 -u -4"), that were added to both ends of Ribo-seq and RNA-seq reads during library preparation, using Cutadapt v.2.5 (Martin 2011).

Quality control plots. RiboToolkit (Liu et al. 2020) was used (parameters: RPF length 26-29 nt, Mismatch allowed 2, Max multi-map 1) to determine the RPF-lengths with good triplet periodicity *(Fig. 4.3-B; Mock rep #1 sample as a representative result),* assess the frame-enrichment *(Fig. 4.4-A, B; all the samples),* and the distribution of reads *(Fig.4.4-C, D; all the*

samples) over different mRNA features. The data was obtained via RiboToolkit but was plotted using GraphPad Prism (GraphPad Software, Inc.).

Read mapping. Firstly, the processed data was mapped to Arabidopsis ncRNA (rRNA, snoRNA, tRNA) sequences (TAIR10) using Bowtie v.1.2 (parameters: "-v 2") (Langmead et al. 2009). The ncRNA-unaligned reads were then mapped to Arabidopsis reference genome (TAIR10) using STAR v.2.5 (parameters: "--outFilterMismatchNmax 2 --outFilterMultimapNmax 1") (Dobin et al. 2013) to yield uniquely-mapped reads. The ncRNA-unaligned reads were also mapped to RCNMV RNA1 and RNA2 using Bowtie v1.2 (parameters: "-v 2 -m 1") (Langmead et al. 2009) to yield uniquely-mapped reads. The read length distribution *(Fig. 4.3-A; all the samples)* was determined using Samtools (Li et al. 2009; Danecek et al. 2021). Subsequently, size filtering was done to retain only the 26-29-nt reads in the Ribo-seq alignment bam file using the reformat function in the BBMap tool (Bushnell 2014). No size filtering was done for RNA-seq reads. The metagene analysis plots *(Fig. 4.3-C Mock rep #1 sample as a representative result)* were generated using RiboTaper (Calviello et al. 2016). From the STAR-aligned files, all the RNA-seq reads were counted (parameters: "-t exon -s 0 -g gene_id") while for Ribo-seq reads, only those mapping to the CDS were counted (parameters: "-t CDS -s 0 -g gene_id") using the featureCounts (Liao et al. 2014). The read statistics, such as the number and proportion of raw, processed, and aligned reads can be found in *Supplemental file 4.1*.

Statistical analysis. Using the DESeq2 package (Love et al. 2014), the regularized-log-transformed data from the Ribo-seq and RNA-seq counts were used for the principal component analysis (PCA) *(Fig. 4.4-E)*. For making correlation plots *(Fig. 4.4-F, G)*, corrplot package (Wei and Simko 2021) was used only with the genes whose sum of read counts was greater than zero

across all the Ribo-seq or RNA-seq samples. DESeq2 package (Love et al. 2014) was also used to identify the differentially expressed genes (DEGs) from the RNA-seq data and the differentially translated genes (DTGs) from the Ribo-seq data. For each of the Ribo-seq or RNA-seq data, separately, only the genes whose sum of read counts was greater than 100 across all the samples were used for analysis. All the comparisons refer to RCNMV-infected vs mock samples. Genes with absolute $\log_2$-fold change (RNA or RPF abundance) >1 and adjusted p-value < 0.05 were considered DEGs or DTGs. The list of DEGs and DTGs can be found in *Supplemental file 4.2* and the DESeq2-normalized read counts can be found in *Supplemental file 4.3*. For *Fig. 4.5-B*, $\log_2$-fold change (RPF abundance) against $\log_2$-fold change (RNA abundance) was plot using only the genes that had a valid output (Non-NA) from DESeq2. The blue-colored genes (only-identified as DTGs) within the yellow-shaded region were considered translationally-regulated and used for protein-domain enrichment analysis via ThaleMine (Krishnakumar et al. 2017). More information about the genes included in the scatterplot can be found in *Supplemental file 4.4*.

KEGG pathway enrichment analysis. For each of the Ribo-seq and RNA-seq datasets, the upregulated and downregulated genes were used together for the enrichment analysis. Firstly, the amino acid sequence for the DEGs/DTGs were downloaded from (Arabidopsis.org/tools/bulk/sequence) with the following parameters: dataset “Araport 11 protein sequences”, search against “get one sequence per locus (representative gene model/splice form only)". Subsequently, KOBAS (kobas.cbi.pku.edu.cn/kobas3/genelist/) (Bu et al. 2021) was used with the following parameters: species “*Arabidopsis thaliana*”, input type “fasta protein sequence”, pathway “KEGG”, statistical method “hypergeometric/Fisher's exact test”, FDR correction method “Benjamin and Hochberg (1995)”, background database “default”.

Pathways with FDR < 0.05 were considered as enriched. More information for the enriched pathways can be found in *Supplemental file 4.5*. For *Fig. 4.6-B*, $\log_2$-fold change (RPF abundance) against $\log_2$-fold change (RNA abundance) was plot using the DEGs or DTGs that were present in the enriched KEGG pathways. There were a few DEGs that did not have a valid output (non-NA) from DESeq2 analysis of Ribo-seq data and hence, were assigned $\log_2$-fold change (RPF abundance) = 0 (green triangles). There were a few DTGs that did not have a valid output (non-NA) from DESeq2 analysis of RNA-seq data and hence, were assigned $\log_2$-fold change (RNA abundance) = 0 (blue triangles). More information about the genes included in the scatterplot and the list of DEGs or DTGs involved in the enriched pathways can be found in *Supplemental file 4.6*.

RCNMV analysis. For *Fig. 4.7-A*, proportion of reads that mapped to RCNMV genome with respect to total number of Arabidopsis- and RCNMV-mapped reads was calculated. See *Supplemental file 4.1* for more details. For *Fig. 4.7-B*, RCNMV read counts were included in the count table from Arabidopsis-mapped reads and input into DESeq2 for normalization. The normalized abundance was transformed via $\log_{10}(x+1)$ transformation. Subsequently, arithmetic mean of $\log_{10}$ values were calculated (equivalent to geometric mean of read counts) and plotted as a scatterplot. See *Supplemental file 4.7* for more details. For *Fig. 4.8*, whole length of the RCNMV positive- and negative-strand-mapped RNA-seq reads (combined across all RCNMV-infected samples) were plotted across RCNMV RNA1 and RNA2 sequences. For *Fig. 4.9* and *Fig. 4.10*, riboSeqR tool was used to visualize the coverage of RNA-seq reads (gray bars) and the Ribo-seq reads (colored bars). Here, only the first nucleotide of the reads were plotted over RCNMV RNA1 and RNA2 sequences. For *Fig. 4.11*, frameshift efficiency was calculated as the ratio of the length-normalized number of RPFs that map to the frameshifted

ORF (100 bp downstream of p27 stop codon to 100 bp upstream of p88 stop codon) to the length-normalized number of RPFs that map to the p27 and p88-overlapping ORF (100 bp downstream of p27 start codon to 100 upstream of the frameshift site). Length-normalized means that the number of RPFs, which map to the ORF region, was divided by the length (nt) of that ORF region. Only 26-29 nt size RPFs were used for calculating the frameshift efficiency.

Data availability

The raw sequencing fastq files will be deposited in the NCBI Gene Expression Omnibus database prior to the submission of the manuscript.

Supplemental Material

Supplemental File 4.1. Read statistics for the raw and processed Ribo-seq and RNA-seq data, xlsx file.

Supplemental File 4.2. DESeq2 output, xlsx file.

Supplemental File 4.3. DESeq2-normalized count data, xlsx file.

Supplemental File 4.4. List of genes in the scatterplot for *Fig. 4.5-B* with annotations, xlsx file.

Supplemental File 4.5. KEGG pathway enrichment output, xlsx file.

Supplemental File 4.6. List of DEGs/DTGs in the enriched KEGG pathways with annotations, xlsx file.

Supplemental File 4.7. List of genes in the scatterplot for *Fig.4.7-B* with annotations, xlsx file.

Acknowledgments

The authors thank Dr. Akshay Yadav and Dr. Gaurav Kandoi for their frequent help with bioinformatics, and Dr. Viraj Muthye for assistance with plant cultivation. The authors would also like to thank Dr. Prakrit Chotewutmontri and Dr. Polly Hsu for their advice on optimizing the Ribo-seq protocol. This project was funded by Iowa State University Plant Sciences Institute Faculty Scholar award to WAM. This paper of the Iowa Agriculture and Home Economics Experiment Station, Ames, IA, Project No. 3808 was supported in part by Hatch Act and State of Iowa funds. The authors thank the DNA facility at Iowa State University for sequencing the services.

Conflict of Interest

The authors declare no conflict of interest associated with the work described in this manuscript.

References

Ahmed MMS, Ji W, Wang M, Bian S, Xu M, Wang W, Zhang J, Xu Z, Yu M, Liu Q, Zhang C, Zhang H, Tang S, Gu M, Yu H. 2017. Transcriptional changes of rice in response to rice black-streaked dwarf virus. Gene 628: 38–47.

Alexander MM, Cilia M. 2016. A molecular tug-of-war: Global plant proteome changes during viral infection. Curr Plant Biol 5: 13–24.

Alexander MR, Brice AM, Jansen van Vuren P, Rootes CL, Tribolet L, Cowled C, Bean AGD, Stewart CR. 2021. Ribosome-Profiling Reveals Restricted Post Transcriptional Expression of Antiviral Cytokines and Transcription Factors during SARS-CoV-2 Infection. Int J Mol Sci 22: 3392.

Allie F, Rey MEC. 2013. Transcriptional alterations in model host, *Nicotiana benthamiana*, in response to infection by South African cassava mosaic virus. Eur J Plant Pathol 137: 765–785.

Andrews S. 2010. FastQC: A Quality Control Tool for High Throughput Sequence Data [Online]. Available online at: http://www.bioinformatics.babraham.ac.uk/projects/fastqc/.

Angelos E, Ruberti C, Kim SJ, Brandizzi F. 2017. Maintaining the factory: the roles of the unfolded protein response in cellular homeostasis in plants. Plant J 90: 671–682.

Barry JK, Miller WA. 2002. A -1 ribosomal frameshift element that requires base pairing across four kilobases suggests a mechanism of regulating ribosome and replicase traffic on a viral RNA. Proc Natl Acad Sci 99: 11133–11138.

Bayless AM, Nishimura MT. 2020. Enzymatic Functions for Toll/Interleukin-1 Receptor Domain Proteins in the Plant Immune System. Front Genet 11: 539.

Bencun M, Klinke O, Hotz-Wagenblatt A, Klaus S, Tsai MH, Poirey R, Delecluse HJ. 2018. Translational profiling of B cells infected with the Epstein-Barr virus reveals 5′ leader ribosome recruitment through upstream open reading frames. Nucleic Acids Res 46: 2802–2819.

Bhatt PR, Scaiola A, Loughran G, Leibundgut M, Kratzel A, Meurs R, Dreos R, O'Connor KM, McMillan A, Bode JW, Thiel V, Gatfield, Atkins JF, Ban N. 2021. Structural basis of ribosomal frameshifting during translation of the SARS-CoV-2 RNA genome. Science 372: 1306–1313.

Bhattacharjee S, Zamora A, Azhar MT, Sacco MA, Lambert LH, Moffett P. 2009. Virus resistance induced by NB-LRR proteins involves Argonaute4-dependent translational control. Plant J 58: 940–951.

Brierley I, Gilbert RJC, Pennell S. 2010. Pseudoknot-Dependent Programmed —1 Ribosomal Frameshifting: Structures, Mechanisms and Models. In Recoding: Expansion of Decoding Rules Enriches Gene Expression (ed. Atkins JF, Gesteland RF), Vol 24, pp. 149–174, Springer, New York, NY.

Bu D, Luo H, Huo P, Wang Z, Zhang S, He Z, Wu Y, Zhao L, Liu J, Guo J, Fang S, Cao W, Yi L, Zhao Y, Kong L. 2021. KOBAS-i: intelligent prioritization and exploratory visualization of biological functions for gene enrichment analysis. Nucleic Acids Res 49: W317–W325.

Bushnell B. 2014. BBMap: A Fast, Accurate, Splice-Aware Aligner. United States.

Calviello L, Mukherjee N, Wyler E, Zauber H, Hirsekorn A, Selbach M, Landthaler M, Obermayer B, Ohler U. 2016. Detecting actively translated open reading frames in ribosome profiling data. Nat Methods 13: 165–170.

Catoni M, Miozzi L, Fiorilli V, Lanfranco L, Accotto GP. 2009. Comparative Analysis of Expression Profiles in Shoots and Roots of Tomato Systemically Infected by Tomato spotted wilt virus Reveals Organ-Specific Transcriptional Responses. Mol Plant-Microbe Interact 22: 1504–1513.

Cheng X, Wang A. 2017. Multifaceted defense and counter-defense in co-evolutionary arms race between plants and viruses. Commun Integr Biol 10: e1341025.

Choi H, Jo Y, Lian S, Jo KM, Chu H, Yoon JY, Choi SK, Kim KH, Cho WK. 2015. Comparative analysis of chrysanthemum transcriptome in response to three RNA viruses: Cucumber mosaic virus, Tomato spotted wilt virus and Potato virus X. Plant Mol Biol 88: 233–248.

Chotewutmontri P, Barkan A. 2016. Dynamics of Chloroplast Translation during Chloroplast Differentiation in Maize. PLoS Genet 12: e1006106.

Chotewutmontri P, Stiffler N, Watkins KP, Barkan A. 2018. Ribosome Profiling in Maize. Methods Mol Biol 1676: 165–183.

Chung BY, Hardcastle TJ, Jones JD, Irigoyen N, Firth AE, Baulcombe DC, Brierley I. 2015. The use of duplex-specific nuclease in ribosome profiling and a user-friendly software package for Ribo-seq data analysis. RNA 21: 1731–45.

Chung BYW, Balcerowicz M, Di Antonio M, Jaeger KE, Geng F, Franaszek K, Marriott P, Brierley I, Firth AE, Wigge PA. 2020. An RNA thermoswitch regulates daytime growth in Arabidopsis. Nat Plants 6: 522–532.

Collum TD, Padmanabhan MS, Hsieh YC, Culver JN. 2016. Tobacco mosaic virus-directed reprogramming of auxin/indole acetic acid protein transcriptional responses enhances virus phloem loading. Proc Natl Acad Sci 113: E2740–E2749.

Collum TD, Stone AL, Sherman DJ, Rogers EE, Dardick C, Culver JN. 2020. Translatome Profiling of Plum Pox Virus–Infected Leaves in European Plum Reveals Temporal and Spatial Coordination of Defense Responses in Phloem Tissues. Mol Plant-Microbe Interact 33: 66–77.

Cook GM, Shang P, Li Y, Brown KA, Dinan A, Fang Y, Firth A, Brierley I. 2019. Ribosome profiling of porcine reproductive and respiratory syndrome virus. Access Microbiol 1: 313.

Dai A, Cao S, Dhungel P, Luan Y, Liu Y, Xie Z, Yang Z. 2017. Ribosome Profiling Reveals Translational Upregulation of Cellular Oxidative Phosphorylation mRNAs during Vaccinia Virus-Induced Host Shutoff. J Virol 91: e01858-16.

Danecek P, Bonfield JK, Liddle J, Marshall J, Ohan V, Pollard MO, Whitwham A, Keane T, McCarthy SA, Davies RM, Li H. 2021. Twelve years of SAMtools and BCFtools. Gigascience 10: 1–4.

Dardick C. 2007. Comparative Expression Profiling of *Nicotiana benthamiana* Leaves Systemically Infected with Three Fruit Tree Viruses. Mol Plant-Microbe Interact 20: 1004–1017.

Deleris A, Gallego-Bartolome J, Bao J, Kasschau KD, Carrington JC, Voinnet O. 2006. Hierarchical Action and Inhibition of Plant Dicer-Like Proteins in Antiviral Defense. Science 313: 68–71.

Deng Y, Humbert S, Liu JX, Srivastava R, Rothstein SJ, Howell SH. 2011. Heat induces the splicing by IRE1 of a mRNA encoding a transcription factor involved in the unfolded protein response in Arabidopsis. Proc Natl Acad Sci 108: 7247–7252.

Deng Y, Srivastava R, Howell S. 2013. Endoplasmic Reticulum (ER) Stress Response and Its Physiological Roles in Plants. Int J Mol Sci 14: 8188–8212.

Dinan AM, Keep S, Bickerton E, Britton P, Firth AE, Brierley I. 2019. Comparative Analysis of Gene Expression in Virulent and Attenuated Strains of Infectious Bronchitis Virus at Subcodon Resolution. J Virol 93: 714–733.

Dinman JD. 2012. Mechanisms and implications of programmed translational frameshifting. WIREs RNA 3: 661–673.

Dobin A, Davis CA, Schlesinger F, Drenkow J, Zaleski C, Jha S, Batut P, Chaisson M, Gingeras TR. 2013. STAR: ultrafast universal RNA-seq aligner. Bioinformatics 29: 15–21.

Dubey N, Singh K. 2018. Role of NBS-LRR Proteins in Plant Defense. In Molecular Aspects of Plant-Pathogen Interaction (ed. Singh A, Singh I), pp. 115–138, Springer Singapore, Singapore.

Echavarría-Consuegra L, Cook GM, Busnadiego I, Lefèvre C, Keep S, Brown K, Doyle N, Dowgier G, Franaszek K, Moore NA, Sidell SG, Bickerton E, Hale BG, Firth AE, Brierley I, Irigoyen N. 2021. Manipulation of the unfolded protein response: A pharmacological strategy against coronavirus infection. PLoS Pathog 17: e1009644.

Eskelin K, Hafren A, Rantalainen KI, Makinen K. 2011. Potyviral VPg Enhances Viral RNA Translation and Inhibits Reporter mRNA Translation In Planta. J Virol 85: 9210–9221.

Eskelin K, Varjosalo M, Ravantti J, Mäkinen K. 2019. Ribosome profiles and riboproteomes of healthy and Potato virus A- and Agrobacterium -infected *Nicotiana benthamiana* plants. Mol Plant Pathol 20: 392–409.

Esse HP, Reuber TL, Does D. 2020. Genetic modification to improve disease resistance in crops. New Phytol 225: 70–86.

Fan H, Zhang Y, Sun H, Liu J, Wang Y, Wang X, Li D, Yu J, Han C. 2015. Transcriptome Analysis of Beta macrocarpa and Identification of Differentially Expressed Transcripts in Response to Beet Necrotic Yellow Vein Virus Infection. PLoS One 10: e0132277.

Fernández-Miragall O, Hernández C. 2011. An Internal Ribosome Entry Site Directs Translation of the 3′-Gene from Pelargonium Flower Break Virus Genomic RNA: Implications for Infectivity. PLoS One 6: e22617.

Finkel Y, Mizrahi O, Nachshon A, Weingarten-Gabbay S, Morgenstern D, Yahalom-Ronen Y, Tamir H, Achdout H, Stein D, Israeli O, Beth-Din A, Melamed S, Weiss S, Israely T, Paran N, Schwartz M, Stern-Ginossar N. 2021. The coding capacity of SARS-CoV-2. Nature 589: 125–130.

Gaffar FY, Koch A. 2019. Catch Me If You Can! RNA Silencing-Based Improvement of Antiviral Plant Immunity. Viruses 11: 673.

Gal-On A, Fuchs M, Gray S. 2017. Generation of novel resistance genes using mutation and targeted gene editing. Curr Opin Virol 26: 98–103.

Garcia-Moreno M, Järvelin AI, Castello A. 2018. Unconventional RNA-binding proteins step into the virus-host battlefront. WIREs RNA 9: e1498.

Garcia-Ruiz H. 2018. Susceptibility Genes to Plant Viruses. Viruses 10: 484.

Garcia-Ruiz H. 2019. Host factors against plant viruses. Mol Plant Pathol 20: 1588–1601.

Garcia-Ruiz H, Szurek B, Van den Ackerveken G. 2021. Stop helping pathogens: engineering plant susceptibility genes for durable resistance. Curr Opin Biotechnol 70: 187–195.

Gerresheim G, Bathke J, Michel A, Andreev D, Shalamova L, Rossbach O, Hu P, Glebe D, Fricke M, Marz M, Goesmann A, Kiniry SJ, Baranov PV, Shatsky IN, Niepmann M. 2019. Cellular Gene Expression during Hepatitis C Virus Replication as Revealed by Ribosome Profiling. Int J Mol Sci 20: 1321.

Ghoshal B, Sanfaçon H. 2014. Temperature-dependent symptom recovery in *Nicotiana benthamiana* plants infected with tomato ringspot virus is associated with reduced translation of viral RNA2 and requires ARGONAUTE 1. Virology 456–457: 188–197.

Girardi E, Pfeffer S, Baumert TF, Majzoub K. 2021. Roadblocks and fast tracks: How RNA binding proteins affect the viral RNA journey in the cell. Semin Cell Dev Biol 111: 86–100.

Gómez-Aix C, Pascual L, Cañizares J, Sánchez-Pina MA, Aranda MA. 2016. Transcriptomic profiling of Melon necrotic spot virus-infected melon plants revealed virus strain and plant cultivar-specific alterations. BMC Genomics 17: 429.

Gould AR, Francki RIB, Hatta T, Hollings M. 1981. The bipartite genome of red clover necrotic mosaic virus. Virology 108: 499–506.

Guenther RH, Sit TL, Gracz HS, Dolan MA, Townsend HL, Liu G, Newman WH, Agris PF, Lommel SA. 2004. Structural characterization of an intermolecular RNA-RNA interaction involved in the transcription regulation element of a bipartite plant virus. Nucleic Acids Res 32: 2819–2828.

Hake K, Romeis T. 2019. Protein kinase-mediated signalling in priming: Immune signal initiation, propagation, and establishment of long-term pathogen resistance in plants. Plant Cell Environ 42: 904–917.

Hanley-Bowdoin L, Bejarano ER, Robertson D, Mansoor S. 2013. Geminiviruses: masters at redirecting and reprogramming plant processes. Nat Rev Microbiol 11: 777–788.

Harwig A, Landick R, Berkhout B. 2017. The Battle of RNA Synthesis: Virus versus Host. Viruses 9: 309.

Hashimoto M, Neriya Y, Yamaji Y, Namba S. 2016. Recessive Resistance to Plant Viruses: Potential Resistance Genes Beyond Translation Initiation Factors. Front Microbiol 7: 1695.

Havelda Z, Vrallyay V, Vlczi A, Burgyn J. 2008. Plant virus infection-induced persistent host gene downregulation in systemically infected leaves. Plant J 55: 278–288.

Herath V, Gayral M, Miller RK, Verchot J. 2020. BIP and the unfolded protein response are important for potyvirus and potexvirus infection. Plant Signal Behav 15: 1807723.

Hetz C. 2012. The unfolded protein response: controlling cell fate decisions under ER stress and beyond. Nat Rev Mol Cell Biol 13: 89–102.

Hetz C, Zhang K, Kaufman RJ. 2020. Mechanisms, regulation and functions of the unfolded protein response. Nat Rev Mol Cell Biol 21: 421–438.

Hiruki C. 1987. The Dianthoviruses: A Distinct Group of Isometric Plant Viruses with Bipartite Genome. Adv Virus Res 33: 257-300.

Howell SH. 2013. Endoplasmic Reticulum Stress Responses in Plants. Annu Rev Plant Biol 64: 477–499.

Hsu PY, Calviello L, Wu HYL, Li FW, Rothfels CJ, Ohler U, Benfey PN. 2016. Super-resolution ribosome profiling reveals unannotated translation events in Arabidopsis. Proc Natl Acad Sci 113: E7126–E7135.

Huang C, Cun Y, Yu H, Tong Z, Xiao B, Song Z, Wang B, Li Y, Liu Y. 2017. Transcriptomic profile of tobacco in response to Tomato zonate spot orthotospovirus infection. Virol J 14: 153.

Huang S, Chen X, Zhong X, Li M, Ao K, Huang J, Li X. 2016. Plant TRAF Proteins Regulate NLR Immune Receptor Turnover. Cell Host Microbe 19: 204–215.

Hyodo K, Okuno T. 2014. Host factors used by positive-strand RNA plant viruses for genome replication. J Gen Plant Pathol 80: 123–135.

Hyodo K, Okuno T. 2016. Pathogenesis mediated by proviral host factors involved in translation and replication of plant positive-strand RNA viruses. Curr Opin Virol 17: 11–18.

Hyodo K, Okuno T. 2020. Hijacking of host cellular components as proviral factors by plant-infecting viruses. Adv Virus Res 107: 37–86.

Hyodo K. 2021. Identification and characterization of host factors involved in plant RNA virus replication. J Gen Plant Pathol 1–3.

Ingolia NT, Ghaemmaghami S, Newman JRS, Weissman JS. 2009. Genome-wide analysis *in vivo* of translation with nucleotide resolution using ribosome profiling. Science 324: 218–23.

Irigoyen N, Firth AE, Jones JD, Chung BYW, Siddell SG, Brierley I. 2016. High-Resolution Analysis of Coronavirus Gene Expression by RNA Sequencing and Ribosome Profiling. PLoS Pathog 12: e1005473.

Irigoyen N, Dinan AM, Brierley I, Firth AE. 2018. Ribosome profiling of the retrovirus murine leukemia virus. Retrovirology 15: 10.

Iwakawa H, Mizumoto H, Nagano H, Imoto Y, Takigawa K, Sarawaneeyaruk S, Kaido M, Mise K, Okuno T. 2008. A Viral Noncoding RNA Generated by cis -Element-Mediated Protection against 5′→3′ RNA Decay Represses both Cap-Independent and Cap-Dependent Translation. J Virol 82: 10162–10174.

Iwakawa H, Mine A, Hyodo K, An M, Kaido M, Mise K, Okuno T. 2011. Template recognition mechanisms by replicase proteins differ between bipartite positive-strand genomic RNAs of a plant virus. J Virol 85: 497–509.

Kanodia P, Prasanth KR, Roa-Linares VC, Bradrick SS, Garcia-Blanco MA, Miller WA. 2020a. A rapid and simple quantitative method for specific detection of smaller coterminal RNA by PCR (DeSCo-PCR): application to the detection of viral subgenomic RNAs. RNA 26: 888–901.

Kanodia P, Vijayapalani P, Srivastava R, Bi R, Liu P, Miller WA, Howell SH. 2020b. Control of translation during the unfolded protein response in maize seedlings: Life without PERKs. Plant Direct 4: e00241.

Kapos P, Devendrakumar KT, Li X. 2019. Plant NLRs: From discovery to application. Plant Sci 279: 3–18.

Karran RA, Sanfaçon H. 2014. Tomato ringspot virus Coat Protein Binds to ARGONAUTE 1 and Suppresses the Translation Repression of a Reporter Gene. Mol Plant-Microbe Interact 27: 933–943.

Kaur H, Yadav CB, Alatar AA, Faisal M, Jyothsna P, Malathi VG, Praveen S. 2015. Gene expression changes in tomato during symptom development in response to leaf curl virus infection. J Plant Biochem Biotechnol 24: 347–354.

Khong A, Bonderoff J, Spriggs R, Tammpere E, Kerr C, Jackson T, Willis A, Jan E. 2016. Temporal Regulation of Distinct Internal Ribosome Entry Sites of the Dicistroviridae Cricket Paralysis Virus. Viruses 8: 25.

Kim KH, Lommel SA. 1994. Identification and Analysis of the Site of -1 Ribosomal Frameshifting in Red Clover Necrotic Mosaic Virus. Virology 200: 574–582.

Kim KH, Lommel SA. 1998. Sequence Element Required for Efficient −1 Ribosomal Frameshifting in Red Clover Necrotic Mosaic Dianthovirus. Virology 250: 50–59.

Koh DCY, Wong SM, Liu DX. 2003. Synergism of the 3′-Untranslated Region and an Internal Ribosome Entry Site Differentially Enhances the Translation of a Plant Virus Coat Protein. J Biol Chem 278: 20565–20573.

Kontos H, Napthine S, Brierley I. 2001. Ribosomal Pausing at a Frameshifter RNA Pseudoknot Is Sensitive to Reading Phase but Shows Little Correlation with Frameshift Efficiency. Mol Cell Biol 21: 8657–8670.

Koonin EV. 1991. The phylogeny of RNA-dependent RNA polymerases of positive-strand RNA viruses. J Gen Virol 72: 2197–2206.

Kraft JJ, Treder K, Peterson MS, Miller WA. 2013. Cation-dependent folding of 3′ cap-independent translation elements facilitates interaction of a 17-nucleotide conserved sequence with eIF4G. Nucleic Acids Res 41: 3398–3413.

Krishnakumar V, Contrino S, Cheng CY, Belyaeva I, Ferlanti ES, Miller JR, Vaughn MW, Micklem G, Town CD, Chan AP. 2017. ThaleMine: A Warehouse for Arabidopsis Data Integration and Discovery. Plant Cell Physiol 58: e4.

Kushwaha NK, Hafrén A, Hofius D. 2019. Autophagy-virus interplay in plants: from antiviral recognition to proviral manipulation. Mol Plant Pathol 20: 1211–1216.

Kusumanegara K, Mine A, Hyodo K, Kaido M, Mise K, Okuno T. 2012. Identification of domains in p27 auxiliary replicase protein essential for its association with the endoplasmic reticulum membranes in Red clover necrotic mosaic virus. Virology 433: 131–141.

Langmead B, Trapnell C, Pop M, Salzberg SL. 2009. Ultrafast and memory-efficient alignment of short DNA sequences to the human genome. Genome Biol 10: 1-10.

Li F, Wang A. 2019. RNA-Targeted Antiviral Immunity: More Than Just RNA Silencing. Trends Microbiol 27: 792–805.

Li F, Zhang C, Tang Z, Zhang L, Dai Z, Lyu S, Li Y, Hou X, Bernards M, Wang A. 2020. A plant RNA virus activates selective autophagy in a UPR-dependent manner to promote virus infection. New Phytol 228: 622–639.

Li FF, Sun HJ, Jiao YB, Wang FL, Yang JG, Shen LL. 2018. Viral infection-induced endoplasmic reticulum stress and a membrane-associated transcription factor NbNAC089 are involved in resistance to virus in *Nicotiana benthamiana*. Plant Pathol 67: 233–243.

Li H, Handsaker B, Wysoker A, Fennell T, Ruan J, Homer N, Marth G, Abecasis G, Durbin R. 2009. The Sequence Alignment/Map format and SAMtools. Bioinformatics 25: 2078–2079.

Liao Y, Smyth GK, Shi W. 2014. featureCounts: an efficient general purpose program for assigning sequence reads to genomic features. Bioinformatics 30: 923–930.

Lilly ST, Drummond RSM, Pearson MN, MacDiarmid RM. 2011. Identification and Validation of Reference Genes for Normalization of Transcripts from Virus-Infected *Arabidopsis thaliana*. Mol Plant-Microbe Interact 24: 294–304.

Lindbo JA, Fitzmaurice WP, Della-Cioppa G. 2001. Virus-mediated reprogramming of gene expression in plants. Curr Opin Plant Biol 4: 181–185.

Liu Q, Shvarts T, Sliz P, Gregory RI. 2020. RiboToolkit: an integrated platform for analysis and annotation of ribosome profiling data to decode mRNA translation at codon resolution. Nucleic Acids Res 48: W218–W229.

Lommel SA, Weston-Fina M, Xiong Z, Lomonossoff GP. 1988. The nucleotide sequence and gene organization of red clover necrotic mosaic virus RNA-2. Nucleic Acids Res 16: 8587–8602.

Lopinski JD, Dinman JD, Bruenn JA. 2000. Kinetics of Ribosomal Pausing during Programmed −1 Translational Frameshifting. Mol Cell Biol 20: 1095–1103.

Love MI, Huber W, Anders S. 2014. Moderated estimation of fold change and dispersion for RNA-seq data with DESeq2. Genome Biol 15: 550.

Lv H, Fang Z, Yang L, Zhang Y, Wang Y. 2020. An update on the arsenal: mining resistance genes for disease management of Brassica crops in the genomic era. Hortic Res 7: 34.

Ma X, Nicole MC, Meteignier LV, Hong N, Wang G, Moffett P. 2015. Different roles for RNA silencing and RNA processing components in virus recovery and virus-induced gene silencing in plants. J Exp Bot 66: 919–932.

Machado JPB, Brustolini OJB, Mendes GC, Santos AA, Fontes EPB. 2015. NIK1, a host factor specialized in antiviral defense or a novel general regulator of plant immunity? BioEssays 37: 1236–1242.

Machado JPB, Calil IP, Santos AA, Fontes EPB. 2017. Translational control in plant antiviral immunity. Genet Mol Biol 40: 292-304.

Machkovech HM, Bloom JD, Subramaniam AR. 2019. Comprehensive profiling of translation initiation in influenza virus infected cells. PLoS Pathog 15: e1007518.

Macho AP, Lozano-Duran R. 2019. Molecular dialogues between viruses and receptor-like kinases in plants. Mol Plant Pathol 20: 1191–1195.

Martin M. 2011. Cutadapt removes adapter sequences from high-throughput sequencing reads. EMBnet.journal 17: 10–12.

Mauck KE, Kenney J, Chesnais Q. 2019. Progress and challenges in identifying molecular mechanisms underlying host and vector manipulation by plant viruses. Curr Opin Insect Sci 33: 7–18.

May J, Johnson P, Saleem H, Simon AE. 2017. A Sequence-Independent, Unstructured Internal Ribosome Entry Site Is Responsible for Internal Expression of the Coat Protein of Turnip Crinkle Virus. J Virol 91: e02421-16.

Medzihradszky A, Gyula P, Sós-Hegedűs A, Szittya G, Burgyán J. 2019. Transcriptome reprogramming in the shoot apical meristem of CymRSV-infected *Nicotiana benthamiana* plants associates with viral exclusion and the lack of recovery. Mol Plant Pathol 20: 1748–1758.

Meteignier LV, Zhou J, Cohen M, Bhattacharjee S, Brosseau C, Caamal Chan MG, Robatzek S, Moffett P. 2016. NB-LRR signaling induces translational repression of viral transcripts and the formation of RNA processing bodies through mechanisms differing from those activated by UV stress and RNAi. J Exp Bot 67: 2353–2366.

Meteignier LV, El Oirdi M, Cohen M, Barff T, Matteau D, Lucier JF, Rodrigue S, Jacques PE, Yoshioka K, Moffett P. 2017. Translatome analysis of an NB-LRR immune response identifies important contributors to plant immunity in Arabidopsis. J Exp Bot 68: 2333–2344.

Miller WA, Shen R, Staplin W, Kanodia P. 2016. Noncoding RNAs of Plant Viruses and Viroids: Sponges of Host Translation and RNA Interference Machinery. Mol Plant-Microbe Interact 29: 156–164.

Mine A, Hyodo K, Takeda A, Kaido M, Mise K, Okuno T. 2010a. Interactions between p27 and p88 replicase proteins of Red clover necrotic mosaic virus play an essential role in viral RNA replication and suppression of RNA silencing via the 480-kDa viral replicase complex assembly. Virology 407: 213–224.

Mine A, Takeda A, Taniguchi T, Taniguchi H, Kaido M, Mise K, Okuno T. 2010b. Identification and Characterization of the 480-Kilodalton Template-Specific RNA-Dependent RNA Polymerase Complex of Red Clover Necrotic Mosaic Virus. J Virol 84: 6070–6081.

Miyakawa T, Hatano K, Miyauchi Y, Suwa Y, Sawano Y, Tanokura M. 2014. A Secreted Protein with Plant-Specific Cysteine-Rich Motif Functions as a Mannose-Binding Lectin That Exhibits Antifungal Activity. Plant Physiol 166: 766–778.

Mizumoto H, Tatsuta M, Kaido M, Mise K, Okuno T. 2003. Cap-Independent Translational Enhancement by the 3′ Untranslated Region of Red Clover Necrotic Mosaic Virus RNA1. J Virol 77: 12113–12121.

Moeller JR, Moscou MJ, Bancroft T, Skadsen RW, Wise RP, Whitham SA. 2012. Differential accumulation of host mRNAs on polyribosomes during obligate pathogen-plant interactions. Mol Biosyst 8: 2153.

Musidlak O, Nawrot R, Goździcka-Józefiak A. 2017. Which Plant Proteins Are Involved in Antiviral Defense? Review on *In Vivo* and *In Vitro* Activities of Selected Plant Proteins against Viruses. Int J Mol Sci 18: 2300.

Nagy PD, Pogany J. 2012. The dependence of viral RNA replication on co-opted host factors. Nat Rev Microbiol 10: 137–149.

Napthine S, Ling R, Finch LK, Jones JD, Bell S, Brierley I, Firth AE. 2017. Protein-directed ribosomal frameshifting temporally regulates gene expression. Nat Commun 8: 15582.

Napthine S, Bell S, Hill CH, Brierley I, Firth AE. 2019. Characterization of the stimulators of protein-directed ribosomal frameshifting in Theiler's murine encephalomyelitis virus. Nucleic Acids Res 47: 8207–8223.

Navickas A, Chamois S, Saint-Fort R, Henri J, Torchet C, Benard L. 2020. No-Go Decay mRNA cleavage in the ribosome exit tunnel produces 5′-OH ends phosphorylated by Trl1. Nat Commun 11: 122.

Nawkar GM, Lee ES, Shelake RM, Park JH, Ryu SW, Kang CH, Lee SY. 2018. Activation of the Transducers of Unfolded Protein Response in Plants. Front Plant Sci 9: 214.

Nicaise V, Candresse T. 2017. Plum pox virus capsid protein suppresses plant pathogen-associated molecular pattern (PAMP)-triggered immunity. Mol Plant Pathol 18: 878–886.

O'Malley RC, Barragan CC, Ecker JR. 2015. A User's Guide to the Arabidopsis T-DNA Insertion Mutant Collections. Methods in Mol Biol 1284: 323–342.

Okamoto K, Nagano H, Iwakawa H, Mizumoto H, Takeda A, Kaido M, Mise K, Okuno T. 2008. cis-Preferential requirement of a −1 frameshift product p88 for the replication of Red clover necrotic mosaic virus RNA1. Virology 375: 205–212.

Okuno T, Hiruki C. 2013. Molecular Biology and Epidemiology of Dianthoviruses. Adv Virus Res 87: 37-74.

Park HH. 2018. Structure of TRAF Family: Current Understanding of Receptor Recognition. Front Immunol 9: 1999.

Pesti R, Kontra L, Paul K, Vass I, Csorba T, Havelda Z, Várallyay É. 2019. Differential gene expression and physiological changes during acute or persistent plant virus interactions may contribute to viral symptom differences. PLoS One 14: e0216618.

Pitzalis N, Heinlein M. 2018. The roles of membranes and associated cytoskeleton in plant virus replication and cell-to-cell movement. J Exp Bot 69: 117–132.

Qi H, Xia FN, Xiao S, Li J. 2021. TRAF proteins as key regulators of plant development and stress responses. J Integr Plant Biol. https://doi.org/10.1111/jipb.13182

Qiao W, Helpio E, Falk B. 2018. Two Crinivirus-Conserved Small Proteins, P5 and P9, Are Indispensable for Efficient Lettuce infectious yellows virus Infectivity in Plants. Viruses 10: 459.

Ramesh SV, Yogindran S, Gnanasekaran P, Chakraborty S, Winter S, Pappu HR. 2021. Virus and Viroid-Derived Small RNAs as Modulators of Host Gene Expression: Molecular Insights Into Pathogenesis. Front Microbiol 11: 614231.

Rodriguez-Hernandez AM, Gosalvez B, Sempere RN, Burgos L, Aranda MA, Truniger V. 2012. Melon RNA interference (RNAi) lines silenced for Cm-eIF4E show broad virus resistance. Mol Plant Pathol 13: 755–763.

Schmitt-Keichinger C. 2019. Manipulating Cellular Factors to Combat Viruses: A Case Study From the Plant Eukaryotic Translation Initiation Factors eIF4. Front Microbiol 10: 17.

Seo JK, Kim MK, Kwak HR, Choi HS, Nam M, Choe J, Choi B, Han SJ, Kang JH, Jung C. 2018. Molecular dissection of distinct symptoms induced by tomato chlorosis virus and tomato yellow leaf curl virus based on comparative transcriptome analysis. Virology 516: 1–20.

Sharma S Das, Kraft JJ, Miller WA, Goss DJ. 2015. Recruitment of the 40S Ribosome Subunit to the 3′-Untranslated Region (UTR) of a Viral mRNA, via the eIF4 Complex, Facilitates Cap-independent Translation. J Biol Chem 290: 11268–11281.

Shen L, Li F, Dong W, Liu W, Qian Y, Yang J, Wang F, Wu Y. 2017. *Nicotiana benthamiana* NbbZIP28, a possible regulator of unfolded protein response, plays a negative role in viral infection. Eur J Plant Pathol 149: 831–843.

Simms CL, Thomas EN, Zaher HS. 2017. Ribosome-based quality control of mRNA and nascent peptides. WIREs RNA 8: e1366.

Sit TL, Vaewhongs AA, Lommel SA. 1998. RNA-mediated trans-activation of transcription from a viral RNA. Science 281: 829–32.

Somogyi P, Jenner AJ, Brierley I, Inglis SC. 1993. Ribosomal pausing during translation of an RNA pseudoknot. Mol Cell Biol 13: 6931–6940.

Souza PFN, Carvalho FEL. 2019. Killing two birds with one stone: How do Plant Viruses Break Down Plant Defenses and Manipulate Cellular Processes to Replicate Themselves? J Plant Biol 62: 170–180.

Srivastava R, Li Z, Russo G, Tang J, Bi R, Muppirala U, Chudalayandi S, Severin A, He M, Vaitkevicius SI, Lawrence-Dill CJ, Liu P, Stapleton AE, Bassham DC, Brandizzi F, Howell SH. 2018. Response to Persistent ER Stress in Plants: A Multiphasic Process That Transitions Cells from Prosurvival Activities to Cell Death. Plant Cell 30: 1220–1242.

Steckelberg AL, Akiyama BM, Costantino DA, Sit TL, Nix JC, Kieft JS. 2018. A folded viral noncoding RNA blocks host cell exoribonucleases through a conformationally dynamic RNA structure. Proc Natl Acad Sci 115: 6404–6409.

Stern-Ginossar N. 2015. Decoding Viral Infection by Ribosome Profiling. J Virol 89: 6164–6166.

Stern-Ginossar N, Ingolia NT. 2015. Ribosome Profiling as a Tool to Decipher Viral Complexity. Annu Rev Virol 2: 335-349.

Sun F, Fang P, Li J, Du L, Lan Y, Zhou T, Fan Y, Shen W, Zhou Y. 2016. RNA-seq-based digital gene expression analysis reveals modification of host defense responses by rice stripe virus during disease symptom development in Arabidopsis. Virol J 13: 202.

Sun T, Sun X, Li F, Ma N, Wang M, Chen Y, Liu N, Jin Y, Zhang J, Hou C, Yang C, Wang D. 2021. H2O2 mediates transcriptome reprogramming during Soybean mosaic virus-induced callose deposition in soybean. Crop J. https://doi.org/10.1016/j.cj.2021.04.005.

Tajima Y, Iwakawa H, Kaido M, Mise K, Okuno T. 2011. A long-distance RNA–RNA interaction plays an important role in programmed − 1 ribosomal frameshifting in the translation of p88 replicase protein of Red clover necrotic mosaic virus. Virology 417: 169–178.

Takken FL, Albrecht M, Tameling WIL. 2006. Resistance proteins: molecular switches of plant defence. Curr Opin Plant Biol 9: 383–390.

Taliansky M, Samarskaya V, Zavriev SK, Fesenko I, Kalinina NO, Love AJ. 2021. RNA-Based Technologies for Engineering Plant Virus Resistance. Plants 10: 82.

Tang Z, Bernards M, Wang A. 2020. Identification and manipulation of host factors for the control of plant viruses. In Applied Plant Virology (ed. L.P. Awasthi), pp. 671–695, Academic Press.

Tena G, Boudsocq M, Sheen J. 2011. Protein kinase signaling networks in plant innate immunity. Curr Opin Plant Biol 14: 519–529.

Tran V, Ledwith MP, Thamamongood T, Higgins CA, Tripathi S, Chang MW, Benner C, García-Sastre A, Schwemmle M, Boon ACM, Diamond MS, Mehle A. 2020. Influenza virus repurposes the antiviral protein IFIT2 to promote translation of viral mRNAs. Nat Microbiol 5: 1490–1503.

Treder K, Pettit Kneller EL, Allen EM, Wang Z, Browning KS, Miller WA. 2007. The 3' cap-independent translation element of Barley yellow dwarf virus binds eIF4F via the eIF4G subunit to initiate translation. RNA 14: 134–147.

Tu C, Tzeng TH, Bruenn JA. 1992. Ribosomal movement impeded at a pseudoknot required for frameshifting. Proc Natl Acad Sci 89: 8636–8640.

Turner KA, Sit TL, Callaway AS, Allen NS, Lommel SA. 2004. Red clover necrotic mosaic virus replication proteins accumulate at the endoplasmic reticulum. Virology 320: 276–290.

Vaattovaara A, Brandt B, Rajaraman S, Safronov O, Veidenberg A, Luklová M, Kangasjärvi J, Löytynoja A, Hothorn M, Salojärvi J, Wrzaczek M. 2019. Mechanistic insights into the evolution of DUF26-containing proteins in land plants. Commun Biol 2: 56.

Ve T, Williams SJ, Kobe B. 2015. Structure and function of Toll/interleukin-1 receptor/resistance protein (TIR) domains. Apoptosis 20: 250–261.

Verchot J, Pajerowska-Mukhtar KM. 2021. UPR signaling at the nexus of plant viral, bacterial, and fungal defenses. Curr Opin Virol 47: 9–17.

Vinutha T, Vanchinathan S, Bansal N, Kumar G, Permar V, Watts A, Ramesh SV, Praveen S. 2020. Tomato auxin biosynthesis/signaling is reprogrammed by the geminivirus to enhance its pathogenicity. Planta 252: 51.

Walter P, Ron D. 2011. The Unfolded Protein Response: From Stress Pathway to Homeostatic Regulation. Science 334: 1081–1086.

Wang A. 2015. Dissecting the Molecular Network of Virus-Plant Interactions: The Complex Roles of Host Factors. Annu Rev Phytopathol 53: 45–66.

Wang C, Wang C, Zou J, Yang Y, Li Z, Zhu S. 2019. Epigenetics in the plant–virus interaction. Plant Cell Rep 38: 1031–1038.

Wang L, Xie H, Zheng X, Chen J, Zhang S, Wu J. 2021. Recent advances and emerging trends in antiviral defense networking in rice. Crop J 9: 553–563.

Wei T, Simko V. 2021. R package "corrplot": Visualization of a Correlation Matrix. (Version 0.90), https://github.com/taiyun/corrplot.

Wu H, Qu X, Dong Z, Luo L, Shao C, Forner J, Lohmann JU, Su M, Xu M, Liu X, Zhu L, Zeng J, Liu S, Tian Z, Zhao Z. 2020. WUSCHEL triggers innate antiviral immunity in plant stem cells. Science 370: 227–231.

Wu M, Ding X, Fu X, Lozano-Duran R. 2019a. Transcriptional reprogramming caused by the geminivirus Tomato yellow leaf curl virus in local or systemic infections in *Nicotiana benthamiana*. BMC Genomics 20: 542.

Wu X, Valli A, García J, Zhou X, Cheng X. 2019b. The Tug-of-War between Plants and Viruses: Great Progress and Many Remaining Questions. Viruses 11: 203.

Xie Z, Allen E, Wilken A, Carrington JC. 2005. DICER-LIKE 4 functions in trans-acting small interfering RNA biogenesis and vegetative phase change in *Arabidopsis thaliana*. Proc Natl Acad Sci 102: 12984–12989.

Xiong Z, Lommel SA. 1989. The complete nucleotide sequence and genome organization of red clover necrotic mosaic virus RNA-1. Virology 171: 543–554.

Xiong Z, Kim KH, Giesman-Cookmeyer D, Lommel SA. 1993. The Roles of the Red Clover Necrotic Mosaic Virus Capsid and Cell-to-Cell Movement Proteins in Systemic Infection. Virology 192: 27–32.

Xu T, Lei L, Shi J, Wang X, Chen J, Xue M, Sun S, Zhan B, Xia Z, Jiang N, Zhou T, Lai J, Fan Z. 2019. Characterization of maize translational responses to sugarcane mosaic virus infection. Virus Res 259: 97–107.

Yang L, Du Z, Gao F, Wu K, Xie L, Li Y, Wu Z, Wu J. 2014. Transcriptome profiling confirmed correlations between symptoms and transcriptional changes in RDV infected rice and revealed nucleolus as a possible target of RDV manipulation. Virol J 11: 81.

Yang Z, Cao S, Martens CA, Porcella SF, Xie Z, Ma M, Shen B, Moss B. 2015. Deciphering Poxvirus Gene Expression by RNA Sequencing and Ribosome Profiling. J Virol 89: 6874–6886.

Ye C, Verchot J. 2011. Role of unfolded protein response in plant virus infection. Plant Signal Behav 6: 1212–1215.

Ye C, Dickman MB, Whitham SA, Payton M, Verchot J. 2011. The Unfolded Protein Response Is Triggered by a Plant Viral Movement Protein. Plant Physiol 156: 741–755.

Yoon YJ, Venkatesh J, Lee JH, Kim J, Lee HE, Kim DS, Kang BC. 2020. Genome Editing of eIF4E1 in Tomato Confers Resistance to Pepper Mottle Virus. Front Plant Sci 11: 1098.

Yu TY, Sun MK, Liang LK. 2021. Receptors in the Induction of the Plant Innate Immunity. Mol Plant-Microbe Interact 34: 587-601.

Yuan S, Liao G, Zhang M, Zhu Y, Wang K, Xiao W, Jia C, Dong M, Sun N, Walch A, Xu P, Zhang J, Deng Q, Hu R. 2021. Translatomic profiling reveals novel self-restricting virus-host interactions during HBV infection. J Hepatol 75: 74–85.

Zaidi SSA, Mukhtar MS, Mansoor S. 2018. Genome Editing: Targeting Susceptibility Genes for Plant Disease Resistance. Trends Biotechnol 36: 898–906.

Zanardo LG, de Souza GB, Alves MS. 2019. Transcriptomics of plant–virus interactions: a review. Theor Exp Plant Physiol 31: 103–125.

Zavriev SK, Hickey CM, Lommel SA. 1996. Mapping of the Red Clover Necrotic Mosaic Virus Subgenomic RNA. Virology 216: 407–410.

Zhang L, Wang A. 2016. ER Stress, UPR and Virus Infections in Plants. In Current Research Topics in Plant Virology (ed. Wang A, Zhou X), pp. 173–195, Springer International Publishing, Cham.

Zhang Z, He G, Filipowicz NA, Randall G, Belov GA, Kopek BG, Wang X. 2019. Host Lipids in Positive-Strand RNA Virus Genome Replication. Front Microbiol 10: 286.

Zhao P, Liu Q, Miller WA, Goss DJ. 2017. Eukaryotic translation initiation factor 4G (eIF4G) coordinates interactions with eIF4A, eIF4B, and eIF4E in binding and translation of the barley yellow dwarf virus 3′ cap-independent translation element (BTE). J Biol Chem 292: 5921–5931.

Zhao Y, Yang X, Zhou G, Zhang T. 2020. Engineering plant virus resistance: from RNA silencing to genome editing strategies. Plant Biotechnol J 18: 328–336.

Zorzatto C, Machado JPB, Lopes KVG, Nascimento KJT, Pereira WA, Brustolini OJB, Reis PAB, Calil IP, Deguchi M, Sachetto-Martins G, Gouveia BC, Loriato VAP, Silva MAC, Silva FF, Santos AA, Chory J, Fontes EPB. 2015. NIK1-mediated translation suppression functions as a plant antiviral immunity mechanism. Nature 520: 679-682.

Figures

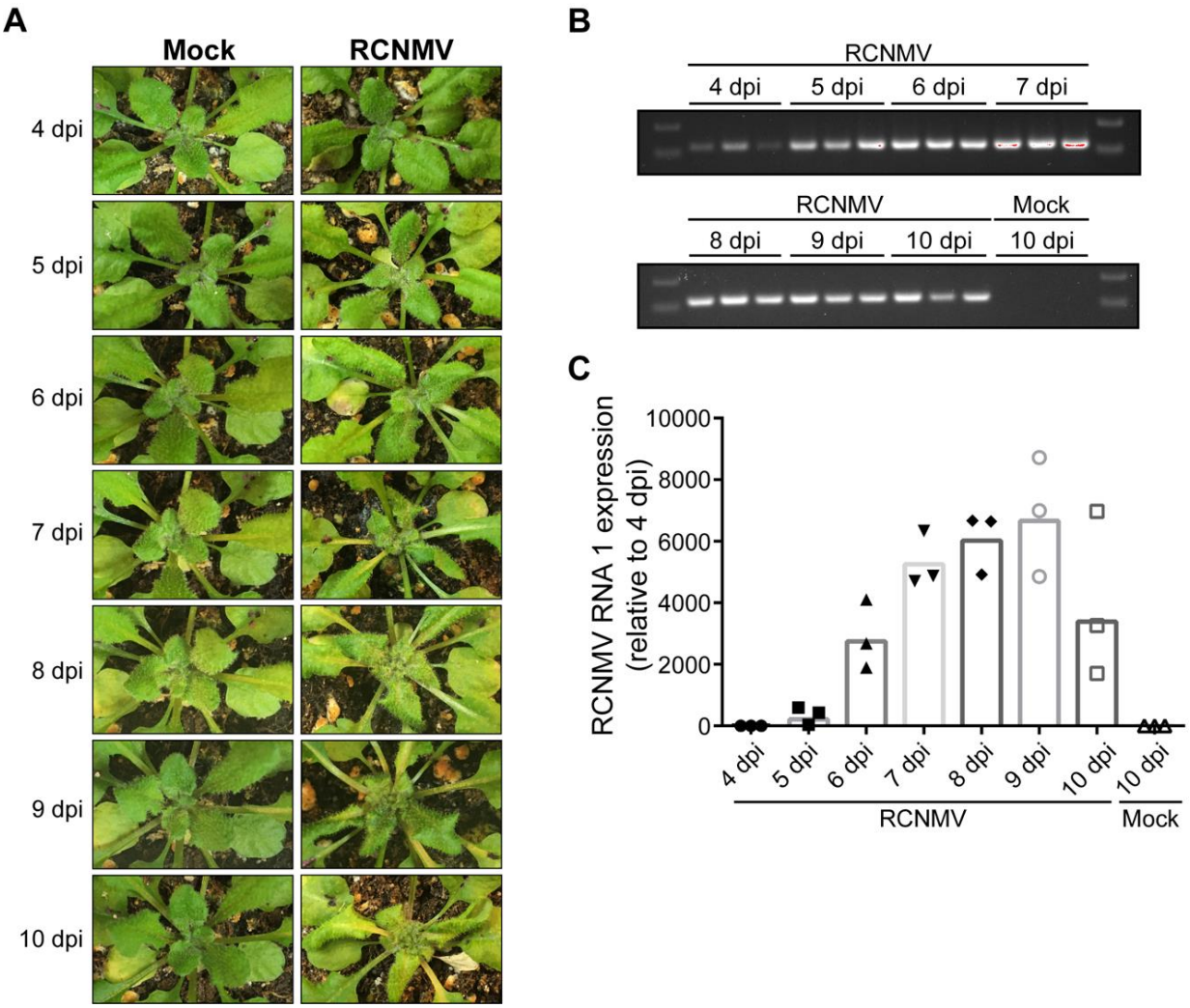

Figure 4.1. Time-course assay in RCNMV-infected *dcl2-1/dcl4-2t Arabidopsis thaliana*. **(A)** Symptom development from 4-10 dpi. Severe symptoms appear on the young systemic leaves at 7 dpi. **(B)** RT-PCR to verify RNA1 accumulation in the systemic young leaves. **(C)** qRT-PCR to assess the increase in RNA1 accumulation from 4 to 10 dpi. AtSAND and AtPDF2 were used as reference genes for qRT-PCR.

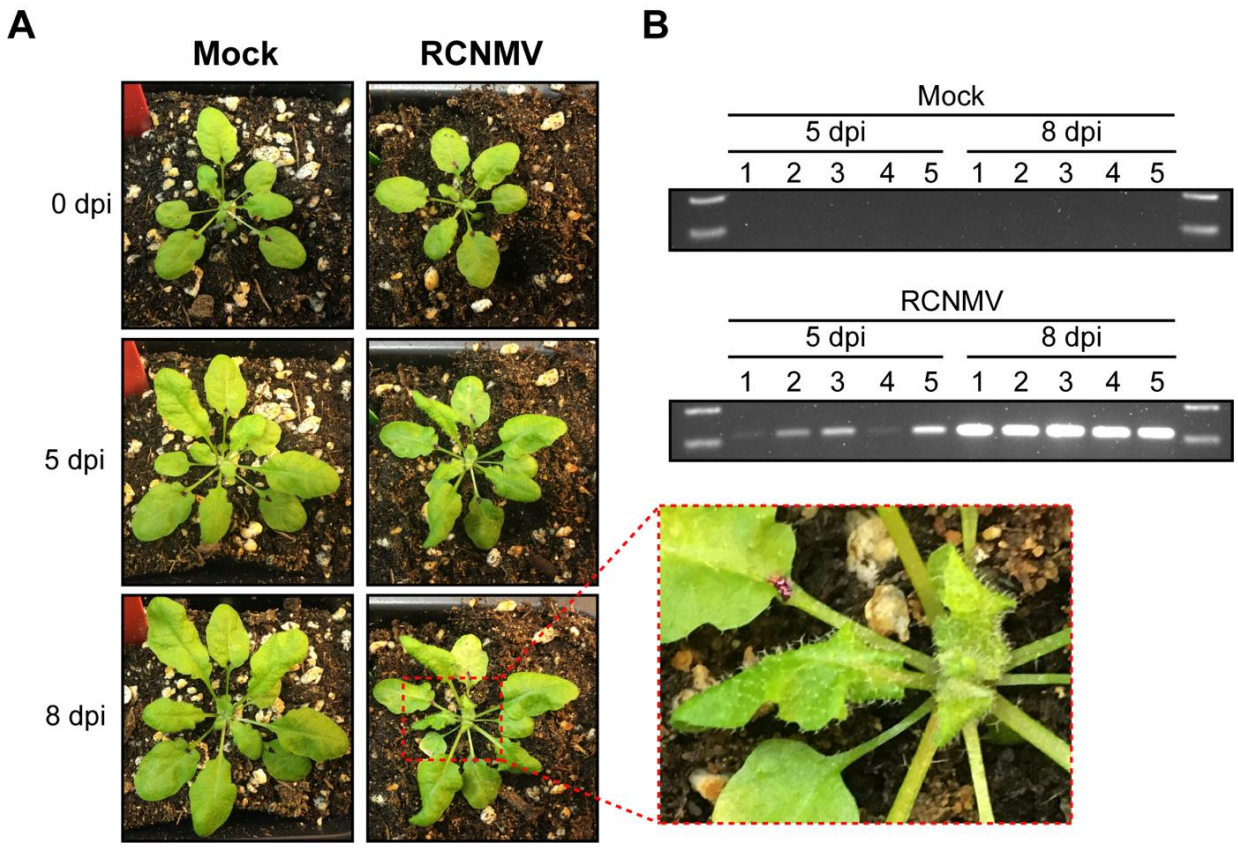

Figure 4.2. Plants used for Ribo-seq and RNA-seq. **(A)** Symptoms at 0, 5, 8 dpi in mock- and RCNMV-infected samples. The zoomed-in image shows the symptoms on the non-inoculated systemic leaves. **(B)** RT-PCR to verify the accumulation of RNA1 in systemic leaves at 5 and 8 dpi in RCNMV-infected plants.

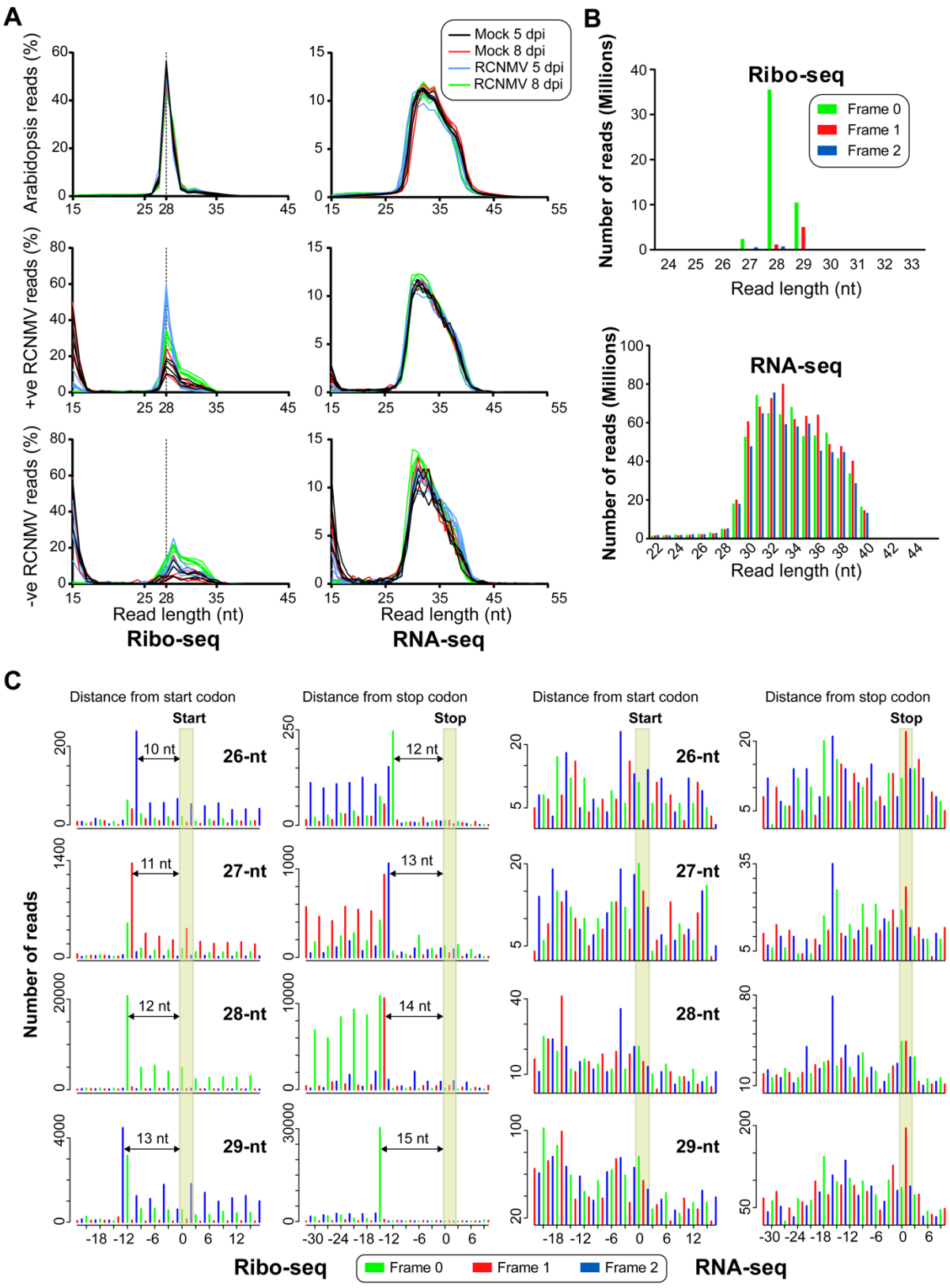

Figure 4.3. Quality assessment of Ribo-seq and RNA-seq data-I. **(A)** Length distribution of Ribo-seq (left) and RNA-seq (right) reads that mapped to Arabidopsis reference genome (top), RCNMV positive-

sense RNAs (middle), and RCNMV negative-sense RNAs (bottom). **(B)** Frame enrichment analysis, using RiboToolkit (Liu et al. 2020), of Arabidopsis-mapped Ribo-seq (top) and RNA-seq (bottom) reads. 27-29 nt RPFs show good triplet periodicity while none of the RNA-seq reads show triplet periodicity. **(C)** Metagene analysis of Arabidopsis-mapped 26-29 nt Ribo-seq reads, using RiboTaper (Calviello et al. 2016), show good triplet periodicity with almost all the reads mapping within the CDS while the RNA-seq reads show lack of triplet periodicity and sufficient reads mapping to the UTRs.

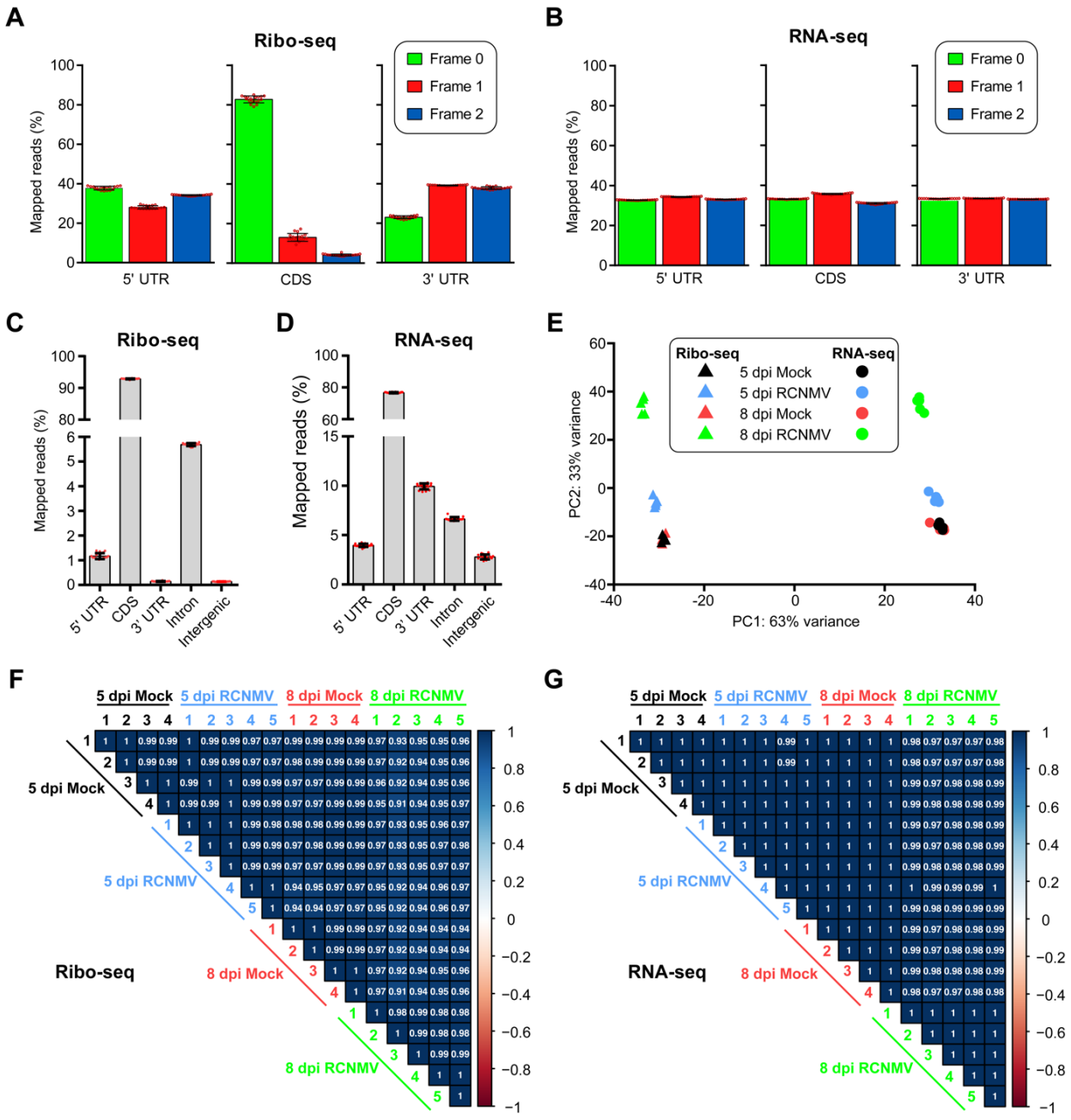

Figure 4.4. Quality assessment of Ribo-seq and RNA-seq data-II. **(A-B)** Frame enrichment analysis, using RiboToolkit (Liu et al. 2020), over the UTRs and the CDS, separately, of Arabidopsis-mapped 26-29nt Ribo-seq (A) and RNA-seq (B) reads. **(C-D)** Distribution of 26-29 nt Ribo-seq (C) and RNA-seq (D) reads over different genomic features using RiboToolkit. **(E)** Principal component analysis using the CDS-mapped 26-29 nt Ribo-seq reads and the exon-mapped RNA-seq reads (all sizes) using DESeq2 (Love et al. 2014). **(F-G)** Pearson correlation analysis, using corrplot package (Wei and Simko 2021), shows high reproducibility among the biological replicates.

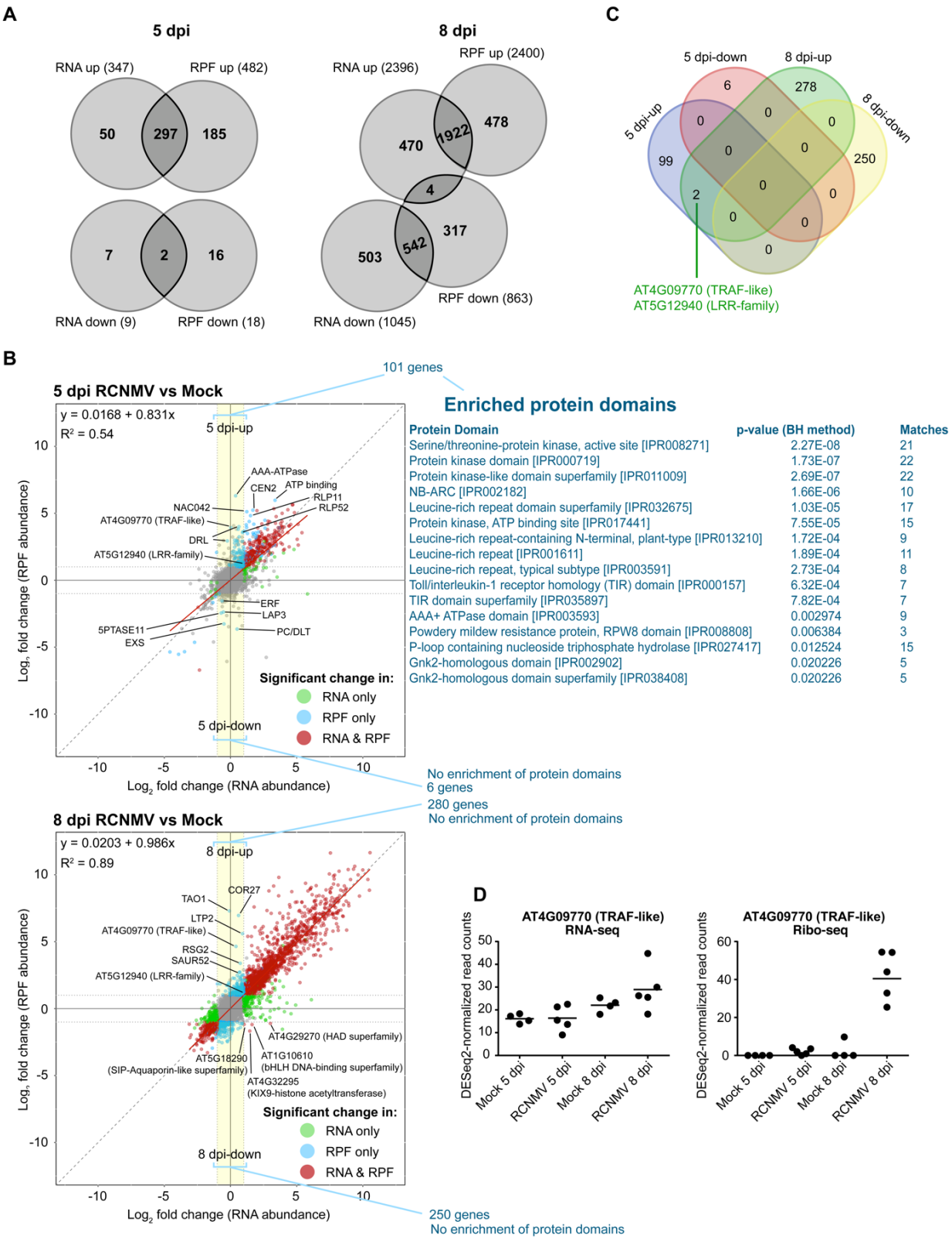

Figure 4.5. Differentially expressed and translated genes in RCNMV-infected plants. **(A)** Venn diagram showing the number of genes identified as DEG from RNA-seq data and DTGs from Ribo-seq data. **(B)**

Scatterplot of log_2-FC (RPF abundance) vs log_2-FC (RNA abundance) with only the genes that had a valid (non-NA) DESeq2 output. **(C)** Venn diagram showing the number of translationally-regulated genes at 5 and 8 dpi (blue-colored genes withing the yellow shaded region). **(D)** DESeq2-normalized read counts of AT4G09770 (TRAF-like) gene in RNA-seq and Ribo-seq datasets across all the treatments. More details can be found in *Supplemental file 4.4*.

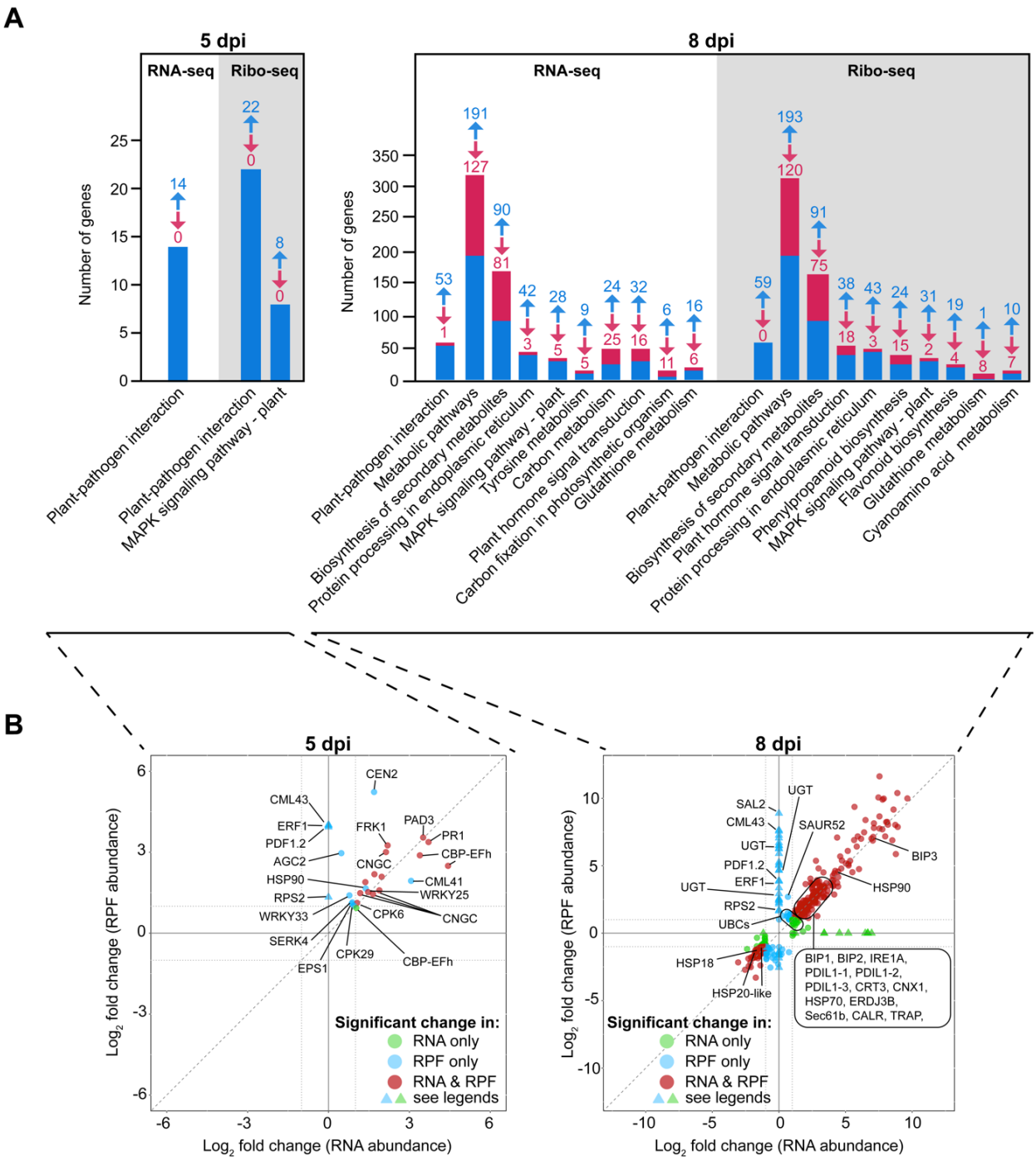

Figure 4.6. KEGG pathway enrichment analysis. **(A)** The enriched pathways were identified via KOBAS (Bu et al. 2021) using the DEGs (RNA-seq) and DTGs (Ribo-seq) at 5 and 8 dpi. The upregulated and downregulated genes were used together for the analysis. The blue and the red arrows with the number denote the number of upregulated and downregulated DEGs/DTGs, respectively, in the enriched pathway. **(B)** Scatterplot of $\log_2$-FC (RPF abundance) vs $\log_2$-FC (RNA abundance) with the DEGs/DTGs in the enriched pathway. The blue triangles refer to the DTGs that did not have a valid output (non-NA) from the RNA-seq data via DESeq2 and therefore, their $\log_2$-FC (RNA abundance) was set to zero. The green triangles refer to the DEGs that did not have valid output (non-NA) from the Ribo-

seq data via DESeq2 and therefore, their log_2-FC (RPF abundance) was set to zero. (DEGs) differentially expressed genes, (DTGs) differentially translated genes, (FC) fold change. More details can be found in *Supplemental file 4.6*.

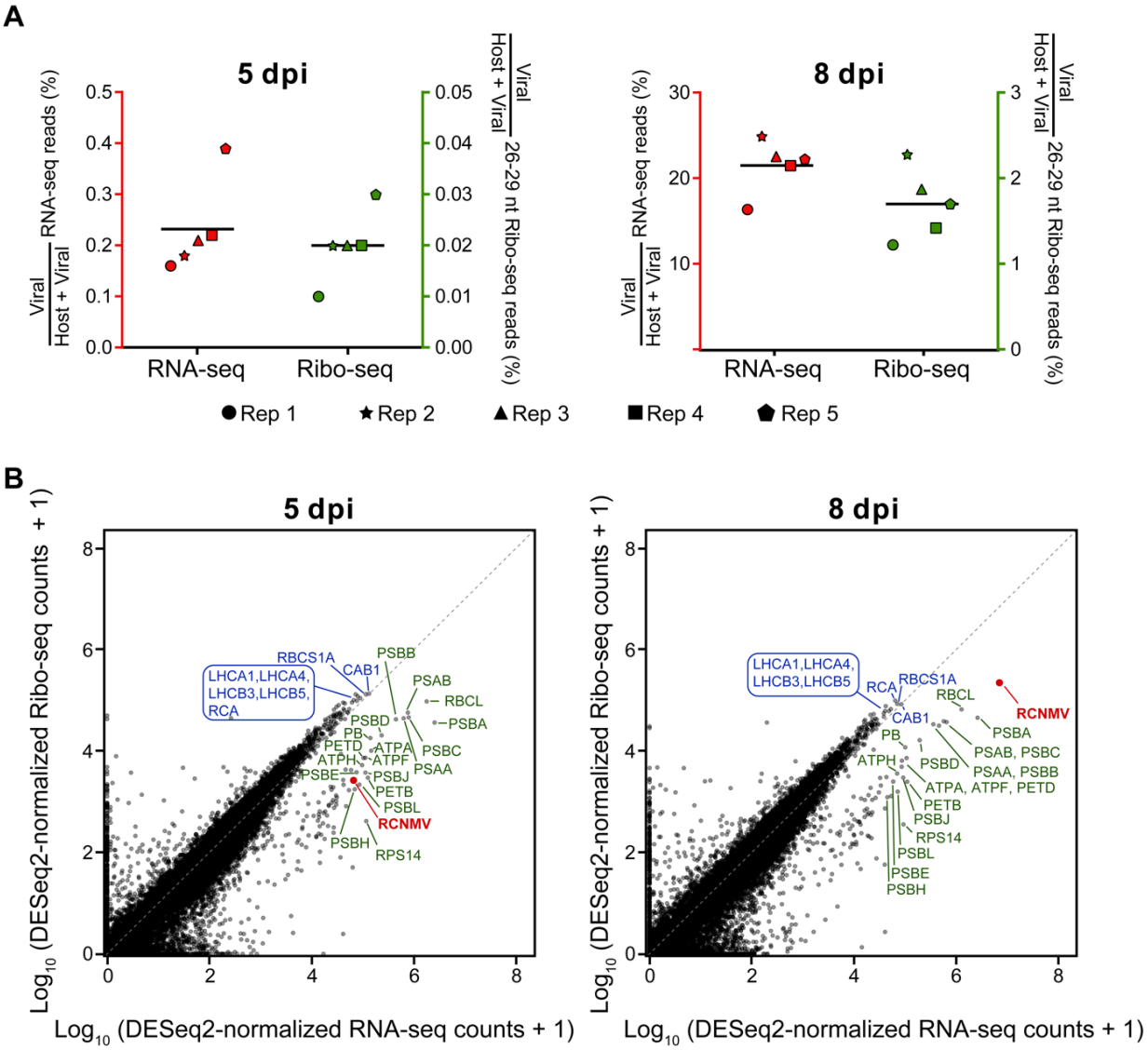

Figure 4.7. Abundance of RCNMV-mapped RNA-seq and Ribo-seq reads. **(A)** Proportion of RNA-seq and Ribo-seq reads in RCNMV-infected plants that map to RCNMV genome. **(B)** Scatterplot display the DESeq2-normalized read counts from RCNMV compared to that from Arabidopsis genome. Values displayed are the arithmetic means of the log_{10} (1+x)-transformed counts across the five biological replicates. Only the Arabidopsis genes that had higher RNA-seq read counts than RCNMV at 5 dpi are labelled in the scatterplot. RCNMV is denoted by red color. Blue-colored labels show nucleus-encoded genes, and green-colored labels show chloroplast-encoded genes. Annotations for the labelled genes can be found in *Supplemental file 4.7*.

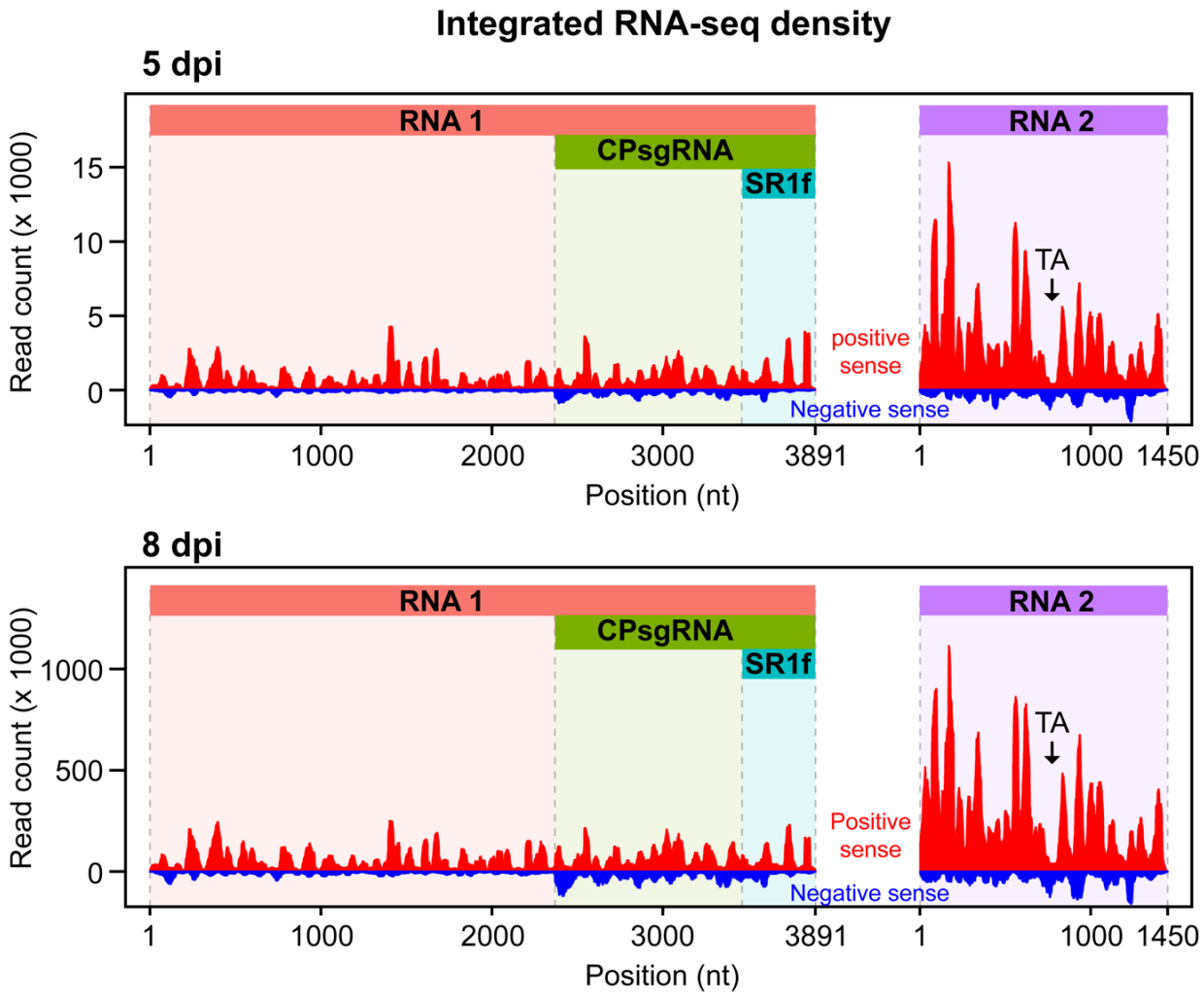

Figure 4.8. Integrated RNA-seq density across RCNMV RNA1 and RNA2. All the nucleotides of RNA-seq reads were plotted as a histogram which represents the integrated read density for all the reads combined from the five biological replicates at each time-point. The red and the blue curve denote the reads mapping to the positive-sense and negative-sense RNA, respectively. The black arrow denotes the location of the TA sequence that interacts with the TA-BS sequence of RNA1 and result in premature transcription termination of CPsgRNA. TA region coincides with the inflection point of RNA-seq density. (nt) nucleotide, (TA) trans-activator.

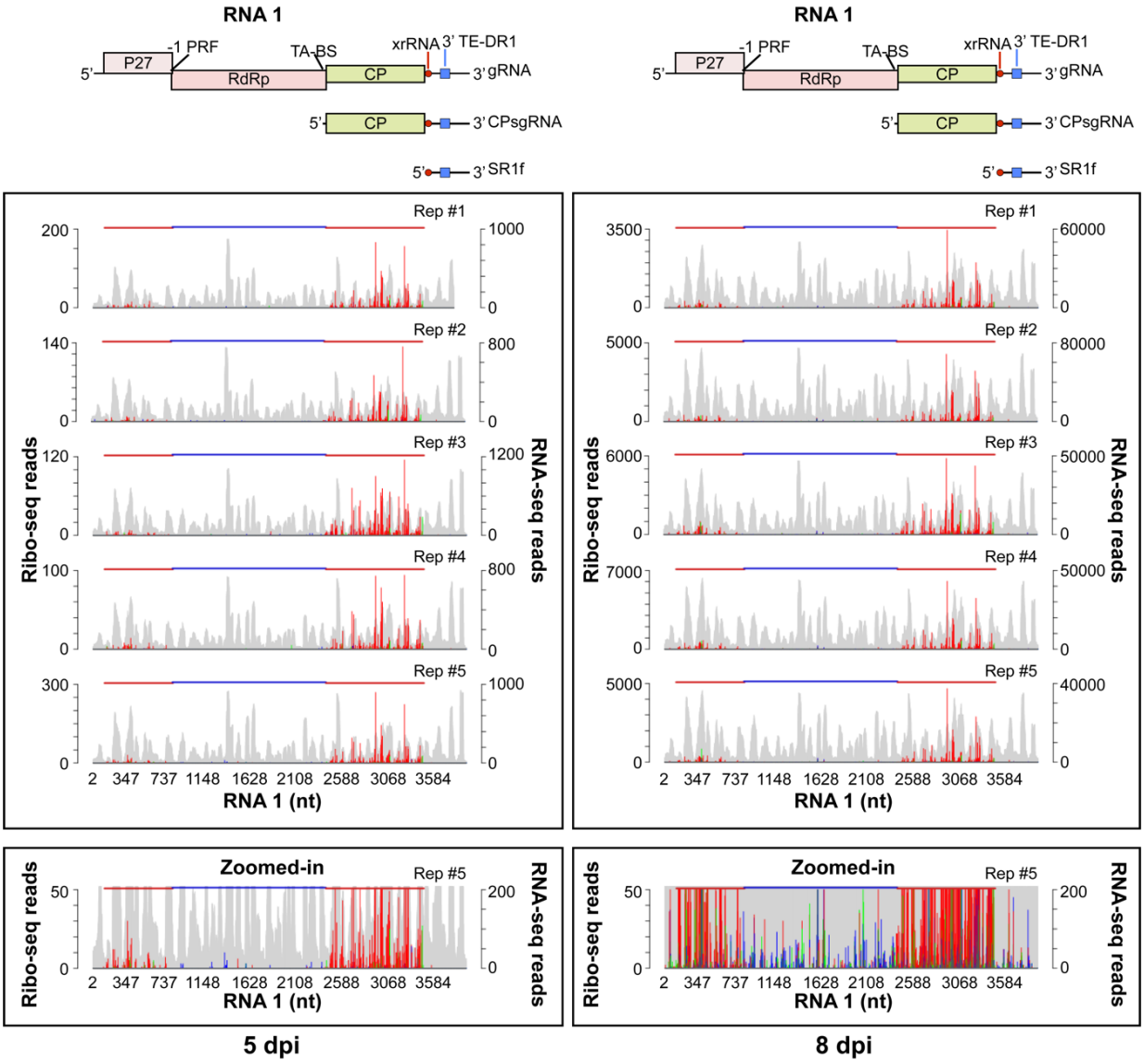

Figure 4.9. Ribo-seq and RNA-seq profiles of RCNMV RNA1. riboSeqR (Chung et al. 2015) was used for plotting the first nt of the RPFs (colored) and RNA reads (gray) as a histogram. The color of the peak is determined by the translating frame (frame 0, 1, 2) at which the first nt of the RPF maps to. The figure shows the profiles of only the 28-nt RPFs and RNA reads for all the five biological replicates at both time-points. The bottom panel depicts a zoomed-in image of replicate 5 to show the RPFs mapping to the RdRp ORF. The translated ORF inferred by riboSeqR (blue and red horizontal line) corresponds to the known RNA1 annotations. -1 PRF can be observed as the red frame (RPFs at p27 ORF) switches to the blue frame (RPFs at RdRp ORF) at the frameshift site. (nt) nucleotide, (RdRp) RNA-dependent RNA polymerase, (PRF) Programmed ribosomal frameshifting.

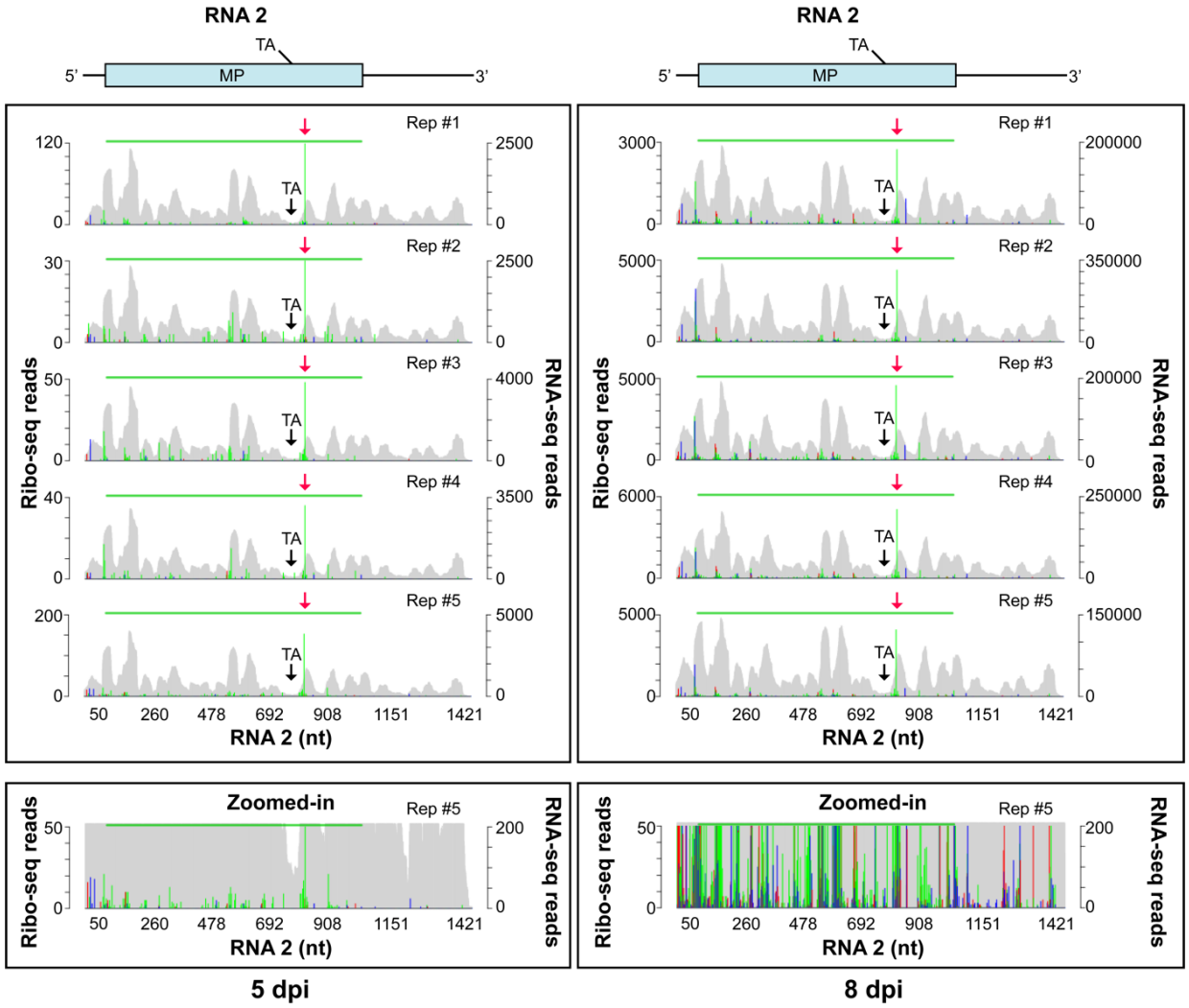

Figure 4.10. Ribo-seq and RNA-seq profiles of RCNMV RNA2. riboSeqR (Chung et al. 2015) was used for plotting the first nt of the RPFs (colored) and RNA reads (gray) as a histogram. The color of the peak is determined by the translating frame (frame 0, 1, 2) at which the first nt of the RPF maps to. The figure shows the profiles of only the 28-nt RPFs and RNA reads for all the five biological replicates at both time-points. The bottom panel depicts a zoomed-in image of replicate 5. The translated ORF inferred by riboSeqR (green horizontal line) corresponds to the known RNA2 annotation. The red arrow denotes a putative ribosomal pause site. The black arrow denotes the location of the TA sequence that interacts with the TA-BS sequence of RNA1 and results in premature transcription termination of CPsgRNA. TA region coincides with the inflection point of RNA-seq density. (nt) nucleotide, (TA) trans-activator, (TA-BS) TA-binding site.

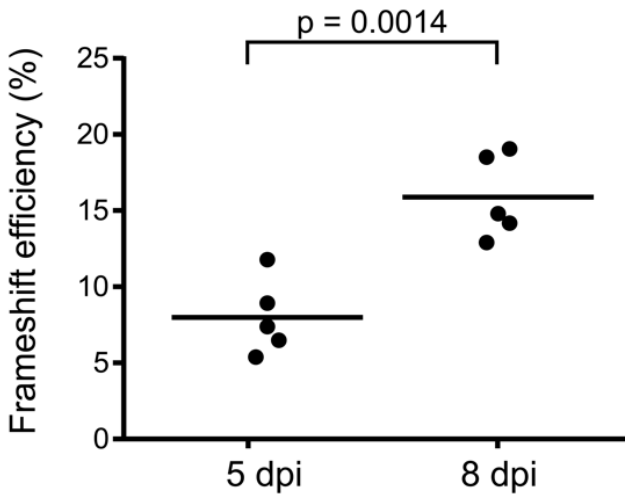

Figure 4.11. Frameshift efficiency of RNA1. Frameshift efficiency was calculated as the ratio of the length-normalized number of RPFs that map to the frameshifted ORF (100 bp downstream of p27 stop codon to 100 bp upstream of p88 stop codon) to the length-normalized number of RPFs that map to the p27 and p88-overlapping ORF (100 bp downstream of p27 start codon to 100 upstream of the frameshift site). Length-normalized means that the number of RPFs, which map to the ORF region, was divided by the length (nt) of that ORF region. The circles represent the biological replicates of RCNMV-infected Arabidopsis samples at each time-point. The horizontal bars depict the arithmetic mean of the frameshift efficiency of the five biological replicates. Unpaired Student's t test was conducted (N=5) using GraphPad and the two-tailed p-value is shown.

CHAPTER 5. CONTROL OF TRANSLATION DURING THE UNFOLDED PROTEIN RESPONSE IN MAIZE SEEDLINGS: LIFE WITHOUT PERKS

Pulkit Kanodia[1,2], Paramasivan Vijayapalani[3], Renu Srivastava[3], Ran Bi[4], Peng Liu[3,4], W. Allen Miller[1,2,3]*, Stephen H. Howell[2,3,5]*

[1] Plant pathology & Microbiology Department, Iowa State University, Ames, IA, USA

[2] Interdepartmental Genetics & Genomics Program, Iowa State University, Ames, IA, USA

[3] Plant Science Institute, Iowa State University, Ames, IA, USA

[4] Department of Statistics, Iowa State University, Ames, IA, USA

[5] Genetics, Development & Cell Biology Department, Iowa State University, Ames, IA, USA

* Corresponding authors: shh@iastate.edu, wamiller@iastate.edu

Modified from a manuscript published in *Plant Direct*

Author Contributions: PK, WAM, and SHH conceived the experiments. PK conducted most of the experimental work. VP produced the polysomes profiling pattern and analyzed the RNAs in polysomes. RS demonstrated the presence of stress granules and analyzed the RNA content in the granules. RB, PK, and PL performed the statistical analyses on the results. RB and PL conceived and applied the proposed statistical method for the analysis of translation efficiency.

Abstract

The accumulation of misfolded proteins in the endoplasmic reticulum (ER) defines a condition called ER stress that induces the unfolded protein response (UPR). The UPR in mammalian cells attenuates protein synthesis initiation, which prevents the piling up of misfolded proteins in the ER. Mammalian cells rely on Protein Kinase RNA-Like Endoplasmic

Reticulum Kinase (PERK) phosphorylation of eIF2α to arrest protein synthesis, however, plants do not have a PERK homolog, so the question is whether plants control translation in response to ER stress. We compared changes in RNA levels in the transcriptome to the RNA levels protected by ribosomes and found a decline in translation efficiency, including many UPR genes, in response to ER stress. The decline in translation efficiency is due to the fact that many mRNAs are not loaded onto polyribosomes (polysomes) in proportion to their increase in total RNA, instead some of the transcripts accumulate in stress granules (SGs). The RNAs that populate SGs are not derived from the disassembly of polysomes because protein synthesis remains steady during stress. Thus, the surge in transcription of UPR genes in response to ER stress is accompanied by the formation of SGs, and the sequestration of mRNAs in SGs may serve to temporarily relieve the translation load during ER stress.

Introduction

A major challenge for plant scientists is to understand how plants adapt to climate change given the prediction for greater weather extremes in the future. Adverse environmental conditions, such as elevated temperatures, tend to exacerbate error-prone processes in plants, such as the folding of proteins in the endoplasmic reticulum (ER) (Howell, 2013; Nakajima & Suzuki, 2013; Strasser, 2018). Errors in protein folding lead to the accumulation of misfolded proteins, a potentially toxic condition termed “ER stress” (Walter & Ron, 2011). ER stress induces an adaptive response called the unfolded protein response (UPR) which helps to mitigate the damage caused by stress and to protect plants from further stress. The UPR upregulates the expression of genes that aid in protein import, folding, quality control, and export (Iwata & Koizumi, 2005; Kamauchi, Nakatani, Nakano, & Urade, 2005; Martinez & Chrispeels, 2003; Srivastava et al., 2018).

The UPR is highly conserved among eukaryotic organisms, and in mammalian cells the UPR leads to an attenuation in protein synthesis initiation (Harding, Novoa, et al., 2000). The slow down in protein synthesis lightens the load for the protein folding machinery and prevents further buildup of misfolded proteins in the ER. Translation initiation in mammalian cells is attenuated by the action of Protein Kinase RNA-Like Endoplasmic Reticulum Kinase (PERK) (Yan et al., 2002), an ER membrane enzyme which is activated by ER stress to phosphorylate the translation initiation factor eIF2α (Harding, Novoa, et al., 2000). Phosphorylation of eIF2α inhibits the guanine nucleotide exchange factor eIF2B and thus downregulates the global protein synthesis (Clemens, 2001). PERK is a key component in one of three arms of the UPR signaling pathway in mammalian cells (Yan et al., 2002). Of the other two arms, one involves membrane-associated bZIP transcription factors, such as ATF6, which are mobilized and relocated to the nucleus in response to ER stress, while the other arm consists of the RNA splicing factor IRE1 that splices XBP1 mRNA in response to stress (*Fig. 5.1*).

Plants have only two arms of the UPR signaling pathway (Howell, 2013). Similar to mammalian cells, plants, such as Arabidopsis, have an arm of the pathway comprised of membrane-associated transcription factors bZIP17 and bZIP28, and an arm involving IRE1, which in the case of plants splices the mRNA for bZIP60 (Deng et al., 2011; Nagashima et al., 2011). Plants do not have a PERK homolog, which leads one to ask whether plants control translation in response to ER stress. This is a critical issue because PERK is essential for translational regulation and cell survival in mammalian cells (Harding, Zhang, Bertolotti, Zeng, & Ron, 2000). Arabidopsis has an eIF2α homolog that is phosphorylated in response to various stresses, including ER stress (Izquierdo et al., 2018; Zhang et al., 2008). However, the phosphorylation of eIF2α in response to ER stress in Arabidopsis is GCN2 dependent (Zhang et

al., 2008). GCN2 is not an ER factor, and so it is not understood how it is activated by ER stress and whether eIF2α phosphorylation affects translation in plants (Browning & Bailey-Serres, 2015). Arabidopsis eIF2α is also phosphorylated following treatment with herbicides, such as glyphosate or chlorsulfuron, that block amino acid biosynthesis (Lageix et al., 2008; Zhang et al., 2008).

Another means by which ER stress can attenuate general protein synthesis is through the activation of regulated IRE1-dependent decay of mRNA (RIDD) (Hollien & Weissman, 2006). RIDD involves the promiscuous attack by IRE1's RNase activity on RNA substrates other than its normal splicing targets. In Drosophila, IRE1 attacks a wide range of substrates consisting of mRNAs encoding secreted proteins (Gaddam, Stevens, & Hollien, 2013). However, in mammalian cells RIDD is more specific, attacking mRNAs with hairpin structures and core sequences comparable to those found in its normal RNA splicing target, XBP1 (Gaddam et al., 2013; Kadowaki & Nishitoh, 2019; Moore & Hollien, 2015). RIDD has also been observed in plants, and in Arabidopsis, RIDD has a wide range of RNA targets encoding secreted proteins (Mishiba et al., 2013). In maize, RIDD appears to have some preferred targets including the mRNAs encoding a family of secreted peroxidases (Srivastava et al., 2018). However, the extent of RIDD activity has not been assessed in maize to determine whether RIDD would have a general effect on translation in response to ER stress.

In this study, we subjected maize seedlings to ER stress and determined the effect on translation. This study was preceded by another in which we reported changes in the transcriptome in response to ER stress induced by tunicamycin (TM) treatment (Srivastava et al., 2018). Most notable among the events was a burst in canonical UPR gene expression from 6 to 12 hr following the imposition of stress. The fate of these RNA transcripts during the burst in

synthesis is not known. A point of interest is whether these UPR transcripts as well as others are translated and thus present on polyribosomes (polysomes) during this period of time.

A fate for some of the UPR gene transcripts could be temporary sequestration in stress granules (SGs). SGs are membraneless aggregates of mRNAs and a variety of other proteins depending on the tissue and developmental stages in which the granules form (Buchan, Yoon, & Parker, 2011; Kosmacz et al., 2019; Wallace et al., 2015). Prominent among the proteins in SGs are RNA-binding proteins such a polyadenylate (poly A)-binding protein, a factor that binds to the poly A tails of mRNAs (Anderson & Kedersha, 2006; Chantarachot & Bailey-Serres, 2018; Kedersha, Gupta, Li, Miller, & Anderson, 1999; Kosmacz et al., 2019). SGs are thought to be formed from mRNAs that are stalled in translation initiation and, therefore, can be found in association with translation initiation factors (Protter & Parker, 2016). SGs are dynamic structures and the mRNAs in the SGs are thought to enter the translation pool once released (Decker & Parker, 2012). SG formation in plants and other organisms has been observed in response to stresses, such as heat, hypoxia, starvation, treatment with metabolic inhibitors, or darkness (Cherkasov et al., 2013; Farny, Kedersha, & Silver, 2009; Jain et al., 2016; Kosmacz et al., 2019; Kroschwald et al., 2015; Sorenson & Bailey-Serres, 2014). However, accumulation of SGs has not been demonstrated in response to ER stress in plants.

Here, we use ribosome profiling (Ingolia, Ghaemmaghami, Newman, & Weissman, 2009; Juntawong, Hummel, Bazin, & Bailey-Serres, 2015) and polysome analyses to determine whether there are general translation changes in response to ER stress in maize seedlings. We find that, despite a burst of UPR gene transcription upon ER stress treatment, there is little change in translation. As a result, translation efficiency declines on a per RNA basis suggesting that some of the transcripts are not engaged by the translational machinery. We provide

evidence that many of the UPR gene transcripts are not loaded onto polysomes, but they accumulate in SGs instead.

Results

Ribosome profiling to assess the level of engagement of UPR gene transcripts by the translational machinery

The UPR is induced in maize seedlings in response to treatment with the ER stress agent, tunicamycin (TM) (Li, Humbert, & Howell, 2012). The induction of the UPR in maize is characterized by a burst in synthesis of mRNAs from the canonical UPR genes (Srivastava et al., 2018). To determine whether these mRNAs became actively engaged in the translational machinery, we conducted ribosome profiling (ribo-seq) utilizing a modification of techniques developed previously for maize (Chotewutmontri et al., 2018). In our protocol, polysomes and total RNA were isolated in biological duplicates from maize seedling roots at 0, 6, and 12 hr after TM stress treatment. Polysomes were treated with RNase 1 to digest mRNA regions that were not protected by ribosomes, and the ribosome-protected fragments (RPFs) were used to generate RPF cDNA libraries. Additionally, total RNA was isolated from the same tissues, fragmented by limited base hydrolysis, and used to generate cDNA libraries *(Fig. 5.2-a)*.

From the sequencing data, we assessed the quality of the ribosome profiling reads based on the following criteria: (a) Size distributions of the sequenced reads in the RPF libraries were distributed around a mean of 32–34 nt with a shoulder at around 30 nt *(Fig. 5.3)*, similar to the sizes reported in Arabidopsis and maize (Chotewutmontri et al., 2018; Hsu et al., 2016; Juntawong et al., 2015). The 30 nt footprints in our study agree with those found previously in maize (Chotewutmontri et al., 2018), but are slightly larger than the 28 nt footprints observed in Arabidopsis (Hsu et al., 2016). The reads in the total RNA library were somewhat more broadly

distributed but also centered around 31 nt. Thus, the two libraries were similar in terms of sizes of cDNA fragments. (b) Both ribo-seq and RNAseq libraries showed a high degree of similarity between duplicates as assessed by Pearson correlation coefficient analysis *(Fig. 5.4)*. (c) Because ribo-seq reads are derived from translating-ribosome protected mRNA fragments, they map predominantly to the coding sequence and minimally to the UTRs *(Fig. 5.2-b, upper profile)*. In contrast, the mapped RNAseq reads have a uniform distribution across the transcripts because they are derived from random fragmentation of total RNA *(Fig. 5.2-c, upper profile)*. (d) During translation, ribosomes display saltatory movements, pausing momentarily at each codon. Therefore, upon metagene analysis, the 5′ ends of RPFs map at every third base in the CDS. This property is known as triplet periodicity and is shown exclusively by ribo-seq data, while the RNAseq data do not show triplet periodicity. Indeed, triplet periodicity was observed in the metagene analysis of RPFs of 30 nt in length *(Fig. 5.2-b, lower profile)*. The 30 nt reads from RNAseq data do not show triplet periodicity *(Fig. 5.2-c, lower profile)*. (e) The 5′ ends of the RPFs mapped 13 nt upstream from the start codon in the P site of the ribosome, and 15 nt upstream from the stop codons, indicating that ribosomes disengage from the RNA when encountering a stop codon. These results are consistent with previous observations that about 30 nt of the mRNA are protected from nuclease by the 80S ribosome with about 15 nt between the first nuclease-accessible nucleotide at the 5’ end of the RPF and the codon in the P site (Ingolia et al., 2009). (f) Another diagnostic feature of true RPFs is the out-of-frame peak 15 nt upstream of the stop codon *(red bar, Fig. 5.2-b)*. The peak (tallest red bar) reveals that ribosome structure is altered upon release factor binding, allowing RNase 1 to digest the mRNA at a position one nucleotide off relative to that which occurs in mRNA on ribosomes during the elongation phase of translation (Alkalaeva, Pisarev, Frolova, Kisselev, & Pestova, 2006; Chung et al., 2015).

RNA sequencing and ribosome profiling data reveal a decrease in mRNA translation efficiencies in response to ER stress

We compared the ribo-seq and RNAseq data to assess the level of translational control following TM treatment. To evaluate the efficiency of translation, the abundance of RPFs was compared to that of RNA transcripts obtained from RNAseq analysis of the same samples. Translation efficiency of a mRNA was expressed as the ratio of RPF read counts to RNAseq read counts (Ingolia et al., 2009) at a given timepoint. A generalized linear model was constructed for simultaneously modeling ribo-seq and RNAseq data, and a hierarchical Bayesian approach was then applied to assess changes of translational efficiency between time points. The number of genes with significant change in translation efficiency (FDR < 0.05) was plotted against log2 fold change in RNA abundance *(Fig. 5.5-a)* and log2 fold change in translation efficiency *(Fig. 5.5-b)*. We were particularly interested in whether there were changes in translation efficiency of the UPR gene transcripts because levels for many of these RNAs rose, reaching a peak at 12 hr following TM treatment (Srivastava et al., 2018). When comparing 12 hr to 0 hr, we observed a decline in translation efficiencies for a sizeable portion of the RNA transcript population *(Fig. 5.5-b)*. The mean level of translation efficiency decline was less than twofold, but substantial considering that it is a change for many genes. Subsequently, edgeR was used with RNAseq and ribo-seq read counts to identify differentially expressed genes (FDR < 0.05). When the log2 fold change in RPF abundance was plotted in a scatterplot against log2 fold change in RNA abundance it could be seen that there was an increase in a sizeable number of RPFs with increasing RNA abundance *(Fig. 5.5-c)*. For many of the UPR genes the increase in RNA abundance exceeded the increase in abundance of RPFs. When the log2 fold change in translation efficiency was plotted in a scatterplot against the abundance of various mRNAs, there was a decline in translation efficiency of a sizeable number of genes with increasing RNA

abundance *(Fig. 5.5-d)*. Also, when the translation efficiencies for mRNAs of some of the canonical UPR genes were compared to the change in abundance of their RNAs, these genes showed a greater increase in RNA abundance compared to most genes, but a decline in translation efficiency *(Fig. 5.5-d)*. For example, Derlin 1, a canonical UPR gene (Oda et al., 2006; Srivastava, Liu, Guo, Yin, & Howell, 2009), its mRNA level was upregulated more than fourfold between 0 and 12 hr, while its translation efficiency declined twofold. Similarly, for ERDJ3a, another UPR induced gene (Genereux et al., 2015; Srivastava et al., 2018), its steady state mRNA level increased more than eightfold, while its translation efficiency declined about 1.5-fold. That trend held for many of the other UPR genes. Because the translation efficiency of these UPR genes declined, we interpret this to mean that there were more RNAs produced from these genes than were translated during this time frame.

No change in global translation rate was observed as assessed by polysome profiling and SUnSET assay

Because the translation efficiency of UPR genes declined, we interpret this to mean that there were more RNAs produced from these genes than loaded onto polysomes during this time frame. To validate this interpretation, other means for assessing translation activity, including polysome profiles and SUnSET assays, were utilized.

The polysome profiles on sucrose gradients have peaks showing ribosomal subunits, monosomes, followed by multiple peaks representing mRNAs with increasing numbers of translating ribosomes loaded on them. Changes in the shape of the overall profiles largely reflect changes in the global rate of initiation of protein synthesis, assuming that protein elongation rates are unchanged (Chasse, Boulben, Costache, Cormier, & Morales, 2017; Ingolia, Brar, Rouskin, McGeachy, & Weissman, 2012). For example, a global decline in protein synthesis initiation

would appear in the polysome profile as an increase in monosomes and free subunits with a concomitant decline in polysomes. We did not observe much change in the polysome/monosome ratio in the polysome profile at 12 hr comparing the TM-treated to untreated samples *(Fig. 5.6-a)*. Therefore, we concluded that there was little, if any change at 12 hr in the overall initiation rate in response to ER stress. As another measure of global translation in response to ER stress, we employed a surface sensing of translation (SUnSET) assay. The SUnSET assay utilizes puromycin to terminate translation and to tag the nascent proteins released from polysomes upon termination (Schmidt, Clavarino, Ceppi, & Pierre, 2009). Puromycin mimics the 3′ terminal nucleoside of a tRNA attached to an amino acid, but by a nonhydrolyzable amide bond. The amino acid mimic is incorporated by the ribosome onto the growing peptide chain, but it cannot be released from the nucleoside, causing chain termination. This assay, developed for animal cells, has been used successfully in plants (Van Hoewyk, 2016). Extracts containing the puromycin-labeled proteins were subjected to gel electrophoresis, immunoblotted using an antibody against puromycin, and the immunoblot was scanned to determine the levels of protein synthesis *(Fig. 5.6-b)*. No significant changes in global translation rates were detected in response to TM treatment. Thus, neither the rate of protein synthesis initiation nor global translation appear to change much in response to the UPR at the peak of UPR transcript accumulation.

mRNAs with levels that increase in response to UPR associate with SGs

Given the decline in translation efficiency for the RNA transcripts for some of the canonical UPR genes, we asked what is the fate of these transcripts? To determine if some of the canonical UPR gene mRNAs were loaded onto polysomes, we obtained polysome fractions at 12 hr after TM treatment and compared the abundance of UPR RNAs on polysomes from TM-

treated samples to mock-treated samples *(Fig. 5.7-a)*. We found that the RNA abundance for some of the prominent UPR genes, BIP2, PDI-2 and ERdJ3a, increased 2 to 5-fold in total RNA fractions following TM treatment. However, the abundance of the mRNAs for these genes in the polysome fractions either held steady following TM treatment or declined somewhat. Thus, some of the UPR mRNAs were not loaded onto polysomes in proportion to their increase in abundance following TM treatment. Derlin1 represents an apparent exception which showed a decline in translation efficiency *(Fig. 5.5-d)* but little difference between its presence in total and polysome RNA at the 12 hr time point *(Fig. 5.7-a)*. The discrepancy may be due to the fact that the former is a time course comparing 12 hr to 0 hr, whereas the latter is a snapshot in time (12 hr only).

We next determined how these mRNAs were being sequestered or stored. Structures well recognized for sequestering and storing mRNAs are SGs (Protter & Parker, 2016). SG formation due to ER stress has not been reported in plants, therefore, we used a poly(A)-binding protein marker (PAB2-YFP), that has been used by others, to visualize SGs in plants (Chantarachot & Bailey-Serres, 2018). We transfected maize protoplasts with the SG marker and treated the protoplasts with TM. Fluorescent granules averaging about 0.5–1 micron in diameter, which increased in number with duration of treatment, became clearly visible *(Fig. 5.7-b)*. (Note that the induction of UPR is more rapid in protoplasts than in seedlings as seen by the upregulation of bZIP60s, BIP2 and calnexin (CNX) at 6 hr *(Fig. 5.8)*).

We investigated whether these granules contain UPR gene mRNAs, such as BIP2 and ERdJ3a mRNAs, by extracting RNA from fractions enriched in SGs. SG-enriched fractions were obtained through a modification of a procedure developed by Wheeler et al. (2017) for the purification of SGs from mammalian cells. The procedure we developed for the purification of

SGs from transfected, TM-treated protoplasts involved similar centrifugation steps, enriching for the recovery of the PAB2-YFP. (To compare the fractions from untreated and TM-treated cells, we repeated the purification procedure without the aid of the PAB2-YFP marker. We then spiked both fractions with recombinant PAB2-YFP RNA and expressed the RNA levels as fold change with respect to PAB2-YFP RNA.) We found that the SG-enriched fraction from the 6 hr TM-treated sample contained RNA transcripts from some of the UPR genes, BIP2 and ERdJ3a *(Fig. 5.7-c).* We also observed that the abundance of BIP2 and ERdJ3a transcripts in the SG fraction increased at 6 hr following TM treatment. We conclude that some RNA transcripts upregulated in the UPR are sequestered in SGs in an abundance comparable to their accumulation as total RNA.

In studies of translation attenuation in response to hypoxic stress, a bias was found in the RNAs which were not sequestered in SGs but which were translated is spite of stress conditions (Sorenson & Bailey-Serres, 2014). During hypoxic stress, the RNAs which remained in the translation pool during hypoxic stress were enriched in functions involving anaerobic metabolism. In our study, we conducted a GO term enrichment analysis of the differentially expressed genes in TM-induced-ER stress, that were identified using RPF reads and total RNA reads and found that GO terms from RPFs were enriched in biological process and molecular function for various aspects of protein folding *(Fig. 5.9-a)*, similar to that found in total RNA *(Fig. 5.9-b).* Therefore, maize does not appear to selectively translate mRNAs, but seems to do so in proportion to their abundance in total RNA in response to ER stress. Even though there is no preferential translation of UPR mRNAs following stress treatment, the upsurge in their mRNA levels enables greater translation of the UPR genes relative to others.

Discussion

Translation initiation is attenuated in mammalian cells in response to ER stress (Harding, Novoa, et al., 2000). It has been reasoned that attenuation prevents the further piling up of misfolded proteins in the ER when the demand exceeds the capacity for folding. The question we have addressed is whether translation is attenuated in plant cells in response to ER stress, and, if so, is it controlled in the same way as it is in mammalian cells. The answer is that translation is affected by ER stress in plants, but not in the same way as in mammalian cells.

Considering that plants lack a PERK homolog, plants cannot use a comparable PERK-eIF2α-P pathway for attenuating translation. Nonetheless, eIF2α is phosphorylated in Arabidopsis in response to various stresses (Zhang et al., 2008). However, eIF2α phosphorylation is not PERK dependent, but is GCN2 dependent (Zhang et al., 2008). Izquierdo et al. (2018) found that treatment of Arabidopsis with the ER stress agent, dithiothreitol (DTT), also induces the phosphorylation of eIF2α and that the phosphorylation is GCN1 and GCN2 dependent. Surprisingly, they found that DTT treatment attenuates protein synthesis as assessed by 35S-Cys/Met incorporation, however the attenuation was not GCN1 and GCN2 dependent and, by inference not eIF2α dependent or UPR dependent. In any case, it has not been shown that eIF2α phosphorylation attenuates protein synthesis in plants. Izquierdo et al. (2018) and others have implied a limited role of eIF2α-P in inhibiting protein synthesis in plants (Browning & Bailey-Serres, 2015; Shaikhin, Smailov, Lee, Kozhanov, & Iskakov, 1992). As for the effect of DTT on protein synthesis, DTT is a strong reducing agent and is likely to affect translation unrelated to its effects on UPR. It is for this reason that we used TM to induce the UPR in this study and in other studies to determine the effects of persistent ER stress in plants (Srivastava et al., 2018).

In our hands, TM-induced ER stress had little effect on the rate of protein synthesis initiation or global translation as assessed by polysome analysis and SUnSET assays. Although the rate of translation was very little affected, there was a reduction in translation efficiency for many mRNAs as assessed by ribosome profiling. The phenomenon is accompanied by a burst in transcription of UPR genes between 6 and 12 hr, during which time some of the transcripts are not loaded onto polysomes. We propose that some of these mRNAs are temporarily stored, presumably to enter the translational pool later *(Fig. 5.10).*

We found that some of the mRNAs are sequestered in SG fractions. SGs are membraneless ribonucleoprotein bodies that consist of a stable core structure enveloped in a diffuse shell (Jain et al., 2016). The diffuse shell is thought to be a dynamic structure formed by liquid-liquid phase separation events. SGs in mammalian cells are formed by or entrap mRNAs, the proteins that bind them, and other proteins, such as G3BP, a Ras-GTPase-activating protein SH3 domain-binding protein that multimerizes in response to stress (Kedersha et al., 2016; Matsuki et al., 2013). SGs from mammalian cells have been isolated by immunoaffinity using G3BP (Khong et al., 2017), revealing that they have a diverse proteome as assessed by mass-spec (Protter & Parker, 2016). SG proteomes have been analyzed in Arabidopsis and consist of many proteins also found in the SGs of human and yeast cells (Kosmacz et al., 2019). A number of the proteins found in Arabidopsis SGs belong together in protein networks that pre-exist before stress treatment. To identify SGs in maize cells, we have used a fluorescent tagged poly(A)-binding protein (PAB2-YFP) which has been used as a marker for SGs in yeast (Brambilla, Martani, & Branduardi, 2017) and in other plants (Sorenson & Bailey-Serres, 2014; Weber, Nover, & Fauth, 2008).

It is thought that messenger RNAs sequestered in SGs in mammalian cells are derived from the disassembly of polysomes as a consequence of translational repression brought about by ER stress (Protter & Parker, 2016). In fact, it is argued that activation of PERK and phosphorylation of eIF2α are required for SG formation during the UPR (Kimball, Horetsky, Ron, Jefferson, & Harding, 2003). Because translation initiation is stalled during ER stress in mammalian cells, SGs are thought to contain mRNAs in 48S preinitiation complexes. In our case with maize, translation initiation is not stalled and polysomes are not disassembled, yet SGs are formed in response to ER stress. We consider the force driving SG formation under these circumstances is the increased concentration of UPR gene transcripts produced during the burst in their synthesis in response to TM treatment. Since SGs are membraneless structures formed by perturbations that alter liquid-liquid phase separations (Wheeler, Matheny, Jain, Abrisch, & Parker, 2016), it is possible that the surge in UPR gene transcription may promote the demixing phase transition that partitions ribonuclear protein complexes into physically discrete cytoplasmic structures such as SGs. The phase transitions that lead to SG formation are concentration dependent, and it could be that the macromolecular crowding of RNAs derived from the surge in RNA synthesis nucleates SG formation (Kedersha, Ivanov, & Anderson, 2013).

It is curious that in maize and mammalian cells, some UPR gene transcripts are sequestered and not all put to work immediately by the translation machinery. In mammalian cells, the translation machinery slows down to prevent the pile up of misfolded protein in the ER (Harding, Calfon, Urano, Novoa, & Ron, 2002; Harding, Novoa, et al., 2000). But it is the same machinery that is needed to produce the proteins, such as chaperones and other protein folding and quality control factors, needed to maintain homeostasis. In maize cells the translation

machinery does not slow down nor does it speed up in response to ER stress, and some of the mRNAs needed to mitigate stress damage are put into reserve in the form of SGs.

In conclusion, we did not find significant changes in protein synthesis initiation in response to ER stress in maize seedlings. That might have been expected since plants have no known PERK homolog, and the attenuation of protein synthesis initiation in mammalian cells is largely due to the action of PERK in phosphorylating and inactivating the translation initiation factor eIF2α. However, in response to ER stress in maize there is a surge in expression of a constellation of canonical UPR genes (Srivastava et al., 2018). While these RNAs increase in numbers following ER stress treatment, we found using riboprofiling that their translation efficiency declines because many of the transcripts are not immediately engaged in the translation machinery, but are sequestered in SGs. This prevents the protein folding machinery in the ER from being overburdened by the translation of new transcripts from the UPR genes, and sequestration in SGs presumably provides a store for these important transcripts so that they can be rationed out as stress continues. Therefore, both plants and animals appear to have ways to prevent overburdening protein folding during ER stress by regulating translation.

Materials and Methods

Plant material

Tunicamycin treatment was performed largely as in Srivastava et al. (2018). In brief, sterile maize B73 seeds were placed in sterile Sigma bottles (Cat No V8630-E100) with two layers of wet filter paper. The seeds were incubated at 30°C for 2 days then transferred to an illuminated incubator at 23°C for 7 days. Seedlings were treated with 5 µg/ml TM in DMSO for 0, 6, 12 hr and 12 hr mock treated.

RT-PCR and qRT-PCR analysis

Total RNA of maize seedling roots was extracted using RNeasy Plant mini kit (Qiagen) according to the manufacturer's instructions. RNA loaded onto polysomes (fractions 17-24) was extracted using TRIzol (Invitrogen). Isolated RNA was reverse transcribed using Maxima H Minus First Strand cDNA Synthesis Kit (Thermo Scientific). For qPCR, 10-fold (polysome RNA) or 20-fold (total RNA) diluted cDNA, 10 pmol primer, and iQ SYBR Green Supermix (Bio-Rad) were used for amplification in an iCycler IQ system (Bio-Rad Laboratories). The qPCR data were normalized using tubulin (Zm00001d013367) as a standard for the polysome RNA analysis and ubiquitin (LOC100192952) for SG RNA analysis. Primer sequences are listed in *Table 5.1*.

Polysome profiling

Polysomes were extracted from root tissue (0.3 g), which was flash frozen, ground in a mortar and pestle with liquid N2, and thawed in polysome extraction buffer (Chotewutmontri, Stiffler, Watkins, & Barkan, 2018) with modifications (50 mM Tris-acetate (pH 8), 0.2 M KCl, 15 mM MgCl2, 0.2 M sucrose, 2 µg/ml pepstatin, 1 tablet/10 ml protease inhibitor, 2% polyoxyethylene-10-tridecyl ether, 1% Triton X-100, 20 mM β-mercaptoethanol, 3 mM DTT, 0.5 mg/ml heparin, 100 µg/ml chloramphenicol, 100 µg/ml cycloheximide). The homogenate was passed through a 40 µ filter followed by centrifugation at 4,700 g for 1 min at 4°C. The supernatant was collected and centrifuged at 21k g for 5 min at 4°C and centrifugation was repeated twice. The polysome extract was either used for fractionation immediately or flash frozen and stored at −80°C. The extract was layered onto 25%–65% sucrose gradient (50 mM Tris acetate (pH 8), 50 mM KCl, 15 mM MgCl2, 100 µg/ml cycloheximide, 100 µg/mL chloramphenicol) and centrifuged in a SW41 rotor (Beckman Coulter) at 35k g, 4°C, for 9 hr.

Polysomes were fractionated using a Piston Gradient Fractionator (BioComp) equipped with a Econo UV monitor (Bio-Rad) according to the manufacturer's instructions. Data were acquired using WinDAQ software (DATAQ Instruments).

Ribosome profiling library preparation

RNase1 digestion. Ribosome profiling protocols from others were used with minor modifications (Chotewutmontri et al., 2018; Chung et al., 2015; Hsu et al., 2016). About 250 mg of 10-day-old maize B73 seedling roots (in biological duplicates) were ground with liquid N2 in 2.5 ml of polysome extraction buffer (PEB; 50 mM Tris-Acetate (pH 8), 200 mM KCl, 15 mM MgCl2, 1% (v/v) Triton X-100, 2% (v/v) polyoxyethelene 10-tridecylether, 200 mM sucrose, 100 µg/ml cycloheximide, 100 µg/ml chloramphenicol, 20 mM β-mercaptoethanol). The crude lysate was filtered through a 40 µm cell strainer (Falcon 08-771-1) by centrifugation at 4,000 g for 2 min. The flow through supernatant was further clarified by centrifugation at 21k g for 15 min. 300 µl of clarified lysate were aliquoted for total RNA extraction. For RPF generation, the remaining lysate was adjusted to A254 = ~10 (Lysate—PEB) with PEB. About 600 µl of the adjusted lysate were digested with 15 µl RNase1 (Ambion AM2295) for 30 min at 28°C on a shaker with slow speed. To terminate RNase digestion, 15 µl SUPERase-In (Ambion AM2696) were added. For each sample, two-aliquots of 600 µl (technical reps) were used and pooled after ultracentrifugation. The RNAse-digested lysate was layered on a precooled 330 µl sucrose cushion (1 M sucrose, 40 mM Tris-acetate (pH 8), 100 mM KCl, 15 mM MgCl2, 100 µg/ml cycloheximide, 100 µg/ml chloramphenicol, 10 mM β-mercaptoethanol) in ultracentrifuge tubes (Thermo Scientific #45237) and subjected to ultracentrifugation at 131k g (57,000 rpm) for 90 min at 4°C in a Sorvall mini ultracentrifuge (Discovery M150) with S150-AT fixed angle rotor

(Thermo Scientific 45582). The pellet was resuspended in 150 µl ribosome dissociation buffer (10 mM Tris-HCl (pH 7.5), 10 mM EDTA (pH 8), 5 mM EGTA (pH 8), 100 mM NaCl).

Preparation of RPFs. RNA was purified by TRIzol extraction method until the phase separations step followed by addition of an equal volume of ice-cold 100% ethanol to the aqueous phase and further purification using Zymo RNA Clean & Concentrator™-5 columns (Zymo R1016) according to the manufacturer's protocol and quantified using a Nanodrop spectrophotometer. Quality of RPFs was assessed by electrophoresis of denatured RNA in a 15% TBE-Urea gel (Invitrogen EC6885BOX) at 120 V for 5 min and 200 V for 55 min, staining the gel with SYBR gold (Invitrogen S11494) and determining the sharpness of the RPF band between the 28 nt and 34 nt RNA size markers. If the RPF bands appeared sharp for all samples, the RNAs from two technical duplicates were pooled for each sample. Subsequently, 10 µg RNA was treated with 1 µl Turbo DNase (Ambion AM2238) in a 50 µl reaction with 1x Turbo DNase buffer at 37°C for 30 min followed by addition of 1 µl more Turbo DNase and incubation at 37°C for additional 30 min, purification by Zymo RNA clean & concentrator −5 columns (Zymo R1016) and quantification with a Nanodrop spectrophotometer. Quality of the DNase-treated RNA was assessed as above. rRNA depletion was carried out using a half reaction of Ribo-Zero for plant seed/root kit (Illumina MRZSR116) per ~5 to 10 µg of DNAse-treated RNA sample followed by RNA clean up using Zymo RNA clean & concentrator −5 columns (Zymo R1016) according to the Illumina TruSeq Ribo Profile kit protocol (Illumina 15066016). RNA was quantified using a Qubit RNA HS kit (Invitrogen Q32852) yielding ~20% recovery from the input.

For size-selecting the RPFs, denatured rRNA-depleted RNA was subjected to electrophoresis on a 15% TBE-Urea gel (Invitrogen EC6885BOX) at 120 V for 5 min and 170 V

for 85 min, stained in the gel with SYBR gold (Invitrogen S11494), and visualized on a blue light transilluminator. The gel region between 28 nt and 34 nt RNA size markers was excised and transferred to a 0.5 ml tube with a hole at the bottom made by a 18 G syringe needle, and the tube was placed a 2 ml microfuge tube. The tube was then centrifuged at 21k g for 2 min at 4°C to crush the gel slice and transfer its contents to the 2 ml microfuge tube. About 500 µl of RNA gel extraction buffer (0.3 M NaOAc (pH5.5), 1 mM EDTA (pH 8), 10 mM Tris-HCl (pH 7.5), 0.25% (w/v) SDS) was added and incubated overnight at 4°C on a shaker. Eluted RPFs were filtered through 0.22 µ SpinX cellulose acetate filter columns (Sigma-Aldrich CL8161). About 2 µl of Glyco Blue (Ambion AM9516) and equal volume of ice-cold 100% isopropanol were added to the supernatant, and RPFs were precipitated at −80°C for 3 hr followed by centrifugation for 45 min at 21k g at 4°C, washing with ice-cold 80% ethanol, and resuspending the pellet in 3.5 µl water.

Prior to library preparation, RPF ends were repaired using T4PNK kit (Thermo Scientific EK0031) as follows: 3.25 µl RNA was incubated at 70°C for 3 min and transferred to ice, followed by addition of 0.5 µl 10x T4 PNK buffer A (no ATP), 0.25 µl superase-IN, 0.5 µl T4PNK enzyme, incubation at 37°C for 30 min, addition of 0.5 µl 10 mM ATP, incubation at 37°C for 1 hr. Following the addition of 5.5 µl water, the reaction was incubated at 75°C for 10 min and transferred to ice. Subsequently, cDNA libraries were prepared using Nextflex small RNAseq kit v3 (Bioo Scientific 5132-05) according to the manufacturer's protocol and 12 cycles of PCR. Quality of the libraries was assessed using an Agilent bioanalyzer high sensitivity DNA Assay kit. Libraries were quantified using Qubit dsDNA HS Assay kit (Invitrogen Q32854), diluted and pooled together with RNAseq cDNA libraries for sequencing at the Iowa State University DNA Sequencing Facility on an Illumina HiSeq 3000 instrument.

RNAseq library preparation

Total RNA was extracted from 300 µl aliquoted clarified lysate using a TRIzol extraction method until the phase separation step and was followed by adding an equal volume of ice-cold 100% ethanol to the aqueous phase and further purification using Zymo RNA clean & concentrator −5 columns (Zymo R1016) according to the manufacturer's protocol and quantified using a Nanodrop spectrophotometer. Integrity of total RNA was assessed by electrophoresis followed by DNase treatment and integrity assessment of DNase-treated total RNA as was done for ribo-seq samples. rRNA depletion was carried out using half reactions of Ribo-Zero for plant seed/root kit (Illumina MRZSR116) per ~5 µg of DNAse-treated total RNA sample followed by RNA clean up using Zymo RNA clean & concentrator −5 columns (Zymo R1016) according to the Illumina TruSeq Ribo Profile kit protocol (Illumina 15066016). Total RNA was subjected to random fragmentation by alkaline hydrolysis as follows: 10 µl total RNA (~1 µg) mixed with 10 µl 2x fragmentation buffer (2 mM EDTA (pH 8), 12 mM Na2CO3, 88 mM NaHCO3), incubated at 95°C in a thermocycler for 20 min. The reaction was terminated by addition of 280 µl stop solution (0.3 M NaOAc, 53.6 µg/ml Glyco Blue) and 750 µl ice-cold 100% ethanol followed by precipitation at −80°C for 3 hr. RNA was precipitated by centrifugation at 21k g for 45 min at 4°C and washed with ice-cold 80% ethanol and resuspended in water. Size-selection was carried out as above by excising the gel region between 28 nt and 34 nt RNA size markers. RNA was purified, end repaired and cDNA libraries were prepared as above. Quality of the libraries was assessed using an Agilent bioanalyzer high sensitivity DNA Assay kit. Libraries were quantified using Qubit dsDNA HS Assay kit (Invitrogen Q32854), diluted and pooled together with ribo-seq cDNA libraries according to the DNA sequencing facility requirements at Iowa State University.

Ribo-seq and RNAseq pooled libraries were multiplexed and sequenced in two lanes using an Illumina HiSeq 3000 to yield single-end 50 bp reads. Because of low depth of ribo-seq sequences, samples were pooled and resequenced in additional two lanes using Illumina HiSeq 3000 to yield single-end 50 bp reads.

Ribo-seq and RNAseq analysis

The quality of raw sequencing reads was assessed using FastQC (http://www.bioinformatics.babraham.ac.uk/projects/fastqc/). Cutadapt 1.16 (http://journal.embnet.org/index.php/embnetjournal/article/view/200) was used to remove adapters from raw sequencing reads using the following parameters: "-a TGGAATTCTCGGGTGCCAAGG—discard-untrimmed—minimum-length 23." Adapter-trimmed reads were further processed to trim the four random bases, that were added to both ends of ribo-seq and RNAseq reads during library preparation, using cutadapt 1.16 with the following parameters: "-u 4 -u -4." Subsequently, ribo-seq reads that were 27 nt to 32 nt in length and RNAseq reads from 25 nt to 40 nt were retained, and the rest were filtered out. Subsequently, noncoding RNA (rRNA, snoRNA and tRNA) was depleted by mapping the reads to the maize ncRNA reference file (ftp://ftp.gramene.org/pub/gramene/CURRENT_RELEASE/fasta/zea_mays/ncrna/) using Bowtie 1.2 (https://genomebiology.biomedcentral.com/articles/10.1186/gb-2009-10-3-r25) with the following parameters: "-n 0 -l 23" and retaining only the unmapped reads. ncRNA-depleted reads were subsequently mapped to maize cDNA and CDS reference transcriptomes (ftp://ftp.gramene.org/pub/gramene/CURRENT_RELEASE/fasta/zea_mays) using Bowtie 1.2 with following parameters: "-l 23 -v 2 -m 20—best -k 1" and only aligned reads were retained. cDNA and CDS-aligned files were converted from sam to bam, sorted, indexed, and read counts

were extracted using samtools view, sort, index, and idxstats tools, respectively (Li et al., 2009). All transcriptome-level read counts were consolidated as gene-level read counts. Pearson correlation data were plotted from CDS-aligned read counts using the tool corrplot (https://github.com/taiyun/corrplot) in R studio after discarding genes that have zero read count in all the samples. True RPF characteristics, that is, RPFs mapping predominately to CDSs and showing triplet periodicity, were assessed with the R package ribo-seqR (Hardcastle, 2014) using cDNA-aligned ribo-seq and RNAseq reads.

Sorted and indexed alignment bam files were run through igvtools with zoom level "7," window function "mean" and window size "10." The tdf files generated were used to make read coverage plots using Integrated Genomics Viewer (Thorvaldsdottir, Robinson, & Mesirov, 2013). Statistical analyses were performed using CDS-aligned ribo-seq and RNAseq read counts as follows. For identification of genes with differential translation efficiency, the CDS-aligned read counts data were normalized to the housekeeping gene, actin. We used a Poisson distribution to model RNAseq data, while a zero-inflated Poisson distribution to model the ribo-seq data for dealing with the excess of zeros in RPF samples. Then we adopted a hierarchical modeling framework to assess the change of translational efficiency between time points. The level 1 model is a generalized linear mixed model that simultaneously models the expression means of ribo-seq and RNAseq data, with abundance level, time point, and change of translational efficiency between time points as fixed effects, pairing signal between RPF and mRNA samples as a random effect. The level 2 models are for each dependent variable involved in level 1 model. For example, the parameter of change of translational efficiency for each gene is modeled as a mixture of 1 (for those genes without change of translational efficiency) and a Gamma distribution (for those genes with change of translational efficiency). Non-informative

priors were utilized to represent all uncertainties within the model. Posterior inferences such as calculating the posterior mean of the change of translational efficiency, or testing whether the translational fold change falls in a certain interval (e.g., at least twofold) while controlling FDR, were implemented via Markov Chain Monte Carlo sampling scheme. Details on the statistical method we proposed can be found as supplemental methods in the published online version of this chapter (doi: 10.1002/pld3.241). The histogram and scatterplots were generated using ggplot2 in R studio (Wickham, 2016).

GO term enrichment analysis

For identification of differentially expressed genes from total reads and RPF reads, edgeR (Robinson, McCarthy, & Smyth, 2010) was used with actin normalization and genes with more than twofold change and with Hochberg multiple correction of FDR <0.05 were retained. AgriGO version 2 (http://bioinfo.cau.edu.cn/agriGO/) was used for singular enrichment analysis using hypergeometric test, multitest adjustment by Hochberg FDR <0.05 and minimum number of mapping entries set as 3. Negative log10 of corrected p-values was calculated and top ten GO terms in each of the three categories were plotted. The background used by AgriGO was locus ID v3.30 (Gramene release 50).

PAB2 cloning

Maize polyA binding protein2 (PAB2) was identified in a blast search of maize sequences from Maize GDB using the Arabidopsis PAB2 (At4g34110) sequence. The ORF of the maize PAB2 homolog, Zm00001d005276 (GRMZM2G102829) was amplified from cDNA and cloned at the AscI and XbaI sites of the vector pSKM36 (Liu, Srivastava, Che, & Howell,

2007). A YFP tag was inserted at the C-terminus of PAB2 to generate ZmPAB2-YFP. The DNA was sequenced and aligned for verification.

Protoplast preparation and treatment

Leaf mesophyll protoplasts were prepared from B73 maize seedlings as described by Sheen et al, (http://molbio.mgh.harvard.edu/sheenweb/protocols_reg.html). DNA was purified using the Plasmid Miniprep Kit from Sigma and adjusted at a concentration of 1 µg/µl for transfection into protoplasts. After transformation, the protoplasts were incubated overnight. TM (5 µg/ml) treatment was carried out the next morning for 3 and 6 hr. Untreated protoplasts and protoplasts TM treated for 3 and 6 hr were visualized for SGs using a Leica SP5X MP confocal laser scanning microscope with a 63X oil immersion objective lens and excitation and emission wavelengths set at 520 and 550 nm for YFP.

SG enrichment

Untreated and 6 hr TM-treated protoplasts were collected by centrifugation and the pellets were frozen for SG isolation. SG purification was adapted from Wheeler, Jain, Khong, and Parker (2017). The protoplasts were resuspended in 1 ml SG lysis buffer. Lysis buffer was prepared fresh before lysing cells; 50 mM Tris-HCl (pH 7.4), 100 mM KOAc, 2 mM MgOAc, 0.5 mM DTT, 50 µg/ml heparin, 0.5% NP40, complete mini EDTA-free protease inhibitor (1 tablet/50 ml lysis buffer, Sigma-Aldrich), 1 U/ml RNasein Plus RNase Inhibitor (N2615, Promega). The resuspended protoplasts were lysed by passage through a 25G needle seven times at 4°C. The lysate was transferred to a microcentrifuge tube, centrifuged at 1,000 g for 5 min at 4°C to remove cell debris. The supernatant was transferred to a new microcentrifuge tube and centrifuged at 18k g for 25 min at 4°C to enrich for SG cores in the pellet. The supernatant

was discarded and the pellet was checked under a microscope for fluorescence. The pellet was resuspended in 1 ml SG lysis buffer and then, centrifuged again at 18k g for 25 min at 4°C. The pellet so obtained was resuspended in 300 µl SG lysis buffer and centrifuged at 850 g for 2 min at 4°C. The supernatant representing the SG core-enriched fraction was transferred to a new microcentrifuge tube, and RNA was extracted from this fraction using TRIzol (Invitrogen) following the manufacturer's protocol.

SUnSET assays

SUnSET assays were carried out using published protocols with minor modifications (Van Hoewyk, 2016). Nine-day-old maize seedlings were treated with water (mock) or 5 µg/ml TM for 6 and 12 hr followed by treatment with 50 µM puromycin solution (Sigma-Aldrich P8833-25MG) or water (no puromycin negative control) for 30 min. Seedlings were rinsed with water and 200–300 mg of roots were ground with mortar and pestle in liquid nitrogen followed by addition of protein extraction buffer (20 mM Tris-HCl (pH 7.5), 50 mM NaCl, 1 mM EDTA (pH 8), 0.1% (v/v) Triton X-100, 10% (v/v) glycerol, 2 mM NaF, 1 mM PMSF, 5 mM DTT, 1 tablet of Mini Complete protease inhibitor cocktail (Roche 4693124001)). The crude lysate was vortexed, centrifuged at 21k g for 3 min at 4°C, and the supernatant was centrifuged again at 21k g for 5 min at 4°C followed by quantification using a Qubit protein assay kit (Invitrogen Q33212). About 20 µg of total protein was mixed with equal volume of 2x Laemmli buffer (with β-mercaptoethanol; BioRad), incubated in boiling water for 5 min and loaded in 4%–15% Mini-protean TGX stain-free protein gel (BioRad). Electrophoresis was carried out in 10x Tris/glycine/SDS buffer (BioRad) at 100 V for 100 min followed by imaging for total protein as a loading control. Subsequently, proteins were transferred from gel to a PVDF membrane using Invitrogen iBlot2 instrument, the membrane was blocked with 5% nonfat milk at room

temperature (RT) for 1 hr, washed with 1x TBST (Tris-buffered saline with Tween 20) at room temperature for 5 min, incubated with anti-puromycin primary antibody (DSHB, University of Iowa, PMY-2A4) in 0.5% nonfat milk (antibody final concentration was 0.48 µg/ml) overnight at 4°C, washed three times with 1x TBST for 5 min, incubated with secondary antibody (anti-mouse IgG from sheep-conjugated with HRP) in 0.5% nonfat milk (3:10,000 dilution) at room temperature for 1 hr and washed three times with 1x TBST for 5 min. Images were developed using a SuperSignal West Pico Plus chemiluminescent kit (Thermo Scientific) according to the manufacturer's protocol.

Accession Numbers

Maize version 4 locus identifiers: BIP2 Zm00001d014993, PDI-1 (protein disulphide isomerase-like 1-1) Zm00001d04099, PDI-2 (protein disulphide isomerase 2-3) Zm00001d005866, Derlin 1 Zm00001d010368, ERDJ3a Zm00001d047726, Alpha tubulin 3 Zm00001d013367, Ubiquitin LOC100192952, Actin2 Zm00001d013873.

Sequence data from this article can be found in NCBI’s Gene Expression Omnibus databases under record number GSE153969.

Acknowledgments

This work was supported by the National Science Foundation Plant Genome Research Program (IOS 1444339) and by Iowa State University's Plant Sciences Institute Research Scholar awards to SHH and WAM.

Conflict of Interest

The authors declare no conflict of interest associated with the work described in this manuscript.

References

Alkalaeva, E. Z., Pisarev, A. V., Frolova, L. Y., Kisselev, L. L., & Pestova, T. V. (2006). *In vitro* reconstitution of eukaryotic translation reveals cooperativity between release factors eRF1 and eRF3. Cell, 125, 1125–1136.

Anderson, P., & Kedersha, N. (2006). RNA granules. The Journal of Cell Biology, 172, 803–808.

Brambilla, M., Martani, F., & Branduardi, P. (2017). The recruitment of the Saccharomyces cerevisiae poly(A)-binding protein into stress granules: New insights into the contribution of the different protein domains. FEMS Yeast Research, 17.

Browning, K. S., & Bailey-Serres, J. (2015). Mechanism of cytoplasmic mRNA translation. The Arabidopsis Book, 13, e0176.

Buchan, J. R., Yoon, J. H., & Parker, R. (2011). Stress-specific composition, assembly and kinetics of stress granules in Saccharomyces cerevisiae. Journal of Cell Science, 124, 228–239.

Chantarachot, T., & Bailey-Serres, J. (2018). Polysomes, stress granules, and processing bodies: A dynamic triumvirate controlling cytoplasmic mRNA fate and function. Plant Physiology, 176, 254–269.

Chasse, H., Boulben, S., Costache, V., Cormier, P., & Morales, J. (2017). Analysis of translation using polysome profiling. Nucleic Acids Research, 45, e15.

Cherkasov, V., Hofmann, S., Druffel-Augustin, S., Mogk, A., Tyedmers, J., Stoecklin, G., & Bukau, B. (2013). Coordination of translational control and protein homeostasis during severe heat stress. Current Biology, 23, 2452–2462.

Chotewutmontri, P., Stiffler, N., Watkins, K. P., & Barkan, A. (2018). Ribosome profiling in maize. Methods in Molecular Biology, 1676, 165–183.

Chung, B. Y., Hardcastle, T. J., Jones, J. D., Irigoyen, N., Firth, A. E., Baulcombe, D. C., & Brierley, I. (2015). The use of duplex-specific nuclease in ribosome profiling and a user-friendly software package for Ribo-seq data analysis. RNA, 21, 1731–1745.

Clemens, M. J. (2001). Initiation factor eIF2 alpha phosphorylation in stress responses and apoptosis. Progress in Molecular and Subcellular Biology, 27, 57–89.

Decker, C. J., & Parker, R. (2012). P-bodies and stress granules: Possible roles in the control of translation and mRNA degradation. Cold Spring Harbor Perspectives in Biology, 4, a012286.

Deng, Y., Humbert, S., Liu, J. X., Srivastava, R., Rothstein, S. J., & Howell, S. H. (2011). Heat induces the splicing by IRE1 of a mRNA encoding a transcription factor involved in the unfolded protein response in Arabidopsis. Proceedings of the National Academy of Sciences of the United States of America, 108, 7247–7252.

Farny, N. G., Kedersha, N. L., & Silver, P. A. (2009). Metazoan stress granule assembly is mediated by P-eIF2alpha-dependent and -independent mechanisms. RNA, 15, 1814–1821.

Gaddam, D., Stevens, N., & Hollien, J. (2013). Comparison of mRNA localization and regulation during endoplasmic reticulum stress in Drosophila cells. Molecular Biology of the Cell, 24, 14–20.

Genereux, J. C., Qu, S., Zhou, M., Ryno, L. M., Wang, S., Shoulders, M. D., Kaufman, R. J., Lasmézas, C. I., Kelly, J. W., & Wiseman, R. L. (2015). Unfolded protein response-induced ERdj3 secretion links ER stress to extracellular proteostasis. The EMBO Journal, 34, 4–19.

Hardcastle, T. J. (2014). riboSeqR: Analysis of sequencing data from ribosome profiling experiments. R package version 1.2.0.

Harding, H. P., Novoa, I., Zhang, Y., Zeng, H., Wek, R., Schapira, M., & Ron, D. (2000). Regulated translation initiation controls stress-induced gene expression in mammalian cells. Molecular Cell, 6, 1099–1108.

Harding, H. P., Zhang, Y., Bertolotti, A., Zeng, H., & Ron, D. (2000). Perk is essential for translational regulation and cell survival during the unfolded protein response. Molecular Cell, 5, 897–904.

Harding, H. P., Calfon, M., Urano, F., Novoa, I., & Ron, D. (2002). Transcriptional and translational control in the Mammalian unfolded protein response. Annual Review of Cell and Developmental Biology, 18, 575–599.

Hollien, J., & Weissman, J. S. (2006). Decay of endoplasmic reticulum-localized mRNAs during the unfolded protein response. Science, 313, 104–107.

Howell, S. H. (2013). ER stress responses in plants. Annual Review of Plant Biology, 64, 477-499.

Hsu, P. Y., Calviello, L., Wu, H. L., Li, F. W., Rothfels, C. J., Ohler, U., & Benfey, P. N. (2016). Super-resolution ribosome profiling reveals unannotated translation events in Arabidopsis. Proceedings of the National Academy of Sciences of the United States of America, 113, E7126-E7135.

Ingolia, N. T., Ghaemmaghami, S., Newman, J. R., & Weissman, J. S. (2009). Genome-wide analysis *in vivo* of translation with nucleotide resolution using ribosome profiling. Science, 324, 218–223.

Ingolia, N. T., Brar, G. A., Rouskin, S., McGeachy, A. M., & Weissman, J. S. (2012). The ribosome profiling strategy for monitoring translation *in vivo* by deep sequencing of ribosome-protected mRNA fragments. Nature Protocols, 7, 1534–1550.

Iwata, Y., & Koizumi, N. (2005). An Arabidopsis transcription factor, AtbZIP60, regulates the endoplasmic reticulum stress response in a manner unique to plants. Proceedings of the National Academy of Sciences of the United States of America, 102, 5280–5285.

Izquierdo, Y., Kulasekaran, S., Benito, P., Lopez, B., Marcos, R., Cascon, T., Hamberg, M., & Castresana, C. (2018). Arabidopsis nonresponding to oxylipins locus NOXY7 encodes a yeast GCN1 homolog that mediates noncanonical translation regulation and stress adaptation. Plant, Cell and Environment, 41, 1438–1452.

Jain, S., Wheeler, J. R., Walters, R. W., Agrawal, A., Barsic, A., & Parker, R. (2016). ATPase-modulated stress granules contain a diverse proteome and substructure. Cell, 164, 487–498.

Juntawong, P., Hummel, M., Bazin, J., & Bailey-Serres, J. (2015). Ribosome profiling: A tool for quantitative evaluation of dynamics in mRNA translation. Methods in Molecular Biology, 1284, 139–173.

Kadowaki, H., & Nishitoh, H. (2019). Endoplasmic reticulum quality control by garbage disposal. The FEBS Journal, 286, 232–240.

Kamauchi, S., Nakatani, H., Nakano, C., & Urade, R. (2005). Gene expression in response to endoplasmic reticulum stress in *Arabidopsis thaliana*. The FEBS Journal, 272, 3461–3476.

Kedersha, N. L., Gupta, M., Li, W., Miller, I., & Anderson, P. (1999). RNA binding proteins TIA-1 and TIAR link the phosphorylation of eIF-2 alpha to the assembly of mammalian stress granules. The Journal of Cell Biology, 147, 1431–1442.

Kedersha, N., Ivanov, P., & Anderson, P. (2013). Stress granules and cell signaling: More than just a passing phase? Trends in Biochemical Sciences, 38, 494–506.

Kedersha, N., Panas, M. D., Achorn, C. A., Lyons, S., Tisdale, S., Hickman, T., Thomas, M., Lieberman, J., McInerney, G. M., Ivanov, P., & Anderson, P. (2016). G3BP-Caprin1-USP10 complexes mediate stress granule condensation and associate with 40S subunits. The Journal of Cell Biology, 212, 845–860.

Khong, A., Matheny, T., Jain, S., Mitchell, S. F., Wheeler, J. R., & Parker, R. (2017). The stress granule transcriptome reveals principles of mRNA accumulation in stress granules. Molecular Cell, 68, 808–820.e805.

Kimball, S. R., Horetsky, R. L., Ron, D., Jefferson, L. S., & Harding, H. P. (2003). Mammalian stress granules represent sites of accumulation of stalled translation initiation complexes. American Journal of Physiology. Cell Physiology, 284, C273–284.

Kosmacz, M., Gorka, M., Schmidt, S., Luzarowski, M., Moreno, J. C., Szlachetko, J., Leniak, E., Sokolowska, E. M., Sofroni, K., Schnittger, A., & Skirycz, A. (2019). Protein and metabolite composition of Arabidopsis stress granules. New Phytologist, 222, 1420–1433.

Kroschwald, S., Maharana, S., Mateju, D., Malinovska, L., Nuske, E., Poser, I., Richter, D., & Alberti, S. (2015). Promiscuous interactions and protein disaggregases determine the material state of stress-inducible RNP granules. Elife, 4, e06807.

Lageix, S., Lanet, E., Pouch-Pelissier, M. N., Espagnol, M. C., Robaglia, C., Deragon, J. M., & Pelissier, T. (2008). Arabidopsis eIF2alpha kinase GCN2 is essential for growth in stress conditions and is activated by wounding. BMC Plant Biology, 8, 134.

Li, H., Handsaker, B., Wysoker, A., Fennell, T., Ruan, J., Homer, N., Marth, G., Abecasis, G., Durbin, R., & 1000 Genome Project Data Processing Subgroup. (2009). The sequence alignment/map format and SAMtools. Bioinformatics, 25, 2078–2079.

Li, Y., Humbert, S., & Howell, S. H. (2012). ZmbZIP60 mRNA is spliced in maize in response to ER stress. BMC Research Notes, 5, 144.

Liu, J. X., Srivastava, R., Che, P., & Howell, S.H. (2007). An endoplasmic reticulum stress response in Arabidopsis is mediated by proteolytic processing and nuclear relocation of a membrane-associated transcription factor, bZIP28. Plant Cell, 19, 4111–4119.

Martinez, I. M., & Chrispeels, M. J. (2003). Genomic analysis of the unfolded protein response in Arabidopsis shows its connection to important cellular processes. The Plant Cell, 15, 561–576.

Matsuki, H., Takahashi, M., Higuchi, M., Makokha, G. N., Oie, M., & Fujii, M. (2013). Both G3BP1 and G3BP2 contribute to stress granule formation. Genes to Cells, 18, 135–146.

Mishiba, K., Nagashima, Y., Suzuki, E., Hayashi, N., Ogata, Y., Shimada, Y., & Koizumi, N. (2013). Defects in IRE1 enhance cell death and fail to degrade mRNAs encoding secretory pathway proteins in the Arabidopsis unfolded protein response. Proceedings of the National Academy of Sciences of the United States of America, 110, 5713–5718.

Moore, K., & Hollien, J. (2015). Ire1-mediated decay in mammalian cells relies on mRNA sequence, structure, and translational status. Molecular Biology of the Cell, 26, 2873–2884.

Nagashima, Y., Mishiba, K., Suzuki, E., Shimada, Y., Iwata, Y., & Koizumi, N. (2011). Arabidopsis IRE1 catalyses unconventional splicing of bZIP60 mRNA to produce the active transcription factor. Scientific Reports, 1, 29.

Nakajima, Y., & Suzuki, S. (2013). Environmental stresses induce misfolded protein aggregation in plant cells in a microtubule-dependent manner. International Journal of Molecular Sciences, 14, 7771–7783.

Oda, Y., Okada, T., Yoshida, H., Kaufman, R. J., Nagata, K., & Mori, K. (2006). Derlin-2 and Derlin-3 are regulated by the mammalian unfolded protein response and are required for ER-associated degradation. The Journal of Cell Biology, 172, 383–393.

Protter, D. S. W., & Parker, R. (2016). Principles and properties of stress granules. Trends in Cell Biology, 26, 668–679.

Robinson, M. D., McCarthy, D. J., & Smyth, G. K. (2010). edgeR: A Bioconductor package for differential expression analysis of digital gene expression data. Bioinformatics, 26, 139–140.

Schmidt, E. K., Clavarino, G., Ceppi, M., & Pierre, P. (2009). SUnSET, a nonradioactive method to monitor protein synthesis. Nature Methods, 6, 275–277.

Shaikhin, S. M., Smailov, S. K., Lee, A. V., Kozhanov, E. V., & Iskakov, B. K. (1992). Interaction of wheat germ translation initiation factor 2 with GDP and GTP. Biochimie, 74, 447–454.

Sorenson, R., & Bailey-Serres, J. (2014). Selective mRNA sequestration by OLIGOURIDYLATE-BINDING PROTEIN 1 contributes to translational control during hypoxia in Arabidopsis. Proceedings of the National Academy of Sciences of the United States of America, 111, 2373–2378.

Srivastava, R., Liu, J. X., Guo, H., Yin, Y., & Howell, S. H. (2009). Regulation and processing of a plant peptide hormone, AtRALF23, in Arabidopsis. The Plant Journal, 59, 930–939.

Srivastava, R., Li, Z., Russo, G., Tang, J., Bi, R., Muppirala, U., Chudalayandi, S., Severin, A., He, M., Vaitkevicius, S. I., Lawrence-Dill, C. J., Liu, P., Stapleton, A. E., Bassham, D. C., Brandizzi, F., & Howell, S. H. (2018). Response to persistent ER Stress in plants: A multiphasic process that transitions cells from prosurvival activities to cell death. The Plant Cell, 30, 1220–1242.

Strasser, R. (2018). Protein quality control in the endoplasmic reticulum of plants. Annual Review of Plant Biology, 69, 147–172.

Thorvaldsdottir, H., Robinson, J. T., & Mesirov, J. P. (2013). Integrative Genomics Viewer (IGV): High-performance genomics data visualization and exploration. Briefings in Bioinformatics, 14, 178–192.

Van Hoewyk, D. (2016). Use of the non-radioactive SUnSET method to detect decreased protein synthesis in proteasome inhibited Arabidopsis roots. Plant Methods, 12, 20.

Wallace, E. W., Kear-Scott, J. L., Pilipenko, E. V., Schwartz, M. H., Laskowski, P. R., Rojek, A. E., Katanski, C. D., Riback, J. A., Dion, M. F., Franks, A. M., Airoldi, E. M., Pan, T., Budnik, B. A., & Drummond, D. A. (2015). Reversible, specific, active aggregates of endogenous proteins assemble upon heat stress. Cell, 162, 1286–1298.

Walter, P., & Ron, D. (2011). The unfolded protein response: From stress pathway to homeostatic regulation. Science, 334, 1081–1086.

Weber, C., Nover, L., & Fauth, M. (2008). Plant stress granules and mRNA processing bodies are distinct from heat stress granules. The Plant Journal, 56, 517–530.

Wheeler, J. R., Matheny, T., Jain, S., Abrisch, R., & Parker, R. (2016). Distinct stages in stress granule assembly and disassembly. eLife, 5, e18413.

Wheeler, J. R., Jain, S., Khong, A., & Parker, R. (2017). Isolation of yeast and mammalian stress granule cores. Methods, 126, 12–17.

Wickham, H. (2016). ggplot2: Elegant graphics for data analysis. New York, NY: Springer-Verlag. ISBN 978-3-319-24277-4, Retrieved from https://ggplot2.tidyverse.org.

Yan, W., Frank, C. L., Korth, M. J., Sopher, B. L., Novoa, I., Ron, D., & Katze, M. G. (2002). Control of PERK eIF2alpha kinase activity by the endoplasmic reticulum stress-induced molecular chaperone P58IPK. Proceedings of the National Academy of Sciences of the United States of America, 99, 15920–15925.

Zhang, Y., Wang, Y., Kanyuka, K., Parry, M. A., Powers, S. J., & Halford, N. G. (2008). GCN2-dependent phosphorylation of eukaryotic translation initiation factor-2alpha in Arabidopsis. Journal of Experimental Botany, 59, 3131–3141.

Figures

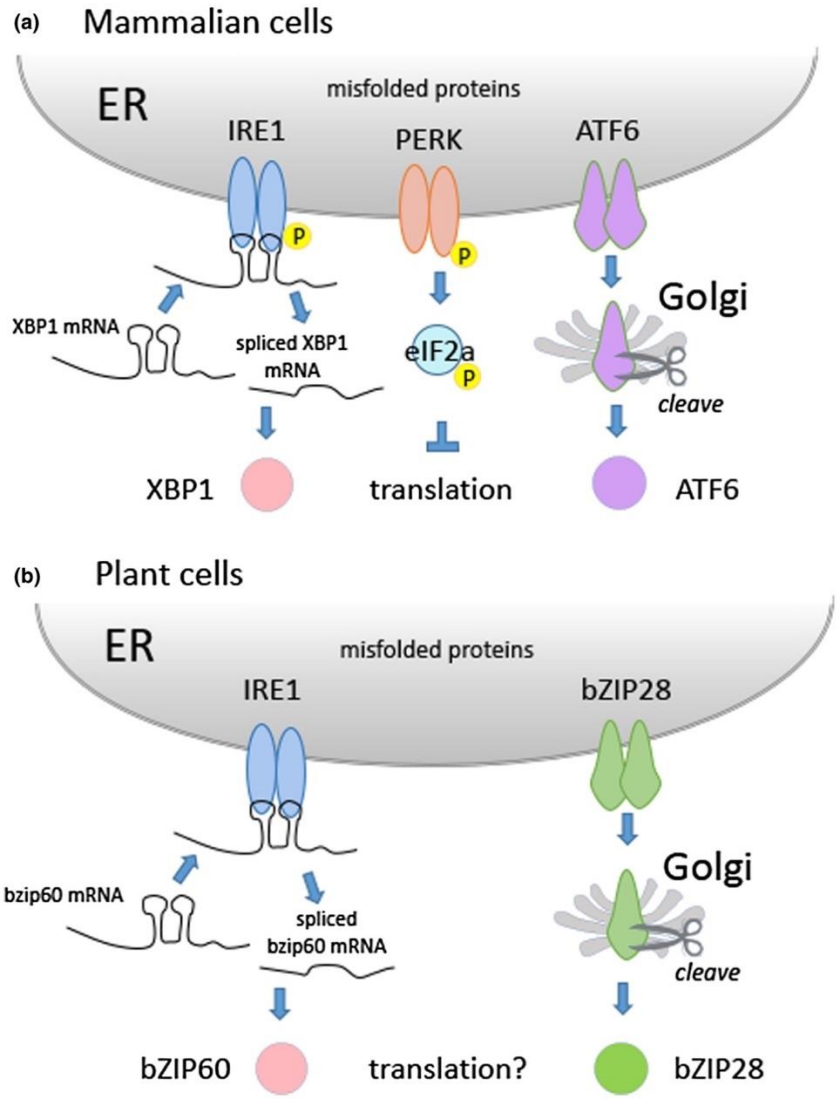

Figure 5.1. Differences between the UPR in mammalian and plant cells. **(a)** Mammalian cells have three arms of the UPR signaling pathway including an arm involving Protein Kinase RNA-Like Endoplasmic Reticulum Kinase (PERK) which phosphorylates eIF2α in response to ER stress, thereby inhibiting translation initiation. **(b)** Plant cells have two arms of the UPR signaling pathway and do not have a PERK homolog leaving open the question as to whether translation is attenuated in response to ER stress in plants. Not shown is the RIDD activity of IRE1 in which this factor attacks other mRNAs on the ER membrane. ER, endoplasmic reticulum; RIDD, regulated IRE1-dependent decay; UPR, unfolded protein response.

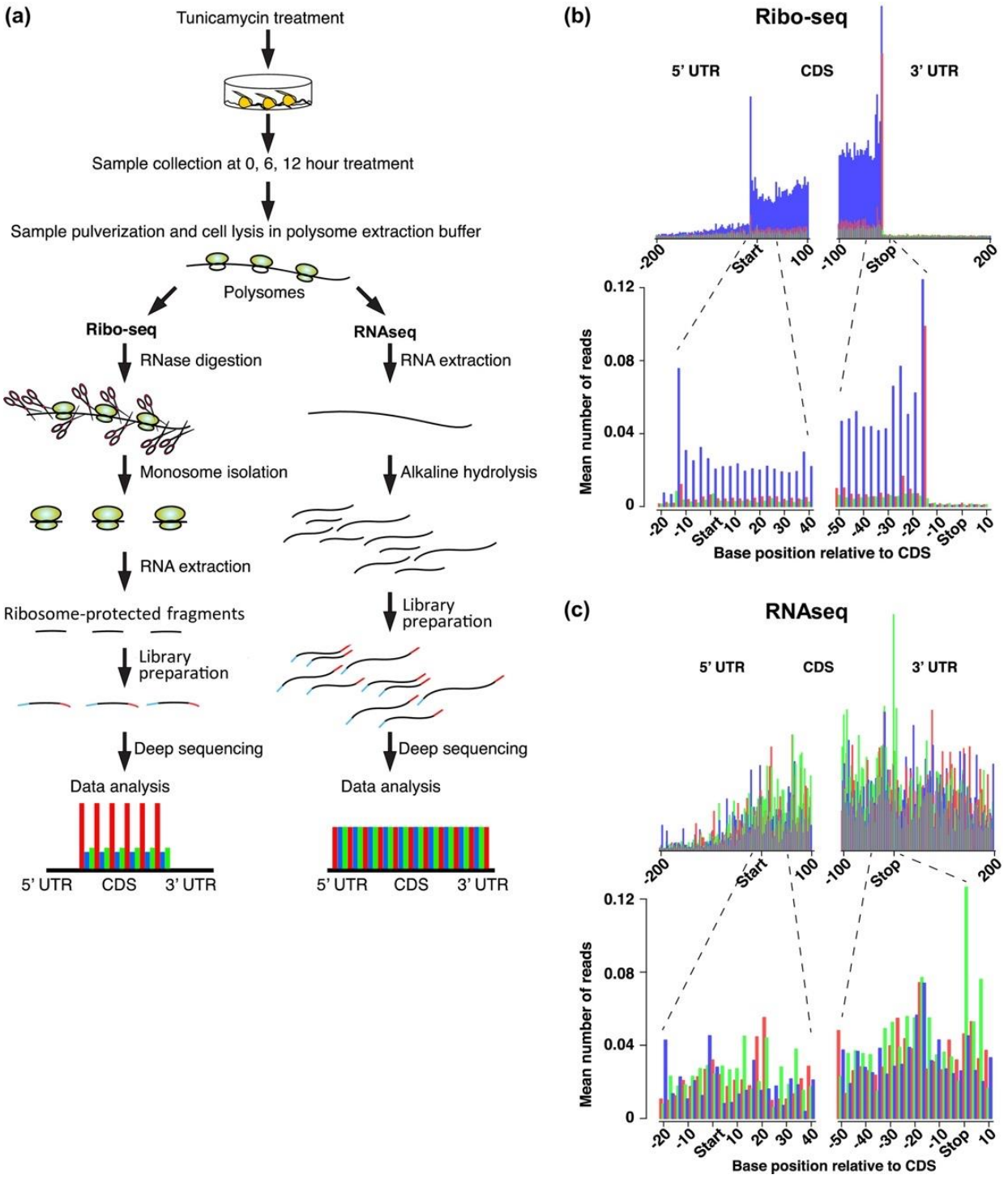

Figure 5.2. Use of riboprofiling to assess translation efficiency. **(a)** Ribosome profiling schematics shows the procedures for performing ribo-seq and RNAseq analysis. **(b)** Metagene analysis conducted for quality control of the ribo-seq analysis. Upper profile is a view of the number of reads in the 5′ and 3′ regions of the coding sequences (CDS) and the 5′ and 3′ UTRs for all genes in the analysis, and the lower profile is an expanded view of the 5′ and 3′ regions of the coding sequences. Profiles are plots of the mean number of ribosome-protected fragments (RPFs) at various positions along expressed maize genes. RPFs exhibit a triplet periodicity reflecting the saltatory movement of ribosomes during translation. Bar

colors correspond to the position in each codon to which the 5′ end of each RPF maps. Alignment of the 5′ ends of the 30 nt RPFs with respect to the base positions of the coding sequence (CDS). Higher peaks indicate ribosome pause sites. **(c)** Metagene analysis of the RNAseq data in which the mean number of total RNA reads are plotted at various positions along expressed maize genes. Alignment of the 5′ ends of the 30 bp cDNAs from the RNAseq analysis with respect to the base positions of the CDS. Neither the condensed (upper) nor the expanded (lower) profiles show, as expected, triplet periodicity as in the RPFs.

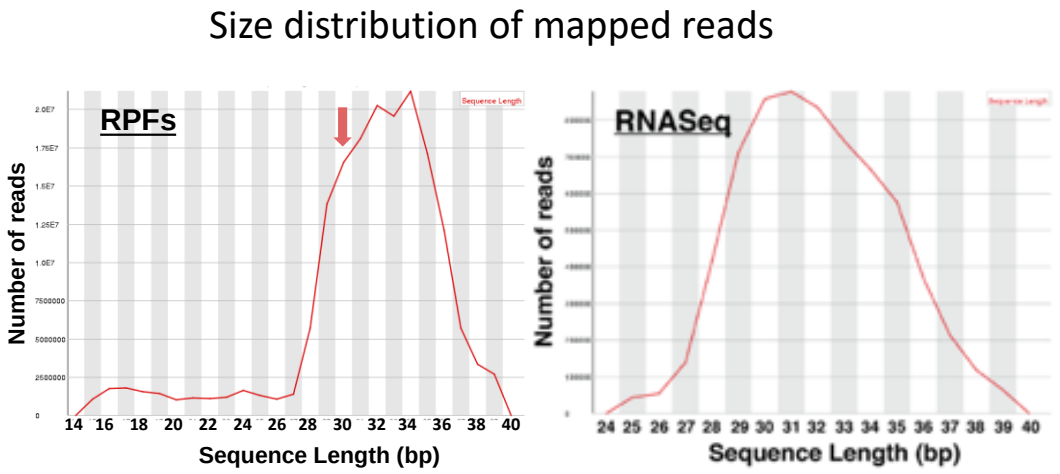

Figure 5.3. Size distribution of mapped reads in the riboseq and RNAseq analyses. Mean cDNA sequence length was 32-34 bp with a shoulder at ~30 bp for the ribosome-protected fragments (RPFs) and about 31bp for the fragmented cDNAs in the RNAseq analysis.

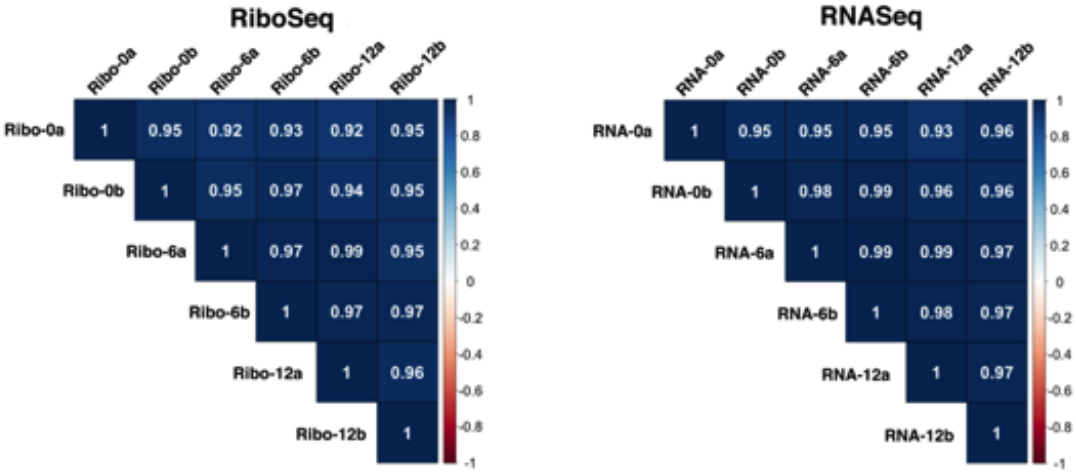

Figure 5.4. Pearson correlation coefficients between replicates. Duplicate samples at the three timepoints for riboseq and RNAseq analyses were compared.

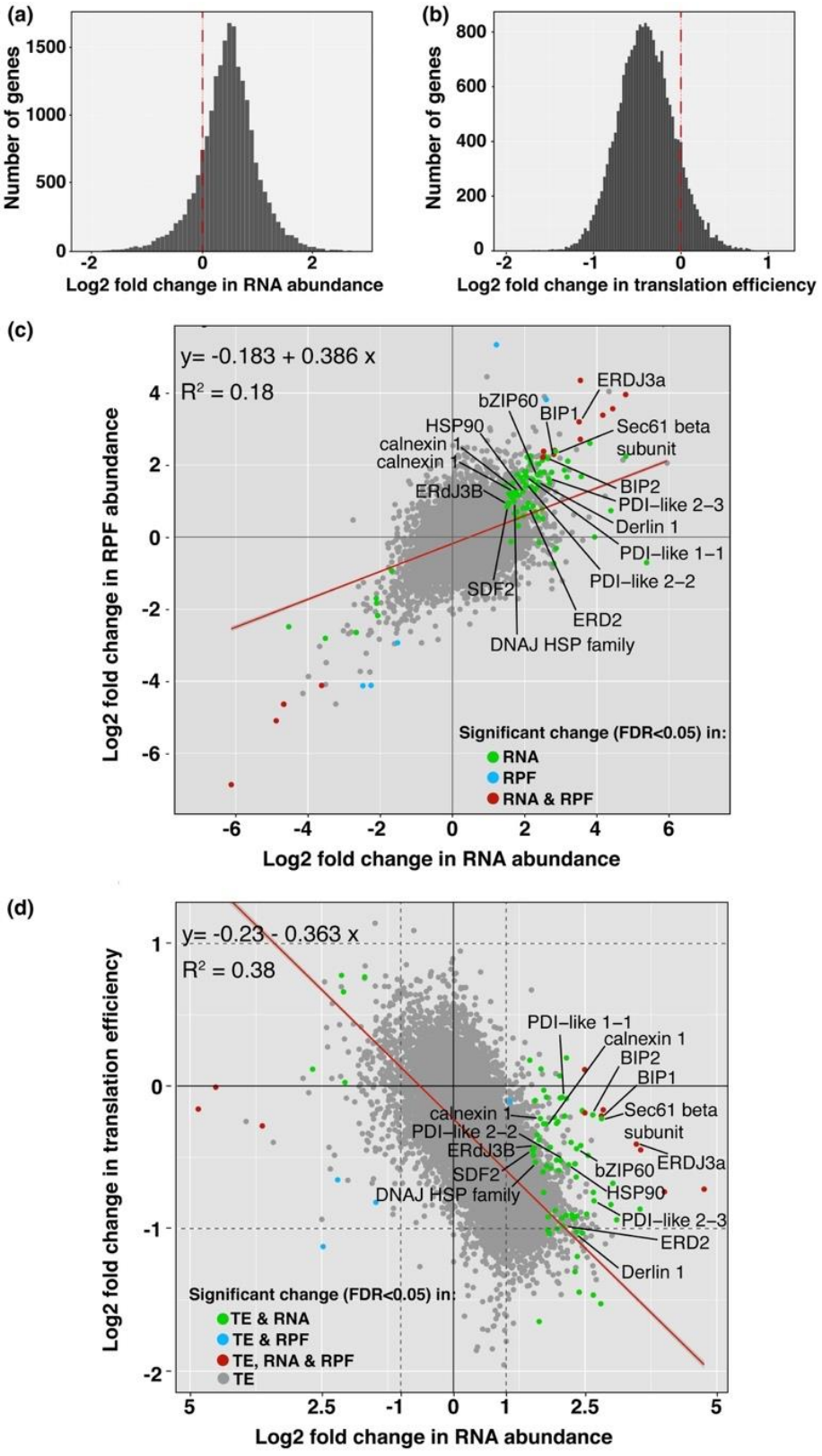

Figure 5.5. Change in RPF abundance and translation efficiency in response to ER stress. **(a)** Graph shows that the log2 fold change in RNA abundance for many genes increases at 12 hr post TM treatment

compared to 0 hr. **(b)** Plot of log2 fold change in translation efficiency. Translation efficiency is the ratio of the abundance of RPFs to RNAs. **(c)** Scatterplot comparing the log2 fold change in RPF abundance versus the log2 fold change in RNA abundance for all the genes indicated with gray dots. UPR genes with significant changes in RNA abundance are highlighted with green dots. Red line is the regression line for which the coefficient of determination is shown. Other colored dots as indicated. **(d)** Scatterplot comparing the log2 fold change in translation efficiency versus the log2 fold change in mRNA abundance. Genes marked with green dots are canonical UPR genes with significant changes in translational efficiency and changes in RNA abundance. Many of these genes tend to have abundant RNAs, but are more downregulated in translation efficiency than the vast majority of other genes. Red line is the regression line for which the coefficient of determination (R^2) is shown. Other colored dots as indicated. ER, endoplasmic reticulum; UPR, unfolded protein response.

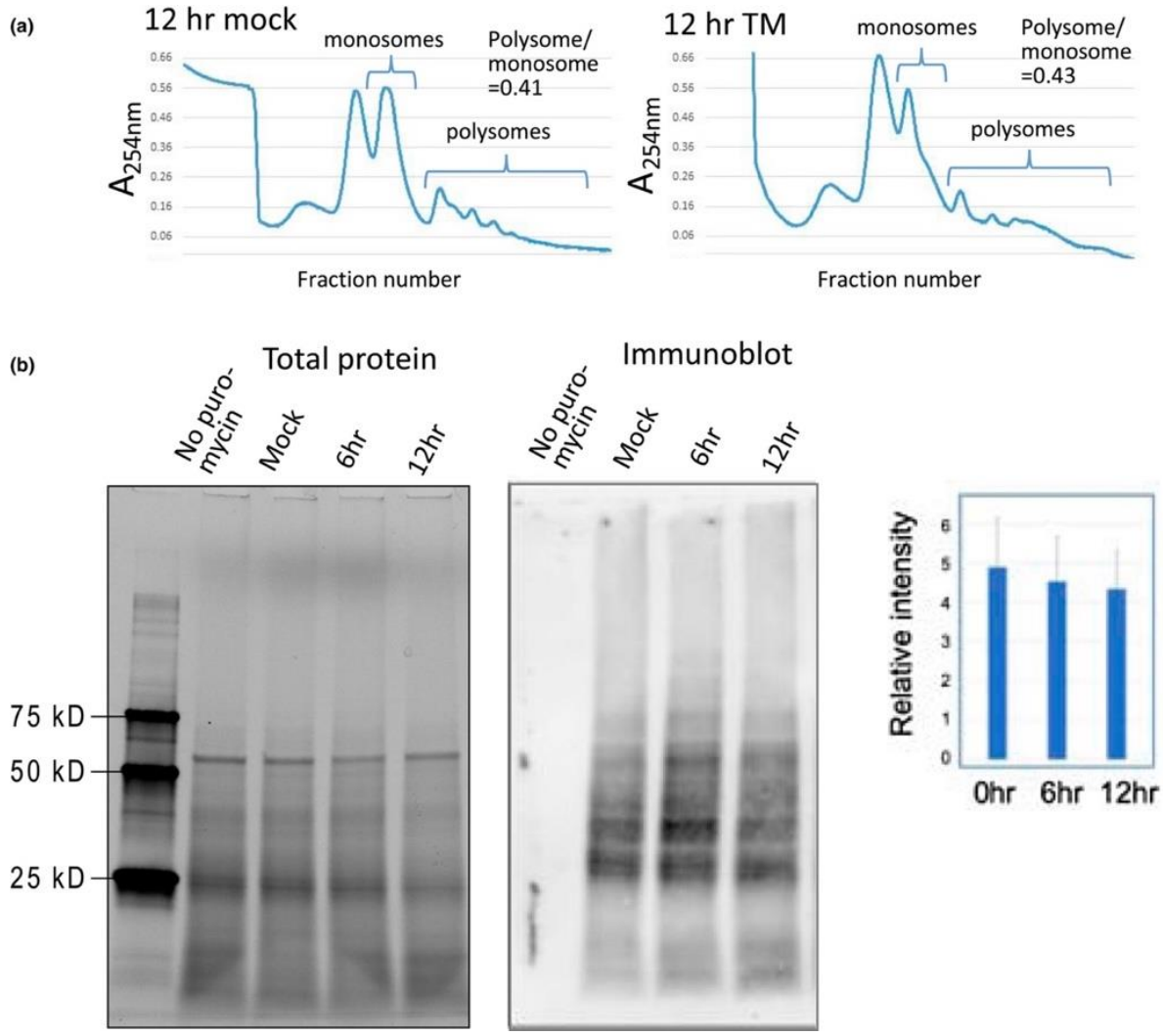

Figure 5.6. Assessments of rates of global protein synthesis. **(a)** Polysomes were profiled to ascertain whether there are global changes in the initiation rate of protein synthesis in the roots of TM treated seedlings. A decline in initiation rate would lead to a reduction in the ratio of polysomes to monosomes. Profiles from 25% to 65% sucrose density gradients show little difference between 12 hr mock and TM-

treated samples. Typical profiles are shown from over 10 gradients analyzed. **(b)** SUnSET assay to assess whether there are changes in rates of protein synthesis following TM treatment in seedlings. In this assay, protein synthesis is terminated and nascent proteins tagged with puromycin. Extracts from treated seedling roots are subjected to gel electrophoresis and immunoblotted with an antibody to puromycin. Bar graph shows the result of integrating the areas under the curves of densitometer scans for the different lanes of the immunoblots in five biological replicates of this experiment. Total protein bands are visualized by trihalo fluorophores in the gel that in the presence of UV light become covalently bound to the proteins, which can be visualized after transfer to membranes. Error bars are SD, n = 5.

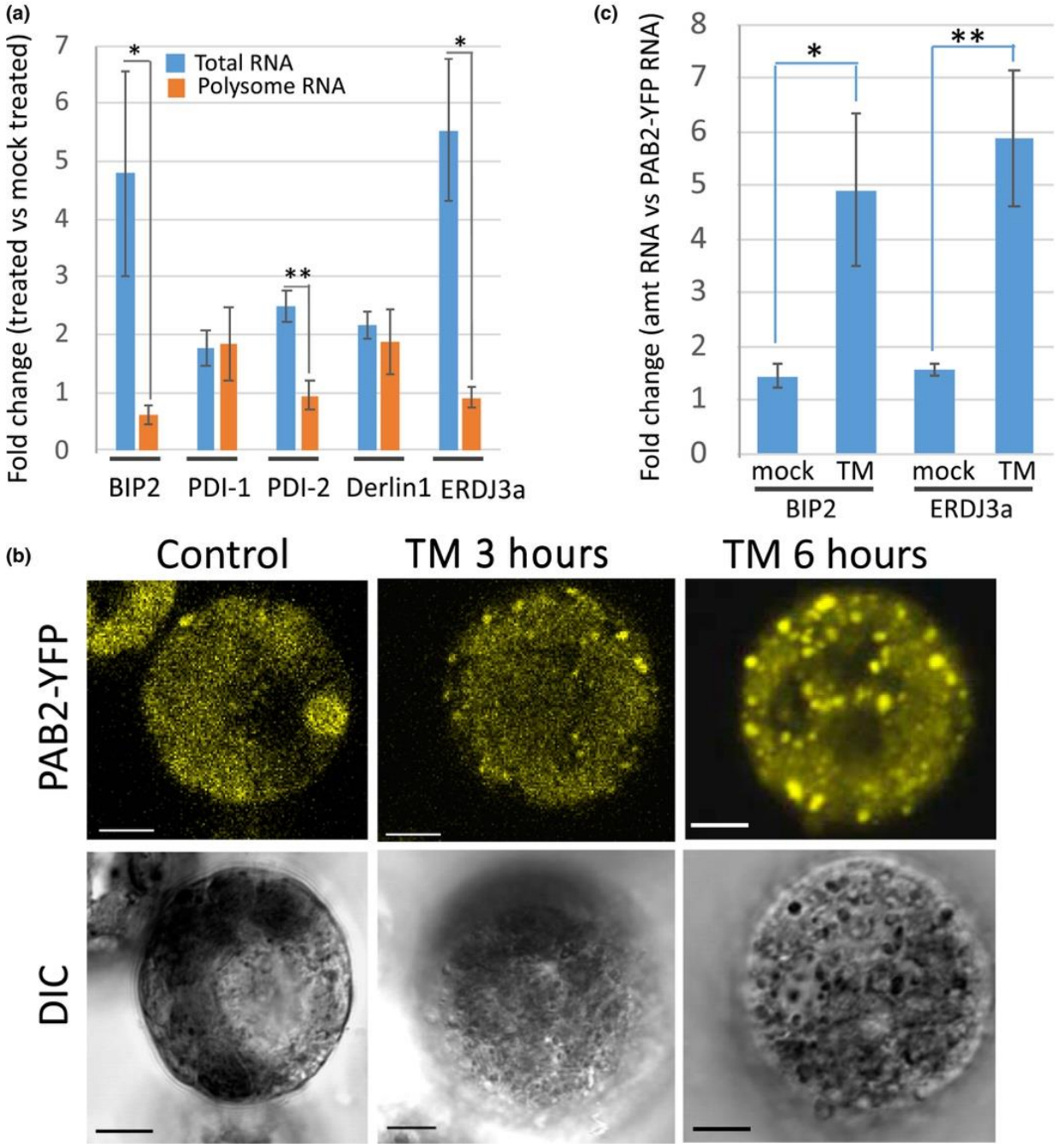

Figure 5.7. Disposition of UPR gene transcripts following ER stress treatment. **(a)** Presence of canonical UPR gene RNAs in total RNA and polysomes. Polysomes from seedling roots untreated or treated with TM for 12 hr were fractionated on sucrose density gradients. RNA was extracted from the polyribosome fractions and analyzed by qRT-PCR. Data are presented as the fold change in RNA levels in fractions from TM-treated versus mock-treated plants. Bars represent the means of the fold changes from three biological reps. BIP2 (Zm00001d014993), PDI-1 (Zm00001d04099), PDI-2 (Zm00001d005866), Derlin 1 (Zm00001d010368), ERDJ3a (Zm00001d047726). Error bars = SEs. Asterisks indicate significance as determined by Student's T test. **(b)** Confocal images of maize leaf protoplasts transfected with the SG marker, PolyA binding protein 2-YFP (PABP2-YFP). Protoplasts were treated with TM and photographed at times indicated. DIC = Differential Interference Contrast

microscopy. Bar = 10µ. **(c)** Canonical UPR gene RNAs found in SG-enriched fractions from untreated and 6 hr TM-treated protoplasts. qRT-PCR analysis of RNA extracted from triplicated SG-enriched fraction samples. The cDNAs synthesized from the extracted RNA were spiked with equal amounts of recombinant PAB2-YFP in order to compare RNA amounts in the treated and untreated samples. The qRT-PCR results were expressed in terms of fold change (FC) over PAB2-YFP mRNA. Error bars = SE. Asterisks indicate significance as determined by Student's t test. *Represents $p < .05$ and **represents $p < .01$. ER, endoplasmic reticulum; SG, stress granule; UPR, unfolded protein response.

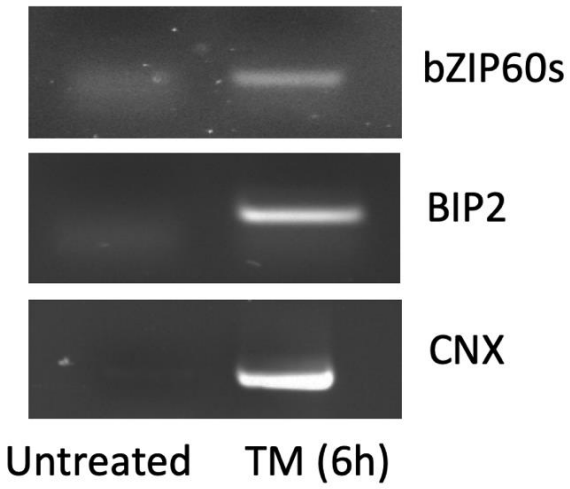

Figure 5.8. UPR canonical gene expression in maize leaf protoplasts as analyzed by RT-PCR in untreated versus 6 hr TM-treated protoplasts.

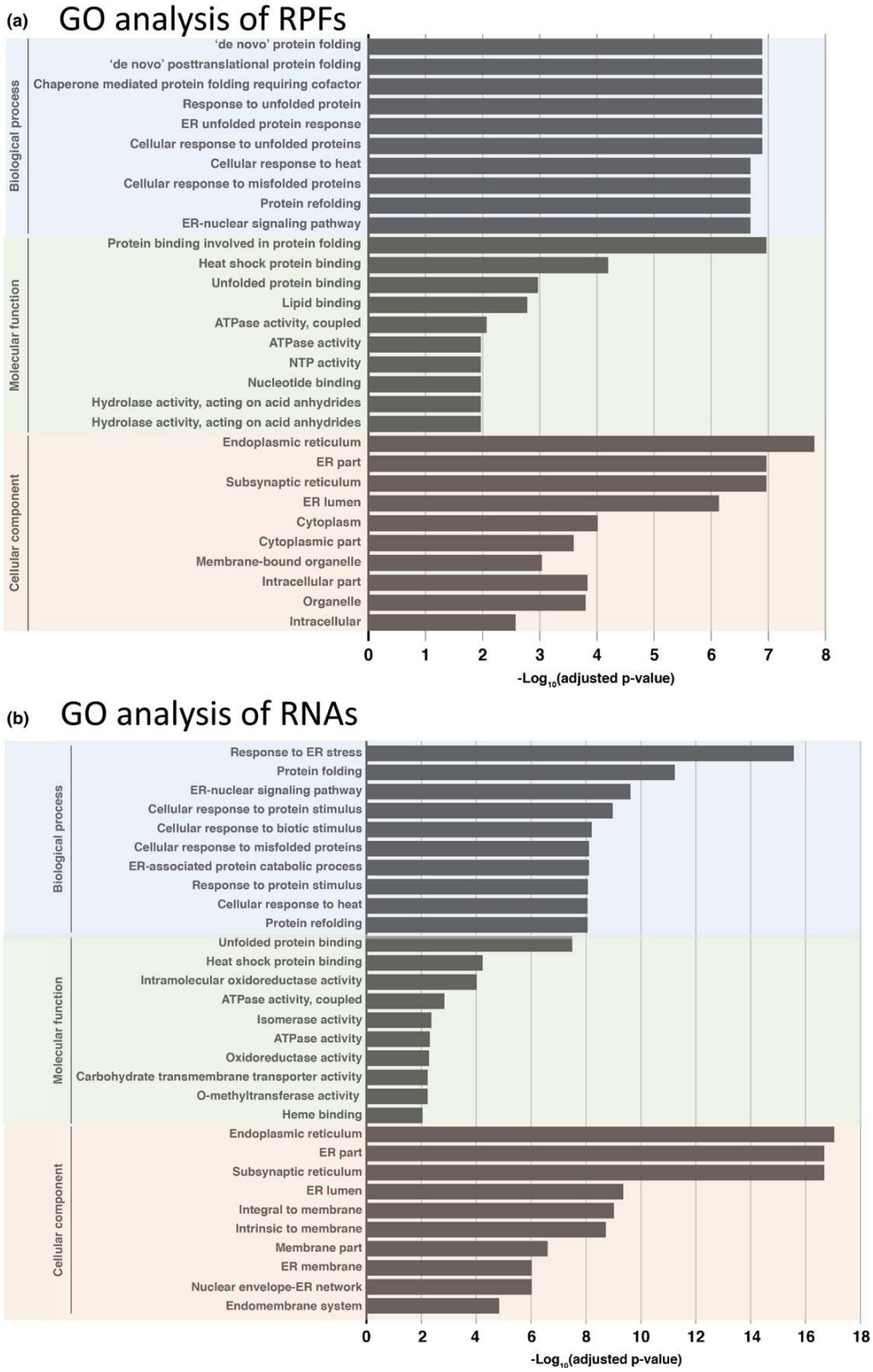

Figure 5.9. Gene ontology (GO) analysis of the RNAs and RPFs following TM treatment. **(a)** GO analysis of RPFs and **(b)** total RNA at 12 hr after TM treatment. GO analysis was conducted using AgriGO (http://bioinfo.cau.edu.cn/agriGO/) for the categories biological process, molecular function, and cellular component.

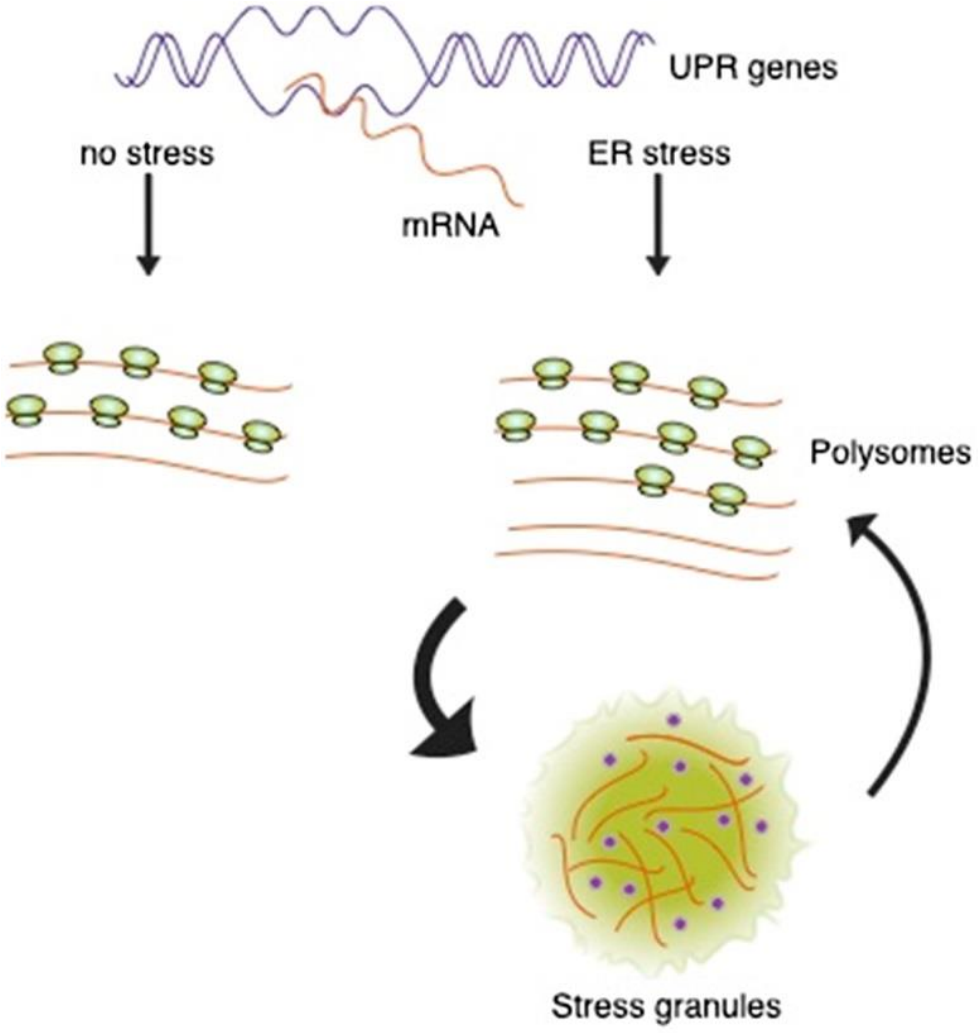

Figure 5.10. Model for the fate of RNA transcripts in response to ER stress. In response to ER stress, there is a surge in transcription which leads to an accumulation of transcripts from UPR genes, not all of which are immediately loaded onto polysomes. The untranslated RNAs drive the formation of stress granules which sequester the RNAs and other RNA-binding proteins (blue dots). With time and dissolution of stress granules, the sequestered RNAs may be progressively liberated to enter the translation pool. ER, endoplasmic reticulum; UPR, unfolded protein response.

Tables

Table 5.1. Sequence of primers used in RT-qPCR.

Primer	**Sequence (5'----3')**
BIP2 F	GTCGGAGAAGATCACGATCAC
BIP2 R	CTTCACCTTCTTGTCCTCCTC
PDI 1-1 F	GTCGCTTGGTTGAAGGAGTA
PDI 1-1 R	CACCTTAACAGGCTCATTGTTG
PDI 2-3 F	GCAAGTACAAGGTGGAAGG
PDI 2-3 R	CCAACTGCTCCAATGCAAAG
Der F	TGGTGCCATCTCACTATTGG
Der R	CTCTCGGCTCCAGACAT
ERD F	GGCCCGTCTCTTCATCTATTC
ERD R	TACCCGTTTGGAGAATCTTGG
Tub F	CTACACCATTGGCAAGGAGAT
Tub R	CCTGGAGACCAGTGCAATTAT
Ubi F	ATCTTCGTGAAGACGCTGAC
Ubi R	GATGCCTTCCTTGTCCTGTATC
PAB2FpAsc	gaaggcgcgccATGGCGACGCAAGGGCAAGC
PAB2RpXba	agtctagaGCTGGAGACGACGCCATCATT

CHAPTER 6. GENERAL CONCLUSIONS

"Civilization as it is known today could not have evolved, nor can it survive, without an adequate food supply. Yet food is something that is taken for granted by most world leaders despite the fact that more than half of the population of the world is hungry." (Norman Borlaug, Nobel Lecture, December 11, 1970)

Plants are continually subjected to an array of biotic and abiotic stresses, such as drought, extreme temperatures, pathogen attack, and pest infestations, among several others. The loss in agricultural productivity due to these stressors will be exacerbated by increasing climate change, which will threaten global food security (1–6). To add to this, the inequality in food distribution across the world mainly affects the under-developed and the developing countries where the population does not even get the basic nutrients to sustain a healthy life (7–9). The underfed and malnourished population are at a higher risk of developing different diseases and disorders (10–15). Therefore, tackling plant diseases can have a significant impact on the overall health of the human population. To do that, we require a comprehensive understanding of the intricate and interconnected mechanisms by which a plant responds to different stressors.

This dissertation encompasses different aspects of a multifaceted research in which I (i) developed a novel assay to detect viral subgenomic (sg)RNAs, (ii) explored the effects of exoribonuclease-resistant (xr)RNA-derived viral noncoding (nc)sgRNAs on the plant's transcriptome, and (iii) investigated how virus infection and unfolded protein response can transcriptionally and translationally affect the plant's cellular gene expression.

In *Chapter 2*, we demonstrated the application of DeSCo-PCR for the specific and quantitative detection of the RCNMV SR1f and ZIKV sfRNA (16). Depending on the research

objective, DeSCo-PCR can be used as a substitute for northern blot hybridization. Because DeSCo-PCR is an RT-PCR-based approach, it has several advantages over northern blots: (i) DeSCo-PCR is simple and does not require any special training. (ii) Number of steps in the DeSCo-PCR protocol is substantially fewer than in the northern blot protocol. Therefore, it is labor-effective and saves hands-on time and the total experiment time. (iii) DeSCo-PCR does not require the use of hazardous formaldehyde gels or radiolabeled probes. Compared to the non-radioactive northern blots, DeSCo-PCR is even quicker and cheaper. (iv) Because PCR is more sensitive, the amount of input RNA required for DeSCo-PCR is much less than northern blots.

In *Chapter 3*, we assessed the role of the xrRNA-derived ncsgRNA of RCNMV, called SR1f, during infection. In *Nicotiana benthamiana* and Arabidopsis plants, wildtype (wt) RCNMV RNAs always accumulated to higher levels than the mutant RCNMVΔSR1f RNAs. Unsurprisingly, symptoms were observed only in wt RCNMV-infected *N. benthamiana* and *dcl2-1/dcl4-2t* Arabidopsis. Because RNA silencing is a major antiviral defense pathway in plants, we tested if SR1f can function as a suppressor of RNA silencing. However, the Arabidopsis loss-of-function mutant *dcl2-1/dcl4-2t*, which lacked functioning RNA silencing machinery, was unable to rescue the replication of RCNMVΔSR1f to wt RCNMV levels, lending to the conclusion that the primary function of SR1f is something other than RNA silencing suppression. We also determined that XRN4, which is the only known cytoplasmic 5'→ 3' exoribonuclease in plants and widely assumed to be responsible for generating xrRNA-derived RNAs (17–20), is not required for the production of SR1f. It is possible that a yet-unidentified cytoplasmic 5'→ 3' XRN exists in plants that makes SR1f or the other 5'→ 3' XRNs (which are presumed only to be nuclear-localized) have redundant functions and can make SR1f in the

absence of XRN4. Because of the lack of a system to disrupt SR1f production from wt RCNMV RNA1, we were unable to attribute our findings to the specific role(s) of SR1f. The six-base substitution in the RCNMV RNA1 mutant (RNA1-m1) that we used for our study may have had some pleiotropic effects. However, we did not find biologically meaningful differences in RNA1 and RNA1-m1 translation *in vitro* in wheat germ extract. Furthermore, the comparative transcriptomic analysis using RCNMV-infected *N. benthamiana* revealed many cellular pathways that were only disrupted in wt RCNMV-infected plants. As expected, a larger number of genes was differentially expressed in wt RCNMV-infected plants that included many defense-related genes such as PR genes and LRR-RLK/RLPs, almost all of which were not expressed in RCNMVΔSR1f-infected plants.

In *Chapter 4*, we investigated the transcriptional and translational control of gene expression in RCNMV-infected *dcl2-1/dcl4-2t* Arabidopsis plants. From a time-course qRT-PCR assay, we determined that the RCNMV RNA 1 accumulation in the systemic non-inoculated leaves increased steeply at 6/7 dpi, which correlated with the appearance of symptoms. Accordingly, we chose 5 dpi as an early time-point, which reflects the pre-symptomatic phase, and 8 dpi as the late time-point, which reflects the late symptomatic phase of the infection. We collected systemic leaves of RCNMV-infected Arabidopsis plants at these two time-points for ribosome profiling (Ribo-seq) and RNA sequencing (RNA-seq) to assess the differential regulation of host and viral gene expression at the level of transcription and translation. We demonstrated the high-quality and reproducibility among the replicates for the Ribo-seq and RNA-seq data. We identified the list of differentially expressed (DEGs) and/or translated (DTGs) genes in RCNMV-infected plants. We determined that at 5 dpi, DTGs were specific to the plant innate immune responses, unlike at 8 dpi, when the DTGs included several

cellular pathways that were regulated or dysregulated during infection. At 8 dpi, we determined that several canonical UPR genes, such as BiP3, were transcriptionally upregulated in RCNMV-infected plants signifying the elicitation of unfolded protein response (UPR). Because RCNMV replicates at the ER membrane, UPR may serve as a proviral mechanism to increase the ER membrane surface area and improve the protein folding capacity of the cell.

We also analyzed the Ribo-seq and RNA-seq reads that mapped to the RCNMV genome. We found that at 5 dpi, even though the RCNMV RNA abundance and the ribosome-protected fragments (RPFs) derived from those constituted only a small percentage of total mapped reads, the viral proteins were synthesized (which depends on mRNA abundance and the translation efficiency of the mRNA) at a much higher rate than the majority of individual Arabidopsis proteins. By 8 dpi, RCNMV RNAs were the most prominent RNAs in the cell. Even though only a fraction of RCNMV RNAs (based on the number of RNA-seq and Ribo-seq reads and the proportion of Ribo-seq reads with respect to total mapped Ribo-seq reads) were being translated, RCNMV proteins were synthesized at a much higher rate than any other Arabidopsis protein. We also assessed the coverage of RNA-seq and Ribo-seq reads across RCNMV genome which correctly identified the annotated RCNMV ORFs. Ribo-seq read coverage across RCNMV RNA1 demonstrated the translation of RdRp domain-containing p88 protein via -1 programmed ribosomal frameshifting. We also found that the frameshifting efficiency increased from ~8% at 5 dpi to ~16% at 8 dpi. Additionally, we identified many similar RNA-seq coverage characteristics that we observed in *Chapter 2*, especially the peculiar profile over RNA2. Lastly, a putative ribosomal pause site in the movement protein ORF of RNA2 downstream of the trans-activator (TA) sequence was also identified.

In *Chapter 5*, we explored if and how translation is regulated during the UPR in maize roots. It is well known that the conserved PERK-dependent pathway of the UPR attenuates the translation initiation globally in mammalian cells by phosphorylating eIF2α (21). However, PERK is absent in the plant system (22). So, is there a global translation inhibition in plants during the UPR? To answer this, we used ribosome profiling in ER-stressed maize roots and found a modest decrease in the translation efficiency of some cellular mRNAs (23). However, we found no global inhibition of translation initiation and a very slight decrease in the translation rate, as assessed by polysome profiles and SUnSET assay, respectively. We observed a surge in the abundance of UPR-responsive mRNAs without a concomitant increase of RPFs from those mRNAs. Consistent with this observation, even though the UPR-responsive mRNA abundance increased in the total RNA fraction during UPR, the increase was not observed in the polysome fraction. We hypothesized that the reduced translation efficiency (ratio of RPF abundance to RNA abundance) occurred because of increased transcription of UPR-responsive mRNAs from which not all of the newly transcribed mRNAs engaged the translation machinery. We detected some of these UPR-responsive mRNAs in stress granules that are formed during the UPR. Therefore, we propose that during UPR, there is an increase in the transcription of UPR-responsive genes, from which subpopulation of mRNAs get sequestered into stress granules to maintain the low protein-folding load on the ER but are released back to the cytoplasm for immediate translation according to the cellular needs.

Future directions and perspectives

Simultaneous visualization of viral gRNA and sgRNAs *in situ*

DeSCo-PCR and northern blots can detect the presence of sgRNAs in infected cells. But, what about the subcellular localization of sgRNAs? Localization of viral RNAs and proteins can

have important implications on the virus life cycle (24–33). Even though many methods exist that can be used to detect the subcellular localization of viral proteins and gRNAs (34–40), sgRNA localization cannot be distinguished from the gRNA for the same reason why the conventional two-primer RT-PCR cannot be used for specific detection of sgRNAs *(Chapter 2).*

Here, I hypothesize that the principle of DeSCo-PCR can be utilized to develop assays for simultaneous detection of gRNA and multiple sgRNAs at their sites of localization. For example, RNA localization can be detected *in situ* by using padlock probes that circularize by ligation only when they anneal to the template. Subsequently, the circular probe undergoes rolling circle amplification (RCA) and the fluorophore-tagged probes can hybridize to the circular probe-derived amplicon and be detected via fluorescence microscopy (41, 42). In this case, padlock probes can be designed that can anneal to the 5' end of the sgRNA *(Fig. 6.1-A, padlock probe B).* Additionally, a blocking oligo, which can anneal to the gRNA at the same sequence that the padlock probe B can anneal to and several nucleotides upstream of that sequence, can be designed *(Fig. 6.1-A).* Therefore, the blocking oligo would prevent the annealing of padlock probe B to the gRNA-derived template whereas it would not prevent the annealing of padlock probe B to the sgRNA *(Fig. 6.1-A).* Thus, there will not be any RCA because of the presence of the gRNA *(Fig. 6.1-A).* However, the padlock probe B would anneal to the sgRNA-derived template, circularize, and initiate the RCA that can be tagged via the fluorophore-probe and detected via fluorescence microscopy *(Fig. 6.1-A).* Another set of padlock probes *(Fig. 6.1-A, padlock probe A)* that would only anneal to gRNA can be used simultaneously, and the resulting amplicon from its RCA could be hybridized to another fluorophore-bound probe *(Fig. 6.1-A).* This could, in theory, enable the researchers to detect multiple coterminal RNAs simultaneously.

Another hypothetical approach is to use a reporter-quencher system where a 3'-tagged reporter probe would anneal to the 5' end of the sgRNA and the same sequence in the gRNA *(Fig. 6.1-B)*. In contrast, a 5'-tagged quencher probe would anneal only to the gRNA just upstream of the region where the reporter probe anneals *(Fig. 6.1-B)*. This approach would result in the quenching of the fluorescence from the reporter probe that anneals to the gRNA whereas the reporter that anneals to sgRNA would continue to fluoresce *(Fig. 6.1-B)*. An additional reporter probe with a different fluorophore can be used that would anneal only to the gRNA and therefore, enable the researchers to detect multiple coterminal RNAs simultaneously *(Fig. 6.1-B)*. However, because this technique is based on fluorescence of one reporter molecule per target molecule, unlike the padlock-probe-based method, it may not have sufficient sensitivity. We speculate that other techniques, such as ampFISH (38), RNAscope (36), etc., could also be adapted for specific detection of sgRNA localization.

Regulation of viral and cellular translation by SR1f

The 3' cap-independent translation element (3' CITE) in the 3 'UTR of RCNMV RNA1, called 3'TE-DR1, which belongs to the BYDV-like translation element (BTE) class of 3' CITEs, binds to the cellular eIF4G for recruitment of translational machinery to RNA1 (43–47). Because RCNMV SR1f, which contains the 3'TE-DR1, accumulates in RCNMV-infected cells, it is hypothesized that SR1f can sequester translation initiation factors and differentially regulate the translation of different RCNMV ORFs and cellular RNAs (48, 49). Using reporter assays, it has been shown previously that SR1f suppresses both cap-dependent and cap-independent translation *in vitro* and *in vivo* (48). However, whether the translation of cellular mRNAs is regulated by SR1f in infected cells has not been investigated. One of my initial objectives included the use of Ribo-seq in plants infected with wt RCNMV (which makes SR1f) and mutant

RCNMV (which does not make SR1f) to investigate the effects of SR1f on cellular and viral mRNA translation. However, I was unable to pursue that experiment because of the following reasons: (i) The mutant, RNA1-m1, and the other SR1f-deficient mutants (48), accumulate to lower levels than wt RCNMV RNAs. Therefore, it was not possible to determine whether the observed difference in translation was because of SR1f or because of differential accumulation of RCNMV, (ii) RNA-m1 did not replicate in wt Arabidopsis and replicated inconsistently in *dcl2-1/dcl4-2t* mutant Arabidopsis. Therefore, for Ribo-seq, another plant system is required in which the mutant RCNMV can replicate to wt RCNMV levels. I considered *N. benthamiana* for the Ribo-seq experiment but because of the poorly annotated genome of *N. benthamiana* and other reasons pointed out above, I decided it would be futile at this moment to conduct Ribo-seq with mutant RCNMV-infected plants. Therefore, for studying the effects of SR1f on the host and viral translation, a system with a well-annotated genome is required in which (i) mutant RCNMV replicates to wt RCNMV levels, and (ii) we can regulate the production of SR1f. An alternative option would be to express replication-deficient (i) RCNMV RNA1 or (ii) RNA1-m1 either via Agrobacterium-mediated transformation or via transgenic Arabidopsis plants. Because the expressed RNA would be transcribed in the nucleus, it would consist of a 5' cap that may affect the generation of SR1f. Therefore, a cis-hammerhead ribozyme at the 5' end of the RNA could be used that would cleave itself and the 5' cap from the expressed RNA. However, this will result in an RNA with a hydroxyl group at the 5' end (50–52). Because the preferential substrate for the 5'→ 3' exoribonuclease is 5' monophosphorylated RNA (53, 54), it needs to be tested if the proposed construct, which will yield a 5' hydroxylated RNA, would result in the production of SR1f *in vivo* from the replication-deficient RNMV RNA1. If the proposed

construct works, this system could be used for Ribo-seq to assess if the presence of SR1f affects the cellular mRNA translation.

xrRNA structure as a biotechnological tool

xrRNAs can increase the stability of the downstream RNA region by protecting it from 5' to 3' degradation (18–20, 48, 55–72). Therefore, it seems like an obvious tool that can be utilized to increase the stability of transiently- or transgenically-expressed RNAs in an organism. Recently, an RNA structure, different from the xrRNA, was identified in the carnation Italian ringspot virus (CIRV) (73). It is called exoribonuclease-evading (xe)RNA. In contrast to the xrRNAs that can stall the progression of 5'→ 3' XRN, xeRNAs can limit the access of 5'→ 3' XRN to the 5' end of an RNA. However, once the 5'→ 3' XRN starts digestion, xeRNA cannot block it (73). The combination of xeRNA and xrRNAs can be a valuable tool for a more stable transgene expression. However, more research is needed to understand the impact of xeRNAs and xrRNAs on the cellular pathways.

Investigate translationally-regulated genes (DTGs) in RCNMV-infected Arabidopsis plants

The length and nucleotide composition of the 5' UTR and the cis-acting elements in the UTRs of an mRNA have been shown to have a profound influence on mRNA translation (74–81). For example, (i) RNA hairpin structures in the 5' UTR of PIF7, WRKY22, and HSFA2 mRNAs in Arabidopsis regulate the translation of these mRNA in response to high temperatures (82), (ii) an uORF in the 5' UTR of AtbZIP11 mRNA in Arabidopsis represses the translation of the main ORF in a sucrose-dependent manner (83), (iii) Poly(U) motifs in the 3' UTR of EBF1 and EBF2 mRNAs subject these mRNAs to EIN2-mediated translation repression (84, 85).

Therefore, one of our future goals is to investigate the UTRs of the mRNAs that are regulated translationally during RCNMV infection *(Chapter 4)* and explore the mechanisms by which translational regulation occurs.

Dissect the coverage of Ribo-seq and RNA-seq reads on RCNMV RNA2

We identified a putative ribosomal pause site in RNA2 via Ribo-seq *(Chapter 4)*. We also observed a peculiar coverage profile of RNA-seq reads across RNA2 in RCNMV- infected *N. benthamiana (Chapter 3)* and RCNMV-infected Arabidopsis plants *(Chapter 4)*. Considering these results together, we hypothesize that there is an authentic pause site in the MP ORF of RNA2, and because of the ribosome pausing or stacking at the pause site, RNA2 undergoes No-Go decay (86, 87). This hypothesis would explain the peculiar pattern of RNA-seq read coverage across RNA2, sparse distribution of RPFs on RNA2, and the big RPF peak from Ribo-seq data on RNA2. Therefore, future experiments would include experimental verification of the pause site and further exploration of RNA sequence, RNA structure, codon composition, etc., at/near the pause site. Subsequently, how the ribosomal pausing on RNA2, if it exists, affects RCNMV infection would be explored.

Concluding remarks

Combinations of different high-throughput genome-wide expression studies that can dissect each layer of regulation of every expressed gene are essential for developing an interactome of pathways. These studies can provide insight into how we might modify the expression of a certain gene or a combination of genes to develop plants that can withstand, if not all, multiple abiotic and biotic stresses simultaneously. In this dissertation, I utilized two NGS techniques, RNA-seq and Ribo-seq, and a variety of molecular tools to explore (i) how

virus infection, with and without the production of ncsgRNAs, affects the plant and viral gene expression at the level of mRNA abundance, (ii) how virus infection affects the plant and viral gene expression both at the level of mRNA abundance and translation, and (iii) how unfolded protein response, which is elicited by a variety of biotic and abiotic stressors, affects plant gene expression at the level of mRNA abundance and translation. My work provides insights into the regulation of gene expression at a genome-wide level which could be utilized by future studies to dissect the mechanism(s) of gene expression regulation at the individual gene- and mRNA- level. This dissertation also provides valuable transcriptomic and translatomic data that can be subjected to rigorous exploration and analyses for the identification of novel ORFs in the plant's transcriptome. In addition, my work on DeSCo-PCR provides a principle that can be utilized for different molecular biology applications where specific detection or visualization of the smaller coterminal RNAs is, otherwise, not possible.

References

1. Luck J, Spackman M, Freeman A, Tre¸bicki P, Griffiths W, Finlay K, Chakraborty S. 2011. Climate change and diseases of food crops. Plant Pathol 60: 113–121.

2. Chakraborty S, Newton AC. 2011. Climate change, plant diseases and food security: an overview. Plant Pathol 60: 2–14.

3. Anyamba A, Small JL, Britch SC, Tucker CJ, Pak EW, Reynolds CA, Crutchfield J, Linthicum KJ. 2014. Recent Weather Extremes and Impacts on Agricultural Production and Vector-Borne Disease Outbreak Patterns. PLoS One 9: e92538.

4. Niu S, Luo Y, Li D, Cao S, Xia J, Li J, Smith MD. 2014. Plant growth and mortality under climatic extremes: An overview. Environ Exp Bot 98: 13–19.

5. Arora NK. 2019. Impact of climate change on agriculture production and its sustainable solutions. Environ Sustain 2: 95–96.

6. Anderson R, Bayer PE, Edwards D. 2020. Climate change and the need for agricultural adaptation. Curr Opin Plant Biol 56: 197–202.

7. Hossain N. 2017. Inequality, hunger, and malnutrition: Power matters, p. 24–29. In Global Hunger Index: International Food Policy Research Institute (IFPRI).

8. Wood SA, Smith MR, Fanzo J, Remans R, DeFries RS. 2018. Trade and the equitability of global food nutrient distribution. Nat Sustain 1: 34–37.

9. FAO, IFAD, UNICEF, WFP, WHO. 2019. The State of Food Security and Nutrition in the World 2019. Safeguarding against economic slowdowns and downturns. Rome, FAO.

10. Chandrasekaran P, Saravanan N, Bethunaickan R, Tripathy S. 2017. Malnutrition: Modulator of Immune Responses in Tuberculosis. Front Immunol 8: 1316.

11. Ibrahim MK, Zambruni M, Melby CL, Melby PC. 2017. Impact of Childhood Malnutrition on Host Defense and Infection. Clin Microbiol Rev 30: 919–971.

12. Yan X, Zhao X, Li J, He L, Xu M. 2018. Effects of early-life malnutrition on neurodevelopment and neuropsychiatric disorders and the potential mechanisms. Prog Neuro-Psychopharmacology Biol Psychiatry 83: 64–75.

13. Farhadi S, Ovchinnikov R. 2018. The relationship between nutrition and infectious diseases: A review. Biomed Biotechnol Res J 2: 168.

14. Campisano S, La Colla A, Echarte SM, Chisari AN. 2019. Interplay between early-life malnutrition, epigenetic modulation of the immune function and liver diseases. Nutr Res Rev 32: 128–145.

15. Siddiqui FJ, Belayneh G, Bhutta ZA. 2021. Nutrition and Diarrheal Disease and Enteric Pathogens, p. 219–241. In Humphries, D, Scott, M, Vermund, S (eds.), Nutrition and Infectious Diseases. Nutrition and Health. Humana, Cham.

16. Kanodia P, Prasanth KR, Roa-Linares VC, Bradrick SS, Garcia-Blanco MA, Miller WA. 2020. A rapid and simple quantitative method for specific detection of smaller coterminal RNA by PCR (DeSCo-PCR): application to the detection of viral subgenomic RNAs. RNA 26: 888–901.

17. Flobinus A, Hleibieh K, Klein E, Ratti C, Bouzoubaa S, Gilmer D. 2016. A Viral Noncoding RNA Complements a Weakened Viral RNA Silencing Suppressor and Promotes Efficient Systemic Host Infection. Viruses 8: 272.

18. Flobinus A, Chevigny N, Charley PA, Seissler T, Klein E, Bleykasten-Grosshans C, Ratti C, Bouzoubaa S, Wilusz J, Gilmer D. 2018. Beet necrotic yellow vein virus noncoding rna production depends on a 5 ′ →3 ′ xrn exoribonuclease activity. Viruses 10: 137.

19. Gunawardene CD, Newburn LR, White KA. 2019. A 212-nt long RNA structure in the Tobacco necrosis virus-D RNA genome is resistant to Xrn degradation. Nucleic Acids Res 47: 9329–9342.

20. Ilyas M, Du Z, Simon AE. 2021. Opium Poppy Mosaic Virus Has an Xrn-Resistant, Translated Subgenomic RNA and a BTE 3′ CITE. J Virol 95: e02109-20.

21. Harding HP, Calfon M, Urano F, Novoa I, Ron D. 2002. Transcriptional and Translational Control in the Mammalian Unfolded Protein Response. Annu Rev Cell Dev Biol 18: 575–599.

22. Howell SH. 2013. Endoplasmic Reticulum Stress Responses in Plants. Annu Rev Plant Biol 64: 477–499.

23. Kanodia P, Vijayapalani P, Srivastava R, Bi R, Liu P, Miller WA, Howell SH. 2020. Control of translation during the unfolded protein response in maize seedlings: Life without PERKs. Plant Direct 4: e00241.

24. Somasundaran M, Zapp ML, Beattie LK, Pang L, Byron KS, Bassell GJ, Sullivan JL, Singer RH. 1994. Localization of HIV RNA in mitochondria of infected cells: potential role in cytopathogenicity. J Cell Biol 126: 1353–1360.

25. Más P, Beachy RN. 1999. Replication of Tobacco Mosaic Virus on Endoplasmic Reticulum and Role of the Cytoskeleton and Virus Movement Protein in Intracellular Distribution of Viral RNA. J Cell Biol 147: 945–958.

26. Miller S, Krijnse-Locker J. 2008. Modification of intracellular membrane structures for virus replication. Nat Rev Microbiol 6: 363–374.

27. Donnelly CJ, Fainzilber M, Twiss JL. 2010. Subcellular Communication Through RNA Transport and Localized Protein Synthesis. Traffic 11: 1498–1505.

28. den Boon JA, Ahlquist P. 2010. Organelle-Like Membrane Compartmentalization of Positive-Strand RNA Virus Replication Factories. Annu Rev Microbiol 64: 241–256.

29. Buxbaum AR, Haimovich G, Singer RH. 2015. In the right place at the right time: visualizing and understanding mRNA localization. Nat Rev Mol Cell Biol 16: 95–109.

30. Chin A, Lécuyer E. 2017. RNA localization: Making its way to the center stage. Biochim Biophys Acta 1861: 2956–2970.

31. Becker JT, Sherer NM. 2017. Subcellular Localization of HIV-1 gag-pol mRNAs Regulates Sites of Virion Assembly. J Virol 91: 2315–2331.

32. Ryder PV, Lerit DA. 2018. RNA localization regulates diverse and dynamic cellular processes. Traffic 19: 496–502.

33. Engel KL, Arora A, Goering R, Lo HYG, Taliaferro JM. 2020. Mechanisms and consequences of subcellular RNA localization across diverse cell types. Traffic 21: 404–418.

34. Zhang F, Simon AE. 2003. A novel procedure for the localization of viral RNAs in protoplasts and whole plants. Plant J 35: 665–673.

35. Tilsner J, Linnik O, Christensen NM, Bell K, Roberts IM, Lacomme C, Oparka KJ. 2009. Live-cell imaging of viral RNA genomes using a Pumilio-based reporter. Plant J 57: 758–770.

36. Wang F, Flanagan J, Su N, Wang LC, Bui S, Nielson A, Wu X, Vo HT, Ma XJ, Luo Y. 2012. RNAscope: A Novel *in Situ* RNA Analysis Platform for Formalin-Fixed, Paraffin-Embedded Tissues. J Mol Diagnostics 14: 22–29.

37. Borah S, Nichols LA, Hassman LM, Kedes DH, Steitz JA. 2012. Tracking expression and subcellular localization of RNA and protein species using high-throughput single cell imaging flow cytometry. RNA 18: 1573–1579.

38. Marras SAE, Bushkin Y, Tyagi S. 2019. High-fidelity amplified FISH for the detection and allelic discrimination of single mRNA molecules. Proc Natl Acad Sci 116: 13921–13926.

39. Wu KE, Fazal FM, Parker KR, Zou J, Chang HY. 2020. RNA-GPS Predicts SARS-CoV-2 RNA Residency to Host Mitochondria and Nucleolus. Cell Syst 11: 102-108.e3.

40. Sánchez Pina MA, Gómez-Aix C, Méndez-López E, Gosalvez Bernal B, Aranda MA. 2021. Imaging Techniques to Study Plant Virus Replication and Vertical Transmission. Viruses 13: 358.

41. Larsson C, Grundberg I, Söderberg O, Nilsson M. 2010. *In situ* detection and genotyping of individual mRNA molecules. Nat Methods 7: 395–397.

42. Schneider N, Meier M. 2017. Efficient *in situ* detection of mRNAs using the Chlorella virus DNA ligase for padlock probe ligation. RNA 23: 250–256.

43. Mizumoto H, Tatsuta M, Kaido M, Mise K, Okuno T. 2003. Cap-Independent Translational Enhancement by the 3′ Untranslated Region of Red Clover Necrotic Mosaic Virus RNA1. J Virol 77: 12113–12121.

44. Treder K, Pettit Kneller EL, Allen EM, Wang Z, Browning KS, Miller WA. 2007. The 3’ cap-independent translation element of Barley yellow dwarf virus binds eIF4F via the eIF4G subunit to initiate translation. RNA 14: 134–147.

45. Kraft JJ, Treder K, Peterson MS, Miller WA. 2013. Cation-dependent folding of 3′ cap-independent translation elements facilitates interaction of a 17-nucleotide conserved sequence with eIF4G. Nucleic Acids Res 41: 3398–3413.

46. Sharma S Das, Kraft JJ, Miller WA, Goss DJ. 2015. Recruitment of the 40S Ribosome Subunit to the 3′-Untranslated Region (UTR) of a Viral mRNA, via the eIF4 Complex, Facilitates Cap-independent Translation. J Biol Chem 290: 11268–11281.

47. Zhao P, Liu Q, Miller WA, Goss DJ. 2017. Eukaryotic translation initiation factor 4G (eIF4G) coordinates interactions with eIF4A, eIF4B, and eIF4E in binding and translation of the barley yellow dwarf virus 3′ cap-independent translation element (BTE). J Biol Chem 292: 5921–5931.

48. Iwakawa H, Mizumoto H, Nagano H, Imoto Y, Takigawa K, Sarawaneeyaruk S, Kaido M, Mise K, Okuno T. 2008. A Viral Noncoding RNA Generated by cis -Element-Mediated Protection against 5′→3′ RNA Decay Represses both Cap-Independent and Cap-Dependent Translation. J Virol 82: 10162–10174.

49. Miller WA, Shen R, Staplin W, Kanodia P. 2016. Noncoding RNAs of Plant Viruses and Viroids: Sponges of Host Translation and RNA Interference Machinery. Mol Plant-Microbe Interact 29: 156–164.

50. Ferre-D'Amare AR, Doudna JA. 1996. Use of Cis- and Trans-Ribozymes to Remove 5' and 3' Heterogeneities from Milligrams of *In Vitro* Transcribed RNA. Nucleic Acids Res 24: 977–978.

51. Ausländer S, Ketzer P, Hartig JS. 2010. A ligand-dependent hammerhead ribozyme switch for controlling mammalian gene expression. Mol Biosyst 6: 807.

52. Ferre-D'Amare AR, Scott WG. 2010. Small Self-cleaving Ribozymes. Cold Spring Harb Perspect Biol 2: a003574–a003574.

53. Jones CI, Zabolotskaya MV, Newbury SF. 2012. The 5′ → 3′ exoribonuclease XRN1/Pacman and its functions in cellular processes and development. WIREs RNA 3: 455–468.

54. Nagarajan VK, Jones CI, Newbury SF, Green PJ. 2013. XRN 5′→3′ exoribonucleases: Structure, mechanisms and functions. Biochim Biophys Acta 1829: 590–603.

55. Kieft JS, Rabe JL, Chapman EG. 2015. New hypotheses derived from the structure of a flaviviral Xrn1-resistant RNA: Conservation, folding, and host adaptation. RNA Biol 12: 1169–1177.

56. Akiyama BM, Laurence HM, Massey AR, Costantino DA, Xie X, Yang Y, Shi PY, Nix JC, Beckham JD, Kieft JS. 2016. Zika virus produces noncoding RNAs using a multi-pseudoknot structure that confounds a cellular exonuclease. Science 354: 1148–1152.

57. Charley PA, Wilusz CJ, Wilusz J. 2018. Identification of phlebovirus and arenavirus RNA sequences that stall and repress the exoribonuclease XRN1. J Biol Chem 293: 285–295.

58. MacFadden A, O'Donoghue Z, Silva PAGC, Chapman EG, Olsthoorn RC, Sterken MG, Pijlman GP, Bredenbeek PJ, Kieft JS. 2018. Mechanism and structural diversity of exoribonuclease-resistant RNA structures in flaviviral RNAs. Nat Commun 9: 119.

59. Slonchak A, Khromykh AA. 2018. Subgenomic flaviviral RNAs: What do we know after the first decade of research. Antiviral Res 159: 13–25.

60. Steckelberg AL, Akiyama BM, Costantino DA, Sit TL, Nix JC, Kieft JS. 2018. A folded viral noncoding RNA blocks host cell exoribonucleases through a conformationally dynamic RNA structure. Proc Natl Acad Sci 115: 6404–6409.

61. Steckelberg AL, Vicens Q, Kieft JS. 2018. Exoribonuclease-Resistant RNAs Exist within both Coding and Noncoding Subgenomic RNAs. MBio 9: e02461-18.

62. Dilweg IW, Gultyaev AP, Olsthoorn RC. 2019. Structural features of an Xrn1-resistant plant virus RNA. RNA Biol 16: 838–845.

63. Steckelberg AL, Vicens Q, Costantino DA, Nix JC, Kieft JS. 2020. The crystal structure of a Polerovirus exoribonuclease-resistant RNA shows how diverse sequences are integrated into a conserved fold. RNA 26: 1767–1776.

64. Szucs MJ, Nichols PJ, Jones RA, Vicens Q, Kieft JS. 2020. A New Subclass of Exoribonuclease-Resistant RNA Found in Multiple Genera of Flaviviridae. MBio 11: 1–15.

65. Jones RA, Steckelberg AL, Vicens Q, Szucs MJ, Akiyama BM, Kieft JS. 2021. Different tertiary interactions create the same important 3D features in a distinct flavivirus xrRNA. RNA 27: 54–65.

66. Vicens Q, Kieft JS. 2021. Shared properties and singularities of exoribonuclease-resistant RNAs in viruses. Comput Struct Biotechnol J 19: 4373–4380.

67. Pijlman GP, Funk A, Kondratieva N, Leung J, Torres S, van der Aa L, Liu WJ, Palmenberg AC, Shi PY, Hall RA, Khromykh AA. 2008. A Highly Structured, Nuclease-Resistant, Noncoding RNA Produced by Flaviviruses Is Required for Pathogenicity. Cell Host Microbe 4: 579–591.

68. Silva PAGC, Pereira CF, Dalebout TJ, Spaan WJM, Bredenbeek PJ. 2010. An RNA Pseudoknot Is Required for Production of Yellow Fever Virus Subgenomic RNA by the Host Nuclease XRN1. J Virol 84: 11395–11406.

69. Moon SL, Anderson JR, Kumagai Y, Wilusz CJ, Akira S, Khromykh AA, Wilusz J. 2012. A noncoding RNA produced by arthropod-borne flaviviruses inhibits the cellular exoribonuclease XRN1 and alters host mRNA stability. RNA 18: 2029–2040.

70. Peltier C, Klein E, Hleibieh K, D'Alonzo M, Hammann P, Bouzoubaa S, Ratti C, Gilmer D. 2012. Beet necrotic yellow vein virus subgenomic RNA3 is a cleavage product leading to stable non-coding RNA required for long-distance movement. J Gen Virol 93: 1093–1102.

71. Chapman EG, Moon SL, Wilusz J, Kieft JS. 2014. RNA structures that resist degradation by Xrn1 produce a pathogenic Dengue virus RNA. Elife 3: e01892.

72. Clarke BD, Roby JA, Slonchak A, Khromykh AA. 2015. Functional non-coding RNAs derived from the flavivirus 3′ untranslated region. Virus Res 206: 53–61.

73. Gunawardene CD, Im JSH, White KA. 2021. RNA Structure Protects the 5′ End of an Uncapped Tombusvirus RNA Genome from Xrn Digestion. J Virol 95: e0103421.

74. Kawaguchi R, Bailey-Serres J. 2005. mRNA sequence features that contribute to translational regulation in Arabidopsis. Nucleic Acids Res 33: 955–65.

75. Matsuura H, Takenami S, Kubo Y, Ueda K, Ueda A, Yamaguchi M, Hirata K, Demura T, Kanaya S, Kato K. 2013. A Computational and Experimental Approach Reveals that the 5′-Proximal Region of the 5′-UTR has a Cis-Regulatory Signature Responsible for Heat Stress-Regulated mRNA Translation in Arabidopsis. Plant Cell Physiol 54: 474–483.

76. Kim Y, Lee G, Jeon E, Sohn EJ, Lee Y, Kang H, Lee DW, Kim DH, Hwang I. 2014. The immediate upstream region of the 5′-UTR from the AUG start codon has a pronounced effect on the translational efficiency in *Arabidopsis thaliana*. Nucleic Acids Res 42: 485–498.

77. von Arnim AG, Jia Q, Vaughn JN. 2014. Regulation of plant translation by upstream open reading frames. Plant Sci 214: 1–12.

78. Kwok CK, Ding Y, Shahid S, Assmann SM, Bevilacqua PC. 2015. A stable RNA G-quadruplex within the 5′-UTR of *Arabidopsis thaliana* ATR mRNA inhibits translation. Biochem J 467: 91–102.

79. Álvarez D, Voß B, Maass D, Wüst F, Schaub P, Beyer P, Welsch R. 2016. Carotenogenesis Is Regulated by 5′UTR-Mediated Translation of Phytoene Synthase Splice Variants. Plant Physiol 172: 2314–2326.

80. Srivastava AK, Lu Y, Zinta G, Lang Z, Zhu JK. 2018. UTR-Dependent Control of Gene Expression in Plants. Trends Plant Sci 23: 248–259.

81. Zhang T, Wu A, Yue Y, Zhao Y. 2020. uORFs: Important Cis-Regulatory Elements in Plants. Int J Mol Sci 21: 6238.

82. Chung BYW, Balcerowicz M, Di Antonio M, Jaeger KE, Geng F, Franaszek K, Marriott P, Brierley I, Firth AE, Wigge PA. 2020. An RNA thermoswitch regulates daytime growth in Arabidopsis. Nat Plants 6: 522–532.

83. Wiese A, Elzinga N, Wobbes B, Smeekens S. 2004. A Conserved Upstream Open Reading Frame Mediates Sucrose-Induced Repression of Translation. Plant Cell 16: 1717–1729.

84. Li W, Ma M, Feng Y, Li H, Wang Y, Ma Y, Li M, An F, Guo H. 2015. EIN2-Directed Translational Regulation of Ethylene Signaling in Arabidopsis. Cell 163: 670–683.

85. Merchante C, Brumos J, Yun J, Hu Q, Spencer KR, Enríquez P, Binder BM, Heber S, Stepanova AN, Alonso JM. 2015. Gene-Specific Translation Regulation Mediated by the Hormone-Signaling Molecule EIN2. Cell 163: 684–697.

86. Simms CL, Thomas EN, Zaher HS. 2017. Ribosome-based quality control of mRNA and nascent peptides. WIREs RNA 8: e1366.

87. Navickas A, Chamois S, Saint-Fort R, Henri J, Torchet C, Benard L. 2020. No-Go Decay mRNA cleavage in the ribosome exit tunnel produces 5′-OH ends phosphorylated by Trl1. Nat Commun 11: 122.

Figures

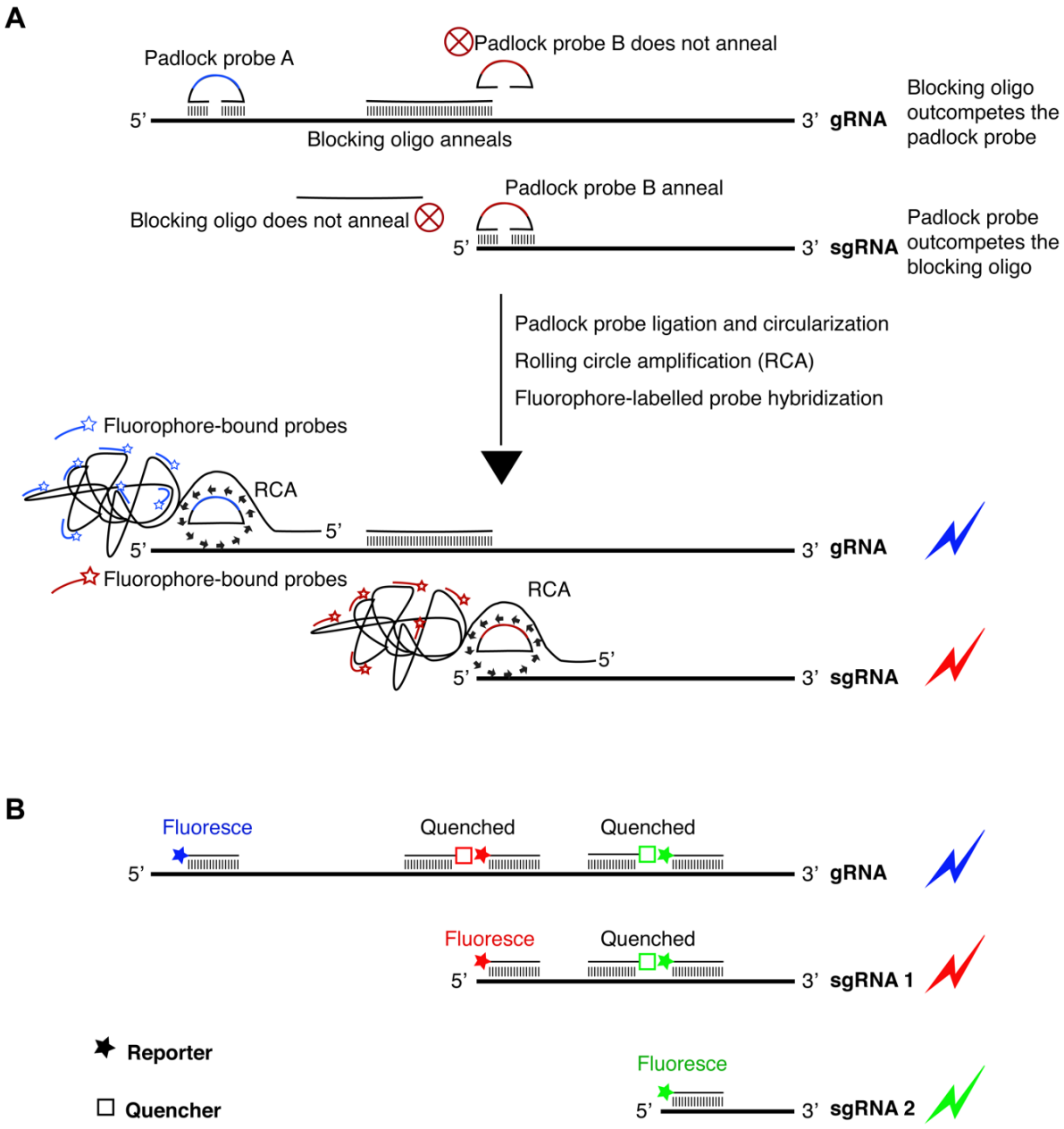

Figure 6.1. Proposed adaptation of DeSCo-PCR principle for specific detection of viral sgRNAs *in situ*. **(A)** Use of a blocking oligo with the padlock probes can inhibit the annealing of the padlock probe to the gRNA template, thereby preventing its circularization and rolling circle amplification from it. In contrast, the padlock probe annealing to the sgRNA would circularize, amplify, hybridize to fluorophore-tagged probes and fluoresce. **(B)** Use of reporter-quencher system in a way that would quench the fluorescence only from the reporter that anneals to the gRNA in the coterminal region. (gRNA) genomic RNA, (sgRNA) subgenomic RNA, (RCA) rolling circle amplification.